Technical Report 1

HF TIME-AND FREQUENCY-DISPERSION EFFECTS--EXPERIMENTAL VALIDATION OF AN FSK ERROR-RATE MODEL

By: B. M. SIFFORD R. N. SHAVER R. F. DALY K. D. FELPERIN

Prepared for:

U.S. ARMY RADIO PROPAGATION AGENCY
FORT MONMOUTH, NEW JERSEY

CONTRACT DA 36-039 SC-90859

STANFORD RESEARCH INSTITUTE
MENLO PARK, CALIFORNIA

*SRI

STANFORD RESEARCH INSTITUTE
MENLO PARK CALIFORNIA

March 1965

Technical Report 4

HF TIME- AND FREQUENCY-DISPERSION EFFECTS-- EXPERIMENTAL VALIDATION OF AN FSK ERROR-RATE MODEL

Prepared for:

U.S. ARMY RADIO PROPAGATION AGENCY
FORT MONMOUTH, NEW JERSEY

CONTRACT DA 36-039 SC-90859

By: B. M. SIFFORD H. N. SHAVER R. F DALY K. D. FELPERIN

SRI Project 4172

Approved: W. R. VINCENT, MANAGER
COMMUNICATION LABORATORY

D. R. SCHEUCH, EXECUTIVE DIRECTOR
ELECTRONICS AND RADIO SCIENCES

Copy No.

ABSTRACT

An experiment has been conducted to determine the sensitivity of an HF FSK communications system to time- and frequency-selective fading phenomena. Binary error rate was measured on AN/FGC-29 teletype terminal equipment over an HF path from Fort Monmouth, New Jersey to Palo Alto, California in the fall of 1964. Simultaneous measurements were made of channel signal-to-noise ratios, channel time-delay profiles, channel Doppler-shift profiles, and signal correlation between spaced antennas. Instrumentation included a phase-stable transmitter-receiver, an oblique-incidence ionospheric sounder, and a special correlation meter. The measured error rates were compared to those predicted by a mathematical model. The model for the channel considers randomly time-varying and frequency-selective effects appropriate for the HF propagation mechanism. The system model approximates the AN/FGC-29 system. Theoretical and measured error-rate curves are presented and discussed. Measured system performance showed a well-defined sensitivity to channel time- and frequency-selective effects. The asymptotic error rates measured at high signal-to-noise ratios are in reasonable agreement with those predicted from the model.

CONTENTS

CONTENTS

CONTENTS

ILLUSTRATIONS

TABLES

ACKNOWLEDGMENTS

Significant support for this experiment was provided by current government-supported SRI projects with related interests. An HF communications and ionospheric sounder link from Fort Monmouth to Palo Alto had previously been established under Contract DA 36-039 SC-87197; these facilities were made available to this effort. The analog-to-digital converter—used to make digital time-delay recordings—and the Doppler-profile computer programs were developed under this contract.

Equipment and personnel support were also provided to this experiment through Contract DA 28-043 AMC-00082(E) sponsored by the U.S. Army Electronics Command. This project had an interest in experimentally demonstrating a relation between error rate on HF communications channels and multipath propagation information provided by oblique sounders.

A project from the Defense Communications Agency (Contract SD-189) was very cooperative in supporting this experiment. The interest of this agency stems from a desire to evaluate the use of ionospheric sounders as an aid to the control of DCS HF trunks. Such use of sounders relies heavily on a channel model and an error-rate formulation to show the sensitivity of a given system to the various parameters a sounder can measure. Almost half of the field experiment expense at the Palo Alto receiver site and essentially all of the data-processing costs associated with the time-delay and Doppler profiles were borne by this project.

I INTRODUCTION

A. HISTORICAL BACKGROUND

Since 1956, the Communication Laboratory at Stanford Research Institute has been active in various fields related to the analysis of strategic military communications networks. This activity has resulted in a series of computer programs that predict the performance and vulnerability of such networks under a wide variety of propagation and electromagnetic environments.[1,2,3,4]* Recently, this work has been expanded to include consideration of time- and frequency-dispersive effects on the performance of selected types of systems. Since the backbone of strategic military communications networks is HF radio—even though there has been recent inclusion of troposcatter, cable, and satellite systems—the emphasis has been on HF systems and propagation. The computational models used in the propagation predictions are based on predictable geophysical factors. As a result, predictions of signal-to-noise ratio (S/N) on a radio path can be computed months and years in advance. Even though these predictions are not exact, they are valuable in day-to-day station operation and in the planning of future networks.

To transform the results of the propagation predictions into estimates of communications link performance, it was necessary to establish a computational model for each communications system used in the particular terminals of the network. It was also necessary to establish a quantitative definition of the performance of these systems and criteria for the utility of the link based on this performance rating. The measure of performance adopted was binary error rate. This parameter has the following advantages:

(1) It can often be evaluated analytically from basic system models by making certain assumptions on the signal and noise statistics.

(2) It can usually be translated further to other user-defined performance criteria, such as character error rate, reliability, or message intelligibility.

(3) It can be directly estimated from nonsubjective measurements.

* References are given at the end of the report.

With the increasing use of data and digital-voice transmission, binary error rate will undoubtedly become the standard measure of communications circuit performance.

Recently, the Communication Laboratory has been active in deriving more detailed error-rate models of specific systems designed for HF. These models are unique in that they consider dispersive channel effects but require the specification of additional channel parameters not predicted by the present propagation programs. It is hoped that these propagation programs can be updated by including the additional parameters so that eventually a computation capability for evaluating entire networks by using these new system and channel models can be obtained.

To gain confidence in error-rate computational models, a direct comparison with actual measured results was needed. Stanford Research Institute was asked to conduct a controlled experiment to determine the accuracy of the error-rate computational model for a particular system when all of the required channel characteristics are known. This experiment was performed in the fall of 1964; results of this experiment are presented in this report.

B. REVIEW OF ERROR-RATE MODELS

Error-rate computational models are based on statistical principles. As such, they do not attempt to predict the exact number of errors that will occur but only to answer the question: What is the *probability* that a receiver will decide that State A was transmitted during a particular signaling interval when State B was actually transmitted? To answer such a question, probabilistic concepts must be introduced and with them certain random variables that can be described only in a statistical sense.

The first attempts to derive an error-rate model for communications channels were based on the following assumptions:

(1) An ideal matched-filter receiver

(2) All signals subject only to fixed attenuation and a fixed time delay in their passage through the propagation medium

(3) Errors in reception caused solely by narrow-band Gaussian noise added to the received signal.

The ideal matched-filter receiver has knowledge of all the possible signal waveforms that can be transmitted by the transmitter for each time

interval. Coherent matched-filter detection requires that the receiver have exact knowledge of all possible phase states of the transmitted waveforms when they arrive at the receiver. Incoherent matched-filter detection does not utilize *a priori* phase information of the received signal. The assumption of an ideal matched-filter receiver implies exact time synchronization with the transmitted data stream and ideal integration and sampling of the received waveform. This is followed by complete energy dumping or quenching of all integrating filters.

The next evolutionary stage in the development of error-rate models was to allow the received signal envelope to vary slowly with respect to a signaling element (*i.e.*, to fade) and to assume a distribution of this variation in calculating the effect on the probability of error. It was also assumed in these models that fading over the transmission bandwidth of the signal was correlated. Such a channel has been termed flat-flat by Bello and Nelin,[5] because the time autocorrelation function of the channel is constant over a time difference on the order of a signaling-element time interval, and the channel frequency-correlation function is constant over a frequency difference comparable to the bandwidth of the transmitted signal. The frequency correlation is directly related to the time-delayed "multipath" propagation modes which are observed at HF and can be predicted by propagation theory. The time autocorrelation is directly related to the difference in Doppler shift associated with these modes. Diversity improvements were modeled by assuming the availability at the receiver of independent fading signals and specifying various combining rules for the receiver. The flat-flat models show a decreasing error rate with increasing S/N.

More recent channel models include the effects of Doppler and delay spreading of the transmitted signals. The use of these models, however, requires additional statistical parameters to describe the spreading of the signal by the channel in time and frequency. These models show asymptotically constant error rates with increasing S/N. The asymptotic values depend critically on interaction of certain system parameters and on the statistical channel spread measures.

At HF, the simpler flat-flat models have generally been used for present binary FSK systems. These are adequate, however, only when gross estimates of performance at moderate error rates are needed. For normal 100-wpm teletype channels predominately handling messages with English-language redundancy, a binary error rate less than 10^{-3} has usually been

considered acceptable. With the present increase in less redundant data traffic and the corresponding increase in reliability requirements, the simpler models are becoming inadequate. As newer modulation systems and higher data-transmission rates are introduced, time and frequency spreading of the channel, even at HF, cannot be ignored in a performance model. But estimating or predicting these channel scattering functions from geophysical parameters presents a problem. Although the present programs can predict individual signal strengths for each propagating mode, together with propagation-time differences, they cannot adequately predict Doppler effects.

C. OUTLINE OF THE VALIDATION EXPERIMENT

The basic plan for the validation experiment was to take a typical HF FSK data modem, a single channel from a standard AN/FGC-29 system, and adapt an appropriate computational model for it. From this model, a series of binary error-rate characteristics were calculated with various values of channel parameters. The next step was to run an experiment on an actual HF link using a system of this type, to measure continuously all of the pertinent channel parameters, together with obtaining a measured estimate of the binary error rate.

Chapter II discusses the computational system and channel models used and the system and channel descriptors that must be specified. Chapter III describes the actual experiment performed, including a description of the instrumentation and of the data-recording procedure. Chapter IV outlines the data-processing operations—the criteria and procedure used to obtain confident measures of the channel parameters and the binary error rate. Chapter V presents the results in the form of computed and measured error-rate curves, together with a discussion of the results.

Chapter VI shows the results of an allied experiment that demonstrates quite dramatically the correlation between frequency-selective effects and detected errors on an HF communications system.

Chapter VII presents some results on the measurement of the correlation of signal fading as received on two space-separated antennas. Comparison of these results with simultaneously measured errors on a dual-diversity system and with measured time-delay characteristics on the channel are also shown.

II DESCRIPTION OF THE COMPUTATIONAL MODEL

A. INTRODUCTION

The computational model used to compute the theoretical error-rate curves was developed in a prior study.[6] In this study, the effects of time- and frequency-selective fading on an idealized FSK system were analyzed for a simple HF channel model. For the purposes of the present effort, the computational model and associated computer programs were modified to include the important effects on a non-zero transition time when the FSK transmitter switches from one frequency to another. The model is more realistic than the previous one which assumed an instantaneous frequency change. It was found that the inclusion of a small transition time (approximately 2 percent of the signaling-element duration) caused the predicted performance of the FSK system to display a moderate deterioration (as opposed to a phase-continuous instantaneous frequency change) at high S/Ns for typical ionospheric time-delay and Doppler conditions.

B. SYSTEM AND CHANNEL MODELS

The system model assumes a single-channel matched-filter receiver with the filters matched to ideal FSK transmissions. A quadratic detector obtains the squared envelope of the output of each matched filter; the receiver then decides which signal was transmitted, on the basis of the larger squared envelope.

With the exception of a linear variation of frequency in the transition intervals, the FSK transmission is assumed to be ideal. If f_m is the mark frequency and f_s is the space frequency, then Fig. 1 displays the linear frequency transition when the sequence SPACE-MARK-SPACE is transmitted. In this figure, T is the signaling-element duration, and $2L$ is the transition time. Observe that in the transition intervals the transmission is a chirp signal that spans all frequencies between the two signaling frequencies. The receiver filters (which are matched to ideal FSK transmissions) are not matched to the above transmissions.

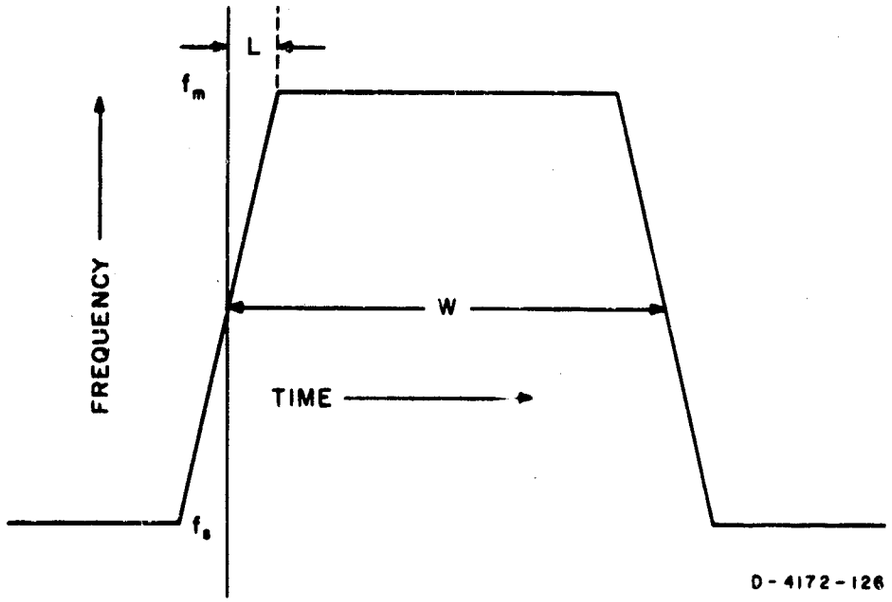

FIG. 1 LINEAR FREQUENCY VARIATION AT TRANSITION INTERVALS

As the transition time, $2L$, is increased, the performance of the FSK system, operating through a time-varying and frequency-selective radio channel, deteriorates. For typical ionospheric Doppler and time-delay conditions and small transition times, the deterioration appears as an increase in the binary error probability for high S/Ns. The randomly selective radio channel transforms the chirp transmissions at the transition times to noise-like signals which impair the detectability of the FSK transmissions.

The channel model has been adequately described in previous Stanford Research Institute reports.[6,7] This model assumes that the randomly time-varying linear channel is composed of a discrete number of independent propagation paths. Each path is described by a time delay, a Doppler shift, and a random complex gain. The model can be considered as an idealized version of the HF channel when the time-delay spread and Doppler spread of the individual paths are small compared to the time-delay differences and Doppler-shift differences between the paths. Alternatively, as the number of paths becomes large, this channel approaches one with a continuum of time delays and Doppler shifts. The channel model accounts for the important signal-distorting effects caused by time- and frequency-selective fading, such as intersymbol interference and fast fading of the signal amplitude within a signaling-element duration.

C. COMPARISON OF THE COMPUTATIONAL SYSTEM MODEL AND THE EXPERIMENTAL SYSTEM

The AN/FGC-29 FSK receiver used in the experiment and the incoherent matched-filter FSK receiver of the computational model display notable differences in detection procedures. The AN/FGC-29 employs discriminator detection without hard limiting and, in contrast to the incoherent matched-filter receiver, does not quench the energy stored from previous signaling elements before processing any given received signaling element. In the absence of hard limiting, the discriminator can be modeled with two linear narrow-band filters with the appropriate center frequencies and bandwidths for the two transmitted FSK signals. Hence, one of the major differences between the computational model and the experimental system lies in the energy-quenching property of the computational model. In the experimental system, the signal energy due to previous signaling elements decays at a rate determined by the filter time constant. In the computational model, the energy in the filters is quenched instantaneously every W seconds, and detection is based only on the signal received in a time interval of length W seconds. If the filters of the experimental system do not decay stored energy rapidly enough, it is possible that frequency-selective fading could cause the stored energy in one filter to differ markedly from the stored energy in the other filter. This anomalous situation would cause an initial bias error which could adversely affect the system's detection capability. The computational model does not account for an unequal biasing of the filters before the processing of a signaling element; however, it does account for the effects of time- and frequency-selective fading occurring during a signaling-element duration. In filtering the received pulses, the experimental system smooths and shapes the time and frequency characteristics of the received signal instead of essentially narrow-band integrating over a signaling-element duration as does the computational model.

D. THE ERROR-RATE PROGRAM

The error-rate program utilizes the simple HF channel model and the idealized FSK system model (including the transition-time modification) to compute a binary error probability. Input parameters to the program describe the particular channel scattering function[7] desired in the error-rate analysis. These parameters include the number of propagation paths and a relative strength, time delay, the Doppler shift for each path.

In the computation of the binary error probability, it is assumed that the channel transfer function is a homogeneous Gaussian random field[7] and that the output of the channel is further perturbed by an additive white Gaussian noise. The details of this computation can be found in Ref. 6, where the cross-ambiguity function [Eq. (33), Ref. 6] has been modified to include the transition-time effect. It is assumed that the time delays (measured from the average time delay determined by the time-delay profile of the channel) of the various propagation paths are all less than a signaling-element duration. Hence intersymbol interference is limited to adjacent signaling elements. The program computes the probability that the MARK in the transmitted sequence SPACE-MARK-SPACE is detected improperly as a SPACE. This sequence corresponds to the actual alternating mark and space sequence that was employed in the experiment, which was chosen to maximize the effects of frequency-selective fading (intersymbol interference and unequal fading of the mark and space frequencies).

The output of the program is a computer-plotted curve of binary error probability versus S/N for the desired channel scattering function. Each plot displays two curves, one for no diversity (labeled FSK1) and one for independent dual diversity (labeled FSK2). Each plot displays a channel-scattering-function diagram in the lower left-hand corner. In this diagram each path is represented by an *X* with size proportional to the strength of the path and with position determined by the time delay and Doppler shift of the path. Time delays relative to the average time delay of the channel are read along the logarithmic horizontal scale and are normalized to the signaling-element duration (T = the time delay of the path divided by the signaling-element duration). Doppler shifts relative to the average Doppler shift of the channel are read along the logarithmic vertical scale and are also normalized to the signaling-element duration (D = Doppler shift of the path multiplied by the signaling-element duration). For example, Fig. 2(a) displays the error-rate curves for an FSK system operating through a propagation medium composed of two equal-strength paths spaced at a time-delay difference equal to 0.2 of the signaling-element duration and with no Doppler spreading in frequency.

E. CHANNEL-SCATTERING-FUNCTION APPROXIMATION

Validation of the theoretical error-rate analysis required simultaneous measurements of the channel scattering function, S/N, and binary error probability. The scope of the experiment (the available time and rate of

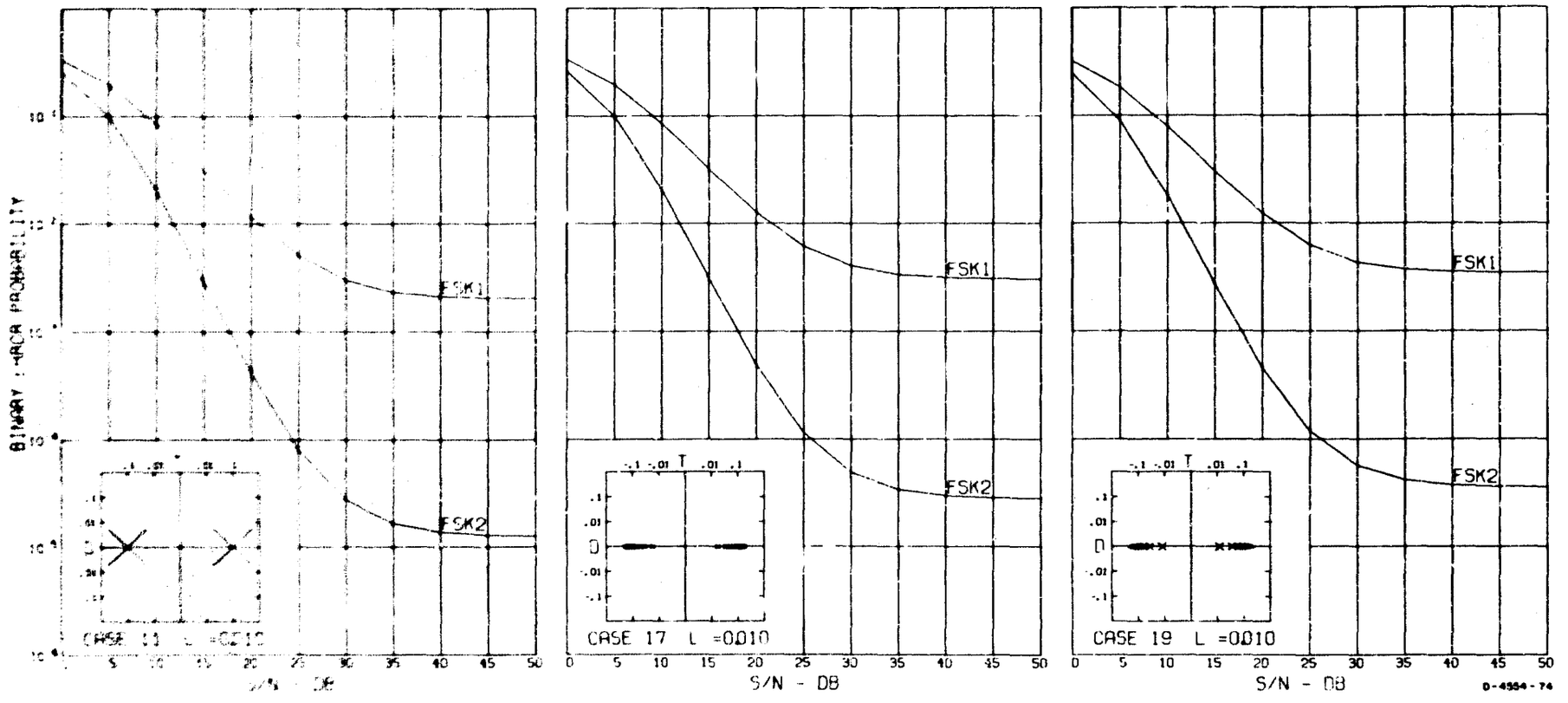

(a) FSK Error Probability, 2 Equal-Strength Paths, $2\sigma_\tau = 0.2$, $2\sigma_\lambda = 0$, $2L = 0.02$

(b) FSK Error Probability, 20 Paths with Uniform-Strength Distribution, $2\sigma_\tau = 0.2$, $2\sigma_\lambda = 0$, $2L = 0.02$

(c) FSK Error Probability, 20 Paths with Triangular-Strength Distribution, $2\sigma_\tau = 0.2$, $2\sigma_\lambda = 0$, $2L = 0.02$.

FIG. 2 ERROR-RATE SENSITIVITY TO THE SHAPE OF THE TIME-DELAY PROFILE

effort) made it necessary to limit the measurement of the channel scattering function to the time-delay and Doppler-shift profiles.[7] It was also necessary to concentrate the major portion of the effort on obtaining data for the no-diversity case, since the dual-diversity case would add another dimension to the classification of data: spacial correlation. The amount of data required to obtain statistically reliable results for dual-diversity operation at all possible states of S/N, time delay, Doppler shift, and spacial correlation far exceeded our single-channel capability for collecting data and available rate of effort for data processing. However, a limited amount of data was obtained for dual-diversity operation; some interesting results concerning spacial correlation are discussed in Chapter VII.

Although time-delay and Doppler-shift profiles were measured on the channel throughout the experiment, it was not feasible or necessary to use all of the information that these functions contain for correlating the observed error rate with the state of the dispersive channel. Various computer programs were run, investigating the sensitivity of the error rate displayed by the theoretical model to the shape of the scattering function. It was found that if the scattering function is approximately symmetrical and of moderate width in the time-delay and Doppler-shift directions, then the error rate is strongly dependent on the time-delay and Doppler-shift second moments and relatively insensitive to the scattering-function shape. Figure 2 illustrates this phenomenon in the time-delay direction. Figure 2(b) and (c) corresponds to error rates computed for a time-delay profile consisting of twenty propagation paths with energy distributed uniformly and triangularly, respectively. In Fig. 2(a) the error rate is computed for two equal-strength paths. In all three of the above scattering functions, the standard deviation of the time-delay profile is equal to 0.1 of the signaling-element duration, or all three shapes possess an rms time-delay spread equal to 0.2 of the signaling-element duration. For most practical applications, the error-rate curves of Fig. 2(a) are reasonable approximations to the curves of Fig. 2(b) and (c), with a tendency to underestimate the error rate. Hence, symmetrical scattering functions with moderate time-delay and Doppler spreads can be approximated with two equal-strength paths spaced in time delay at the time-delay spread of the scattering function and spaced in Doppler at the Doppler spread of the scattering function. This approximation introduces a major simplification in the analysis of the data; when valid, it allows one to use only the second moments associated with the time-delay and Doppler profiles.

For scattering functions possessing large spreads with strongly asymmetrical distributions, the tendency of this approximation to underestimate the error rate becomes excessive. For example, Fig. 3(a) displays the error-rate curves for a channel with two unequal paths spaced at 0.5 of the signaling-element duration, with one path five times the strength of the other path. The rms time-delay spread of this channel is 0.35 of the signaling-element duration. Application of the approximation of two equal-strength paths spaced at 0.35 of the signaling-element duration yields the curves of Fig. 3(b) which excessively underestimate the error rate. In analyzing phase systems, Gaarder of Stanford Research Institute found that asymmetrical scattering functions of the type illustrated in Fig. 3(a) can be effectively approximated with two equal-strength paths spaced at the identical spacing of the original unequal-strength paths and that this approximation remains valid for a wide range of relative path strengths.[8] Application of this approximation to Fig. 3(a) yields the curves of Fig. 3(c) which were computed for two equal-strength paths spaced at 0.5 of the signaling-element duration. For this case, the curves of Fig. 3(a) and (c) are essentially identical.

F. TRANSITION-TIME SENSITIVITY AND IRREDUCIBLE ERROR PROBABILITY

The sensitivity of system performance as a function of transition time is illustrated by Fig. 4. In this figure, error-rate curves are displayed for a fixed scattering function that describes a channel composed of two equal-strength paths spaced in time delay at 0.1 of the signaling-element duration and with zero Doppler shift. Deterioration of system performance with increasing transition time is clearly indicated; the transition times are 0.005, 0.01, and 0.02 of the signaling-element duration in Fig. 4(a), (b), and (c), respectively.

A significant property of the error-rate curves for an incoherent matched-filter system, operating through a dispersive channel, is the existence of an irreducible error probability at infinite S/Ns. Hence the irreducible error probability serves as a meaningful measure of the limitations imposed on system performance by the dispersive properties of the propagation medium. Irreducible error probability as a function of the time-delay spread of two equal-strength paths with zero Doppler is plotted in Fig. 5. Similarly, irreducible error probability as a function of the Doppler spread of two equal-strength paths with a

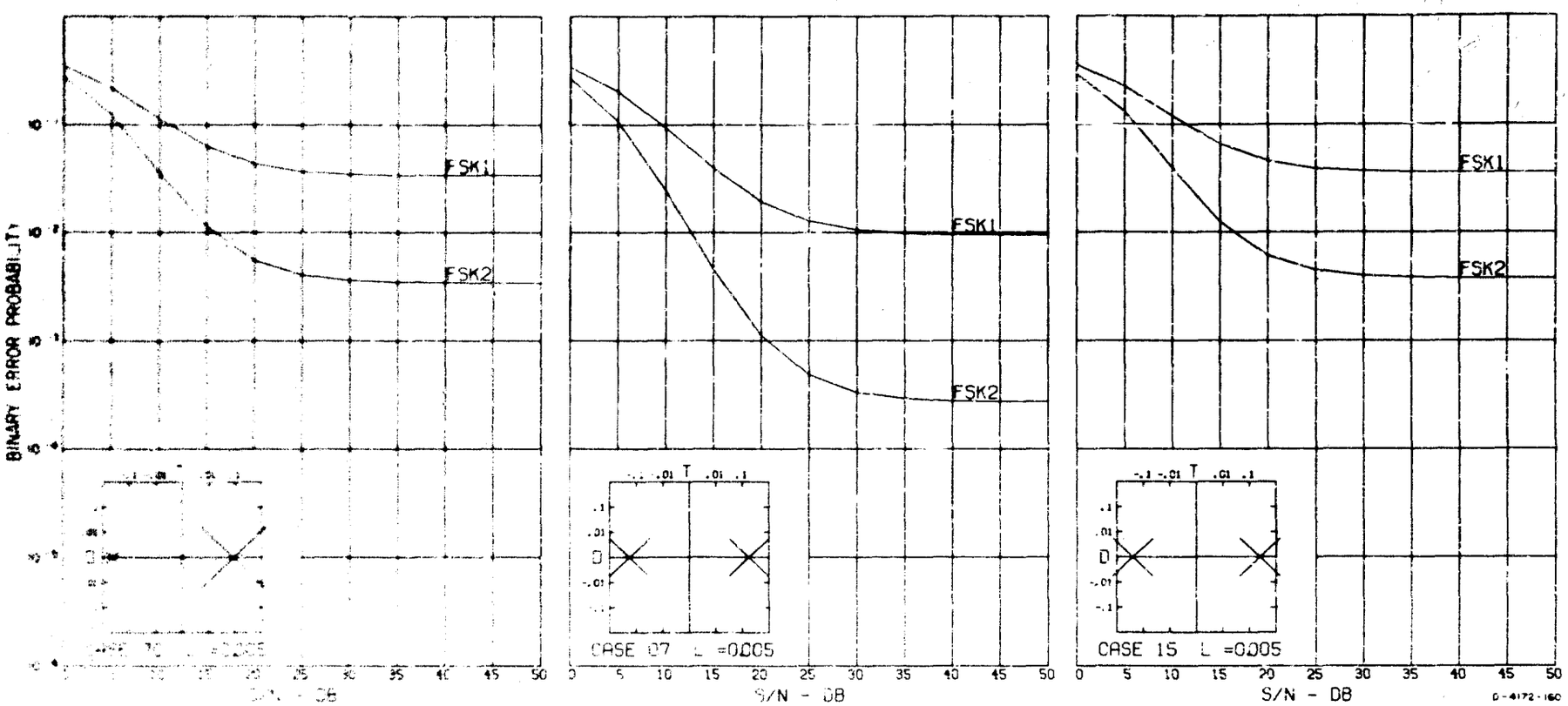

(a) FSK Error Probability, 2 Unequal-Strength Paths, with One Path 5 Times the Strength of the Other $2\sigma_\tau = 0.35$, $2\sigma_\lambda = 0$, $2L = 0.01$

(b) FSK Error Probability, 2 Equal-Strength Paths, $2\sigma_\tau = 0.35$, $2\sigma_\lambda = 0$, $2L = 0.01$.

(c) FSK Error Probability, 2 Equal-Strength Paths, $2\sigma_\tau = 0.5$, $2\sigma_\lambda = 0$, $2L = 0.01$.

FIG. 3 AN APPROXIMATION OF A STRONGLY ASYMMETRICAL TIME-DELAY PROFILE

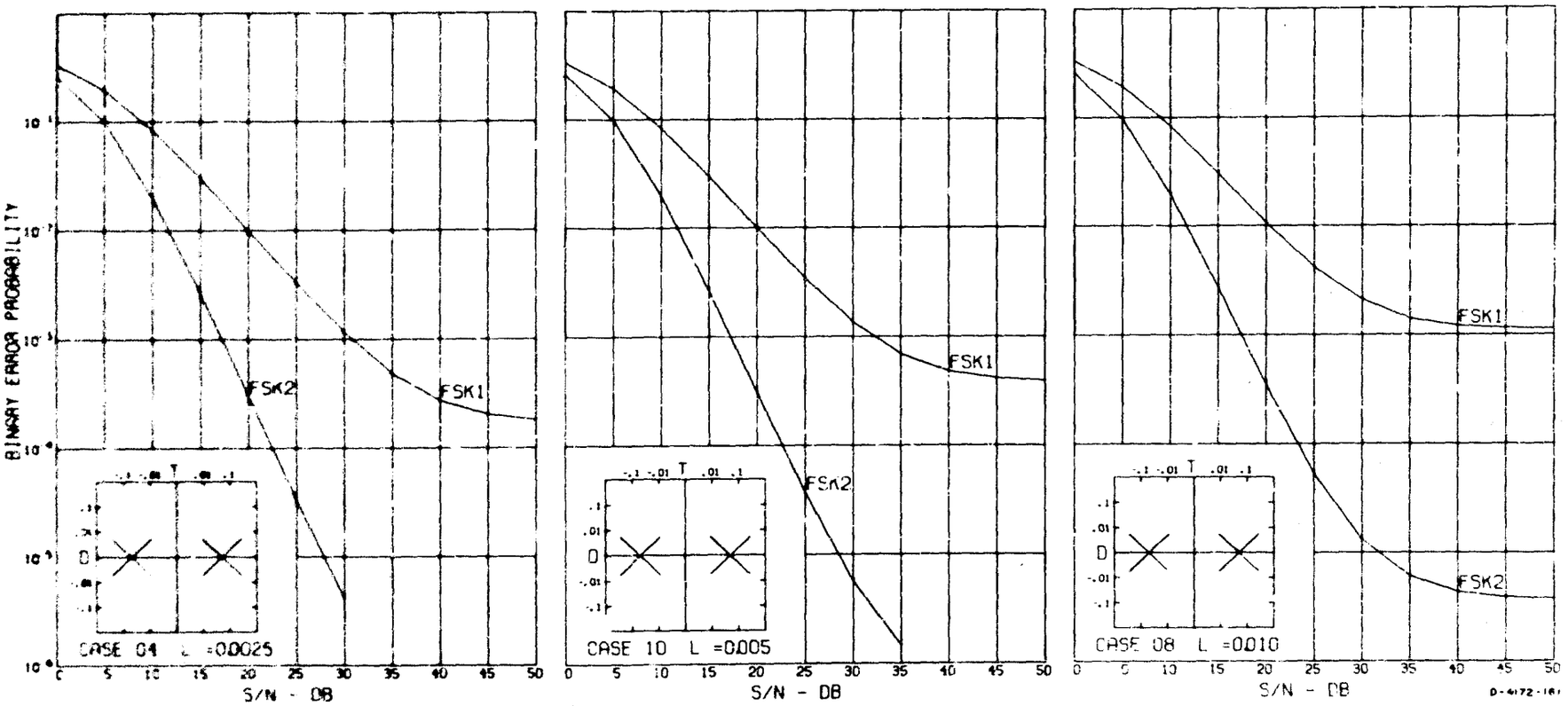

(a) FSK Error Probability, 2 Equal-Strength Paths, $2\sigma_T = 0.2$, $2\sigma_\lambda = 0$, $2L = 0.005$.

(b) FSK Error Probability, 2 Equal-Strength Paths, $2\sigma_T = 0.1$, $2\sigma_\lambda = 0$, $2L = 0.01$.

(c) FSK Error Probability, 2 Equal-Strength Paths, $2\sigma_T = 0.1$, $2\sigma_\lambda = 0$, $2L = 0.02$.

FIG. 4 ERROR-RATE SENSITIVITY TO TRANSITION TIME

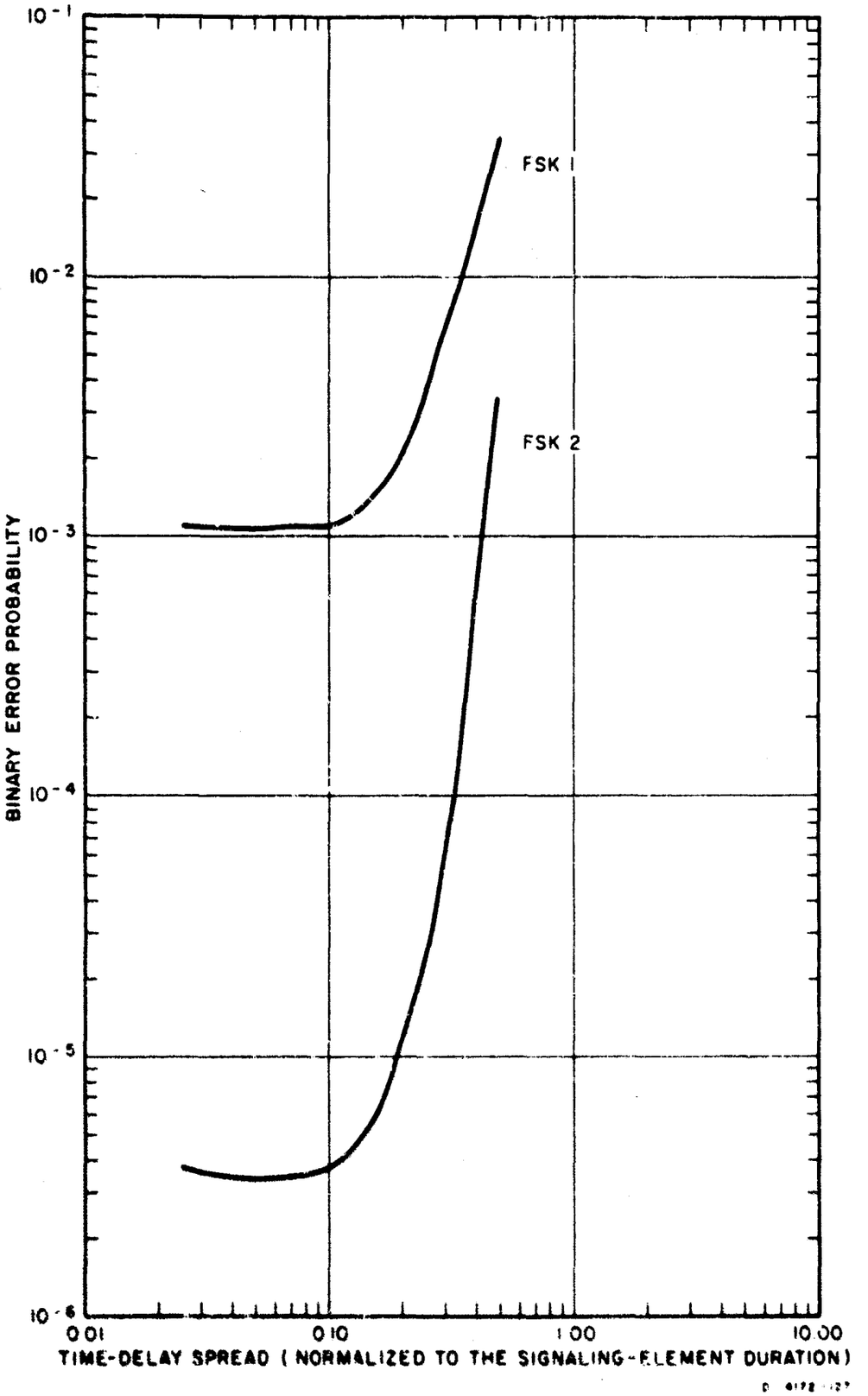

FIG. 5 IRREDUCIBLE ERROR PROBABILITY AS A FUNCTION OF TIME-DELAY SPREAD, $2\sigma_A = 0$, $2L = 0.02$

time-delay spread equal to the transition time is plotted in Fig. 6. Both the time-delay and Doppler-shift irreducible-error-probability curves were plotted for a transition time equal to 0.02 of the signaling-element duration.*

The irreducible-error-probability curves exhibit an interesting transition-time phenomenon. For small time-delay or Doppler-spreads and high S/Ns, the system performance is essentially limited by transition time; this limitation is illustrated by the flat portion of the irreducible-error-probability curves at low spread values. At lower spread values, the curves maintain a constant error probability; at higher spread values, the irreducible error probability increases as the spread raised to some positive power.

* The curves do not display irreducible error probability for time-delay spreads less than the transition time. As the time-delay spread is decreased below the transition time, the irreducible error probability begins to decrease again.

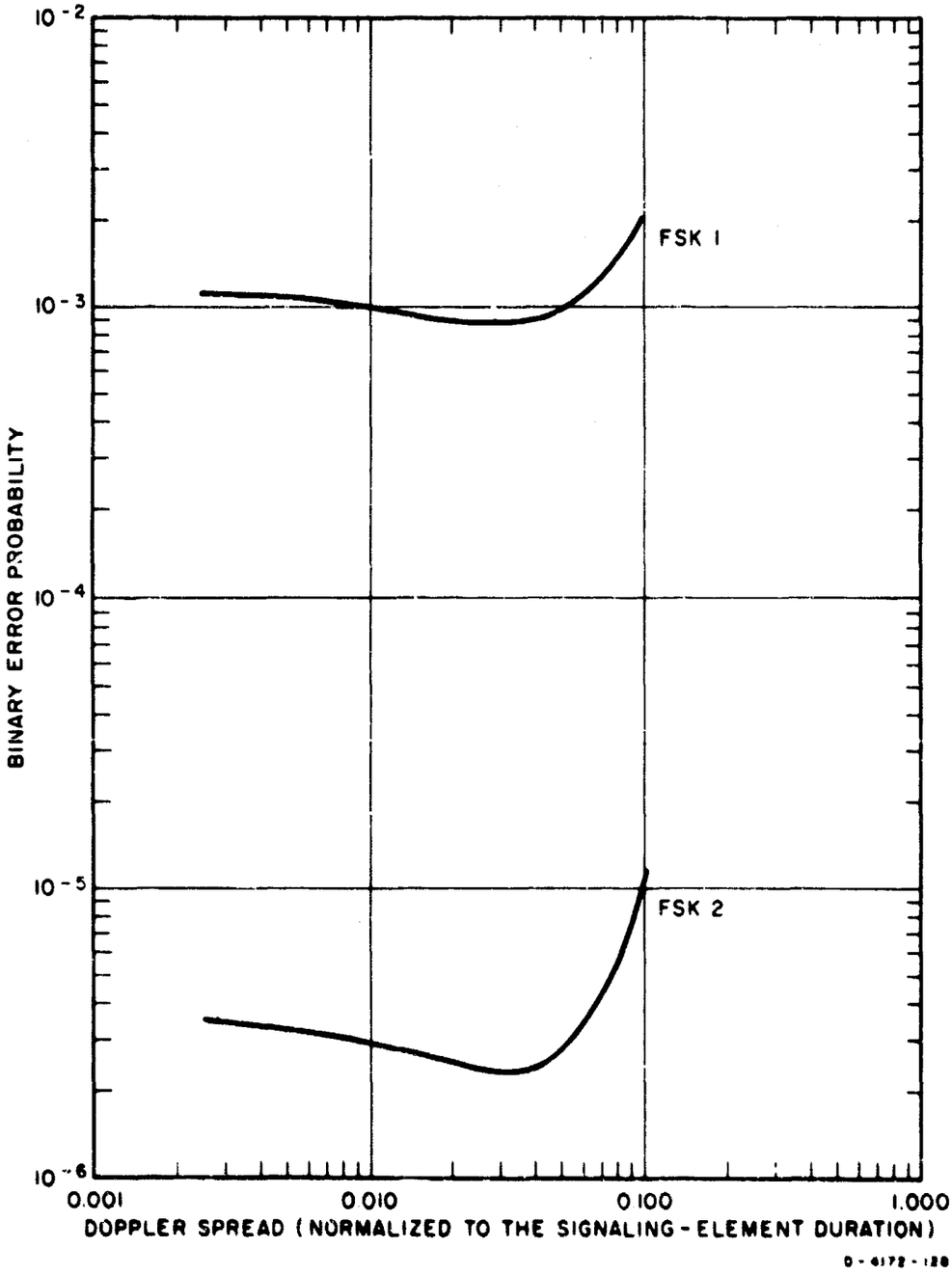

FIG. 6 IRREDUCIBLE ERROR PROBABILITY AS A FUNCTION OF DOPPLER SPREAD, $2\sigma_r$ = 0.02, 2L = 0.02

III DESCRIPTION OF THE EXPERIMENT

A. INTRODUCTION

The purpose of the experimental program was to compare measured error-rate S/N characteristics with predicted characteristics derived from a theoretical error-rate model for an HF FSK communications system. The design of the experiment was so formulated that the experimental program could logically be divided into several distinct subexperiments. All the subexperiments were performed simultaneously, and the results were used to compare measured error rates with predicted error rates for the measured channel conditions. The subexperiments will be catagorized as follows:

(1) Error-rate and S/N measurement

(2) Doppler profile measurement

(3) Time-delay profile measurement.

Each measurement with its associated equipment is described in detail in this chapter.

The measurements were performed on a single binary data channel using two-stage modulation. The input binary data frequency-modulated a subcarrier. The resulting FSK tones single-sideband-modulated the HF carrier, with a substantial portion of the carrier being retained. The data rate was 100 baud, which is slightly higher than that of a single 100-wpm teletype channel. The operating frequencies were 14.360 and 7.366 Mc, used for approximately the same amount of time. These frequencies were chosen to maximize the amount of data collected in the scheduled experiment time and to obtain data under a variety of propagation conditions. The transmitter was located at the Earle Test Site, Fort Monmouth, New Jersey, the receiver site was at an SRI field site near Palo Alto, California. The great-circle distance between the sites is 4100 km.

B. ERROR-RATE AND S/N MEASUREMENT

1. Discussion of the Experiment

The purpose of this experiment was to measure binary error rate and S/N for an FSK data channel using HF ionospheric propagation. The data modem consisted of a single-channel AN/FGC-29 transmitter unit (FSK modulator) and the corresponding AN/FGC-29 receiver unit. The RF transmitter was a modified AN/FRT-51 operated into a horizontal log-periodic antenna. Dipole antennas were used for reception with R-390 receivers and CV-157 sideband converters. The receiving antennas were so positioned that space-diversity reception was also available. The data were simulated by an alternating mark-space sequence with a bit or element length of 10 msec The error rate was estimated by measuring the number of errors detected at the receiver relative to the number of binary digits transmitted. The S/N was measured by sequentially sampling a linearly detected and filtered version of the signal within the data channel with signal plus noise (S/N) present (FSK data tones on) and noise only present (FSK data tone off). The choice of obtaining signal and noise samples at adjacent times but within the same bandwidth—rather than the alternative of obtaining signal and noise samples at adjacent bandwidths but at the same time—was based on the assumption that noise, particularly narrow-band man-made interference, would be more correlated over a short time interval than over a small bandwidth separation.

The data-gathering technique was synchronous in the sense that pertinent operations were performed within a time accuracy of less than a millisecond at both the transmitting and receiving sites A 30-second interval was chosen as the basic data-gathering interval. During each 30-second interval, six data samples were taken, 5 seconds apart. Each data sample consisted of a three-digit counter readout and a digital voltmeter readout. The counter readout contained the number of errors that had been detected in the binary data stream since the start of the 30-second interval. The voltmeter reading represented a linearly detected and filtered version of the received signal contained within the 170-cps bandpass of the data channel. During the first five samples, the data tones were on so that received S N was detected. During the sixth sample, the data tones were off, and noise only was detected

The data tones were gated off at the transmitter from the 25th second until the end of the 30-second period. This period was long

enough for the various detector filters at the receiver to stabilize and the noise level to be sampled and recorded. A loss of the data tones would normally affect the receiver gain through the AGC. To avoid such an effect, the AGC control voltage was derived exclusively from the carrier signal, which remained on continuously through all data-gathering periods.

The error-totalizing counter was reset to zero at the beginning of each 30-second data interval. The fifth data sample contained the fifth S/N voltage reading and the cumulative error count for approximately 23 seconds of data tramsmission. This cumulative error count when divided by the total number of binary digits transmitted during that interval represents the binary error rate. The error count for the sixth data sample was discarded because the data tones had been turned off for the noise measurement. A binary error in the received signal was detected by comparing the loop keyer output of the AN/FGC-29 "combiner" unit with a locally generated replica of the transmitted signal (with path and equipment delays taken into consideration).

2. Data Timing Cycle

The automated collection of data resulted in data collection cycles. The time relationships within the 30-second data period are shown in Fig. 7. This basic cycle started at 7 minutes after the hour and was repeated eighteen times for a total of 9 minutes. The tenth minute was used for a sounder transmission at the receiver site, and data transmission was not attempted then. This minute provided an opportunity for the call sign to

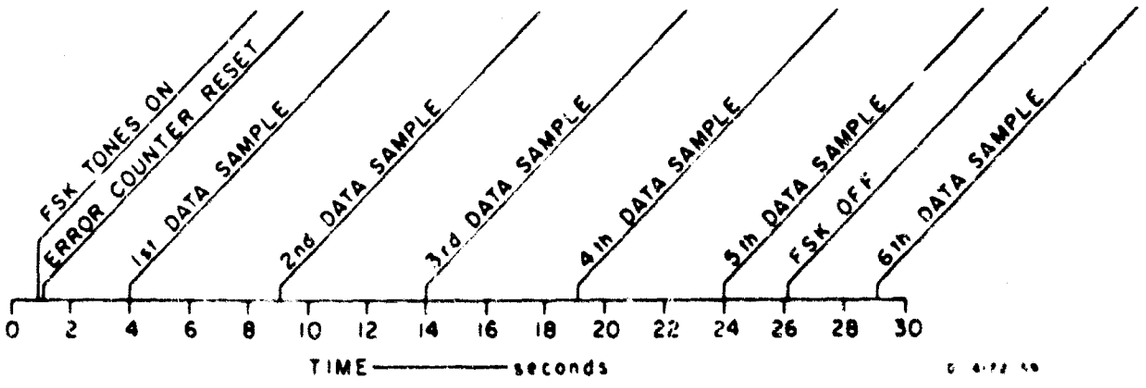

FIG. 7 TIME RELATIONSHIPS WITHIN THE BASIC 30-SECOND DATA-GATHERING INTERVAL

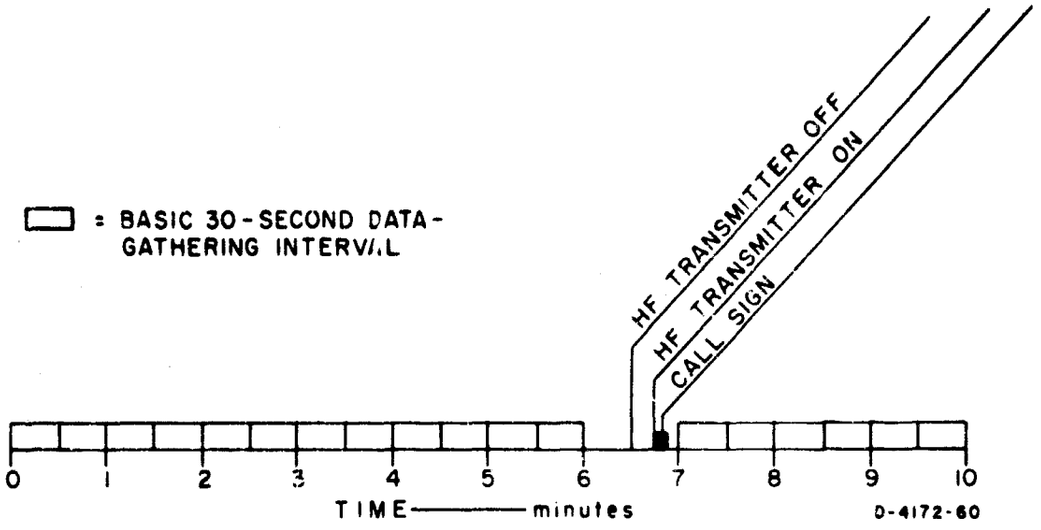

FIG. 8 TIME RELATIONSHIPS WITHIN A 10-MINUTE DATA-COLLECTION PERIOD

be transmitted, minor adjustments to be made on the equipment, and a time reference to be printed on the data tape. The time relationships within a 10-minute period are shown in Fig. 8.

Because timing was of utmost importance in this experiment, both the transmitting and the receiving site used frequency standards that were maintained in synchronization with receptions from WWV. These standards drove digital clocks that delivered timing pulses at programmed times to generate the desired data-gathering cycle.

3. Description of the Experimental Setup

a. Transmitting Terminal Equipment

A block diagram of the equipment located at the transmitting site is shown in Fig. 9. The frequency standard supplied 100-kc and 1-Mc signals. The frequency synthesizer generated a series of phase-stable frequencies for the mixers so that the transmitter could operate at either 7.366 Mc or 14.360 Mc. The requirement for high phase stability was associated with the Doppler profile measurement, which is described in more detail in Sec. C of this chapter.

The Granger Associates (G A) Model 340 programmer[9] was also driven by the 100-kc frequency standard. This programmer is an accurate digital clock with a series of programmable timing outputs. The clock

was set to an accuracy of 1 msec by using WWV. The programmer provided the following timing signals:

(1) Clock pulses, occurring every 10 msec, which drove the digital word generator

(2) A blocking signal which, when applied to the AN/FGC-29 transmitter, turned off the modulation so that periodic in-channel noise measurements could be made at the receiving sites

(3) A timing signal that initiated the call sign transmission each time the transmitter was turned on

(4) A timing signal that turned off the transmitter for 15 seconds once every 10 minutes.

The exact time relationship between these operations has been indicated in Figs. 7 and 8.

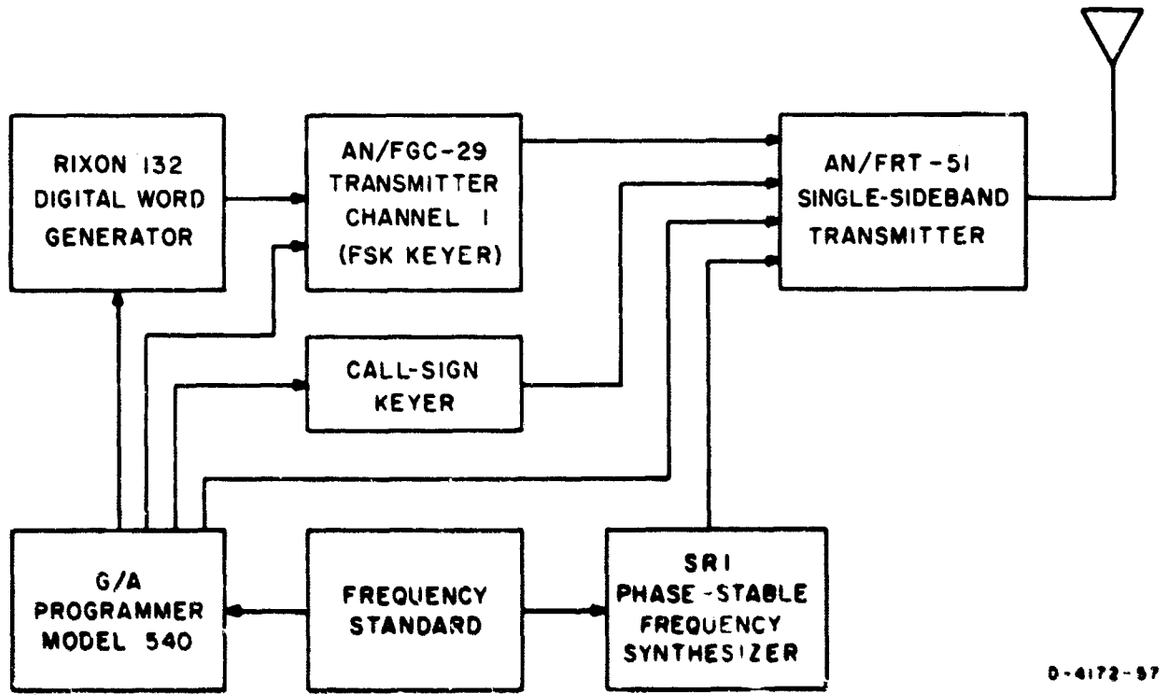

FIG. 9 BLOCK DIAGRAM OF ERROR-RATE EXPERIMENT TRANSMITTER SITE

The Rixon Model 132 digital word generator[10] is capable of providing a selected repetitive binary sequence of any length up to 32 binary digits. In this experiment, a simple alternating sequence was used, because this was the type of signal assumed for the theoretical error-rate curves. Therefore, the word generator in this case was essentially

a time-synthronized square-wave generator. The only required input for the word generator was the 10-msec clock pulses derived from the programmer. The output binary data stream was used to drive the FSK keyer.

The binary output signal from the word generator consists of the voltage levels, zero, and -5 volts. The signal normally required by the AN/FGC-29 transmitter keyer is a 0- or 60-ma current source. Therefore, minor modifications were made to the FSK keyer unit to make the units compatible. The AN/FGC-29 Channel 1 transmitter unit is essentially a subcarrier modulator or FSK keyer. The center frequency for the channel is 1785 cps with MARK at 1827.5 cps and SPACE at 1742.5 cps. The FSK output of this unit was used directly to modulate a single-sideband transmitter. The FSK tone output was blocked (*i.e.*, the modulation signal was turned off) by grounding the keyer output through a set of relay contacts in the programmer so that an in-channel noise voltage sample could be taken at the receiver.

The AN/FRT-51 consists of a twin-sideband modulator, a system of mixers, an exciter, and the final power amplifier. The unit is capable of providing a power of 5 kw; however, under these operating conditions, the total output power was limited to 2 kw, with approximately half the power in the carrier and half in the sideband. The sideband in this case was the upper sideband, which consisted of the single channel FSK data tones. All of the signals used in the modulating and mixing operations, other than the modulation signal itself, were derived from the phase-stable frequency synthesizer or its source, the frequency standard. A block diagram of the modulator-mixer chain (Fig. 10) shows how the upper sideband and carrier were generated. Each mixer was followed by a Q-multiplier so that only the desired signals were retained.

The transmitter site was located at Fort Monmouth (Earle), New Jersey. A horizontal log-periodic antenna directed toward Palo Alto, California, was used on both 7.366 Mc and 14.360 Mc.

b. RECEIVING-TERMINAL EQUIPMENT

The receiving-terminal for the error-rate experiment was located at an SRI site near Palo Alto, California. A block diagram of the receiving system is shown in Fig. 11. The system used two pairs of horizontal dipole antennas—one pair tuned for each of the operating frequencies. The antennas

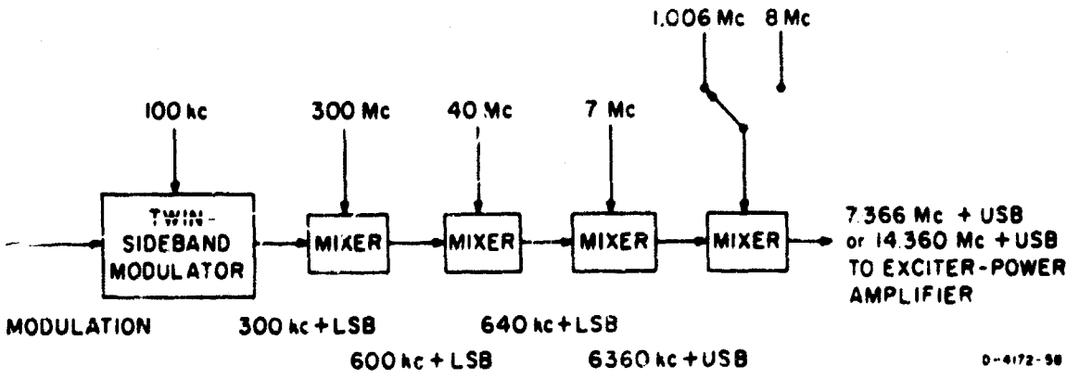

FIG. 10 PHASE-STABLE MODULATOR-MIXER CHAIN IN MODIFIED AN/FRT-51 TRANSMITTER

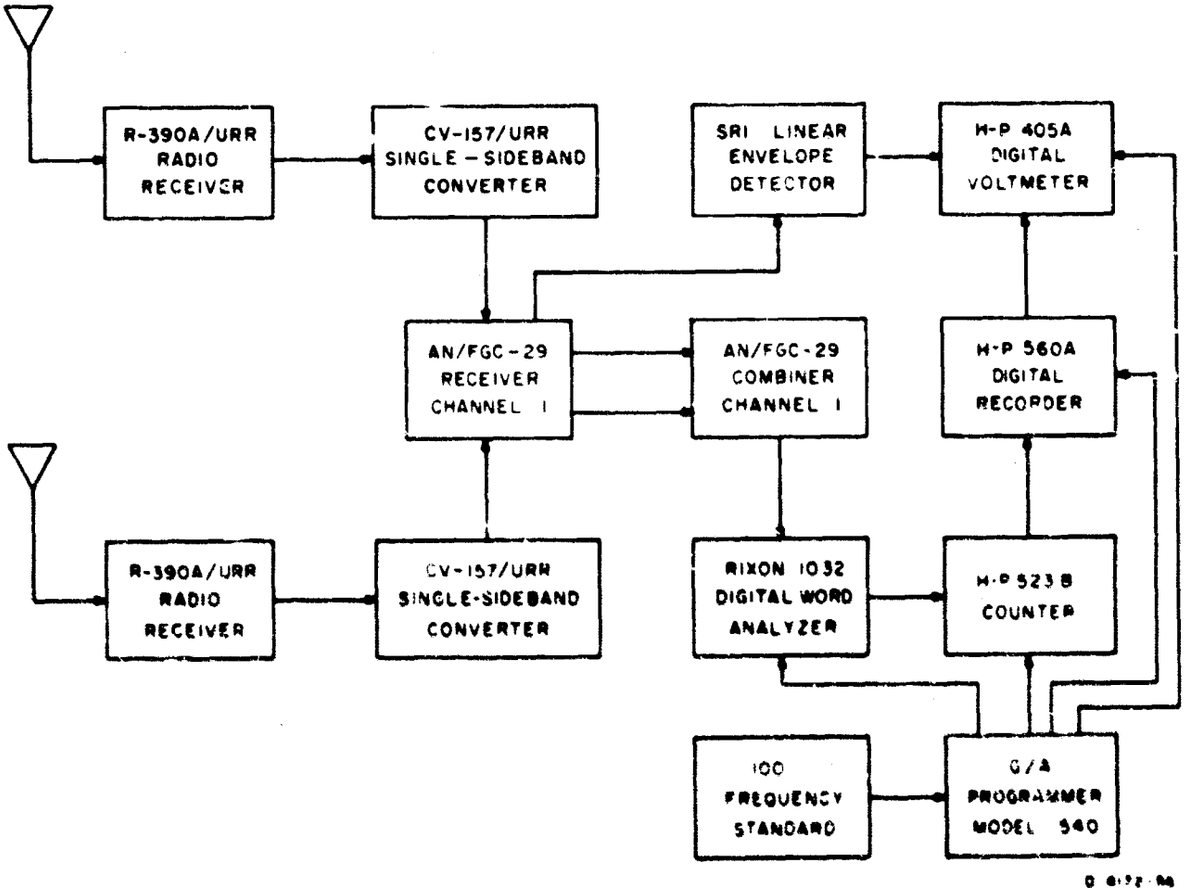

FIG. 11 BLOCK DIAGRAM OF DUAL SPACE-DIVERSITY ERROR-RATE EXPERIMENT RECEIVER SITE

of each pair were physically separated by a distance of approximately 800 feet. The spaced antennas were used for diversity reception.

A set of spaced antennas was connected directly to separate R-390A/URR radio receivers[12] tuned to the transmission frequency. The R-390A/URR is a standard military receiver with a frequency range from 0.5 to 32 Mc. For the demodulation of single-sideband signals, the IF signal from the R-390/URR was used as the input for a single-sideband converter.

The single-sideband converters used were standard military types designated CV-157/URR.[3] The 455-kc IF from the R-390A/URR was mixed to 100 kc in the converter. The converter separates the transmitted carrier frequency from its sideband frequencies and detects the audio in the sidebands. The audio in this case was the subcarrier-modulated (FSK) tones. The availability of both the carrier and the sideband channels provided several alternatives for the generation of the AGC voltage. The choice of appropriate AGC for the experiment was considered at some length and is discussed in a following paragraph. The upper sideband was selected to carry the FSK tones, and the audio from this channel was fed to the Channel 1 input in the AN/FGC-29 receiver unit.

Up to this point in the signal processing, two identical channels were available from the space-diversity antennas. The two distinct channels were processed further through the AN/FGC-29 receiver unit. In the receiver unit, the signals were appropriately weighted for post-detection diversity combining. Prior to the weighting, both diversity channels had equal gain. Within each channel in the AN/FGC-29 receiver, the FSK signal was first passed through a 170-cps bandpass filter centered at 1785 cps (Channel 1). Provisions were available for adjusting the relative gain and relative delay in both channels.

After the two diversity channels had been amplified, the FSK tones were detected in discriminators in the AN/FGC-29 combiner unit. The two resulting dc telegraph signals were then added to complete the combining operation. The combined signal was hard-limited and drove the loop keyer which provided the binary teletype output.

To determine the range of system linearity, the relationship between sideband input S/N and output S/N was measured. This measurement is significant, because a signal measurement (with sideband tones on)

followed by a noise measurement (with sideband tones off) was used to estimate S/N with carrier continuously present. In a sense, this measurement is similar to a measurement of linear dynamic range of the system for different AGC levels. A fixed noise level was added at the input of the R-390A/URR because the noise figure of the receiver is a function of the AGC level. By deriving the AGC from the carrier, sideband signal and noise output levels were measured by alternately turning on and off the sideband modulation. The input signal was fed to the R-390A/URR followed by the CV-157/URR and the receiver unit in the AN/FGC-29. The output S/N was measured at a point following the 170-cps band-pass filter in the AN/FGC-29 receiver. The AGC was developed in the carrier channel of the CV-157/URR and applied in the R-390A/URR. The results of the measurement, as shown in Fig. 12, indicate that the sequential measuring technique estimates S/Ns with reasonable accuracy up to about 60 db.

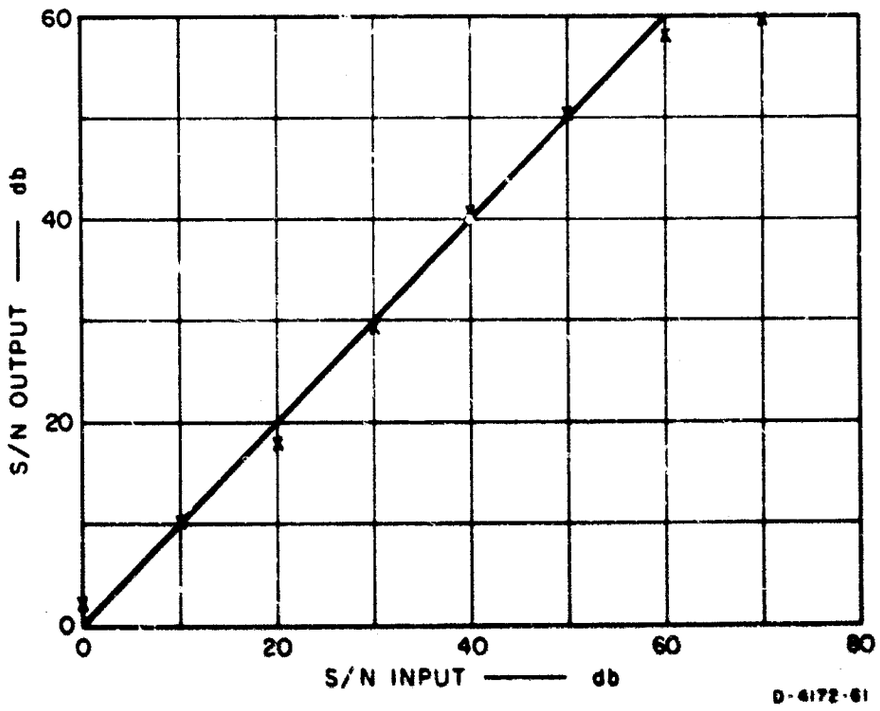

FIG. 12 INPUT-OUTPUT S/N CHARACTERISTICS

The channel weighting for the combining operation was performed in the AN/FGC-29 receiver unit, and the post-detection addition of the signals was performed in the AN/FGC-29 combiner unit. Before combining a series of voltages representing S+N (diversity channels), it is generally advantageous to weight the individual voltages in some manner. If the

noises are mutually independent, a maximization of the output S/N is achieved by weighting each incoming signal in proportion to its ratio of signal voltage to noise power. On the assumption that the noise is constant and relatively small compared to the signal, the combined output is approximately the sum of the squares of the inputs. This type of combining is called maximal-ratio or optimum combining.[14] The combining characteristics of AN/FGC-29 receiver that were used in this experiment approximated this rule; they are shown in Fig. 13.

For the combiner to perform the combining operation that it is designed to perform, the gain through the two diversity channels up to the point where the weighting takes place should be the same. To insure this, both channels must be balanced for equal gain, and any AGC control voltage other than the combiner weighting must be the same for both channels. For the experimental program, the channels were balanced, and a special AGC selector circuit was used. Within each channel, an AGC voltage was developed by placing the FUNCTION switch on the R-390A/URR in the MGC position. In this position, no AGC voltage was developed in the R-390A/URR. On the CV-157/URR, the AGC SELECT switch was placed in the CARRIER position and the AGC TIME switch in the SLOW position. Thus, for each channel, an AGC voltage was developed that was slowly varying and roughly proportional to the carrier level in that channel. The separate AGC voltages were combined in a diode network in which the larger of the two voltages was "selected" and used to operate the AGC control circuits in both of the R-390A/URRs. In this manner, approximately identical channel characteristics were achieved up to the point of combiner weighting. The AGC voltages developed by the R-390A/URR CV-157/URR combinations are shown in Fig. 14.

The measurement of the voltages for the computation of S/N was made in one of the diversity channels following the 170-cps bandpass filter in the AN/FGC-29 receiver unit. This filter was centered at 1785 cps. The signal level at the filter output was estimated by passing the signal through a linear envelope detector-filter combination and monitoring the dc voltage on a digital voltmeter. (The detector is briefly discussed in Appendix A.) The signal responses at the input of the voltmeter to step on and off envelope changes of a fixed-frequency sideband at the input to the R-390A/URR are shown in Fig. 15. The input-output characteristic

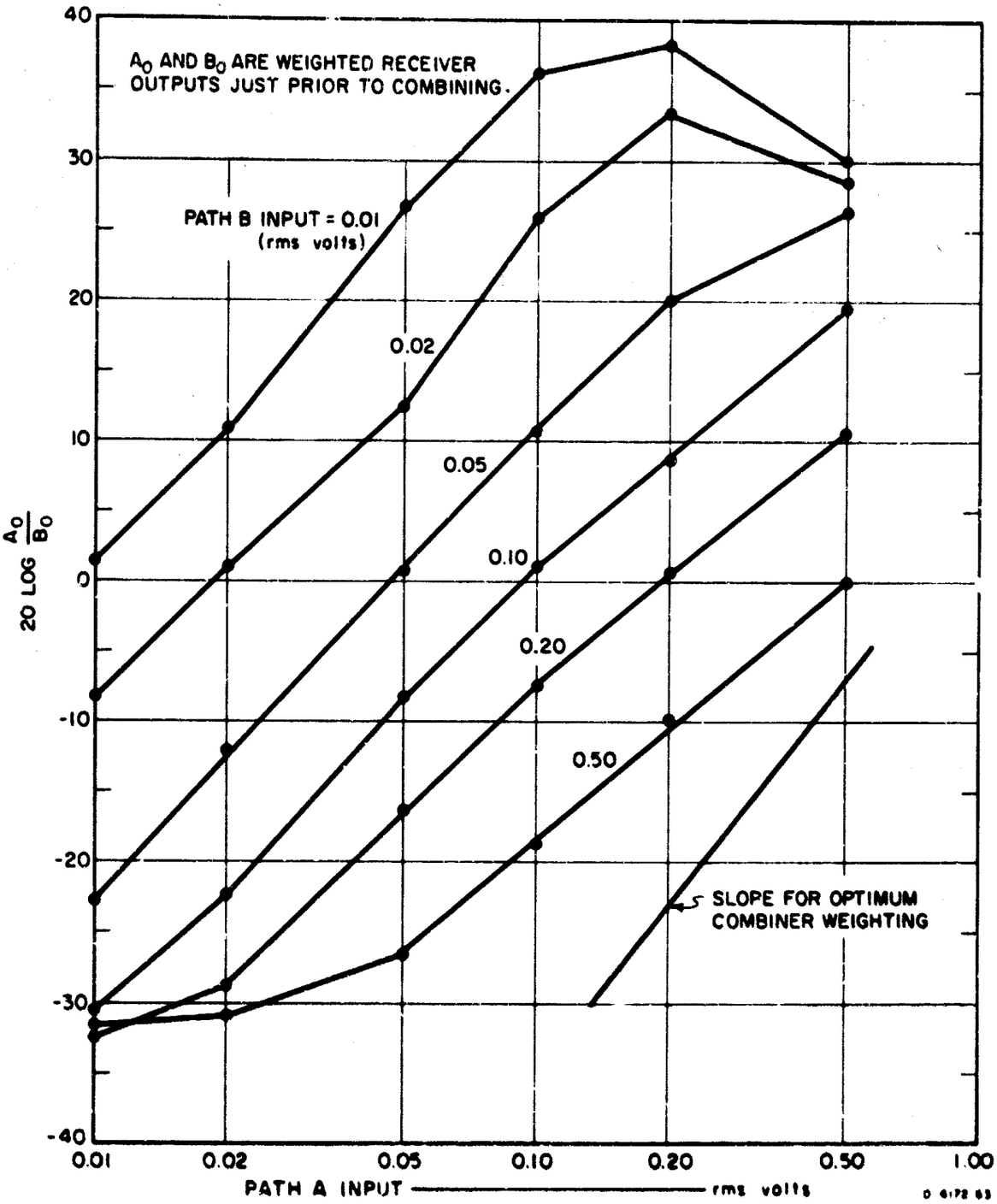

FIG. 13 AN/FGC-29 COMBINER WEIGHTING

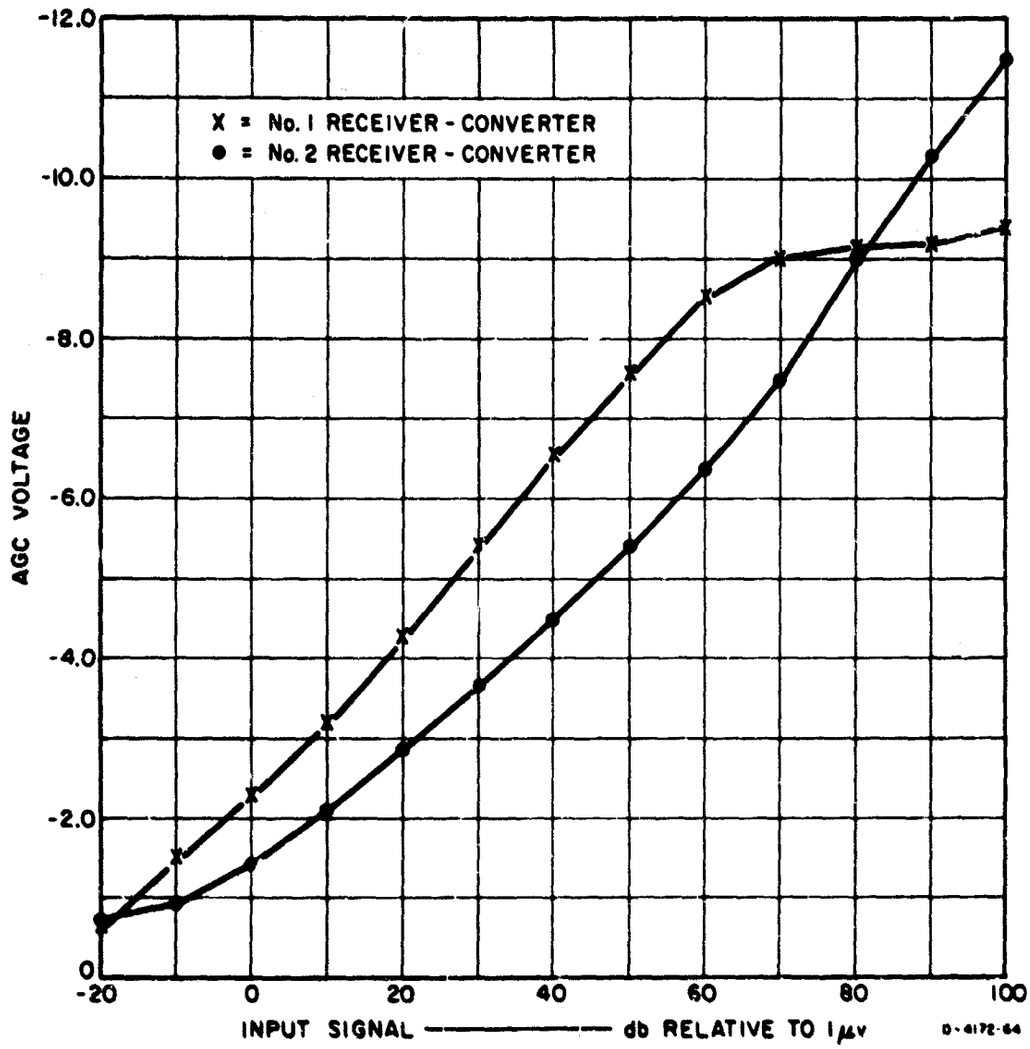

FIG. 14 AGC VOLTAGE vs. INPUT SIGNAL LEVEL

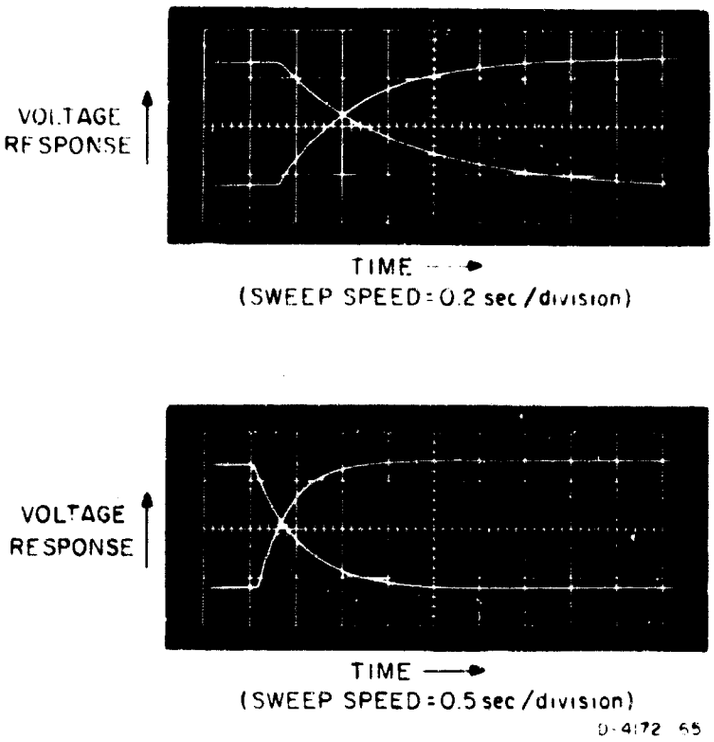

FIG. 15 RESPONSE OF SIGNAL-LEVEL DETECTION SYSTEM TO ON AND OFF STEP CHANGES IN ENVELOPE

of the detection system where the input is considered to be the input to the AN/FGC-29 receiver unit is given in Fig. 16. The nonlinearity is introduced by the AN/FGC-29 receiver unit. By monitoring the detected signal levels on the digital voltmeter, an attempt was made to maintain the output level below 15 volts. In this way, most of the nonlinear effects in the AN/FGC-29 receiver were avoided.

The digital voltmeter, a Hewlett-Packard (H-P) Model 405A, was set to range automatically and was triggered by the G A programmer once every 5 seconds. When a voltmeter reading was completed, it was printed on paper tape on the H-P Model 560A digital recorder. The G A programmer, essentially a digital clock with programable output timing pulses, is identical to the unit used at the transmitter site. This clock was maintained on the correct time by comparison with WWV and was driven by a frequency standard periodically compared with NBA. For 1 minute in each 10 minutes, a negative voltage was applied to the digital voltmeter input through relay contacts in the programmer unit. During this minute, voltage samples were taken once every 10 seconds. The negative polarity caused an asterisk to be printed by each voltage sample. The series of six asterisks was used as a time indicator on the paper data tape.

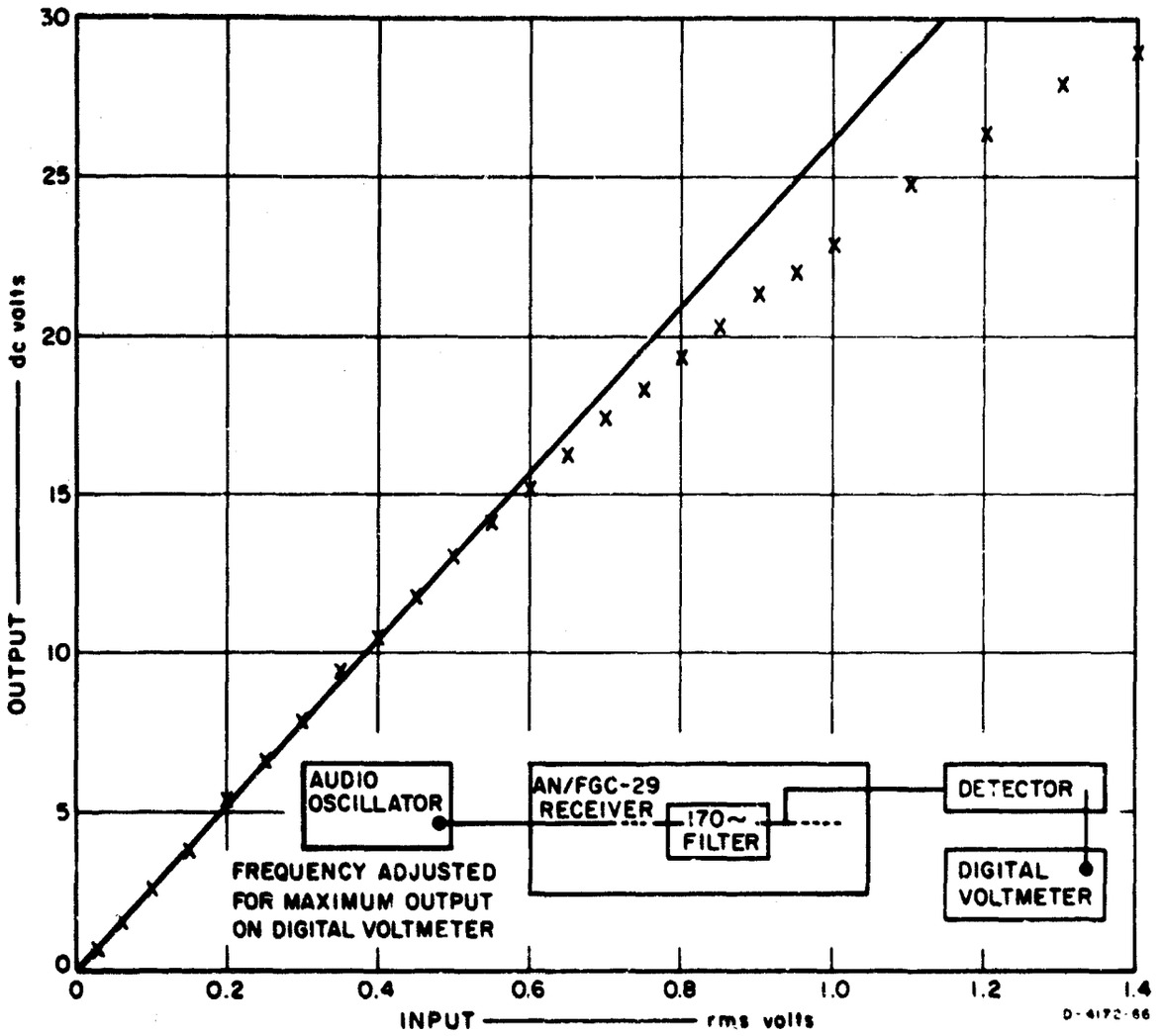

FIG. 16 SIGNAL-LEVEL DETECTION SYSTEM CHARACTERISTICS

The binary received signal from the AN/FGC-29 combiner unit (the output from the loop keyer) was fed into the Rixon Model 1032 digital word analyzer.[10] The analyzer was driven by 10-msec clock pulses from the programmer and generated a synchronized copy of the binary sequence generated at the transmitter. The clock pulses were so adjusted in the programmer that nominal path delay and any system delay were taken into consideration. After initial synchronization of the transmitted signal and the locally generated sequence, synchronization was maintained at both transmitting and the receiving terminal through use of a common time standard (WWV). In the analyzer, the loop-keying waveform was sampled at the nominal center of each received bit. The value of each sample was compared with that of the corresponding bit of the locally generated sequence; a pulse was generated each time these values differed. Although an error counter was available in the analyzer unit, an external counter compatible with the H-P digital printer was used (H-P 523B counter). As has been indicated in the timing diagram (Fig. 7), provisions were made to reset the counter at the beginning of each 30-second data-gathering interval. The three least-significant decades on the counter were connected to three of the printer columns on the H-P 560A digital recorder.

The raw data output from the error-rate and S/N measurement consisted of the printed paper-tape output from the H-P digital recorder. An example of a portion of a data tape—with notes to aid in the interpretation of the format—is given in Fig. 17. For the exact timing of the data-gathering operation, one should refer to Figs. 7 and 8. Each data tape was dated and appropriately identified by the operators at the receiving site. In addition, at least once an hour, the time to the nearest minute was written near a series of six asterisks on the tape. In this manner the exact time associated with any data gathering interval could be determined.

A brief discussion of some of the computational problems and possible biases associated with the estimation of power and power ratios is given in Appendix B. The results indicate that because of the statistical characteristics of the noise and the use of a linear envelope detector, the S/N estimate may be 2 or 3 db high. The propagation of error in the power estimates into the error in S/N expressed in decibels is examined in Appendix C. If one excludes the bias that has been indicated and admits a percentage error of 25 percent in the power estimates, the resulting S/N estimate has an error bound of ±2 db. The complete error bound is also given in Appendix C.

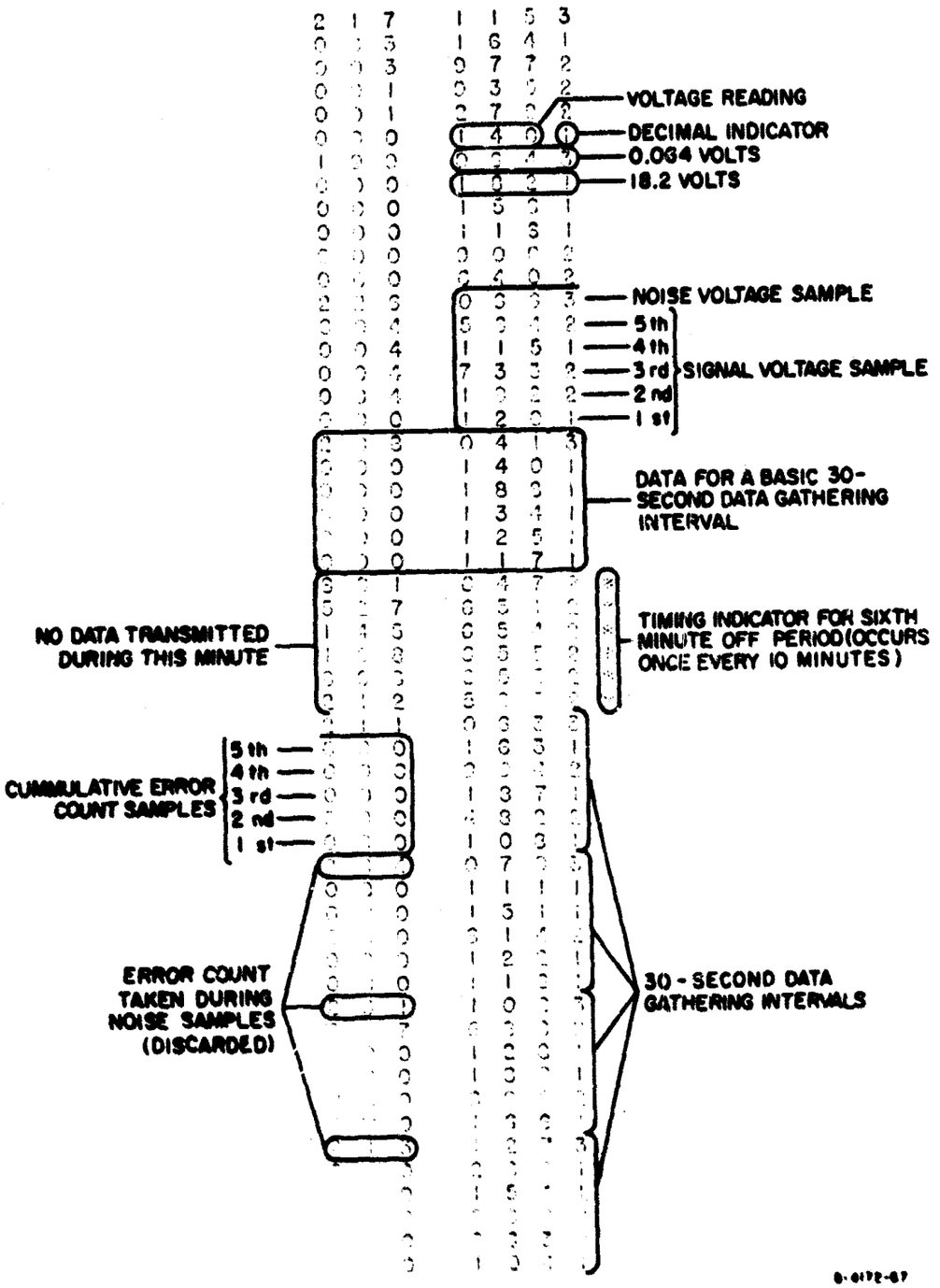

FIG. 17 AN ANNOTATED EXAMPLE OF THE PAPER-TAPE DATA OUTPUT FOR THE ERROR-RATE AND S/N MEASUREMENTS

C. DOPPLER PROFILE MEASUREMENT

1. Discussion of the Experiment

The purpose of this experiment was to provide a measure of the frequency-spreading characteristics of the communication channel. One should refer to Daly,[7] Gallager,[15] Kailath,[16] or Bello[17] for an explanation of some of the details motivating the measurement. The normalized Doppler profile $q_D(\lambda)$, and such measures as the second central moment of $q_D(\lambda)$ have been chosen to display the frequency-spreading characteristic of the channel. The normalized Doppler profile is defined in terms of the channel scattering function, $S_V(\lambda,\tau)$, by

$$q_D(\lambda) = \frac{\int S_V(\lambda,\tau)\,d\tau}{\iint S_V(\lambda,\tau)\,d\tau\,d\lambda} \quad .$$

The channel scattering function may be interpreted as the density of power scattered by the channel as a function of Doppler shift and time delay. An alternate expression for $q_D(\lambda)$ is

$$q_D(\lambda) = \frac{\int R_H(\alpha,0)e^{-i2\pi\lambda\alpha}d\alpha}{\iint R_H(\alpha,0)e^{-i2\pi\lambda\alpha}d\alpha\,d\lambda} = \int \left[\frac{R_H(\alpha,0)}{R_H(0,0)}\right] e^{-i2\pi\lambda\alpha}d\alpha$$

where $R_H(\alpha,0)$ is given by

$$R_H(\alpha,0) = E\{H^*(t,f)H(t+\alpha,f)\} \quad .$$

The function $H(t,f)$ is called the time-variant channel transfer function, it is a complex random variable assumed to be wide-sense stationary in both time and frequency. The symbol E is used to indicate the mathematical expectation. The quantity $H(t,f)$ may be defined as the complex envelope of the channel response to a CW tone relative to the frequency of the transmitted tone. Thus the goal of the experiment was to measure the complex envelope of the channel response to a sinusoidal transmission over a given period of time. Given the complex envelope, the computations required for estimating the Doppler profile have been considered in detail by Daly.[17]

The measurement required for the estimation of the Doppler profile has been reduced to a measurement of the complex envelope (real envelope and phase) of the signal received over the channel when the transmitted signal is a *CW* tone. The complex envelope must be measured relative to the frequency of the transmitted signal; thus high phase stability is required at both the transmitter and the receiver.

2. Description of the Experimental Setup

With a few minor modifications, the experimental setup for this measurement is the same as that described by Shepherd.[19] The experimental setup was made more flexible by introducing operation at 14.360 Mc, as well as at 7.366 Mc. The transmitter portion of the system is the same as that used in the error-rate S/N measurement (block diagrams are given in Figs. 9 and 10). As has been mentioned, half the power is retained in the carrier, and half is used for the transmission of sideband information. The carrier is synthesized from a phase-stable source and is in fact, the transmitted *CW* tone used for the Doppler profile measurement. Since the carrier is synthesized, its stability depends upon the stability of the frequency standard. The standard used at both the transmitting and the receiving site was an H-P Model 103 AR, which has a stability of 5 parts in 10^{10} per day.

Although the error-rate experiment and the Doppler profile experiment shared the same transmitter unit, separate receivers were required at the receiver site. However, one of the dual-diversity receiving antennas was used in common for both experiments. A block diagram of the phase-stable receiving system is shown in Fig. 18. The crystal oscillators were available for calibration of the tape-recorded values of phase and amplitude through the entire system. The R-390A/URR receiver was modified to accept synthesized local oscillator signals, and an IF of 459 kc was generated. For operation at 14.36 rather than 7.366 Mc, the second local oscillator frequency was changed from 27 to 16.994 Mc; the receiver was tuned to the higher frequency; and the antenna was changed. The IF output from the receiver was mixed to 13 kc and bandpass filtered to a passband of 200 cps. The output from the filter went to the phase detector and the envelope detector. The output of the envelope detector was recorded as the level of the received signal and was used as the AGC control voltage in the R-390A/URR receiver. The output level as a function of the input has been given by Shepherd[19] and is shown in Fig. 19. The phase detector also has been described in detail by Shepherd. Briefly, the phase of the received

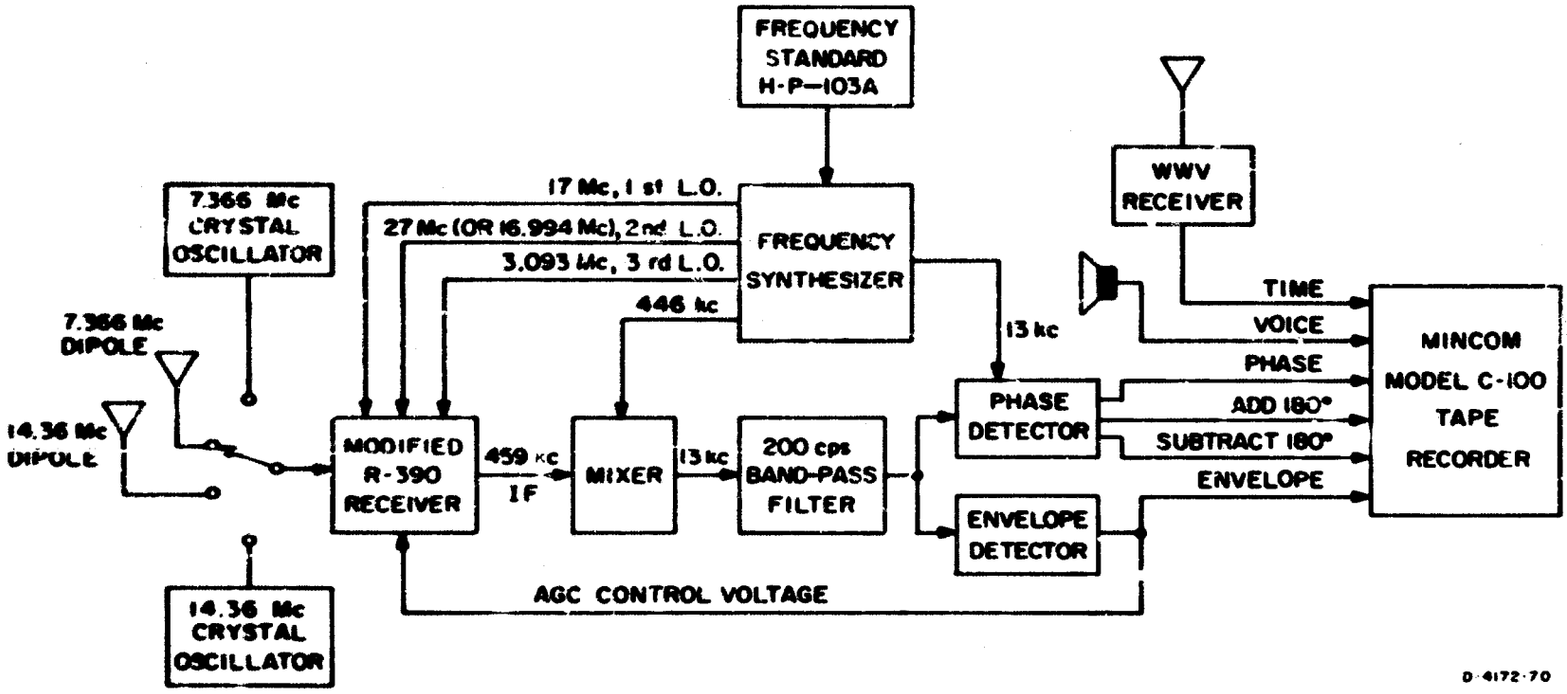

FIG. 18 BLOCK DIAGRAM OF RECEIVING SYSTEM FOR DOPPLER-PROFILE MEASUREMENT

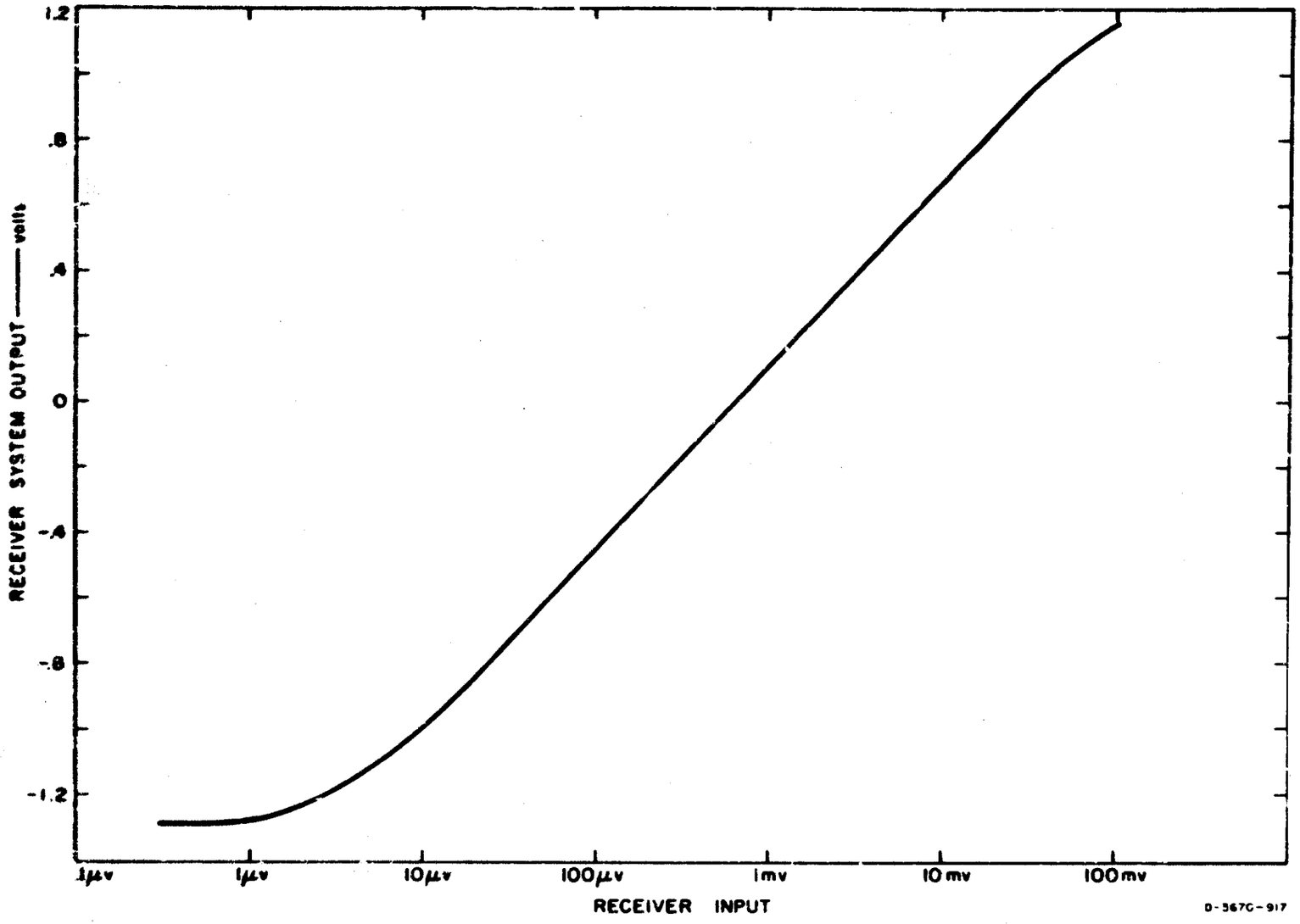

FIG. 19 DYNAMIC RANGE OF THE RECEIVER SYSTEM

signal, nominally at 13 kc, is compared with the phase of a locally synthesized phase-stable 13-kc reference signal. The relative phase of the received signal is recorded by recording the detected phase angle modulo 180 degrees and all positive and negative transitions through an integral multiple of 180 degrees. Thus, over any specified interval of time, both the envelope and phase of the received signal are recorded. The time as received on a *WWV* receiver and any operator notes are also recorded on the magnetic tape.

Data were collected for the Doppler profile measurement from 1800 to 2300 GMT on 14.36 Mc and from 0000 to 0500 GMT on 7.366 Mc. During these intervals, data were collected on chart paper continuously, and magnetic tape recordings were made starting at 6, 26, and 46 minutes after the hour. Each of these recordings lasted for a period of 6 minutes.

3. Output Data and Preprocessing

The output data for the Doppler profile measurement consist of a six-channel tape recording representing phase, envelope, time, and a voice recording of the operator's comments. An additional supplementary two-channel Sanborn chart-paper recording of envelope and phase modulo 180 degrees was also available. This recording is identical to the magnetic-tape recording of two of the channels. An example of this chart is given in Fig. 20. The scale for the signal envelope record is roughly logarithmic. A Doppler shift in addition to the spread is indicated by the phase having a nominal rate of change in one direction (from the bottom of the record to the top). The chart recordings were monitored at the site to ensure proper equipment operation and to provide data for a preliminary evaluation.

The six-channel magnetic-tape data required preprocessing. The phase and envelope signals were passed through constant-time-delay low-pass filters with a cutoff frequency of approximately 50 cps. Finally, the data were converted into digital form and recorded in the appropriate format on digital tape.

D. TIME-DELAY PROFILE MEASUREMENT

1. Discussion of the Experiment

The purpose of this subexperiment was to provide a measure of the time-spreading characteristics of the channel. The significant effects of time spreading of the communication channel at HF have been recognized

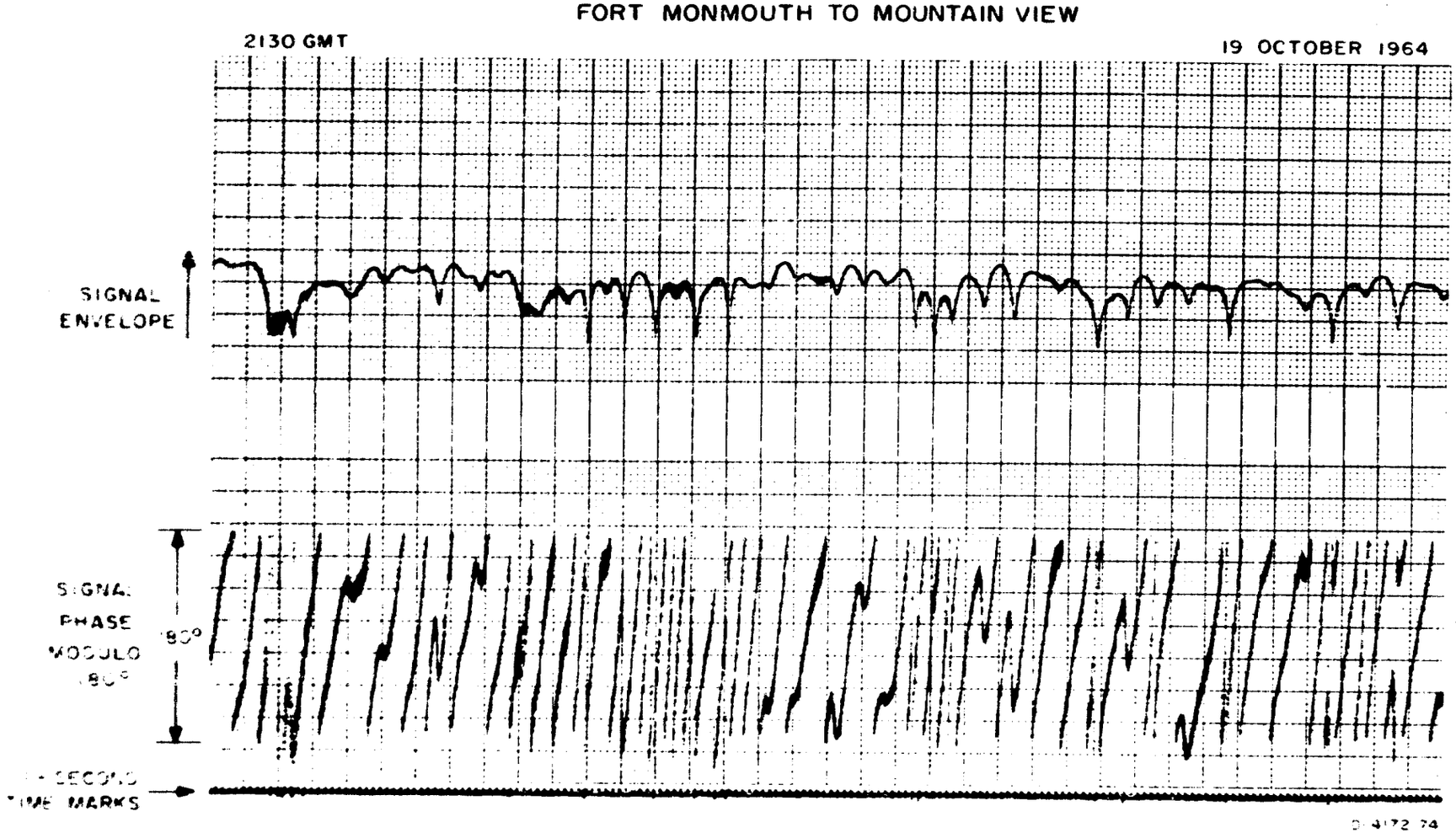

FIG. 20 AN EXAMPLE OF THE RECORDING SHOWING PHASE AND ENVELOPE OF THE RECEIVED SIGNAL RELATIVE TO THE FREQUENCY OF THE TRANSMITTED SIGNAL (14.36 Mc)

for many years. Multipath differential delays have been measured by oblique-incidence ionospheric sounders for some time. Recent developments in channel modeling suggest alternate measures which include consideration of the relative amplitude of various modes.[7,15,16,17] In a manner similar to that indicated for the Doppler profile measurement (Sec. C.1) the normalized delay profile, $q_T(\tau)$ may defined as

$$q_T(\tau) = \frac{\int S_V(\lambda,\tau)\,d\lambda}{\iint S_V(\lambda,\tau)\,d\tau\,d\lambda} .$$

The normalized delay profile and twice the second central moment of $q_T(\tau)$ have been chosen to represent the time-spreading characteristics of the channel.

An alternate expression[7] upon which a measurement technique may be developed is

$$E\{|z(t)|^2\} = \int T(\tau)E\{|x(t-\tau)|^2\}\,d\tau$$

where $z(t)$ and $x(t)$ are the complex envelopes of received and transmitted waveforms, respectively, and $T(\tau)$ is the time-delay profile before normalization. This expression suggests the transmission of a pulse that is short relative to the resolution desired in the estimation of $T(\tau)$. Signals of other types are also useful as long as the quantity $|x(t-\tau)|^2$ performs the desired sifting operation on $T(\tau)$. An estimate of $T(\tau)$ with a series of short pulses is given by

$$\hat{T}(\tau) = \frac{\frac{1}{n}\sum_{i=1}^{n} |z(\tau - t_i)|^2}{\int |x(t-\tau)|^2\,d\tau} ,$$

and the normalized estimate is given by

$$\hat{q}_T(\tau) = \frac{\sum_{i=1}^{n} |z(\tau - t_i)|^2}{\sum_{i=1}^{n} \int |z(\tau - t_i)|^2\,d\tau} .$$

To achieve the desired resolution in $\hat{q}_T(\tau)$, the real envelope of the transmitted signal, $|x(t)|$ was chosen to be a sounder short pulse of 100 μsec. A special modification was incorporated in the G/A sounder transmitter to provide single-frequency operation. At the chosen frequency, a series of fifteen short-pulse transmissions were made to provide confidence in the estimate. Modifications were also made in the G/A sounder receiver unit to permit repetitive reception at a single frequency. The video signal from the sounder occurring in the window of 10 msec was supplied to a unit designated Sounder-Computer Link (SCL) MK I. This unit used the sounder receiver timing signal and provided analog-to-digital (A-D) conversion of the received signals. The digital output was recorded on digital tape, along with timing and other identifying information. The digital tape format was designed to be directly compatible with tape input requirements for IBM computers. Further processing, including refined detection based on the series of samples, was carried out in the computer. This process is described in Sec. D of Chapter IV.

2. Description of the Experimental Setup

The sounder system used to measure the channel characteristics consisted of a G/A Model 901 transmitter unit located at Earle, New Jersey and a G/A Model 903 receiver unit located near Palo Alto, California. For this experiment, certain of the automatic features were de-activated by relays to allow repetitive operation on a single frequency on both the transmitter and the receiver units. A block diagram of the time-delay profile measurement system is given in Fig. 21. The frequency standards supplied both the sounder and the programmer; they had a frequency stability of 5 parts in 10^{10} per day. The frequency accuracy was maintained through periodic calibration to NBA. The programmers provided accurate timing for both the transmission and reception of the sounding pulses.

The sounder was operated at a frequency near the frequencies of operation of the Doppler profile experiment—7.366 Mc and 14.360 Mc—that was also relatively free of interference. This generally resulted in a choice of the G/A sounder Frequency Bands A-32 (7.25 Mc) or A-33 (7.35 Mc) and B-32 (14.5 Mc) or B-33 (14.7 Mc). A brief description of general sounder characteristics has been given by Shepherd.[19] The modifications made de-activated the frequency-stepping features through the use of relays. Both sounder transmitter and the sounder receiver were modified to provide single-frequency operation as an optional operational mode.

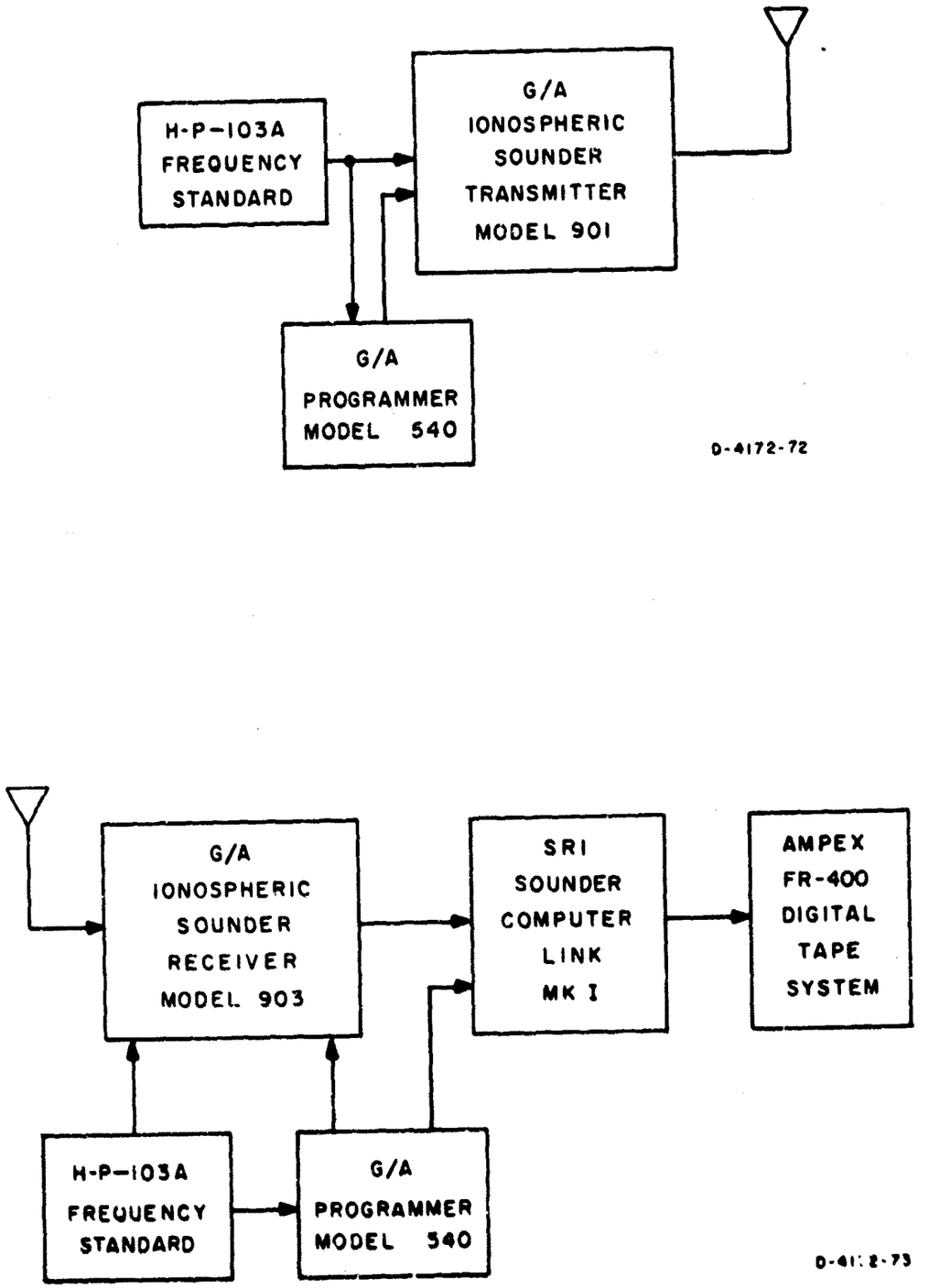

FIG. 21 TIME-DELAY-PROFILE MEASUREMENT SYSTEM

The single-frequency soundings at 14 Mc were taken once every 5 minutes, starting at 1802 GMT and continuing until 2257 GMT. On 7 Mc, soundings were made from 2357 GMT until 0457 GMT. Operation thus concided with the collection of data on all of the other experiments. Each single-frequency sounding was affected by the transmission of a series of fifteen 100-μsec 30-kw pulses with a 2-second spacing between pulses. Thus approximately 30 seconds was required for the complete sounding. At the receiver, the detected RF signal was used to observe the response of the channel to each of the fifteen pulses. The detected signal from the sounder was supplied to the SCL for further processing. The SCL performed the A-D conversion and interface operations between the sounder and a computer. This unit has been described in detail by Sifford.[20] During a predetermined time interval of 10.2 msec, samples were taken once every 50 μsec for a total of 204 samples. Each sample was quantized into one of the thirty-two levels and encoded into a five-bit code word. The digital samples with parity checking bits were recorded on the digital tape. The SCL provided an identification preamble in digital form, including the time that the data were taken. The data format on the tape was designed to be used as direct input to further computer processing programs.

IV DATA PROCESSING

A. INTRODUCTION

Data from the experiments were recorded on various media and in unique formats. To extract meaningful results and to present them efficiently, high-speed computers were employed in a data-processing phase. A flow chart illustrating the basic components of this processing phase is shown in Fig. 22. The end result was a determination of confident experimental estimates of the correlation of measured S/Ns with measured binary error rate for an FSK communications system on an HF channel. Measured time delay and frequency spreading of the channel and spaced antenna correlation were parameters.

Accumulated binary errors detected over a 30-second interval, together with simultaneous samples of received signal and noise voltages, were recorded on adding-machine tape from a digital printer. Time-delay-spread data were recorded in digital form on magnetic tape directly from the output of an ionospheric sounder receiver. Frequency-spread or Doppler data were recorded in analog form on magnetic tape in the form of CW amplitude and phase measurements. Correlation of signals received on a pair of spaced antennas was recorded on chart paper directly from the output of a special correlation instrument. The antenna-correlation data processing is further discussed in Chap. VII.

Partial processing of the 30-second S/N and bit-error data was done on a Burroughs B5000 computer at the SRI Computer Center. The time-delay-spread processing was run on the IBM 7090 computer at Stanford University. The CW analog amplitude and phase measurements were converted to digital form and recorded on magnetic tape on an A-D converter and CDC 160A computer at SRI. Those data were than processed to extract the channel Doppler profiles on the 7090 computer at Stanford University. The results of these three processing programs provided the input to the final classification and summation program. This program, which tabulated the S/N and bit-error rates for various measured channel spread conditions, was run on the B5000 at SRI.

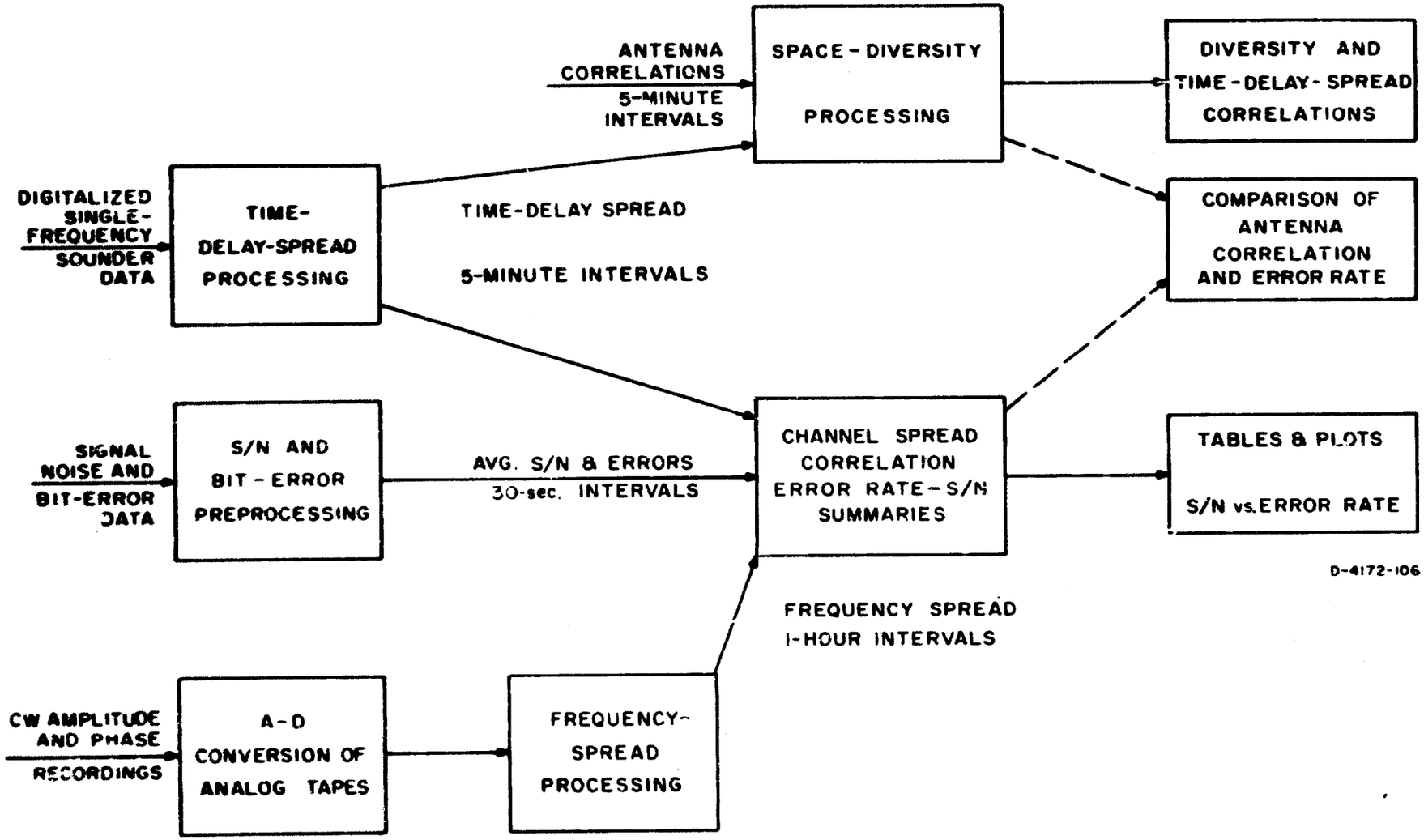

FIG. 22 DATA-PROCESSING FLOW DIAGRAM

B. PRE-EDITING OF S/N AND BIT ERROR DATA

The S/N and bit-error data were manually edited before being punched onto IBM cards. This editing consisted primarily of grouping the data for each 30-second interval into the five signal readings and the one noise reading together with the accumulated bit-error totals during these samples. In addition, the legibility and completeness of each data block were checked, and data suspected of being faulty were deleted from the tape.

The five signal-sample readings and the noise sample, together with the bit-error totals at these sample times, were punched onto IBM cards from this edited tape. The format for this card is shown in Fig. 23. Each card contained the data for one 30-second data period. Time header cards were inserted in the deck to indicate the starting time of a sequence.

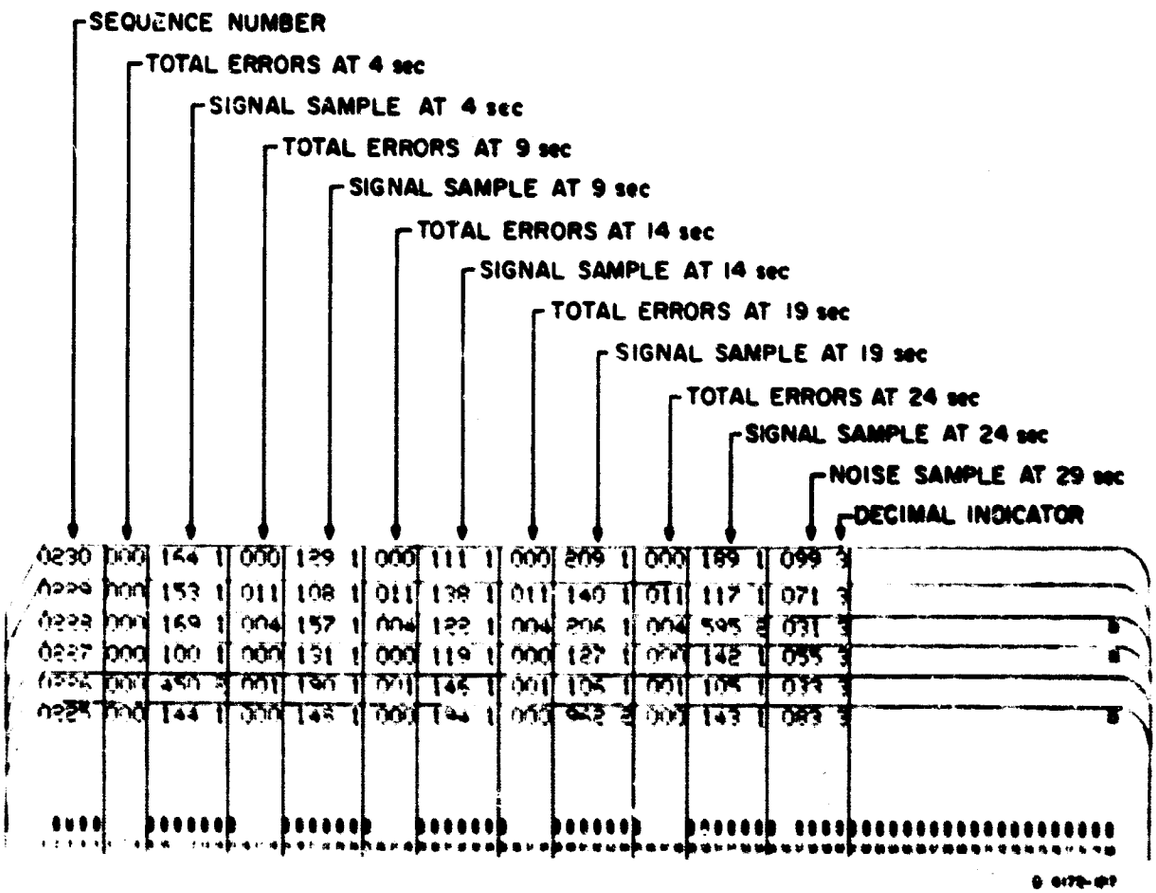

FIG. 23 BASIC 30-SECOND SIGNAL, NOISE, AND BIT-ERROR DATA CARD FORMAT

C. S/N AND BIT ERROR PREPROCESSING

1. S/N Estimation

Five samples of the received S + N, taken five seconds apart, were recorded from the output of a linear rectifier/low-pass filter combination. It is shown in Appendix B that if the signal and noise are independent zero-mean processes, then the best estimate of the total S + N is proportional to the square of the average of the five sample readings. Furthermore, this estimate represents the sum of the power in the signal and noise components.

The noise-power estimate was made from the average of the two noise samples immediately before and after the corresponding five S + N readings. In the event that a valid noise reading was not taken immediately before or after each of the five signal readings, a search procedure was initiated to obtain two usable noise samples. The search procedure, based on cursory observations on the autocorrelation of the noise, was as follows. If a valid noise sample was not available immediately before (or after) a 30-second signal data block, then the noise reading for the preceding (or following) interval was used. This reading was weighted by 80 percent, however, in calculating the average noise estimate with the other sample. However, if the preceding (or following) noise sample was also missing, the next preceding (or following) 30-second noise reading in time was used, and an additional 80-percent de-emphasis was applied to this reading in determining the average. The search for two valid noise samples was continued in this manner. If two noise samples were not found within four 30-second periods removed from the signal data, then all data for this 30-second period were rejected.

The formula used by the processor for calculating the noise average was

$$AN(T) = \frac{(1.2 - 0.2KM)N(T - KM) + (1.0 - 0.2KP)N(T + KP)}{2.2 - 0.2KM - 0.2KP}$$

where

T is an integer designating a particular 30 second block of signal samples followed by a noise sample

KM is the lowest integer from one to four where the noise sample at $T - KM$ is valid.

KP is the lowest integer from zero to three where the noise sample at $T + KP$ is valid.

N(T) is the noise value at time T.

The procedure was used at least once every 10 minutes, since no data were recorded during the sixth minute of each 10-minute data-gathering period. For the first 30-second data period of the seventh minute, the procedure bridged the gap by using the noise reading taken at the end of the second 30-second block of data during the fifth minute to estimate the noise for the first block of data during the seventh minute.

The S/N in decibels was calculated for each 30-second data period as follows:

$$S/N = 10 \log \left(\frac{Ps}{Pn} \right)$$

where

$$\frac{Ps}{Pn} = \frac{Ps + Pn - Pn}{Pn} = \frac{P(s+n)}{Pn} - 1 = \frac{\overline{Z(s+n)}^2}{\overline{Zn}^2} - 1$$

$\overline{Z(s+n)}$ is the average of the five S + N samples

$\overline{Zn}$ is the average of the two noise samples.

If the ratio, Ps/Pn was less than one, then the S/N was assigned a value of −100 db.

2. Validation of Bit Error Count

It was theoretically possible to accumulate as many as 2,251 bit errors during each 30-second data-gathering period. Because only the first three digits of the error counter were recorded, this counter occasionally overflowed during a data period. To sense an overflow in the counter, the processing program was instructed to monitor the error count during each 5-second period. Whenever the accumulated error count for any 5-second recording period was less than the preceding count, an additional 1,000 errors were added to the recorded total.

On numerous occasions, excessive errors were recorded during the experiment, even with a high S/N. These errors were principally caused by difficulty with the automatic frequency control and by occasional loss of

bit synchronism. Even though an attempt was made to detect such conditions and reject the resulting data as they occurred during the experiment, many incidences were not detected. Therefore, a criterion was established in this program to reject data if the total errors made during a data period were judged to be excessive on the basis of the average S/N measured during the data period. The 30-second data were rejected if the *product* of the *maximum* number of errors detected in any five-second period when data were transmitted *times* the S/N in decibels was greater than 2,000. For example, assume the S/N was 20 db. The number of errors made during any 5-second interval then must not be greater than 100 for the data to be accepted. The test was not applied, however, if the measured S/N was less than ten db.

3. Preprocessed Output

Averaged S/N in decibels together with corresponding total bit errors for each accepted 30-second time period were punched onto IBM cards by the preprocessing program. The format for this card is shown in Fig. 24. Each data card included the date and time for convenience in

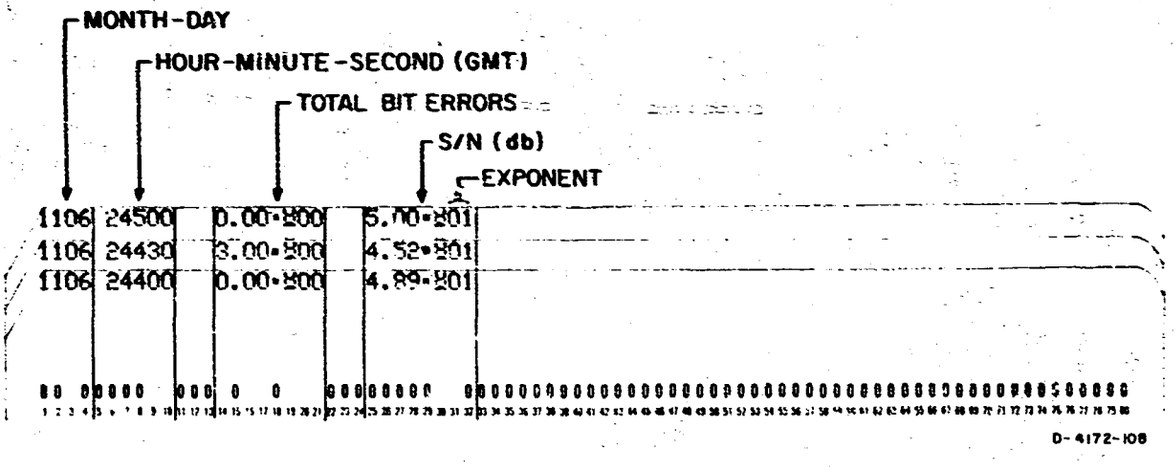

FIG. 24 PREPROCESSED 30-SECOND S/N AND BIT-ERROR DATA CARD FORMAT

correlating later with channel-spread measurements and antenna correlations. A listing of these values for each 30-second period was also produced on the page printer, together with notations indicating where and why data were rejected (see Table I). The notations of rejected data permitted the cause of the data rejection to be investigated and, if possible, corrected. In many cases, mispunched or misordered input cards were detected by the various data-rejection tests.

Table 1

SAMPLE OF PREPROCESSED 30-SECOND DATA

TIME	AVSIG*	ERRORS	AVN**	S/N	BER
DATE IS 1106					
4530	5.41E+01	9	2.30E-03	43.7	4.00E-03
4600	NO DATA				
4630	NO DATA				
4700	1.11E+02	15	2.88E-03	45.9	6.66E-03
4730	ABNORMAL ERRORS FOR S/N, DATA REJECTED				
4730	1.67E+02	465	4.36E-03	45.8	2.07E-01
4800	DATA OUT OF SYNCH				
4830	DATA OUT OF SYNCH				
4900	DATA OUT OF SYNCH				
4930	DATA OUT OF SYNCH				
5000	DATA OUT OF SYNCH				
5030	DATA OUT OF SYNCH				
5100	INSUFFICIENT DATA TO COMPUTE AVERAGE NOISE				
5130	6.51E+01	23	1.33E-03	46.9	1.02E-02
5200	1.23E+02	4	2.70E-03	46.6	1.78E-03
5230	3.34E+01	5	8.37E-03	36.0	2.22E-03
5300	5.66E+01	2	5.55E-03	40.1	8.88E-04
5330	7.34E+01	1	2.35E-03	44.9	4.44E-04
5400	8.54E+01	0	3.02E-03	44.5	0.00E+00
5430	1.06E+02	4	3.84E-03	44.4	1.78E-03
5500	6.20E+01	43	3.60E-03	42.4	1.91E-02
5530	4.59E+01	19	3.42E-03	41.3	8.44E-03
5600	NO DATA				
5630	NO DATA				
5700	1.33E+02	1	4.47E-03	44.7	4.44E-04
5730	1.16E+02	5	3.72E-03	44.9	2.22E-03
5800	1.04E+02	8	2.55E-03	46.1	3.55E-03
5830	1.04E+02	1	2.55E-03	46.1	4.44E-04
5900	1.90E+02	0	6.08E-03	44.9	0.00E+00
5930	7.22E+01	9	6.97E-03	40.2	4.00E-03
10000	1.20E+02	2	2.40E-03	47.0	8.88E-04
10030	1.03E+02	0	1.37E-03	48.8	0.00E+00
10100	6.50E+01	1	2.26E-03	44.6	4.44E-04
10130	7.43E+01	2	2.86E-03	44.1	8.88E-04
10200	7.44E+01	8	2.26E-03	45.2	3.55E-03
10230	1.43E+02	2	3.25E-03	46.4	8.88E-04
10300	9.27E+01	3	3.72E-03	44.0	1.33E-03
10330	8.41E+01	11	2.76E-03	44.8	4.89E-03
10400	1.04E+02	6	4.42E-03	43.7	2.67E-03
10430	1.64E+02	0	4.49E-03	45.6	0.00E+00
10500	1.90E+02	6	3.42E-03	47.4	2.67E-03
10530	4.15E+01	0	2.55E-03	42.1	0.00E+00
10600	NO DATA				
10630	NO DATA				
10700	8.53E+01	2	2.94E-03	44.6	8.88E-04
10730	1.42E+02	11	2.92E-03	46.9	4.89E-03
10800	1.93E+02	0	1.98E-03	49.9	0.00E+00
10830	2.06E+02	5	3.36E-03	47.9	2.22E-03
10900	1.36E+04	0	4.76E-03	64.6	0.00E+00

* AVSIG = Average of five signal readings.

** AVN = Average of two noise readings.

TIME	AVSIG	ERRORS	AVN	S/N	BER
DATE IS 1106					
10930	1.64E+02	2	4.16E-03	46.0	8.88E-04
11000	1.46E+02	0	3.36E-03	46.4	0.00E+00
11030	9.98E+01	4	2.81E-03	45.5	1.78E-03
11100	1.33E+02	0	3.31E-03	46.1	0.00E+00
11130	1.68E+02	0	7.06E-03	43.8	0.00E+00
11200	9.72E+01	0	6.24E-03	41.9	0.00E+00
11230	5.46E+01	0	3.97E-03	41.4	0.00E+00
11300	6.95E+01	1	3.97E-03	42.4	4.44E-04
11330	5.09E+01	6	3.54E-03	41.6	2.67E-03
11400	3.76E+01	2	4.56E-03	39.2	8.88E-04
11430	1.68E+01	5	5.11E-03	35.2	2.22E-03
11500	5.54E+01	2	8.93E-03	37.9	8.88E-04
11530	8.74E+01	2	7.40E-03	40.7	8.88E-04
11600	NO DATA				
11630	NO DATA				
11700	1.16E+02	0	8.21E-03	41.5	0.00E+00
11730	4.20E+01	11	5.04E-03	39.2	4.89E-03
11800	4.91E+01	1	1.76E-03	44.4	4.44E-04
11830	6.29E+01	1	3.54E-03	42.5	4.44E-04
11900	2.66E+01	0	4.16E-03	38.1	0.00E+00
11930	4.64E+01	2	2.55E-03	42.6	8.88E-04
12000	4.63E+01	0	5.63E-03	39.2	0.00E+00
12030	9.99E+01	3	9.60E-03	40.2	1.33E-03
12100	8.35E+01	11	8.28E-03	40.0	4.89E-03
12130	5.73E+01	5	6.48E-03	39.5	2.22E-03
12200	4.73E+01	0	5.63E-03	39.2	0.00E+00
12230	1.09E+02	10	7.57E-03	41.6	4.44E-03
12300	1.04E+02	0	1.05E-02	40.0	0.00E+00
12330	1.29E+02	1	1.10E-02	40.7	4.44E-04
12400	3.57E+01	2	3.42E-02	30.2	8.88E-04
12430	1.75E+01	0	3.59E-02	26.9	0.00E+00
12500	9.88E+01	2	2.87E-02	35.4	8.88E-04
12530	1.34E+02	7	2.34E-02	37.6	3.11E-03
12600	NO DATA				
12630	NO DATA				
12700	1.85E+02	0	2.44E-02	38.8	0.00E+00
12730	9.09E+01	0	2.21E-02	36.2	0.00E+00
12800	8.94E+01	3	7.83E-03	40.6	1.33E-03
12830	5.20E+01	3	8.37E-03	37.9	1.33E-03
12900	7.94E+01	3	7.14E-03	40.5	1.33E-03
12930	1.92E+02	0	4.76E-03	46.0	0.00E+00
13000	1.22E+02	19	4.22E-03	44.6	8.44E-03
13030	9.99E+01	4	1.23E-02	39.1	1.78E-03
13100	5.29E+01	3	1.53E-02	35.4	1.33E-03
13130	2.02E+02	6	1.21E-02	42.2	2.67E-03
13200	1.21E+02	5	1.07E-02	40.5	2.22E-03
13230	6.48E+01	1	4.76E-03	41.3	4.44E-04
13300	6.12E+01	0	4.62E-03	41.2	0.00E+00

TIME	AVSIG	ERRORS	AVN	S/N	BER
DATE IS 1106					
13330	9.14E+01	1	7.92E-03	40.6	4.44E-04
13400	6.15E+01	0	2.04E-02	34.8	0.00E+00
13430	4.65E+01	0	1.40E-02	35.2	0.00E+00
13500	6.50E+01	0	5.55E-03	40.7	0.00E+00
13530	7.91E+01	0	8.01E-03	39.9	0.00E+00
13600	NO DATA				
13630	NO DATA				
13700	4.25E+02	1	4.35E-02	39.9	4.44E-04
13730	3.00E+02	0	3.28E-02	39.6	0.00E+00
13800	6.50E+01	0	3.78E-03	42.3	0.00E+00
13830	8.06E+01	0	4.76E-03	42.3	0.00E+00
13900	1.22E+02	0	1.24E-02	39.9	0.00E+00
13930	7.28E+01	0	1.19E-02	37.9	0.00E+00
14000	7.89E+01	5	5.70E-03	41.4	2.22E-03
14030	7.88E+01	0	1.29E-02	37.9	0.00E+00
14100	5.59E+01	3	1.48E-02	35.8	1.33E-03
14130	3.47E+01	18	5.18E-03	38.3	8.00E-03
14200	4.06E+01	6	3.02E-03	41.3	2.67E-03
14230	7.20E+01	0	2.40E-03	44.8	0.00E+00
14300	7.54E+01	8	6.72E-03	40.5	3.55E-03
14330	6.44E+01	33	1.56E-02	36.2	1.47E-02
14400	8.58E+01	0	1.06E-02	39.1	0.00E+00
14430	6.67E+01	18	6.16E-03	40.3	8.00E-03
14500	7.04E+01	0	6.72E-03	40.2	0.00E+00
14530	4.73E+01	5	7.31E-03	38.1	2.22E-03
14600	NO DATA				
14630	NO DATA				
14700	6.00E+01	6	9.90E-03	37.8	2.67E-03
14730	6.84E+01	15	1.50E-02	36.6	6.66E-03
14800	7.25E+01	6	1.56E-02	36.7	2.67E-03
14830	ABNORMAL ERRORS FOR S/N, DATA REJECTED				
14830	1.11E+02	92	1.48E-02	38.8	4.09E-02
14900	4.42E+01	50	4.49E-02	29.9	2.22E-02
14930	2.72E+01	0	3.76E-02	26.6	0.00E+00
15000	7.68E+01	10	8.28E-03	39.7	4.44E-03
15030	3.61E+01	0	6.97E-03	37.1	0.00E+00
15100	4.68E+01	0	5.11E-03	39.6	0.00E+00
15130	ABNORMAL ERRORS FOR S/N, DATA REJECTED				
15130	6.32E+01	615	2.50E-03	44.0	2.73E-01
15200	4.94E+01	23	7.66E-03	38.1	1.02E-02
15230	1.13E+02	0	7.48E-03	41.8	0.00E+00
15300	7.72E+01	1	7.22E-03	40.3	4.44E-04
15330	6.63E+01	6	1.00E-02	38.2	2.67E-03
15400	7.65E+01	4	2.81E-03	44.3	1.78E-03
15430	4.64E+01	5	1.52E-03	44.8	2.22E-03
15500	6.68E+01	0	2.97E-03	43.5	0.00E+00
15530	7.44E+01	0	4.03E-03	42.7	0.00E+00
15600	NO DATA				
15630	NO DATA				
15700	7.20E+01	7	2.86E-03	44.0	3.11E-03

TIME	AVSIG	ERRORS	AVN	S/N	BER
DATE IS 1106					
15730	1.26E+02	9	2.76E-03	46.6	4.00E-03
15800	3.84E+01	2	2.21E-03	42.4	8.86E-04
15830	1.75E+02	0	2.21E-03	49.0	0.00E+00
15900	9.34E+01	5	2.97E-03	45.0	2.22E-03
15930	5.20E+01	0	3.60E-03	41.6	0.00E+00
20000	1.03E+02	3	3.36E-03	44.9	1.33E-03
20030	9.78E+01	0	3.54E-03	44.4	0.00E+00
20100	6.08E+01	0	6.08E-03	40.0	0.00E+00
20130	9.40E+01	6	4.90E-03	42.8	2.67E-03
20200	5.25E+01	0	2.60E-03	43.1	0.00E+00
20230	1.19E+02	0	2.60E-03	46.6	0.00E+00
20300	3.92E+01	11	1.98E-03	43.0	4.89E-03
20330	5.53E+01	0	3.36E-03	42.2	0.00E+00
20400	1.18E+02	0	5.16E-03	43.6	0.00E+00
20430	1.47E+02	3	3.14E-03	46.7	1.33E-03
20500	5.56E+01	0	2.70E-03	43.1	0.00E+00
20530	1.17E+02	0	3.60E-03	45.1	0.00E+00
20600	NO DATA				
20630	NO DATA				
20700	1.87E+02	4	5.06E-03	45.7	1.78E-03
20730	ABNORMAL ERRORS FOR S/N, DATA REJECTED				
20730	1.16E+02	245	3.02E-03	45.8	1.09E-01
20800	7.25E+01	6	3.60E-03	43.0	2.67E-03
20830	ABNORMAL ERRORS FOR S/N, DATA REJECTED				
20830	1.04E+02	968	6.48E-03	42.1	4.30E-01
20900	ABNORMAL ERRORS FOR S/N, DATA REJECTED				
20900	7.74E+01	82	2.33E-02	35.2	3.64E-02
20930	3.60E+01	0	2.33E-02	31.9	0.00E+00
21000	8.07E+01	18	7.83E-03	40.1	8.00E-03
21030	1.31E+02	13	7.83E-03	42.2	5.78E-03
21100	4.66E+01	9	4.42E-03	40.2	4.00E-03
21130	8.19E+01	0	5.11E-03	42.0	0.00E+00
21200	6.04E+01	18	5.40E-03	40.5	8.00E-03
21230	7.74E+01	9	4.62E-03	42.2	4.00E-03
21300	5.43E+01	1	3.78E-03	41.6	4.44E-04
21330	9.89E+01	0	2.60E-03	45.8	0.00E+00
21400	1.17E+02	0	3.92E-03	46.0	0.00E+00
21430	4.84E+01	5	3.06E-03	42.0	2.22E-03
21500	1.35E+02	0	3.42E-03	46.0	0.00E+00
21530	3.69E+01	0	3.78E-03	39.9	0.00E+00
21600	NO DATA				
21630	NO DATA				
21700	1.10E+02	0	3.66E-03	44.8	0.00E+00
21730	4.78E+01	6	2.40E-03	43.0	2.67E-03
21800	2.78E+01	6	2.02E-03	41.4	2.67E-03
21830	4.28E+01	4	4.69E-03	39.6	1.78E-03
21900	1.10E+02	7	1.55E-02	38.5	3.11E-03
21930	2.05E+02	0	1.09E-02	42.7	0.00E+00
22000	ABNORMAL ERRORS FOR S/N, DATA REJECTED				
22000	8.56E+01	126	2.30E-03	45.7	5.60E-02
22030	1.19E+02	11	1.81E-03	48.2	4.89E-03
22100	9.36E+01	0	3.25E-03	44.6	0.00E+00

TIME	AVSIG	ERRORS	AVN	S/N	BER
DATE IS 1106					
22130	3.16E+01	21	6.81E-03	36.7	9.33E-03
22200	1.40E+02	0	6.16E-03	43.6	0.00E+00
22230	5.23E+01	0	6.01E-03	39.4	0.00E+00
22300	3.80E+01	4	1.48E-02	34.1	1.76E-03
22330	1.49E+02	2	1.61E-02	39.7	8.86E-04
22400	9.88E+01	2	9.41E-03	40.2	8.86E-04
22430	1.54E+02	0	7.06E-03	43.4	0.00E+00
22500	3.72E+01	2	2.86E-03	41.1	8.66E-04
22530	8.98E+01	0	1.72E-03	47.2	0.00E+00
22600	NO DATA				
22630	NO DATA				
22700	1.90E+02	0	2.50E-03	46.6	0.00E+00
22730	5.14E+01	6	2.02E-03	44.0	2.67E-03
22800	5.03E+01	3	6.01E-03	39.2	1.33E-03
22830	1.22E+02	5	7.31E-03	42.2	2.22E-03
22900	7.69E+01	0	3.25E-03	43.9	0.00E+00
22930	4.71E+01	0	2.21E-03	43.3	0.00E+00
23000	6.89E+01	0	9.61E-04	48.6	0.00E+00
23030	5.34E+01	0	6.50E-04	49.1	0.00E+00
23100	7.70E+01	0	1.44E-03	47.3	0.00E+00
23130	8.16E+01	1	1.44E-03	47.5	4.44E-04
23200	1.43E+02	0	1.33E-03	50.3	0.00E+00
23230	1.11E+02	0	4.90E-03	43.5	0.00E+00
23300	3.14E+01	0	6.08E-03	37.1	0.00E+00
23330	6.11E+01	5	2.86E-03	43.3	2.22E-03
23400	1.18E+02	0	3.84E-03	44.9	0.00E+00
23430	6.35E+01	0	5.85E-03	40.4	0.00E+00
23500	7.22E+01	8	5.70E-03	41.0	3.55E-03
23530	1.13E+02	0	6.48E-03	42.4	0.00E+00
23600	NO DATA				
23630	NO DATA				
23700	9.02E+01	0	9.93E-03	39.6	0.00E+00
23730	1.42E+02	9	1.24E-02	40.6	4.00E-03
23800	7.65E+01	0	7.74E-03	39.9	0.00E+00
23830	1.96E+02	0	2.70E-03	48.6	0.00E+00
23900	7.41E+01	0	1.85E-03	46.0	0.00E+00
23930	3.54E+01	23	2.86E-03	40.9	1.02E-02
24000	1.26E+02	9	2.26E-03	47.5	4.00E-03
24030	1.00E+02	0	9.00E-04	50.5	0.00E+00
24100	8.80E+01	0	6.50E-04	51.3	0.00E+00
24130	2.63E+01	0	1.56E-03	42.3	0.00E+00
24200	1.92E+03	13	2.50E-03	58.8	5.76E-03
24230	1.33E+02	0	2.97E-03	46.5	0.00E+00
24300	1.35E+02	0	2.35E-03	47.6	0.00E+00
24330	6.95E+01	4	1.06E-03	48.2	1.76E-03
24400	7.53E+01	0	9.61E-04	48.9	0.00E+00
24430	4.62E+01	3	1.41E-03	45.2	1.33E-03
24500	1.25E+02	0	1.26E-03	50.0	0.00E+00

TIME	AVSIG	ERRORS	AVN	S/N	BER
DATE IS 1106					
24530	3.29E+01	2	1.02E-03	45.1	8.86E-04
24600	NO DATA				
24630	NO DATA				
24700	5.51E+01	0	7.43E-04	46.7	0.00E+00
24730	6.53E+01	0	1.72E-03	45.8	0.00E+00
24800	4.06E+01	3	2.81E-03	41.6	1.33E-03
24830	2.05E+02	6	2.02E-03	50.1	2.67E-03
24900	7.45E+01	0	3.42E-03	43.4	0.00E+00
24930	1.23E+02	0	4.16E-03	44.7	0.00E+00
25000	8.52E+01	4	1.81E-03	46.7	1.78E-03
25030	5.98E+01	5	2.86E-03	43.2	2.22E-03
25100	8.55E+01	15	3.08E-03	44.4	6.66E-03
25130	6.91E+01	7	3.19E-03	43.4	3.11E-03
25200	7.12E+01	0	6.56E-03	40.4	0.00E+00
25230	7.16E+01	3	2.35E-03	44.8	1.33E-03
25300	1.90E+04	0	2.35E-03	69.1	0.00E+00
25330	4.38E+01	0	3.76E-03	40.6	0.00E+00
25400	8.01E+01	0	3.60E-03	43.5	0.00E+00
25430	2.07E+01	13	3.31E-03	38.0	5.78E-03
25500	5.60E+01	7	9.00E-04	47.9	3.11E-03
25530	3.82E+01	31	1.16E-03	45.2	1.38E-02
25600	NO DATA				
25630	NO DATA				
25700	1.45E+02	0	1.86E-03	48.9	0.00E+00
25730	6.27E+01	0	2.30E-03	44.3	0.00E+00
25800	3.15E+02	0	7.83E-03	46.0	0.00E+00
25830	1.29E+02	3	9.31E-03	41.4	1.33E-03
25900	3.57E+01	8	5.11E-03	38.4	3.55E-03
25930	3.70E+01	0	3.14E-03	40.7	0.00E+00
30000	1.29E+02	0	8.41E-04	51.8	0.00E+00
30030	4.82E+01	0	1.37E-03	45.5	0.00E+00
30100	4.45E+01	0	1.56E-03	44.5	0.00E+00
30130	7.06E+01	0	9.30E-04	48.8	0.00E+00
30200	1.07E+02	0	2.16E-03	46.9	0.00E+00
30230	4.03E+01	6	1.76E-03	43.6	2.67E-03
30300	7.67E+01	3	4.84E-04	52.1	1.33E-03
30330	1.16E+02	7	4.41E-04	54.2	3.11E-03
30400	1.35E+02	1	2.35E-03	47.6	4.44E-04
30430	1.46E+02	0	2.81E-03	47.2	0.00E+00
30500	1.04E+02	0	1.16E-03	49.5	0.00E+00
30530	8.50E+01	0	1.26E-03	48.3	0.00E+00
30600	NO DATA				
30630	NO DATA				
30700	1.40E+02	0	1.96E-03	48.5	0.00E+00
30730	3.90E+02	0	1.68E-03	53.7	0.00E+00
30800	1.61E+02	0	6.50E-04	53.9	0.00E+00
30830	8.88E+01	0	1.19E-03	46.7	0.00E+00
30900	3.26E+02	0	3.78E-03	49.4	0.00E+00

A binary error-rate estimate (BER) was also calculated and printed on this listing for each 30-second data period. However, because of the limited number of data bits transmitted during the period (*i.e.*, 2,251) the confidence in the estimate is quite low. No further use was made of this figure.

D. CHANNEL TIME-DELAY-SPREAD PROCESSING

1. Raw Data Format

Time-delay-spread estimations of the channel were made from digitized recordings of the signal received from a remote pulsed transmitter. The raw data consisted of a time series of 204 amplitude samples, spaced 50 μsec apart, of a receiver envelope detector where each sample was quantized into 32 amplitude levels and recorded digitally on magnetic tape. The timing for the series of samples was synchronized with the transmission of a 100-μsec pulse at the remote transmitter. A time-delay-spread estimate was made from an ensemble of fifteen such recordings spaced two seconds apart.

2. Standard Deviation-to-Mean Test

An ensemble mean and standard deviation was calculated for each of the 204 time samples over the fifteen recordings. To eliminate extraneous impulse noise and interference from the data, a limit was placed on the ratio of the standard deviation to ensemble mean. If this ratio was greater than 2.0, the ensemble mean for the time sample was set to zero. The standard deviation-to-mean threshold of 2.0 was chosen so that normal Rayleigh fading signals would not be rejected. (See Appendix A.)

3. Noise-Based Threshold Test

A noise power estimate was made from the average of the square of the first twelve and last twelve ensemble mean time samples. The synchronized timing of samples with respect to the transmissions insured that no actual signal from the remote transmitter was received at these times. This noise average was multiplied by a constant and used as a threshold by which the received power, represented by the ensemble mean squared (EMS), in each time sample was compared. The multiplying factor used was 3.0. If the EMS for a time sample did not exceed or equal the noise-based threshold, then the EMS for that sample time was set to zero. If it equaled or exceeded this threshold, it was unaltered.

4. Adjacent Time-Cell Test

To further discriminate against impulse interference, it was required that at least two successive time samples be above the noise-based threshold in order to be classified as signal. For each EMS found above the noise-based threshold, a test of the EMS in adjacent time cells was made. If neither of the two adjacent EMS samples was above the noise-based threshold, then the EMS for this time sample was set to zero. If either of the two adjacent EMS exceeded the noise threshold, it was accepted as true signal and totalized.

5. S/N Test

A final test on the confidence of the time-delay-spread data was made on the basis of the total received S/N. This test required the total S/N to be 10 db or greater..

At this stage in the process, a plot of the EMS samples—normalized to the total power—as a function of the time samples was sometimes produced. These time-delay profiles were used for detailed examination of the channel time-delay dispersion. Examples of these plots are shown and discussed in Chapter V.

6. Time-Delay Spread Calculations

From the series of EMS at the various time samples, a mean time, defined as the average time delay of the path, was found. Finally, a second moment about this mean-time sample was determined. Twice the square root of this moment, converted to milliseconds, was used as a measure of the time-delay spread of the channel. The exact computational form was

$$2\sigma_\tau = 0.1 \sqrt{\frac{\sum_{N=1}^{204} (i - I)^2 P_i}{\sum_{N=1}^{204} P_i}}$$

where $2\sigma_\tau$ is the second-moment time-delay spread of the channel in milliseconds

P_i is the EMS at time sample i

I is the mean time-delay sample.

This spread calculation together with the time of the recording in GMT was punched on IBM cards. The format for this card is shown in Fig. 25.

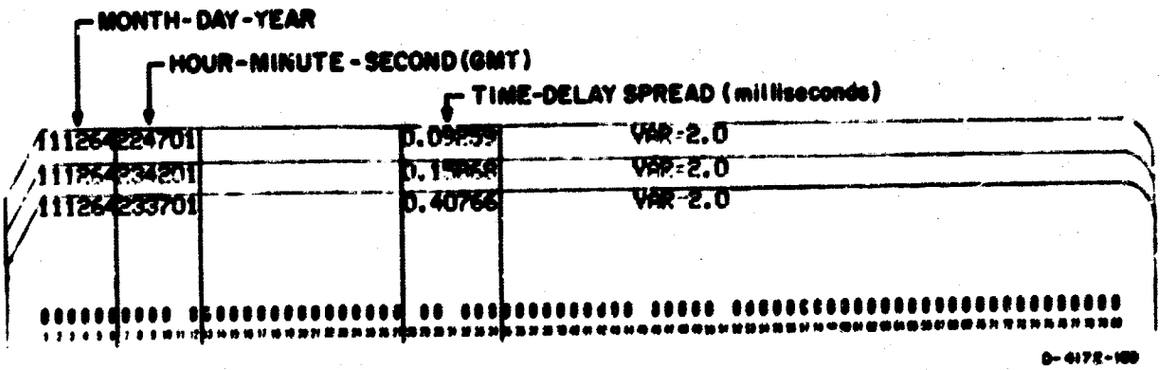

FIG. 25 TIME-DELAY-SPREAD DATA CARD FORMAT

These cards were used as input to the final classification processing of S/N and bit-error data by channel spread conditions.

E. CHANNEL FREQUENCY-SPREAD PROCESSING

Doppler-frequency-spread estimates for the channel were made from recordings of the phase and amplitude of a CW transmission over the channel. The instrumentation for this experiment, previously developed by another SRI project,[6] has been described in Chapter III. Calibrated voltages representing phase and amplitude of the received CW signal were recorded in analog form for 6-minute intervals every 20 minutes on magnetic tape. These amplitude and phase records were then digitized through an Adcom A-D converter and CDC 160A computer combination and recorded in digital form on magnetic tape. Amplitude and phase samples were taken every 10-msec, and each sample was quantized into one of the 256 discrete levels.

The digitized phase and amplitude recordings were further processed on an IBM 7090 computer to extract a Doppler-frequency profile. Daly has described this program.[8] The procedure consists of the following basic steps:

(1) Determination of the quadrature components of the received signal from the phase and amplitude samples

(2) Calculation of the autocorrelation and cross-correlation functions associated with the components

(3) Estimation of the Doppler profile by a Fourier transform of these autocorrelations.

Each Doppler-profile calculation was based on 1,200 samples of amplitude and phase spaced at 100-msec intervals. This yielded a 10-cps bandwidth spectrum with a power estimate every 1/60 cps. The results at this stage were often plotted; examples of these plots are shown in Chapter V.

A single-parameter estimate of the energy spreading in frequency by the channel was based on the variance of the frequency spread by a technique similar to that used in the time-delay-spread calculation: a mean Doppler-shift frequency was found and a second moment about this mean was determined. The square root of this moment, multiplied by two, was used as the frequency-spread parameter for this time.

The frequency-spread calculations together with the date and time were punched onto IBM cards in a format identical to that shown in Fig. 25 for the time-delay-spread calculations.

F. TABLES FOR CHANNEL-SPREAD CLASSIFICATIONS

The classification of channel-spread conditions was based on two considerations:

(1) Theoretical differences in error rates at high S/N would be detectable for different channel-spread conditions.

(2) Sufficient data would be collected in each channel grouping to form confident estimates of S/Ns and error rates, particularly at high S/Ns.

To provide flexibility in these classification decisions, the groupings were defined to the processing program in the form of a two-dimensional matrix as shown in Fig. 26. Each row was subjectively defined by a time-delay-spread range for the channel, and each column was assigned a frequency-spread range. Next, each element in the matrix was assigned a table number defining classifications into which data with these channel-spread conditions would be grouped. As the amount of data in each classification became apparent, the classifications were easily altered by simply redefining the column or row limits or changing the elements in the matrix.

Each table in the processor consisted of two 80-element arrays. One of the arrays contained the total number of 30-second data periods found

at each S/N from 0 to 80 db in 1-db intervals. All S/Ns less than 0 db were grouped with the 0-db entries, while S/Ns greater than 80 db were added to those in the 80-db interval. The other array contained accumulated bit errors at the corresponding S/N intervals.

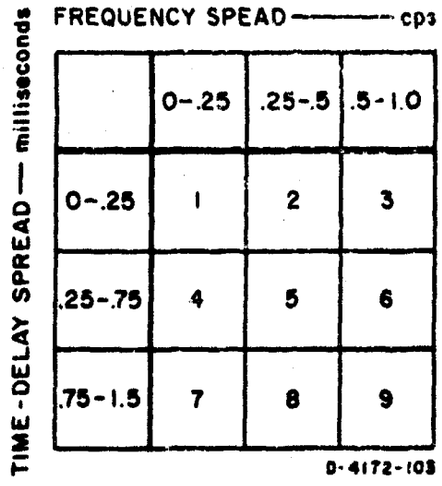

FIG. 26 DEFINITION MATRIX FOR CLASSIFICATION OF TIME-DELAY- AND DOPPLER-SPREAD DATA

G. CLASSIFICATION OF S/N AND BIT-ERROR DATA

Channel time-delay- and frequency-spread data as a function of date and time were generated by the time-delay- and frequency-spread processing programs. These data, on punched cards, were arranged chronologically into two decks, one for time-delay-spread data and the other for frequency-spread data. Each deck was entered into the classification program where chronological time intervals were established during which a particular channel-spread classification was assigned. The time interval was determined from the recorded time-delay- and frequency-spread values. The start of the time interval was determined by calculating one-half the difference between recorded time and the recorded time for the preceding spread measurement. The end of the time interval was determined by calculating one-half the difference between that recorded time and the recorded time for the following spread measurement. In this manner, any missing data were simply bridged over by the bracketing spread measurements. Each time interval was then associated with a particular classification table by matching the time- and frequency-spread measurements for the time interval with the channel-spread classification matrix. A listing of these time intervals and the table numbers assigned to each interval is shown in Appendix E according to the definitions of tables given in Fig. 26.

H. S/N ERROR-RATE DATA

All of the 30-second S/N and error data were then grouped according to channel-spread conditions observed at the time the data were taken. Finally, the data in each classification or table were processed further to produce as many confident error-rate and corresponding S/N ratio points

as possible. Considerations used to establish confident error-rate estimates are discussed in Appendix D. The resulting processing rule was to require that the total observed errors for S/N intervals in each classification equal or exceed 100. The computational procedure for emptying the contents of each table was as follows:

(1) The total number of errors recorded for an S/N of 0 db was noted.

(2) If this number was greater than 100, a binary-error-rate estimate was made by dividing the number of errors by the total bits received at this S/N. The total bits received were determined by the product of the number of 30-second data entries at this S/N and 2,251, the number of bits transmitted during each 30-second data period. The procedure was then repeated for the next higher S/N decibel interval.

(3) If the total number of errors in the 0-db S/N interval was less than 100, the errors at the next higher S/N interval (i.e., 1 db) were added to the total. If the total errors were then greater than 100, a weighted average S/N was calculated, based on the number of entries at each of the two S/N intervals. The corresponding binary error rate was determined from the total errors and the total number of entries at both the 0- and 1-db S/N intervals.

(4) If the total number of errors in the 0 and 1-db intervals was still less than 100, Step (3) above was repeated, taking the errors and entries at the next higher S/N until the error total exceeded 100. At this time, a weighted average S/N was calculated along with a binary error rate.

(5) After the highest S/N interval had been entered, the average S/N and binary error rate were determined, even if the total errors did not exceed 100.

Both punched cards, for use in data plotting, and a printout of the average S/N and corresponding error-rate calculations were produced. Printouts of all results, sorted into various channel-spread classifications, are shown in Appendix F.

V PRESENTATION AND DISCUSSION OF RESULTS

A. CHANNEL MEASUREMENTS

1. Ray-Path Geometry

The character of radio signals propagated via the ionosphere varies greatly with time of day and season and with transmission frequency. Two reflecting layers are responsible for the return of HF transmissions on the path from Fort Monmouth, New Jersey to Palo Alto, California. The principal layer is the *F* layer nominally located at a height of 300 km above the earth. The other is the *E* layer at about 100-km height.

On this path, a great-circle distance of 4100 km, it is normal for signals to arrive at the receiver in many combinations of reflections from these layers and the ground. Each of these propagation paths or modes has a characteristic propagation time depending on the total distance traveled and the group velocity of propagation along the path.

Movements and turbulence of these layers cause a Doppler-frequency shift and spread of the received signal from that transmitted. Each mode contributes a Doppler component to the total received signal. This component may be a fixed frequency shift of all transmission frequencies or a smearing of the received signal over a band of frequencies.

2. Ionograms

Propagation time for each mode can change drastically with transmission frequency. Characteristic patterns of propagation time with transmission frequency are often used to identify experimentally the various propagation modes present on a path. Oblique-incidence ionosphere sounders measure and display this time delay-frequency characteristic directly; such a sounder has been used on this particular path for many years. Typical ionograms produced on this path during the error-rate experiment are shown in Fig. 27. The MOF of each mode is defined as the highest frequency propagated by that mode, as determined by the ionogram, while the LOF is the lowest detectable frequency for the mode.

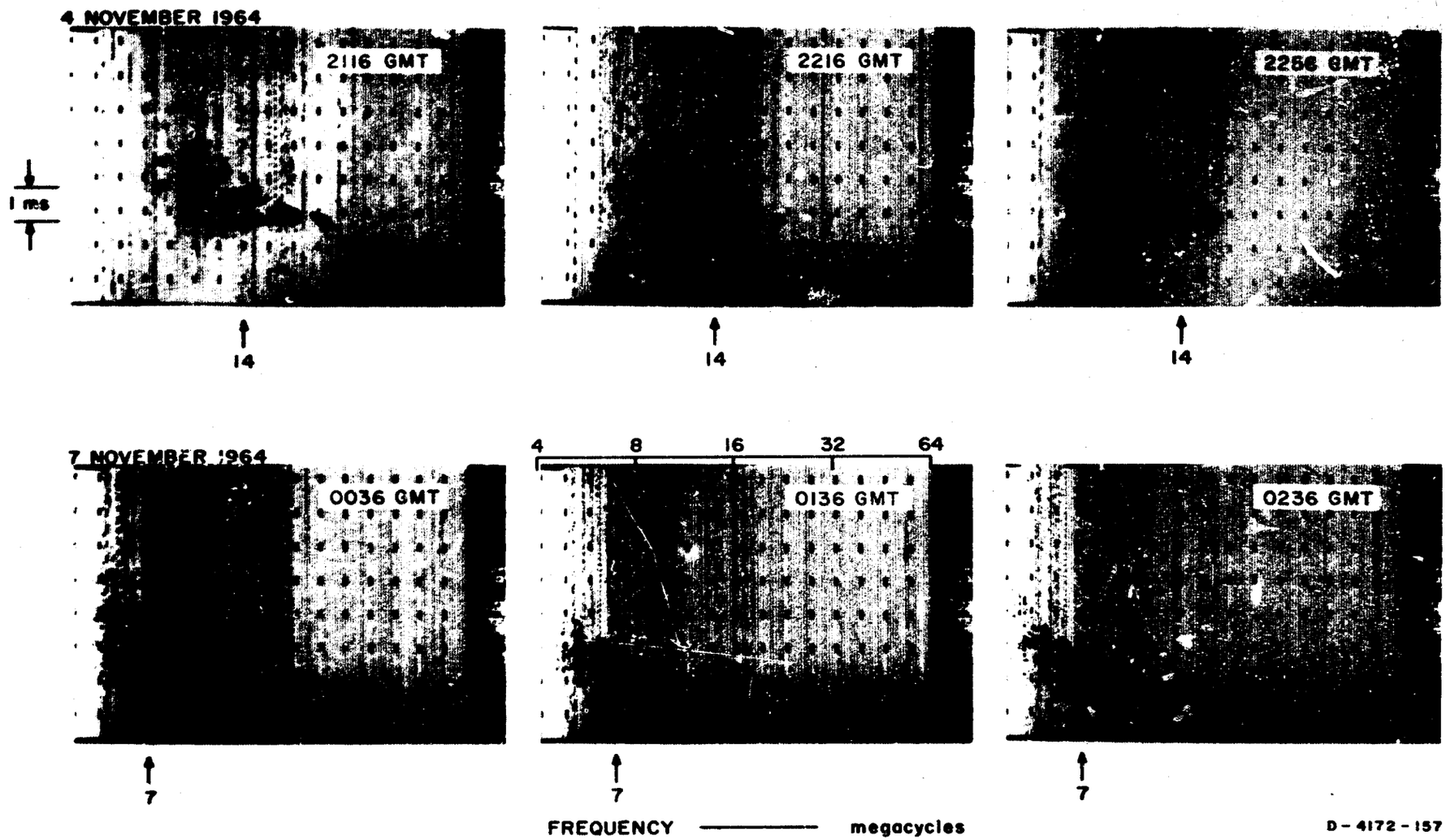

FIG. 27 OBLIQUE-INCIDENCE IONOGRAMS — FORT MONMOUTH TO PALO ALTO

3. Characteristics at 14 Mc

From 1800 to 2300 GMT (1200 to 1700 local time at midpath), the error-rate experiment was operated at 14 Mc. The predominant mode at these times is normally a strong two-hop *F*-layer reflection (*i.e.*, *2F*). The high ray from this mode (*2FH*) often propagates also. The signal from the *2FH* is often unresolvable in time delay from the normal *2F*, but can arrive up to 0.5 msec after the *2F* low ray. At times, usually when the MOF of the *2F* is lower than 14 Mc, it is possible to receive signals from the one-hop *F*-layer high ray. However, the normal *1F* low-ray mode is usually not present on this path because of the earth's curvature.

From path geometry, it is impossible for propagation to occur by a single hop from the *E* layer. However, it is possible for propagation to occur by two or three hops from this layer. A two-hop *E* mode is somewhat rare during the daylight hours at 14 Mc, but a three-hop *E* mode is more common. The *3E* mode arrives approximately 0.2 msec before the arrival of the normal *2F* mode.

A very common and strong propagation mode from 1800 to 2300, at 14 Mc, is the so-called *N* mode. This is a two-hop combination mode consisting of a one-hop reflection from the *F* layer and a one-hop reflection from the *E* layer. The *N*-mode signal arrives a small fraction of a millisecond after the *3E* mode, if present, or about 0.2 msec before the *2F* mode. A typical range of time-delay difference between the first and last arriving mode at this frequency and time of day is from 0 to 1.0 msec.

Background noise is either of local origin or is propagated from great distances by the ionosphere. Local noise is generally man-made interference. Propagated noise is either atmospheric noise or interference.

The heavy *D*-region absorption during the day acts as a substantial attenuator to all propagated signals, particularly those at low frequencies. The signal strength of each mode is affected by its total path length and the distance traveled in the absorbing *D* region. Variation in absorption introduces long-term fading. Of more practical importance, however, is the effect of the antenna gain pattern on the strength of the signals received (and transmitted) from the various modes which arrive (and leave) at different vertical angles. Short-term variations of mode signal strength are also caused by polarization fading and fading within resolvable modes.

4. Characteristics at 7 Mc

The experiment was operated at 7 Mc after sunset on the path (1600-2000, local midpath). Initially, at this frequency the path is characterized by the propagation of higher-order modes (*i.e.*, 3*F*, 4*F*, and 5*F*). However, as the evening wears on, the electron density of the lower ionosphere diminishes, and the absorption in the *D* region lessens. The initial effect, therefore, is a strengthening of the higher-order modes. But shortly thereafter, the electron density of the *F* region diminishes, and the MOF of all modes begins to drop. As a result, the number of modes propagating at this frequency is large at first, may increase slightly, and then decreases as the MOF of the higher-order modes drop through 7 Mc. The two- and three-hop *E* modes are prevalent at this frequency and time of day. A typical range of time-delay differences from the modes propagated at this frequency and time of day is 0.2 to 2.0 msec.

Loss of the *D* region at night also causes the propagated noise and interference to increase significantly. The geographical origin of this noise is more widely spread than during the day.

Other modes are possible on this path, particularly off-path modes due to ionospheric anomalies. These modes, if present, arrive with appreciably longer time delays.

5. Time-Delay Profiles

Accurate error-rate performance estimations of an HF communications systems require a rather detailed picture of the scattering of the signal energy by the channel in time and frequency. A time-delay scattering picture was obtained by actually measuring and displaying an average of several impulse responses of the channel. The measurement technique has been described in Sec. D. 2 of Chapter III. Selected examples of time-delay profiles at 14 and 7 Mc produced directly from the data processor output by a CalComp plotter are shown in Figs. 28 through 33. The time-delay scale has been shifted so that zero time delay corresponds to the average delay of the path. The power density, measured at 50-μsec intervals, is normalized to the total received power.

Twice the second-moment spread, $2\sigma_\tau$, calculated for each of these profiles, is also shown. This spread measure tends to be less than the time difference from the first to last arriving mode, as measured from ionograms, because it weights the amplitude found at each differential time delay.

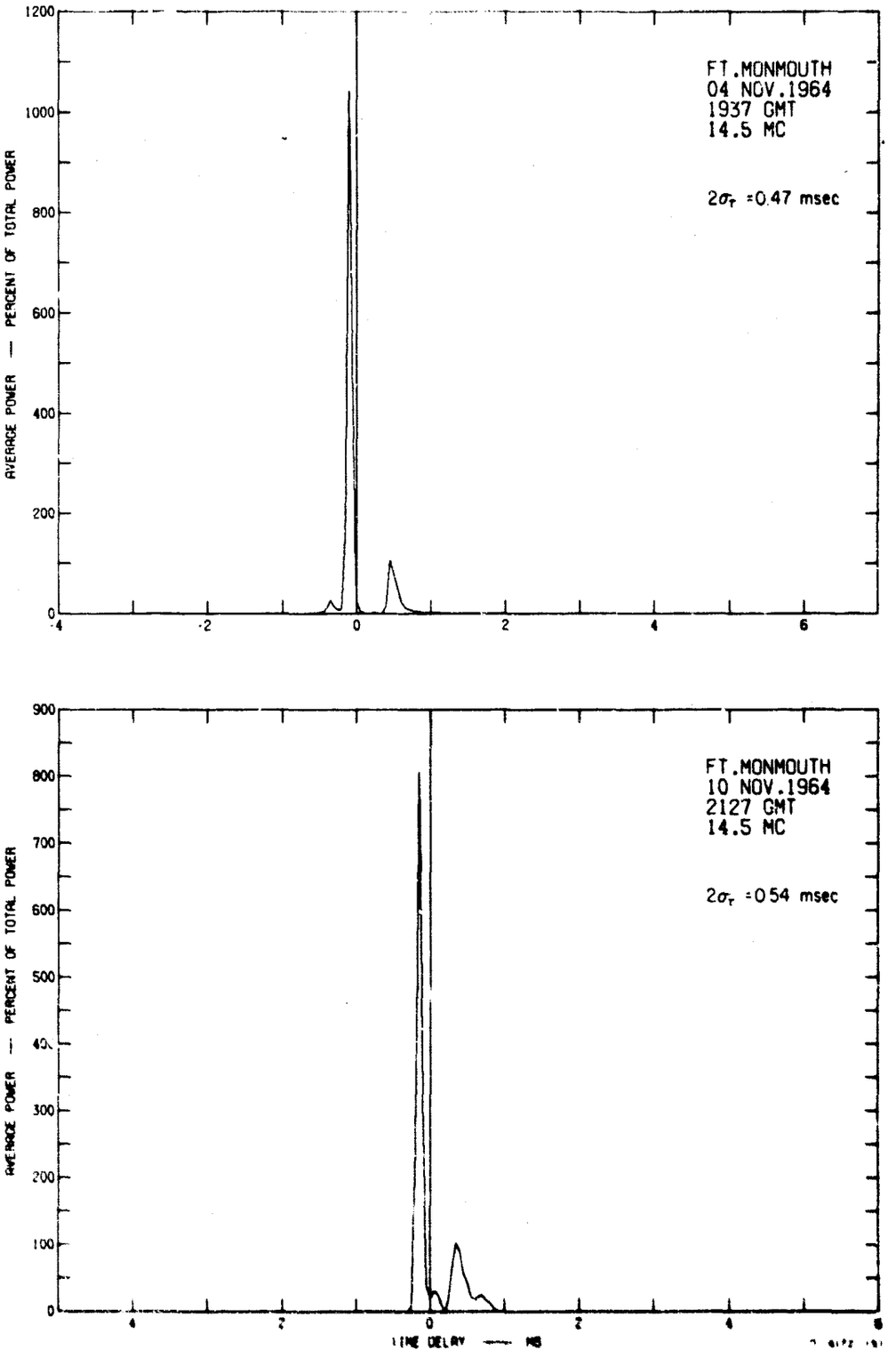

FIG. 28 TIME-DELAY PROFILES

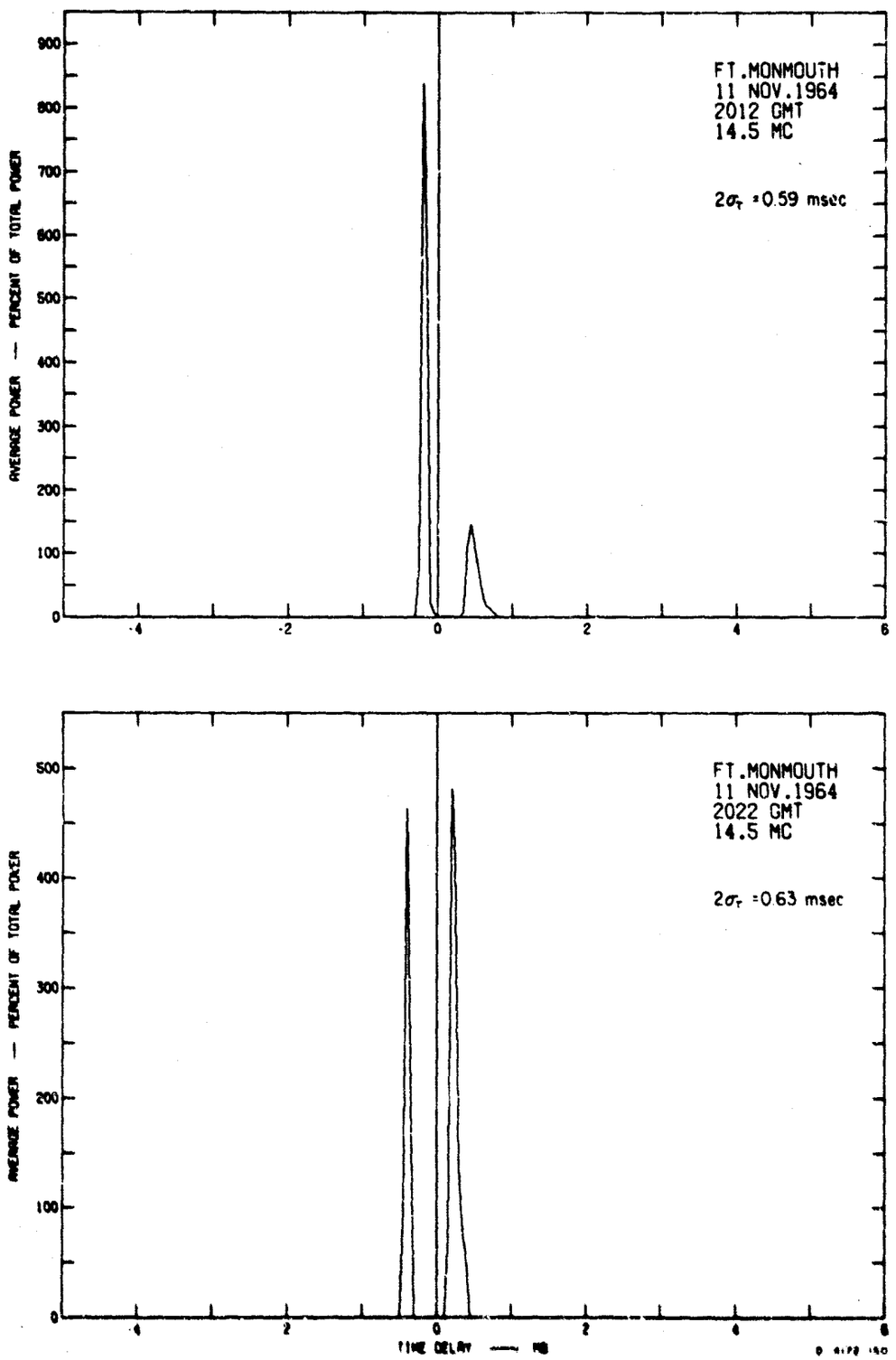

FIG. 29 TIME-DELAY PROFILES

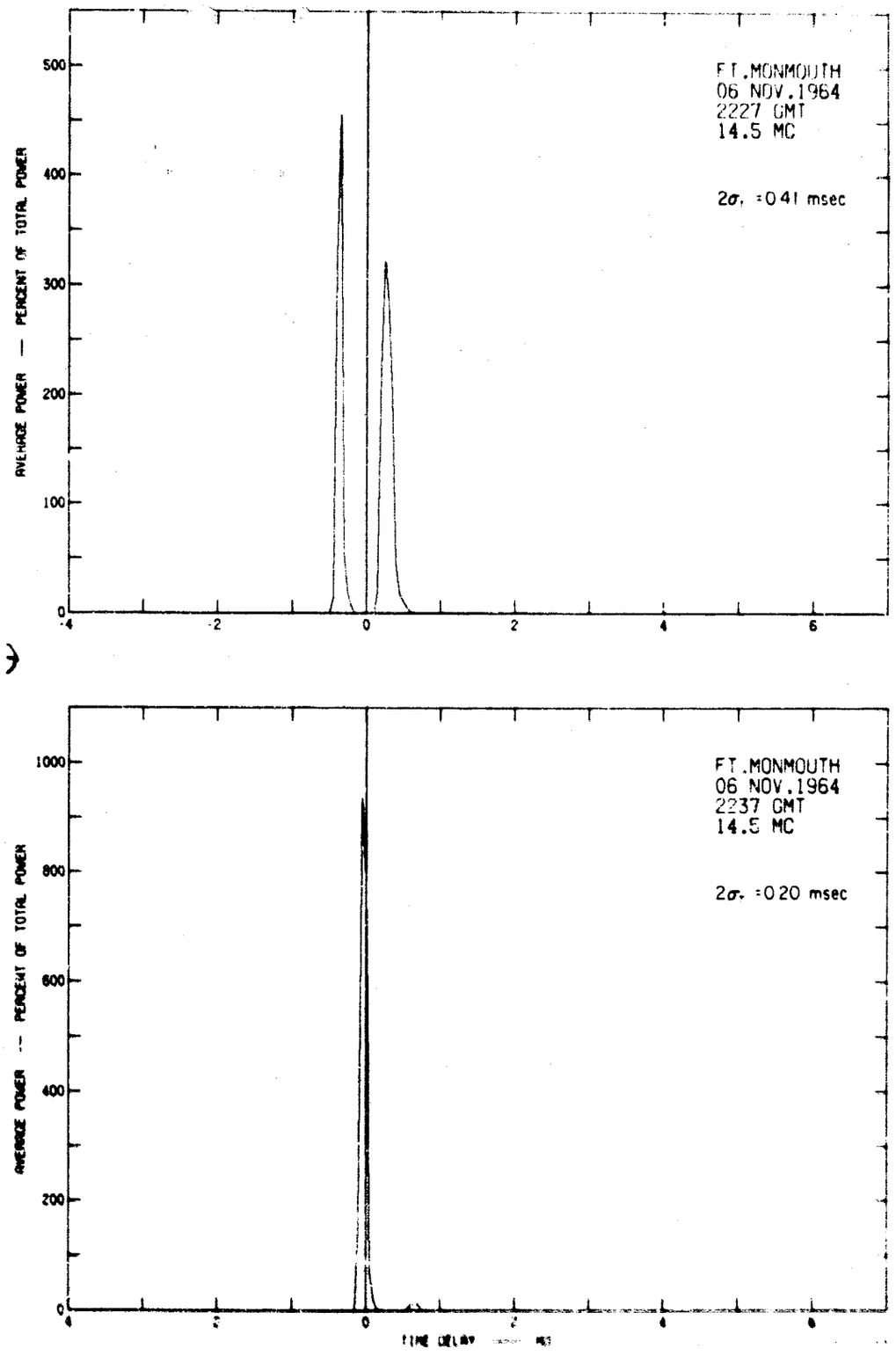

FIG. 30 TIME-DELAY PROFILES

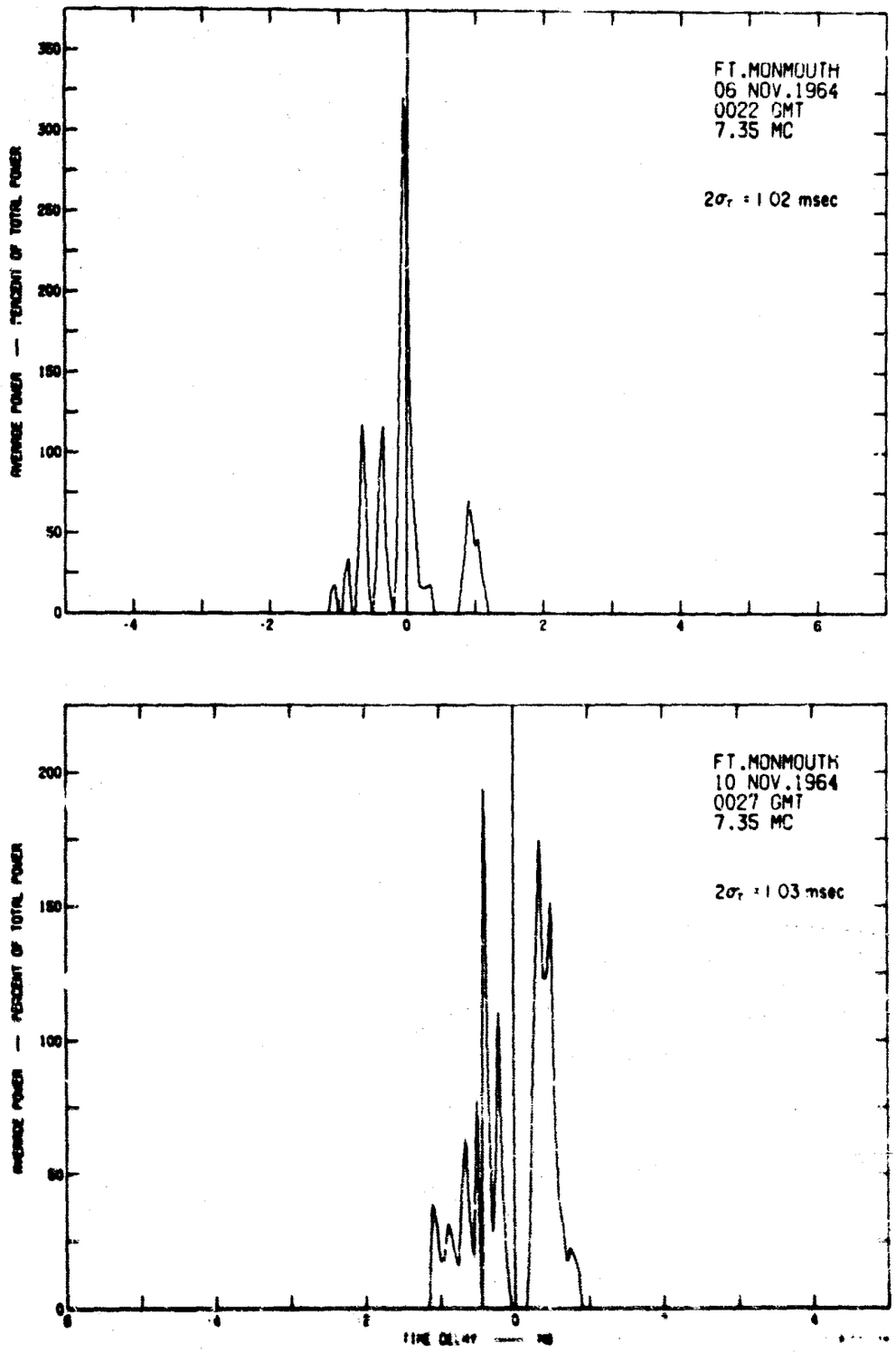

FIG. 31 TIME-DELAY PROFILES

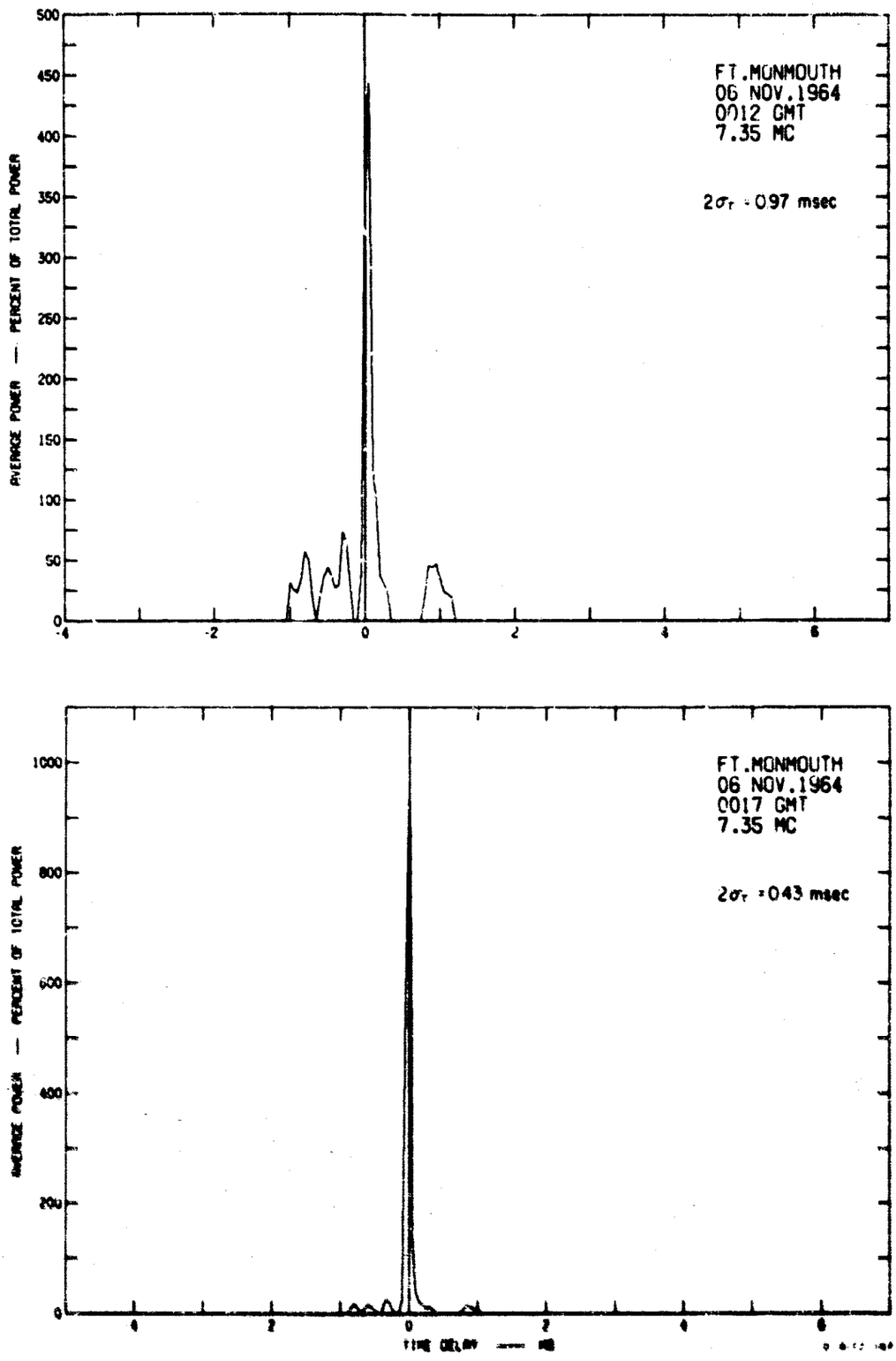

FIG. 32 TIME-DELAY PROFILES

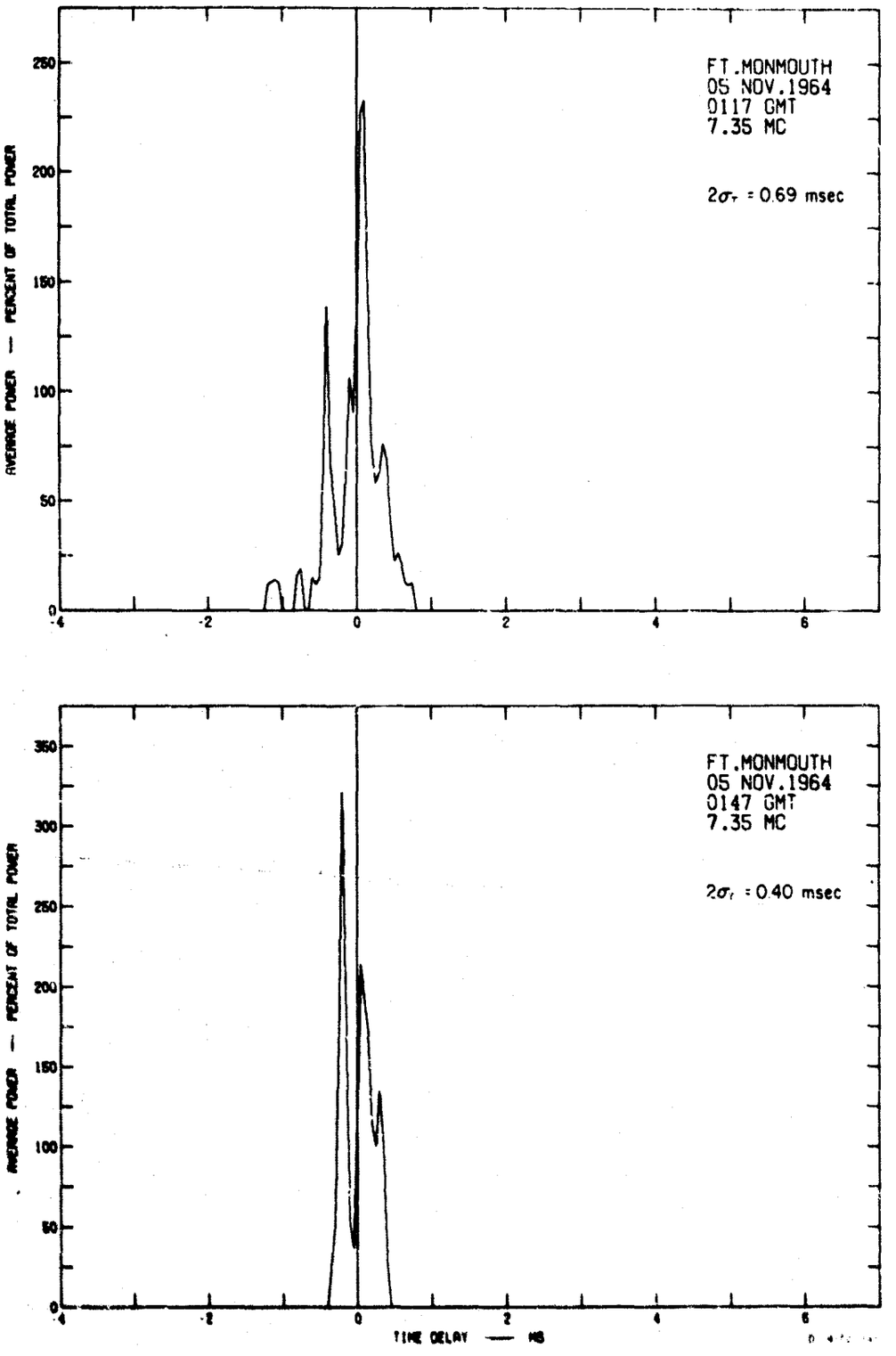

FIG. 33 TIME-DELAY PROFILES

The time-delay profile is a transform of the frequency-selective-fading characteristics of the channel. In general, the wider the time-delay spread, the more severe is the frequency-selective fading. It should be noted that a single mode with a slowly varying time delay will not cause frequency-selective fading but only a shift in the arrival time of the transmitted pulse. Slowly varying mean time shifts are normally corrected by resynchronization in baud-synchronous communications systems or by automatic adjustment in nonsynchronous systems.

Discrete peaks in the time-delay profile are indicative of the propagation of discrete modes with different time delays. The reciprocal of the time-delay difference between these peaks corresponds to a strong frequency-selective fading component in the received signal. If the profile indicates only two, equal-strength modes, deep frequency-selective nulls equally spaced can be predicted.

6. Diurnal Time-Delay Spreads

Diurnal variations in the time-delay spread are shown in Figs. 34 through 41. Diurnal trends in time-delay spread can be discerned; however, there is a wide variation in the data from day to day, particularly at 7 Mc. The high-multipath time-delay spread generally occurred in the early evening at 7 Mc.

7. Time-Delay-Spread Histograms

Histograms for all observed time-delay spreads calculated at 14 and 7 Mc for all data from 3 to 14 November are shown in Fig. 42. The time-delay spread histogram at 14 Mc shows a double peak. The first peak indicates a predominant single-mode propagation condition with little time-delay spreading. The second peak indicates a two-mode condition with a time-delay separation averaging about 0.5 msec.

At 7 Mc, time-delay spreads are more evenly distributed. The rather large tail in the distribution is worth noting since it indicates the possibility of high values of the time-delay spreads.

8. Doppler-Shift Profiles

A Doppler scattering picture was obtained by actually measuring and displaying the frequency dispersion of the channel. The measurement technique has been described in Sec. C.2 of Chapter III. Examples of

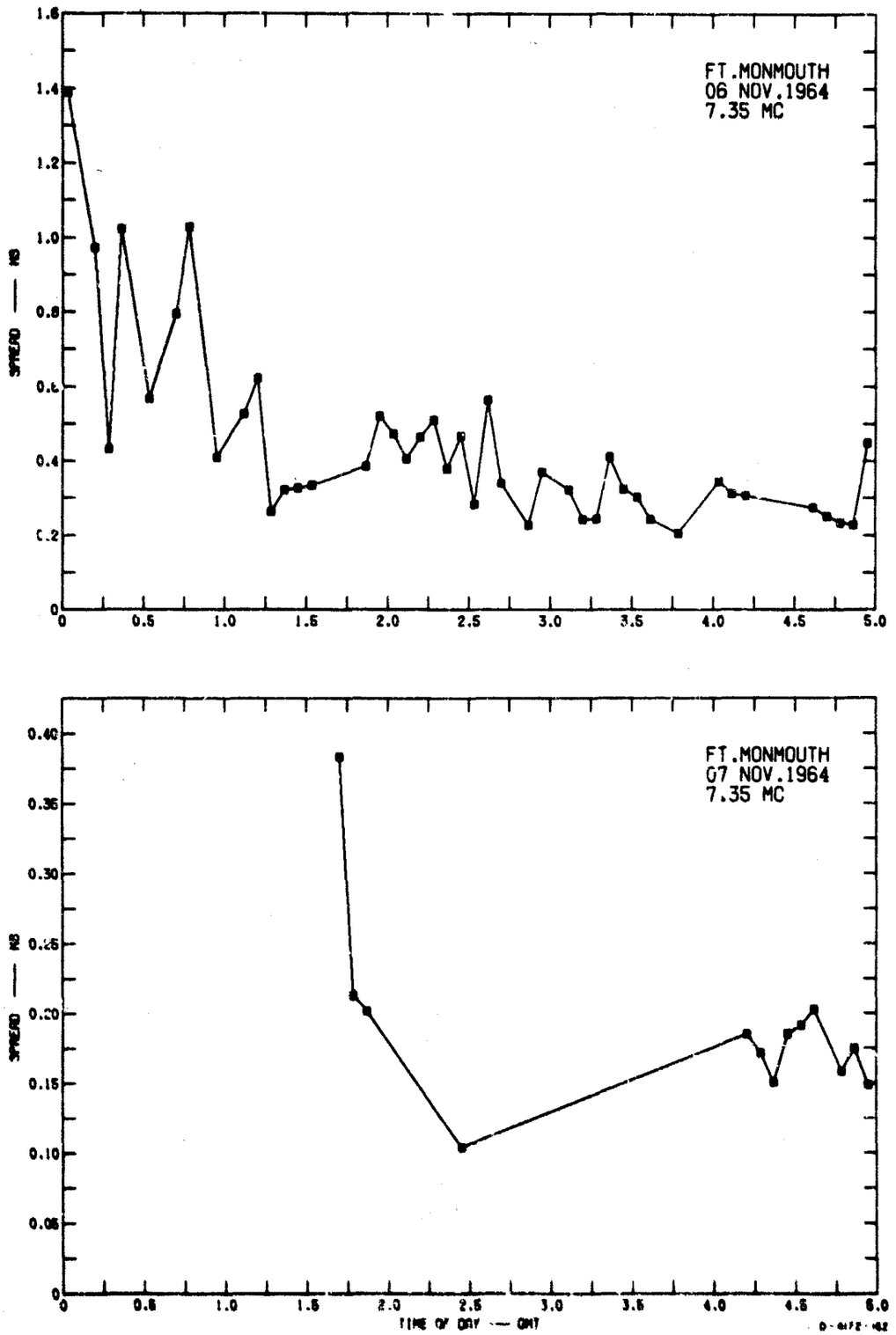

FIG. 34 DIURNAL TIME DELAY — 6 AND 7 NOVEMBER, 7.3 Mc

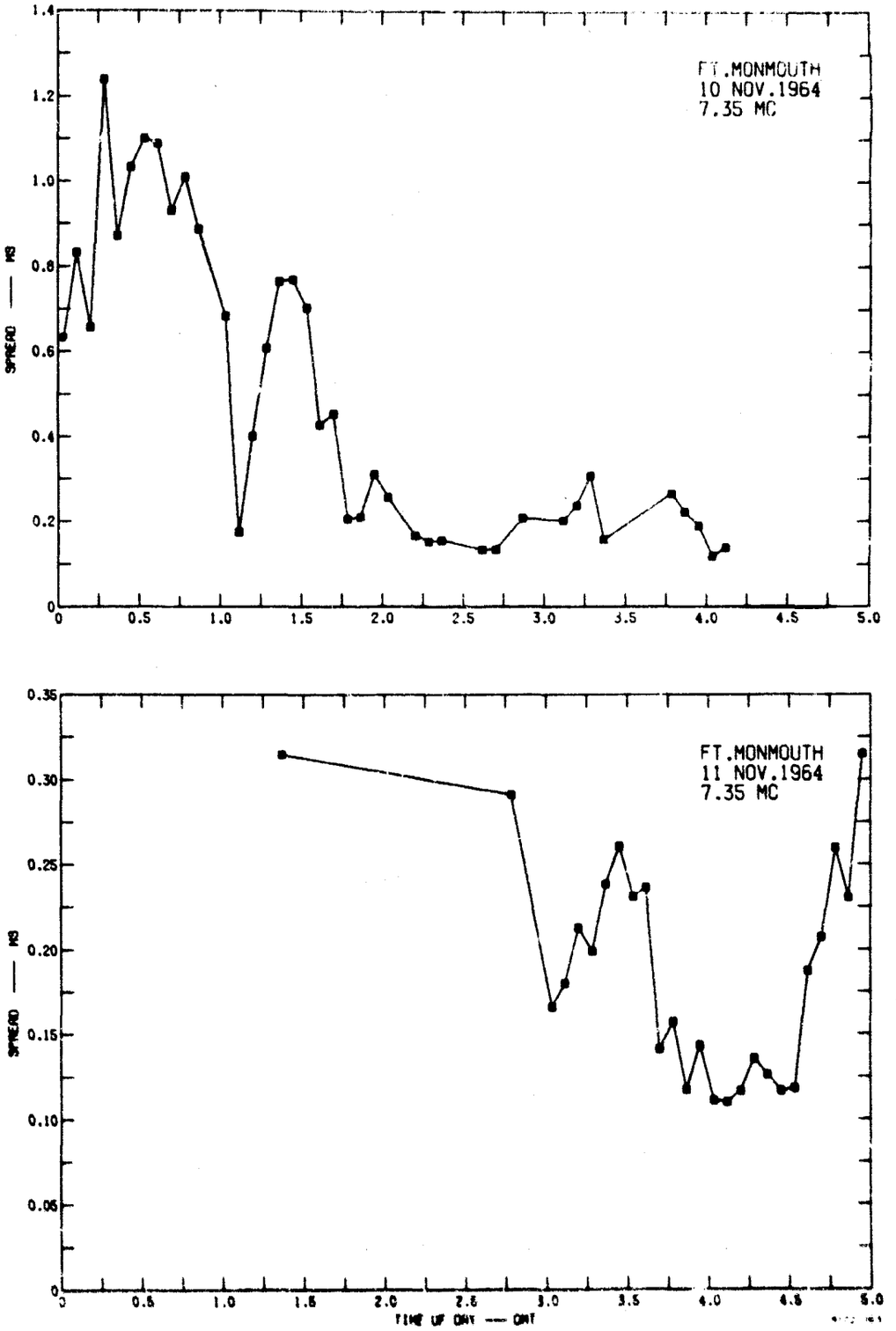

FIG. 35 DIURNAL TIME DELAY — 10 AND 11 NOVEMBER, 7.3 Mc

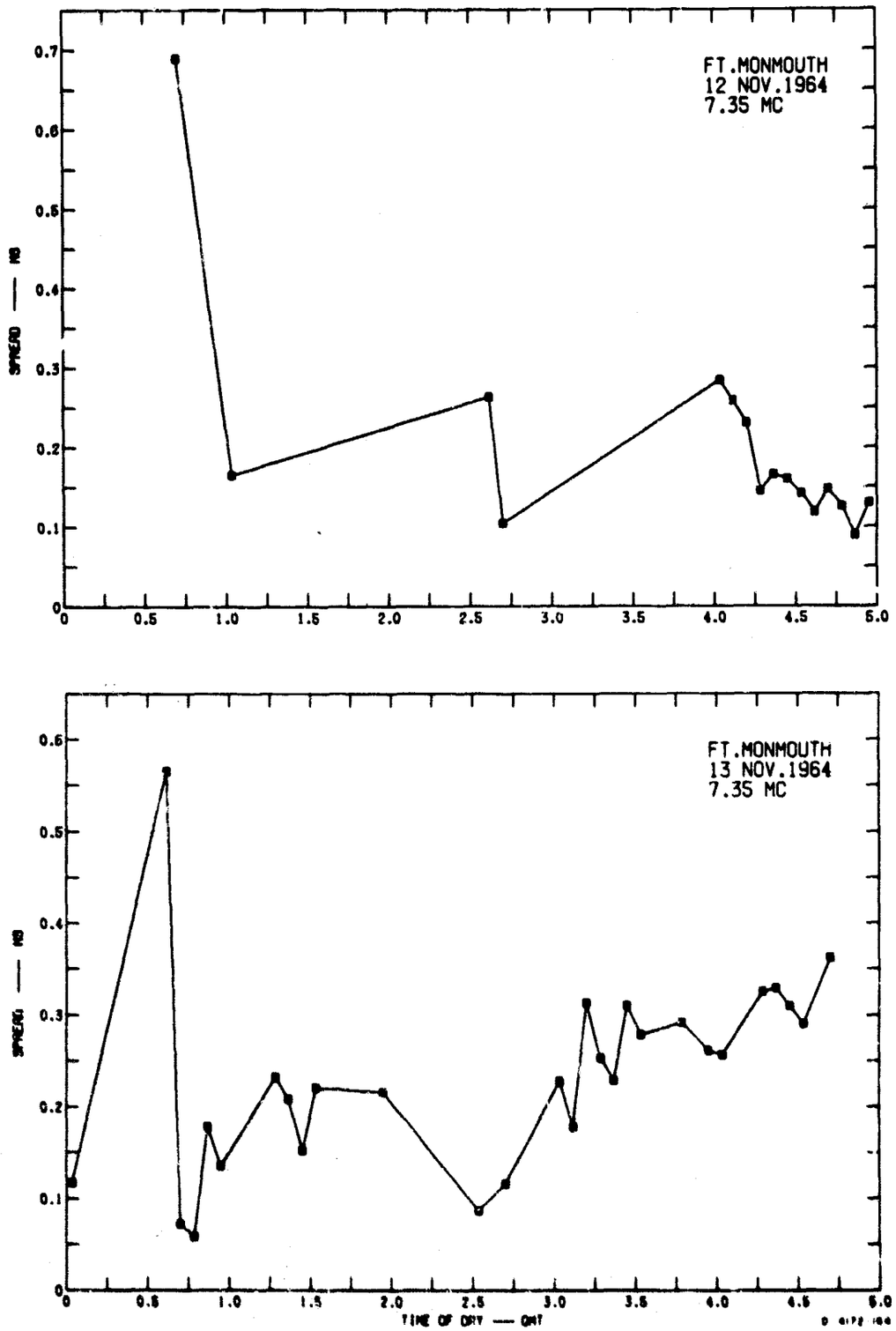

FIG. 36 DIURNAL TIME DELAY — 12 AND 13 NOVEMBER, 7.3 Mc

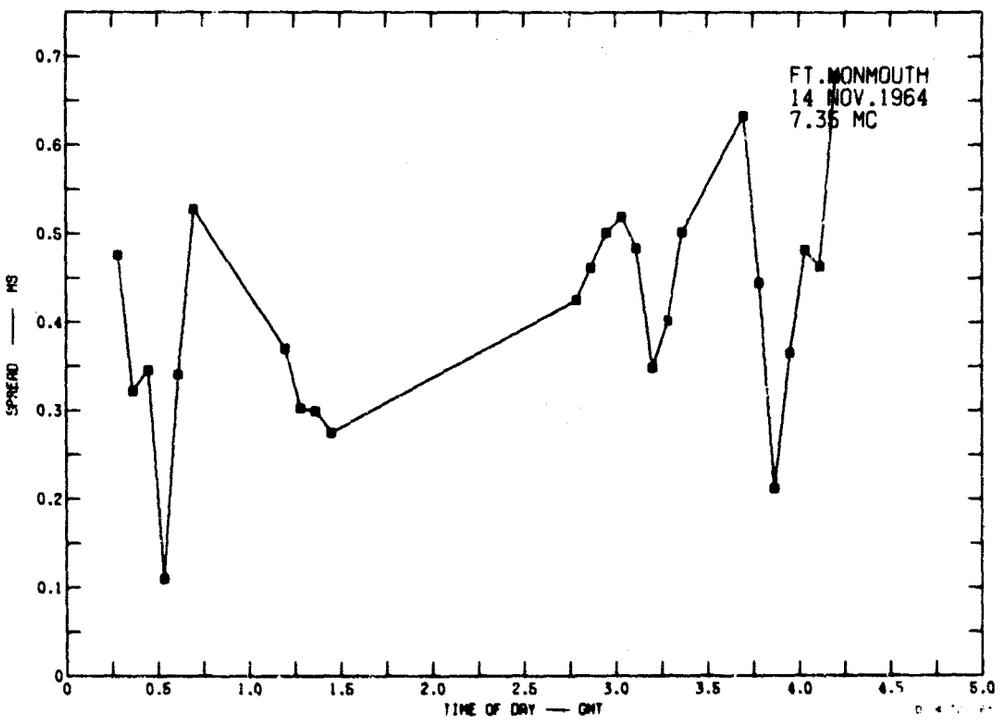

FIG. 37 DIURNAL TIME DELAY — 14 NOVEMBER, 7.3 Mc

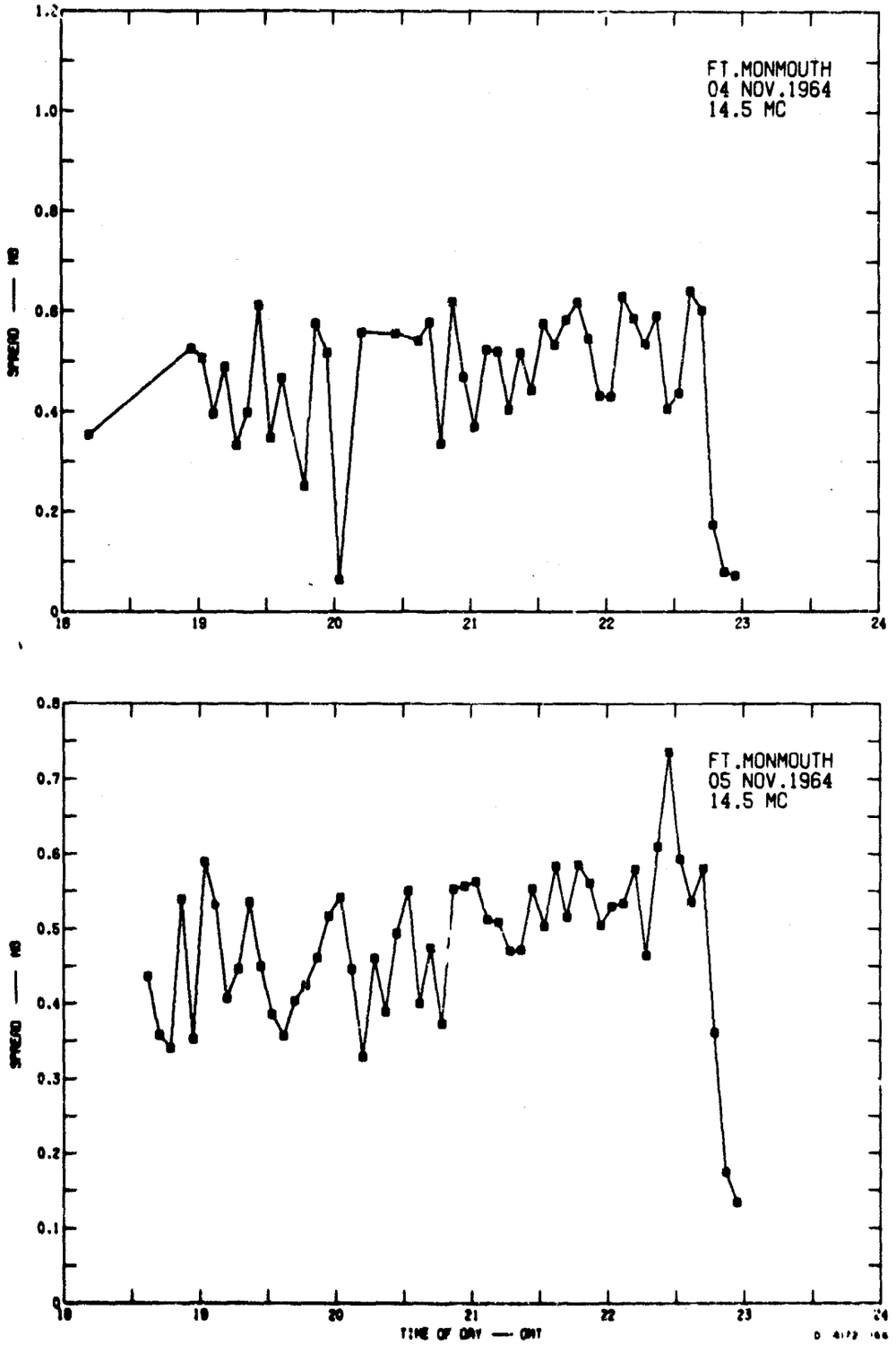

FIG. 38 DIURNAL TIME DELAY — 4 AND 5 NOVEMBER, 14.5 Mc

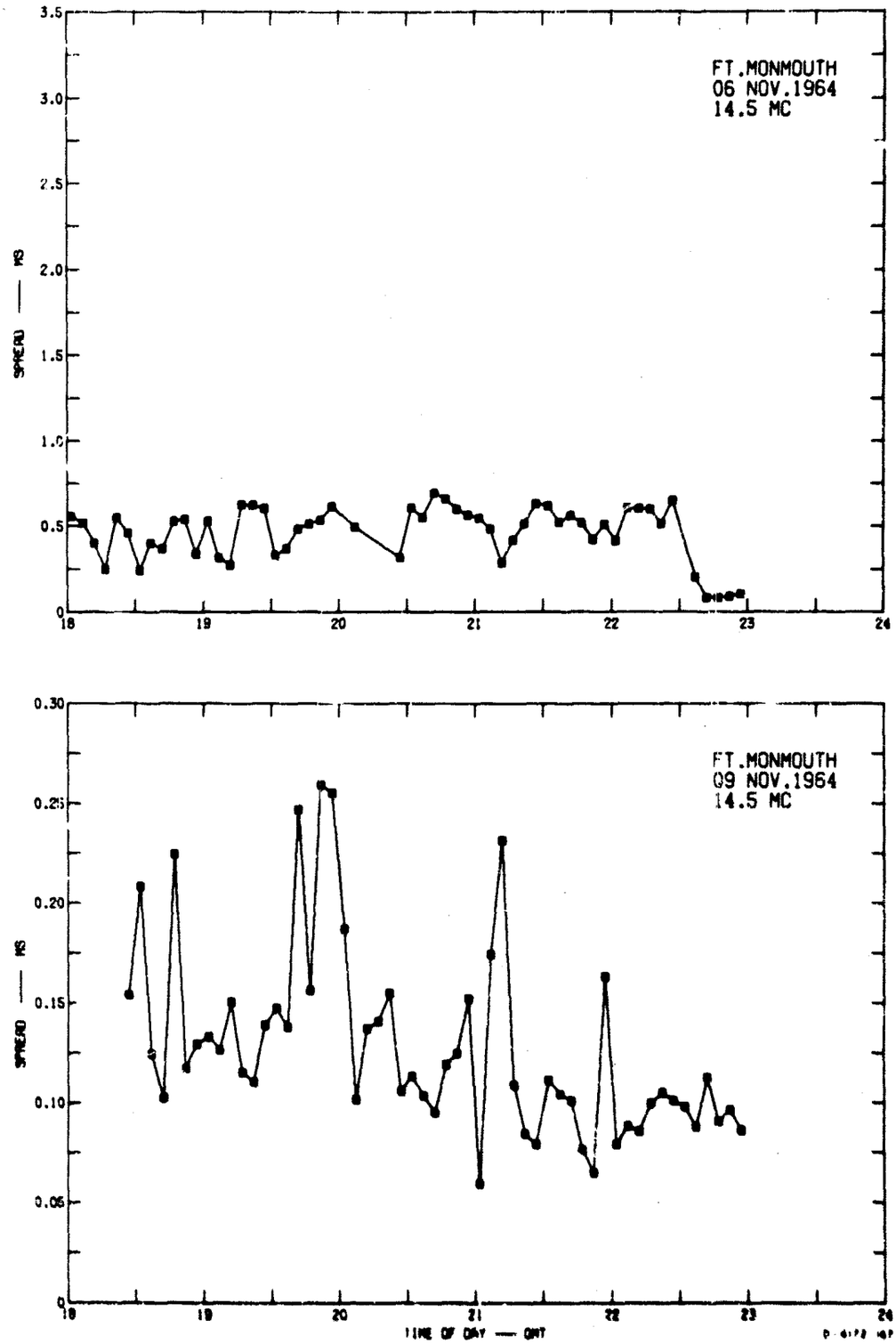

FIG. 39 DIURNAL TIME DELAY — 6 AND 9 NOVEMBER, 14.5 Mc

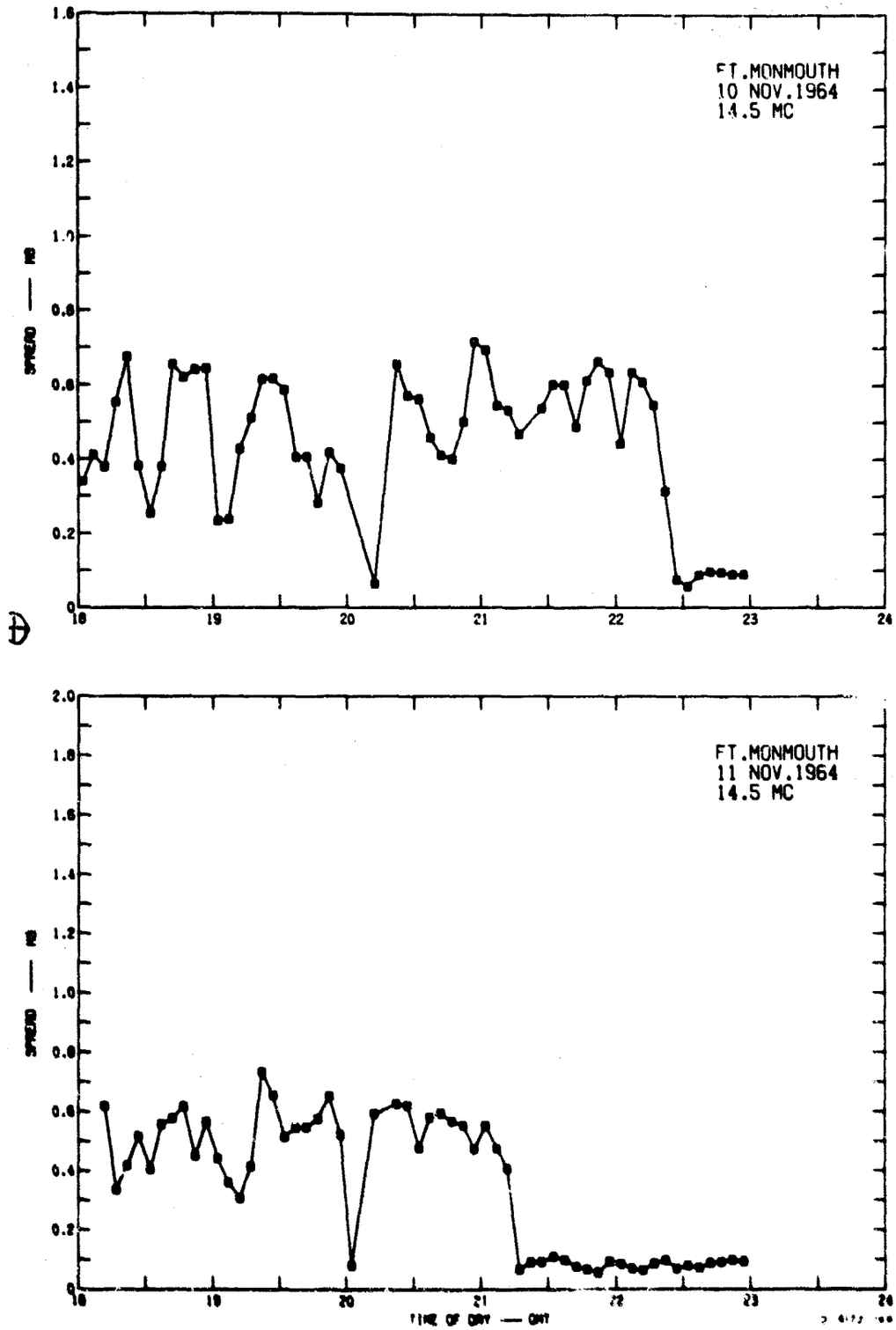

FIG. 40 DIURNAL TIME DELAY — 10 AND 11 NOVEMBER, 14.5 Mc

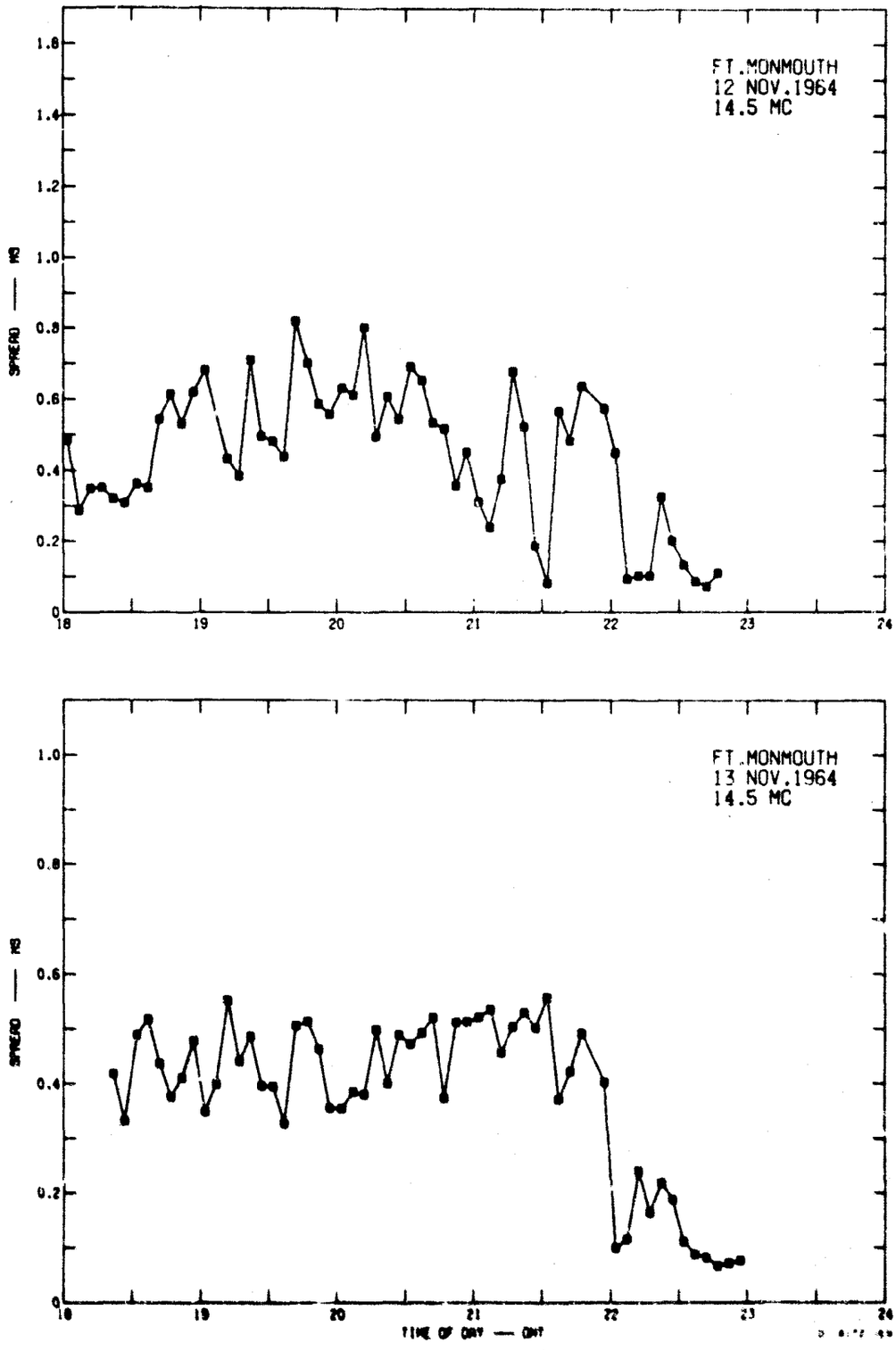

FIG. 41 DIURNAL TIME DELAY — 12 AND 13 NOVEMBER, 14.5 Mc

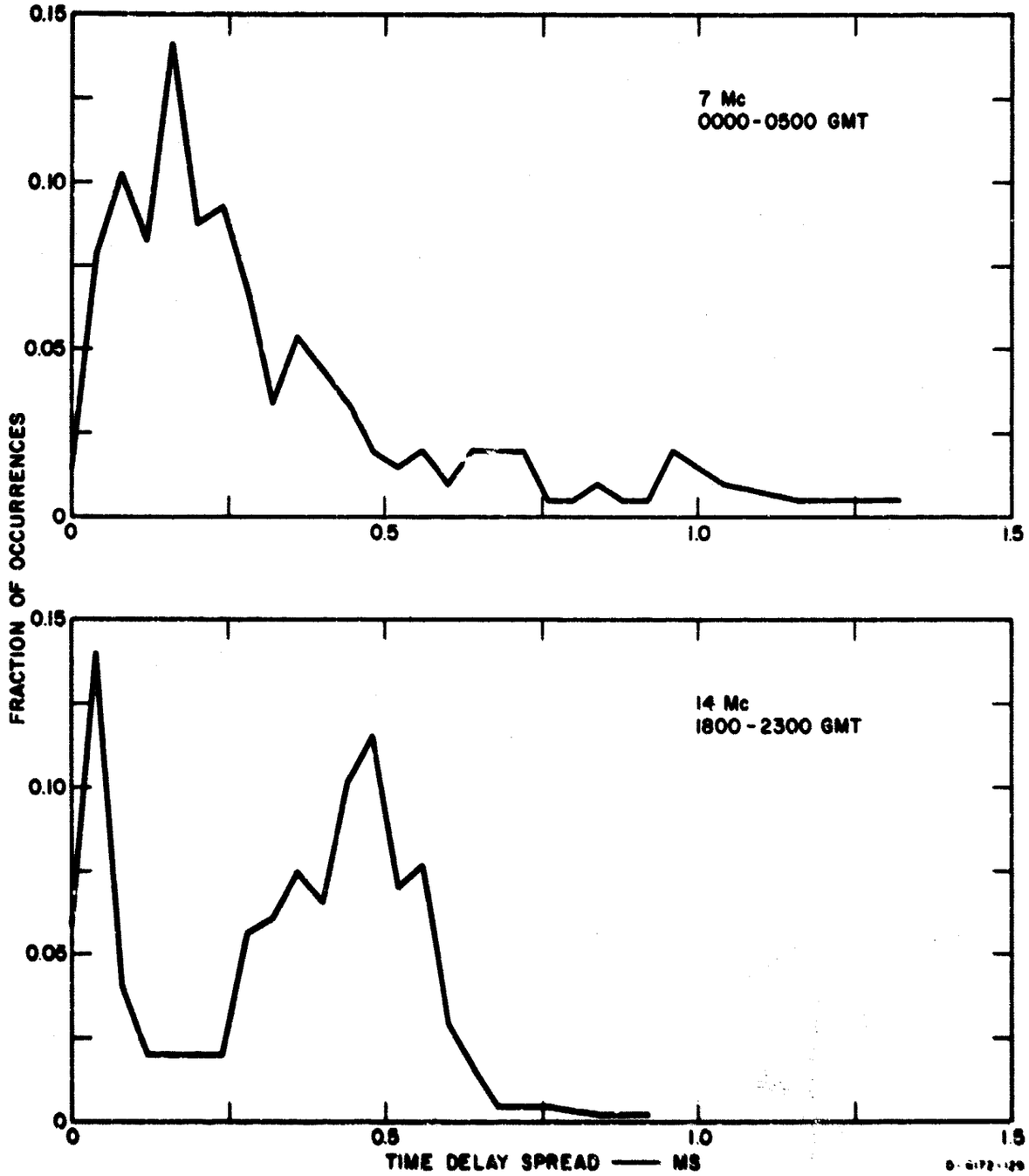

FIG. 42 TIME-DELAY HISTOGRAMS

Doppler-frequency profiles are shown in Figs. 43 through 46. The frequency scale is referenced to the frequency of the transmitted *CW* tone. The power density, measured at 1/80-cps intervals, is normalized to the total ac power detected. Twice the second-moment spread measure, $2\sigma_\tau$, is also shown on these profiles, as is R, the ratio of the dc to ac power. The dc power is the on-frequency power often referred to as the specular component of the received signal.

The Doppler-frequency profile is a transform of the time-selective-fading characteristics of the channel. In general, the wider the Doppler spread, the more rapid is the time fading. It should be noted that a single mode with a slowly varying mean Doppler frequency will not cause time fading but only a shift in the frequency of the arriving signal. In communications systems, slow frequency shifts are normally corrected by AFC circuits in the receiver but, if not, are normally small enough to stay within the bandwidth of the receiver filters.

Discrete peaks in the Doppler profile are indicative of the propagation of discrete modes with different Doppler shifts. The frequency difference between these peaks corresponds to a strong time-fading components in the received signal. If the profile indicates only two, equal-strength modes, deep time-fading nulls equally spaced can be predicted.

B. ERROR-RATE MEASUREMENTS

1. Introduction

Before embarking on a discussion of the results obtained in the error rate experiment, it is well to consider once again that the experimental FSK system and the idealized FSK system model used to compute the theoretical error-rate curves display important differences in detection procedures. The computational model is an energy-quenching system; on the other hand, the experimental system decays received signal energy at a rate determined by its filter time constant. In filtering the received pulses, the computational model merely narrow-band integrates over a signaling-element duration, while the experimental system smooths and shapes the time and frequency characteristics of the received signal in a more complex manner. In any critical experimental or theoretical analysis, these differences will be apparent as the time- and frequency-dispersive effects of the channel are isolated and analyzed in sufficient detail. A complete analysis of the experimental system is not available at the present time, and it was not

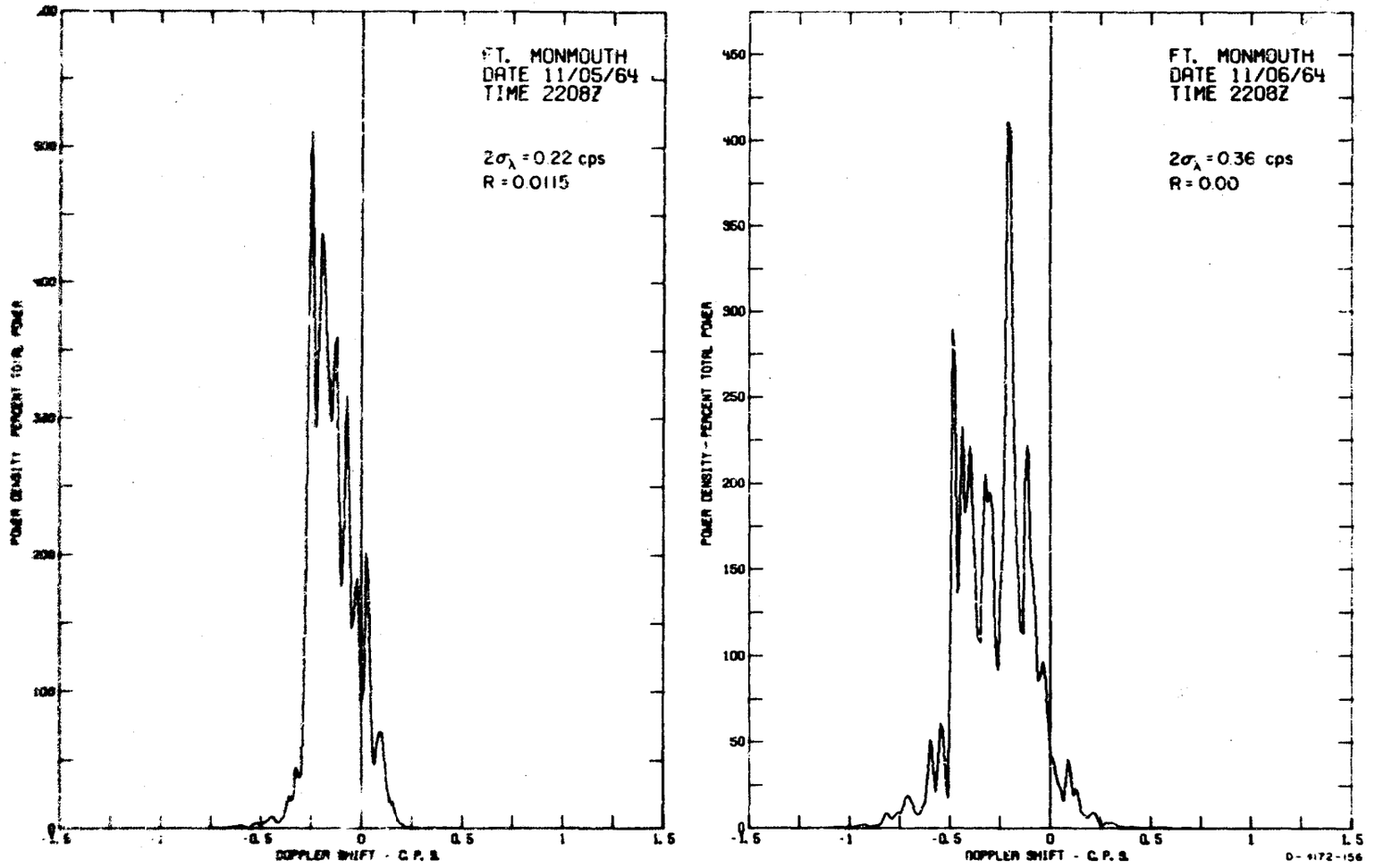

FIG. 43 DOPPLER–FREQUENCY PROFILES

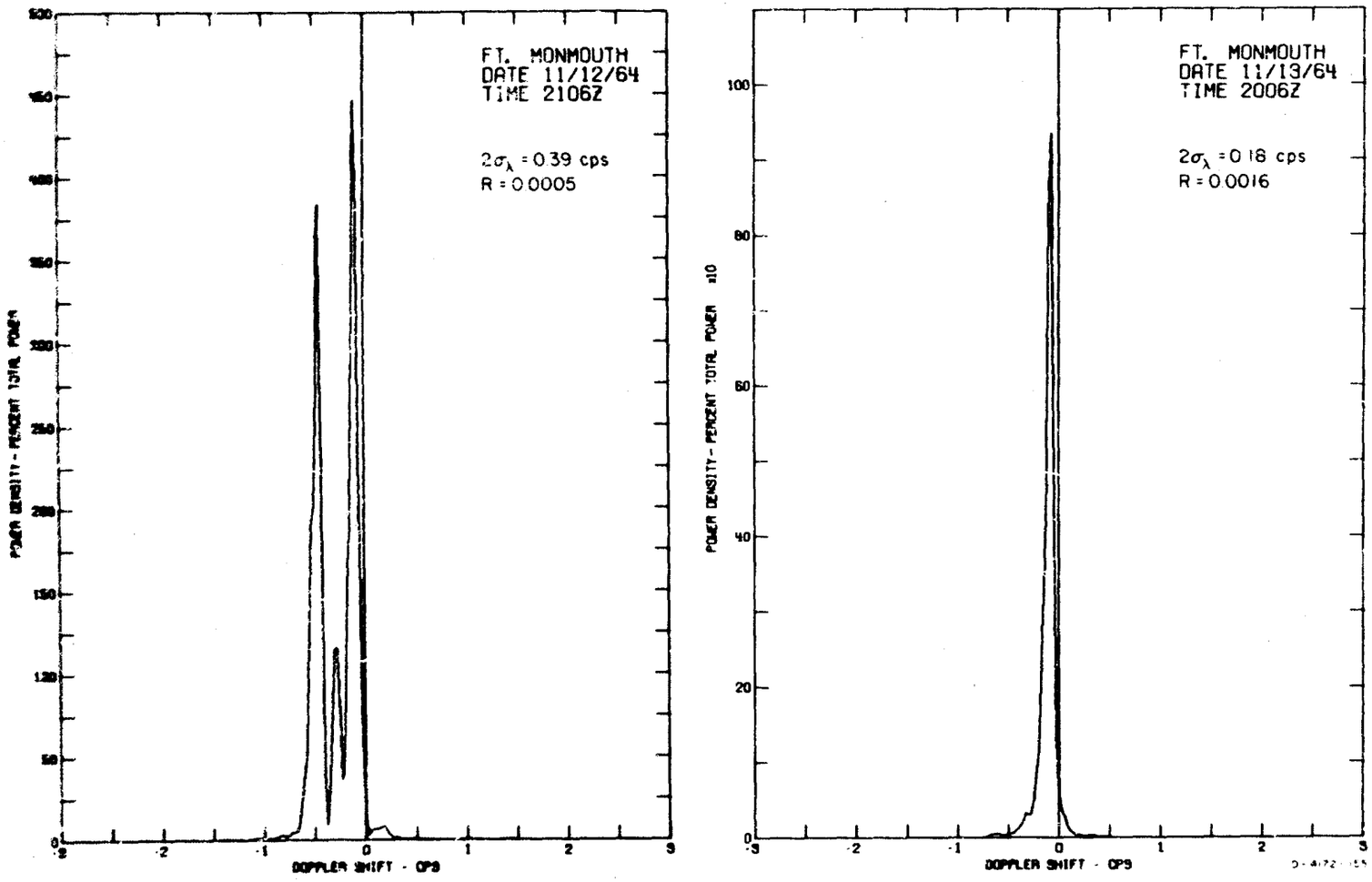

FIG. 44 DOPPLER-FREQUENCY PROFILES

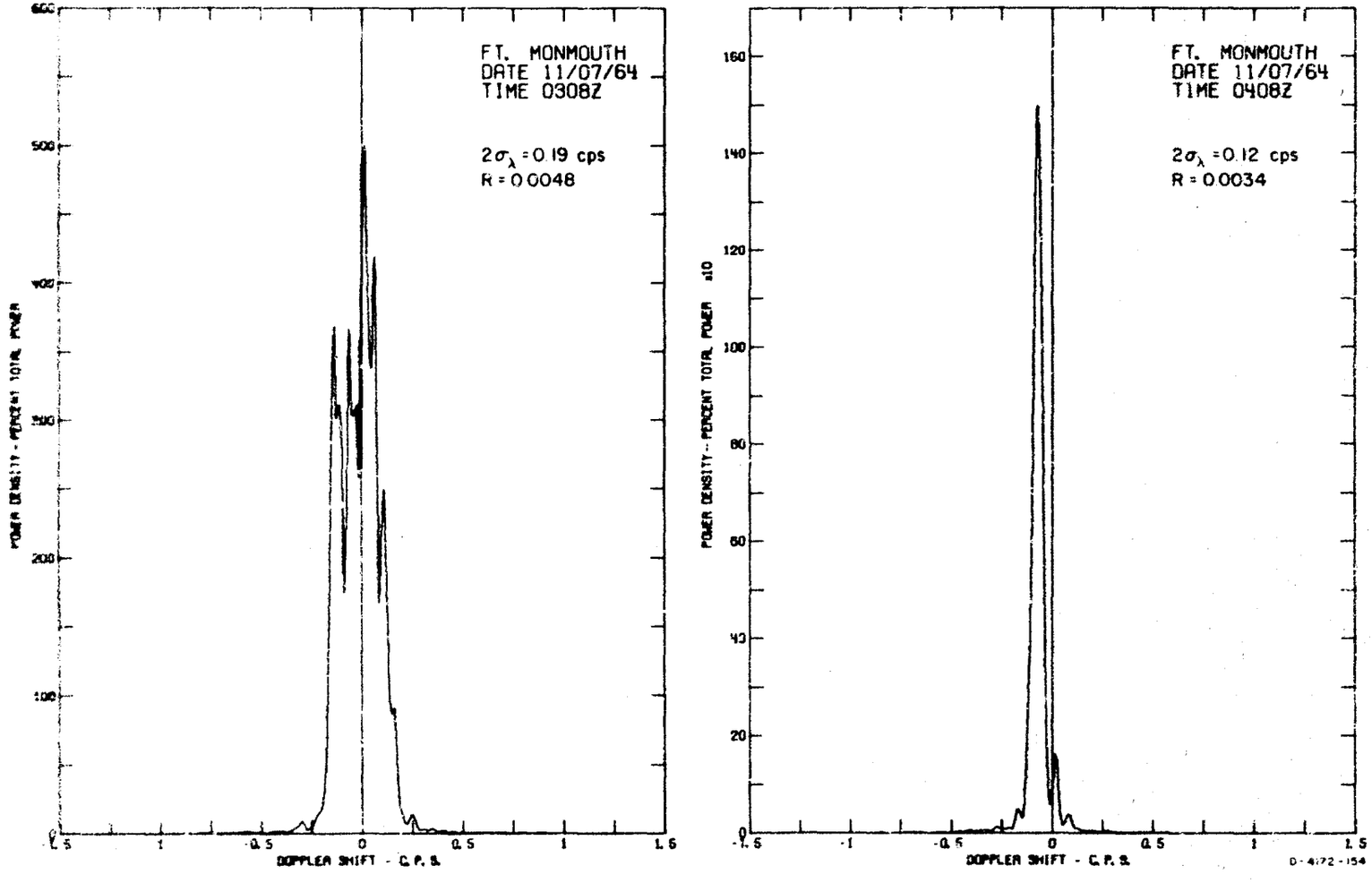

FIG. 45 DOPPLER–FREQUENCY PROFILES

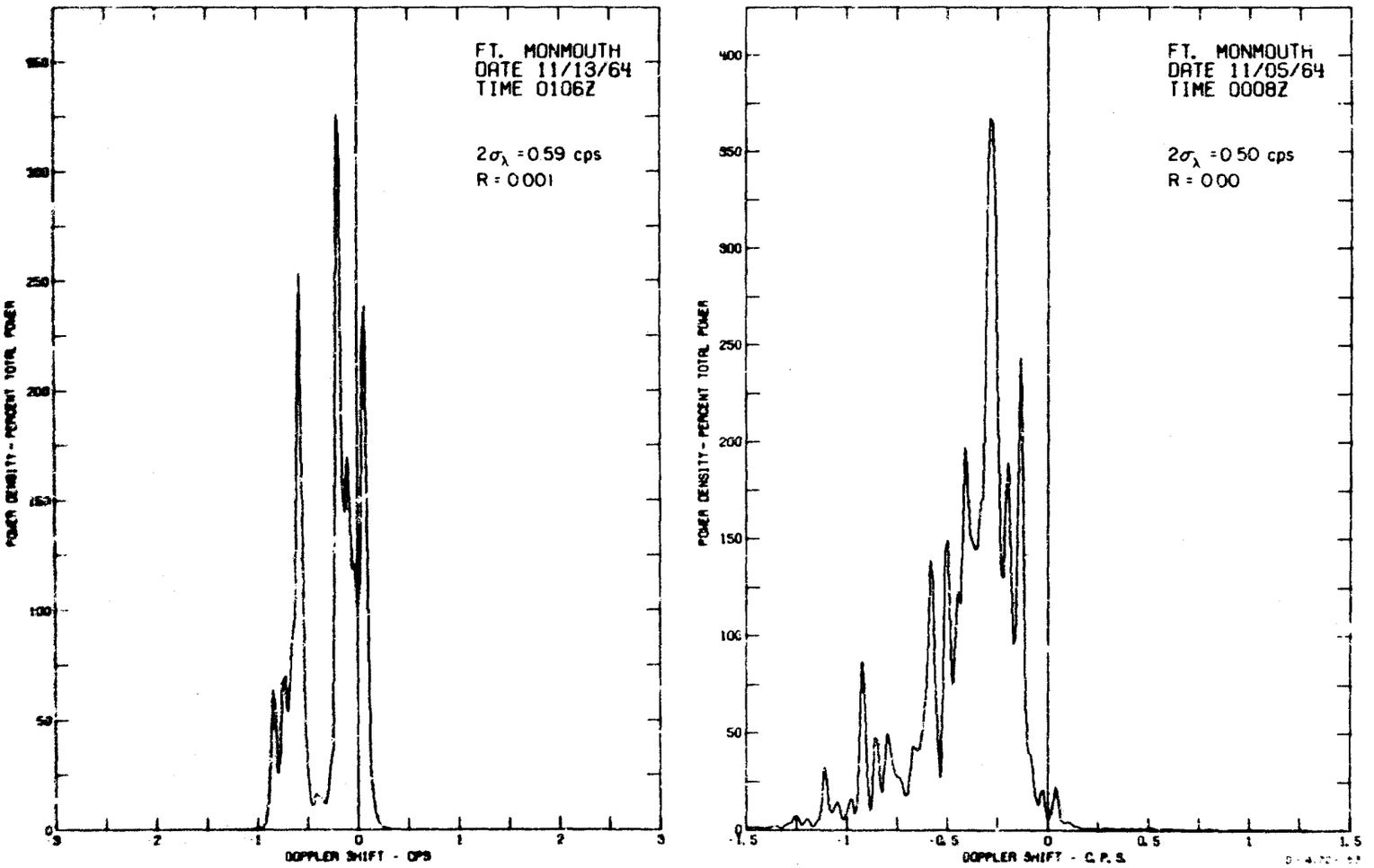

FIG. 46 DOPPLER-FREQUENCY PROFILES

the purpose of this project to generate such an analysis. The purpose of the experiment entailed measuring dispersive effects on the performance of an operational FSK system and comparing these effects with those predicted by the existing theoretical model of an idealized FSK system. The idealized theoretical model was developed in the early stages of a continuing effort which is delving into the complexities of modeling real channels in order to more accurately predict the performance of various communications systems in the presence of arbitrary dispersive conditions. This model serves as a tool that allows the communications engineer to study the effects of a dispersive propagation medium on the performance of a particular FSK system, a tool which, however idealized the system, yields important and useful information about the class of communications systems represented by the theoretical model.

In addition to the problem of adequately modeling the pecularities of a given communication system, the experimental validation of an error-rate analysis is fraught with difficulties when the time- and frequency-selective nature of the channel is modeled. These difficulties are of a practical nature rather than conceptual and concern the validity of the statistical assumptions that are required in the computation of the error probability. For example, it is assumed that the channel transfer function is a homogeneous Gaussian random field[7] on the time-frequency plane, yet this fact was not verified experimentally during the course of the experiment. Such a verification was completely outside the scope of this effort and, indeed, in its entirety would be an unavailing task in the present framework of obtaining approximate answers to an exceedingly complex problem. The various assumptions concerning the statistical behavior of the dispersive mechanisms of the propagation medium are based on physical reasoning and experience with radio channels. These assumptions are general enough to adequately approximate the behavior of a physical radio channel but at the same time simple enough to yield error-rate expressions that can be effectively solved on a large digital computer.

Apart from their use for verifying a theoretical model, which involves comparing measured and predicted results, the measured data, obtained in a carefully planned and executed experiment, are very valuable for assessing the performance of an operational communications system in a dispersive environment. These data can be used to indicate problem areas in the present model and to greatly assist in the development of an improved model.

In addition to the error-rate data, useful measurements of propagation phenomena, such as the time-delay and Doppler-shift profiles of the channel, were obtained.

It is hoped that this preliminary discussion indicates the degree of approximation that is inherent in the formulation and solution of an engineering problem that involves developing a statistical characterization of the dispersive effects of a natural radio channel on a communication system.

2. Data Classification

The basic data obtained in the experiment included estimates of the binary error probability and S/N over a 30-second interval. The data were supplemented with measurements of the channel time-delay and Doppler profiles, which were obtained often enough to follow the important variations of these functions. Hence any binary error probability measured during a 30-second interval was associated with an S/N, a time-delay profile, and a Doppler profile. This experimental procedure made it possible to classify the error-rate data according to time-delay and Doppler spreads. This classification yields an experimental determination of error rate as a function of S/N in which time- and frequency-selective fading effects can be isolated and observed in various degrees and combinations. In addition to being subjected to this classification procedure, the 30-second estimates of binary error probability and S/Ns were also appropriately grouped and averaged so that a minimum of 100 observed errors was obtained in the final estimate of the error rate at any given S/N. This grouping procedure insured the statistical reliability of the resulting estimate of the binary error probability; many of the final error-rate estimates at a given S/N are based on more than 100,000 transmitted bits. The classification and grouping procedures are explained in more detail in Chapter IV, and the statistical reliability of error-rate measurements is considered in Appendix D. The error-rate data were subjected to four different classification procedures; to facilitate reference to the resulting data classes, it is convenient to refer to them with data-class designators as defined by Table II.

Table II

DATA CLASS DESIGNATORS

DATA CLASS DESIGNATOR	DESCRIPTION OF DATA CLASS
A	The class composed of all data in which the measured error rate is a function of S/N only.
TDn	The *n*th of nine classes obtained by classifying the data according to both time-delay and Doppler spread. Each class yields measured error rate as a function of S/N for a particular range of time-delay and Doppler spread.
Tn	The *n*th of three classes obtained by classifying the data according to time-delay spread only. Each class yields measured error rate as a function of S/N for a particular range of time-delay spread independent of the associated Doppler spread.
Dn	The *n*th of three classes obtained by classifying the data according to Doppler spread only. Each class yields measured error rate as a function of S/N for a particular range of Doppler spread independent of the associated time-delay spread.

The range of the second-moment spread measures associated with each of these data classes appears in Table III.

Table III

TIME-DELAY - AND DOPPLER-SPREAD RANGE ASSOCIATED WITH EACH DATA CLASS

DATA CLASS	TIME-DELAY SPREAD ($2\sigma_\tau$) (msec)	DOPPLER SPREAD ($2\sigma_\lambda$) (cps)
A	0 - 1.5	0 - 1
TD1	0 - 0.25	0 - 0.25
TD2	0 - 0.25	0.25 - 0.5
TD3	0 - 0.25	0.5 - 1
TD4	0.25 - 0.75	0 - 0.25
TD5	0.25 - 0.75	0.25 - 0.5
TD6	0.25 - 0.75	0.5 - 1
TD7	0.75 - 1.5	0 - 0.25
TD8	0.75 - 1.5	0.25 - 0.5
TD9	0.75 - 1.5	0.5 - 1
T1	0 - 0.25	0 - 1
T2	0.25 - 0.75	0 - 1
T3	0.75 - 1.5	0 - 1
D1	0 - 1.5	0 - 0.25
D2	0 - 1.5	0.25 - 0.5
D3	0 - 1.5	0.5 - 1

The range of spreads associated with Data Class A indicates the relatively low second-moment spreads observed on the channel during the course of the experiment. A channel displaying a greater variation in the spread

measures would have been more suitable for the experiment; however, the variations of the observed spread values were sufficient to cause a detectable sensitivity of system performance to time- and frequency-selective fading phenomena.

3. Error-Rate Data

The results of classifying the error-rate data according to the four preceding classification procedures are presented and discussed in this section. Measured error rate is plotted as an X on the corresponding theoretical error-rate curve. The theoretical error-rate curves are computed for a transition time equal to 0.02 of the signaling-element duration, which would be 200 μsec for a 10-msec signaling element. This choice of transition time was based on a rough measurement performed on the actual transmitting equipment with a special wide-band discriminator. All measured data are for the no-diversity case with a 10-msec signaling-element duration. A limited amount of dual-diversity data was processed; these data are presented in Chapter VII.

a. DATA CLASS A

All measured error-rate data, without regard to time-delay or Doppler spread, are plotted as a function of S/N in Fig. 47. The theoretical error-rate curve of Fig. 47 was computed for two equal-strength paths with a time-delay spread of 1 msec and a Doppler spread of 1 cps, which are typical of the spreads observed on this channel. The relatively smooth variation of measured error rate with S/N is indicative of the degree of statistical reliability achieved by the experiment. Figure 47 illustrates the important and interesting "bottoming-out" characteristic generally displayed by the measured error-rate data: the measured error rate ceases to decrease with increasing S/N and essentially maintains a constant irreducible value at high S/Ns, as predicted by the theoretical model.

The close agreement between the measured error rate of Data Class A and the theoretical error rate indicates that the theoretical model yields a good approximation to the *average* performance of the experimental system over the range of time-delay and Doppler spreads observed on the channel. It is to be stressed that Fig. 47 is concerned with comparing the measured performance of the experimental system averaged over all dispersive states of the channel with a theoretical curve based on the average state of the channel. Close agreement between

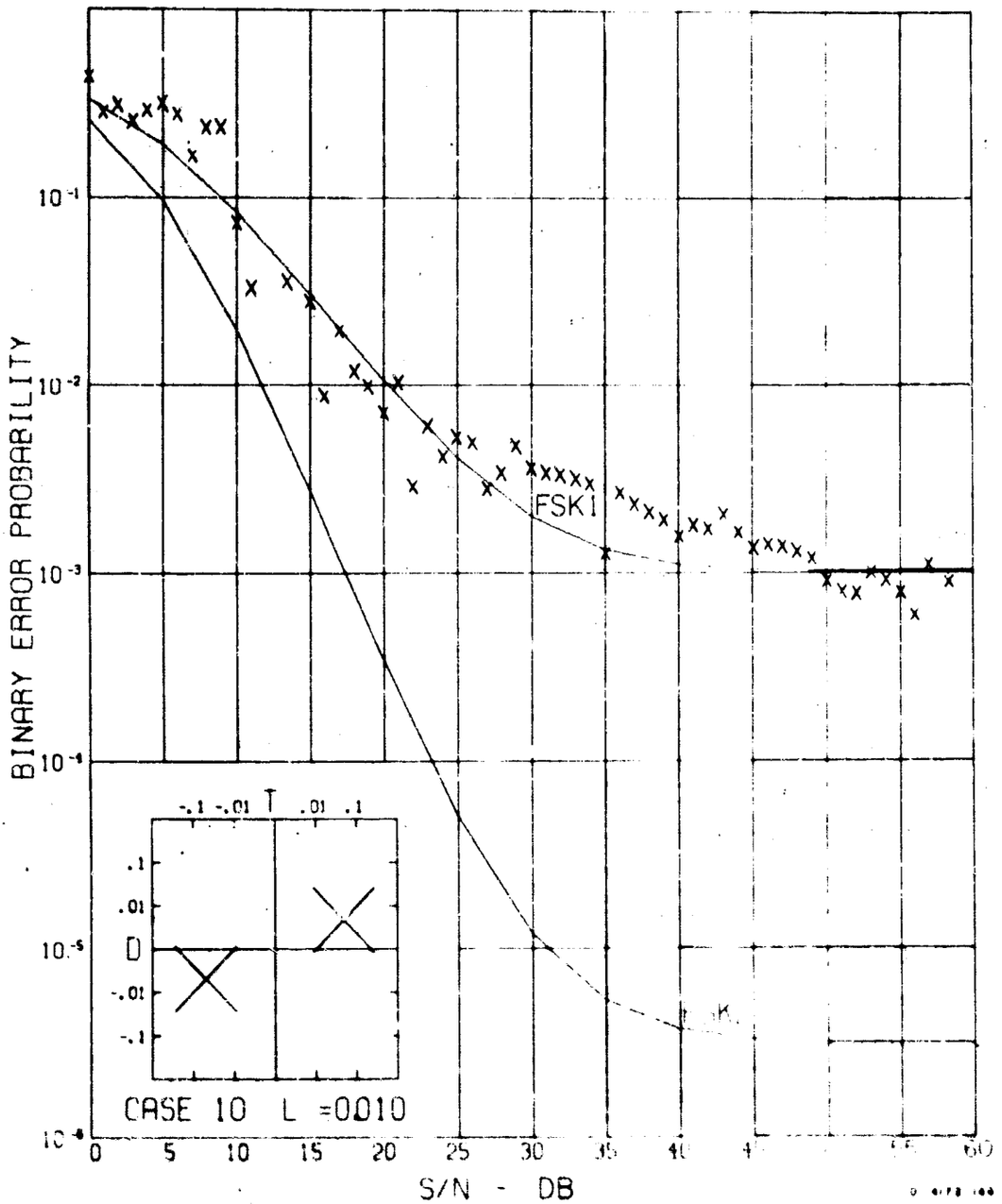

FIG. 47 DATA CLASS A — ALL DATA

measured and theoretical results in this case does not necessarily imply that close agreement will be obtained when measured and theoretical error rates are compared for a particular dispersive state of the channel. Although a Doppler spread of 1 cps was the maximum observed, the theoretical error-rate curves of Fig. 47 are essentially determined by the time-delay spread and transition time and would not display a discernible difference when computed for a zero Doppler spread.

b. DATA CLASSES TD1 THROUGH TD9

The results of classifying the data according to both time-delay and Doppler spread are plotted in Figs. 48 through 55. It is interesting to observe that no data were found in Data Class TD7, which corresponds to the combination of maximum time-delay spread and minimum Doppler spread. In other words, during the course of the experiment, minimum Doppler spreads were not observed when the time-delay spread was maximum. The theoretical error-rate curve associated with each data class was computed for two equal-strength paths possessing a time-delay spread and a Doppler spread equal to the maximum time-delay spread and Doppler spread of the data class plotted on the curve.

Observe that the theoretical error-rate curves associated with Data Classes TD1 through TD6 (minimum and median observed time-delay spreads) are essentially identical and those associated with Data Classes TD8 and TD9 (maximum observed time-delay spreads) are essentially identical. Hence, the theoretical model is relatively insensitive to variations of time-delay and Doppler spread in the range of spreads observed on the channel.

The measured error rate is these classes illustrates the bottoming-out phenomenon; what is more important, this phenomenon can now be observed as a function of time-delay and Doppler spread. The most striking and important characteristic of the measured error-rate data is the evident sensitivity of the experimental system to time- and frequency-selective fading phenomena, notwithstanding the predicted insensitivity of the theoretical model within the range of spreads observed on the channel.

There is reasonable agreement between the measured data and the theoretical error-rate curves for the median time-delay classes (TD4, TD5, and TD6). The error-rate data associated with data classes TD1,

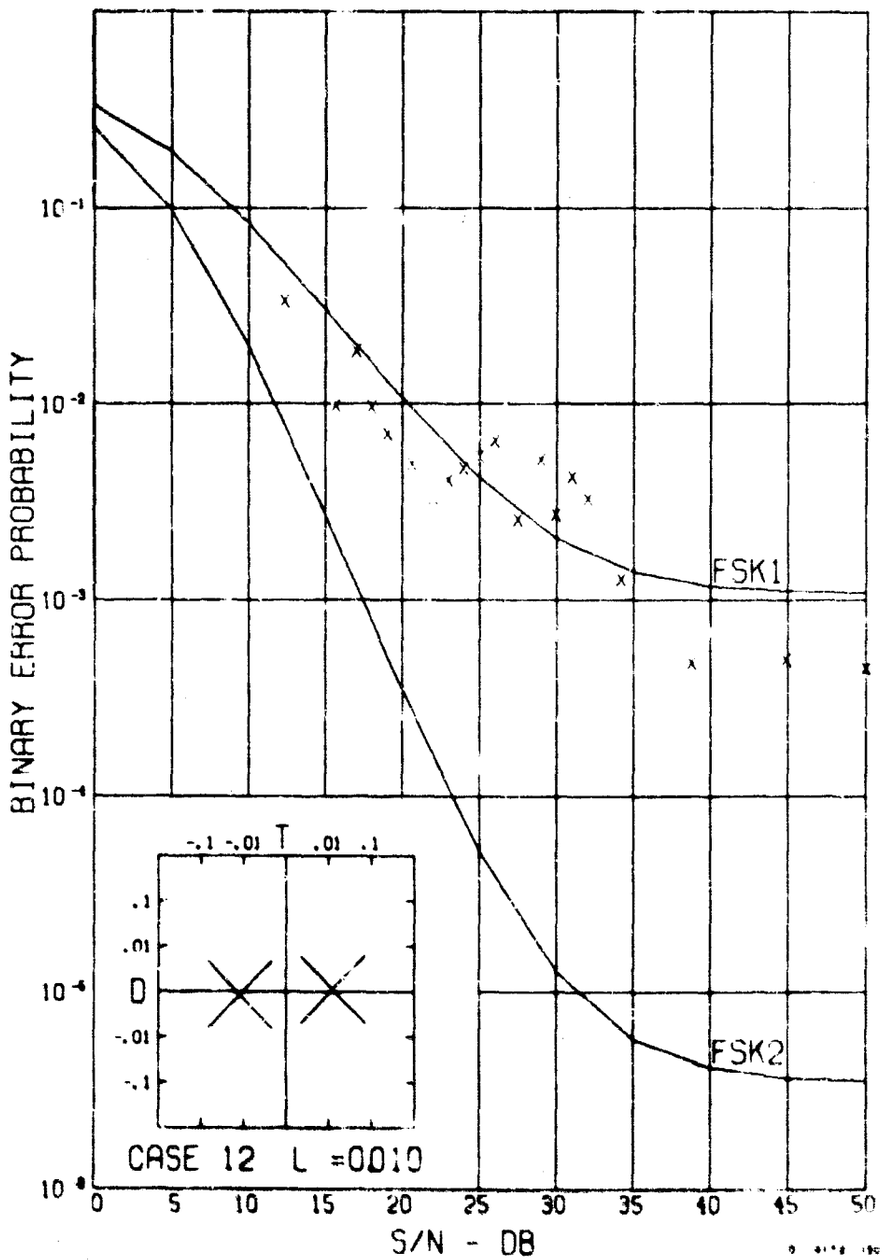

FIG. 48 DATA CLASS TD1 — 0 2·. 0.25, 0 2·\ 0.25

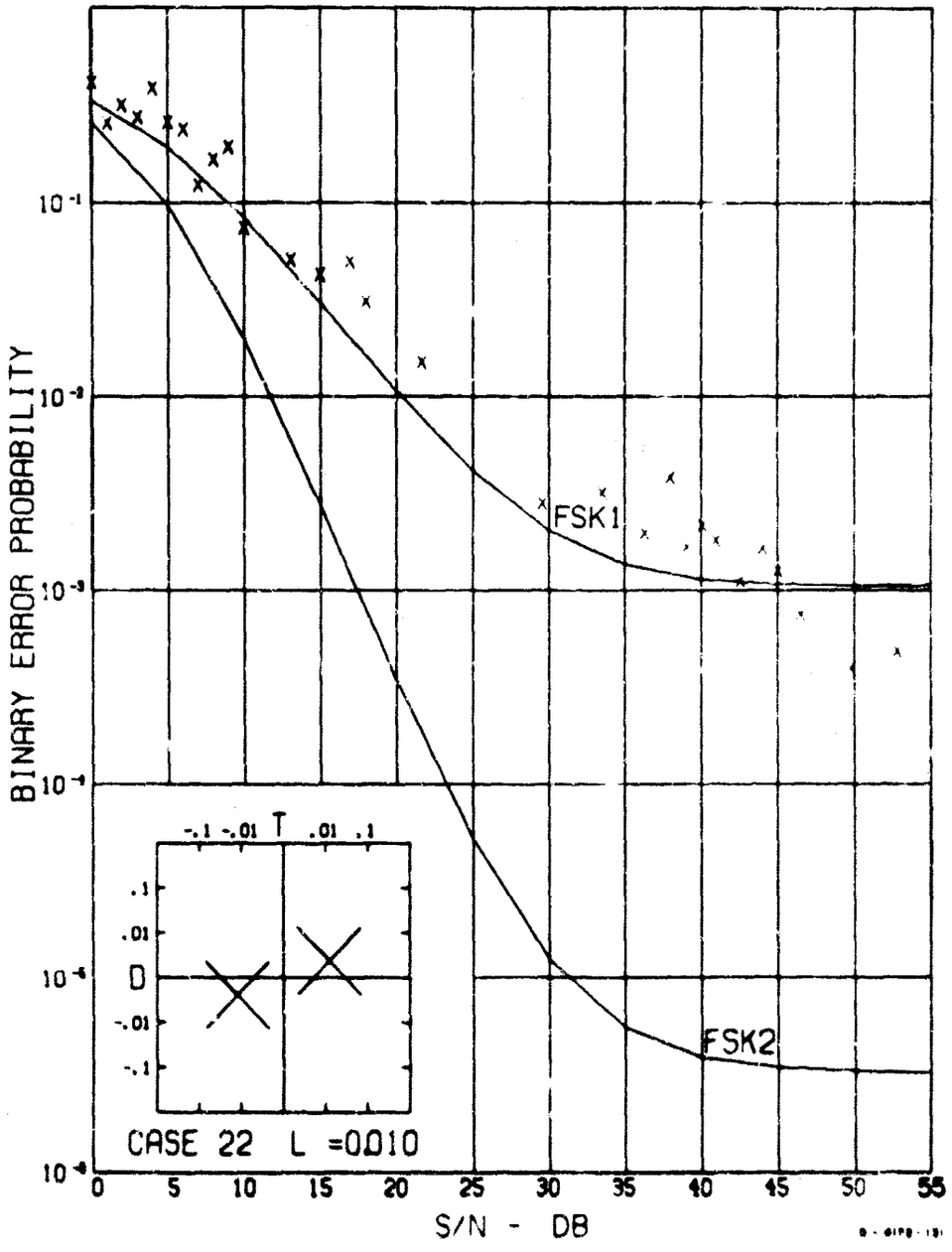

FIG. 49 DATA CLASS TD2 — 0 · $2\nu_p$ · 0.25; 0.25 ν_A · 0.5

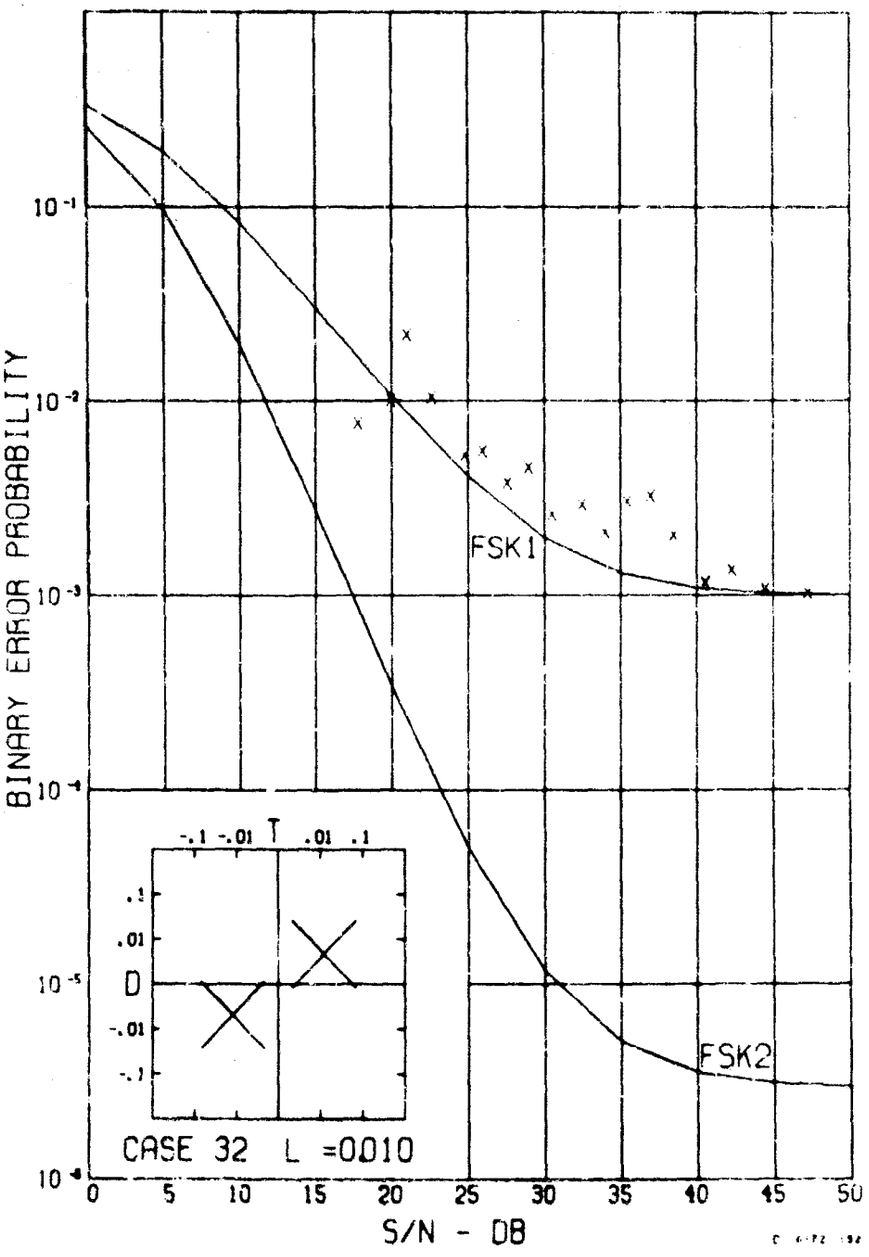

FIG. 50 DATA CLASS TD3 — 0 2ν, 0.25, 0.5 2ν, 1.0

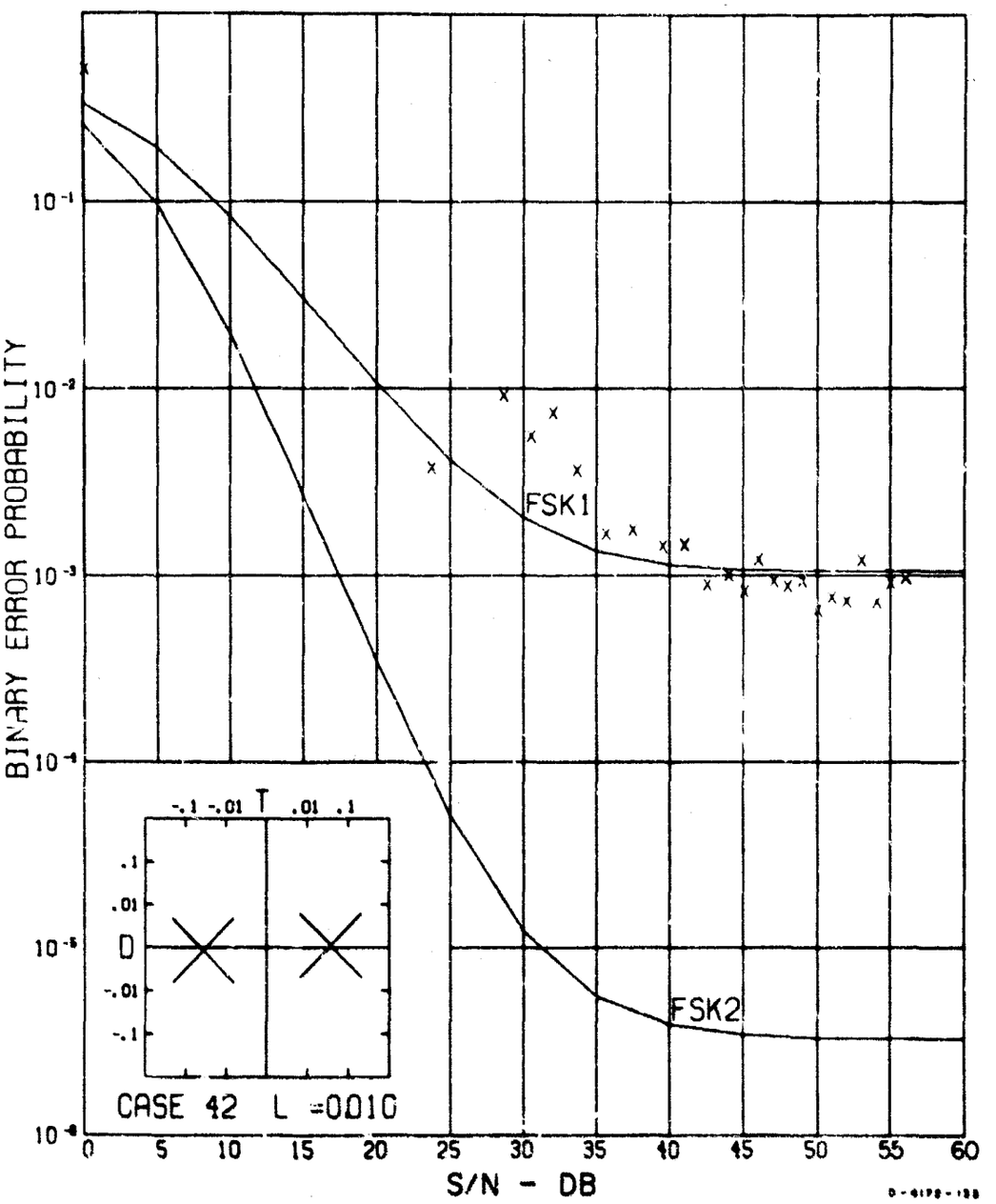

FIG. 51 DATA CLASS TD4 — $0.25 \leq 2\sigma_\tau \leq 0.75$; $0 \leq 2\sigma_\lambda \leq 0.25$

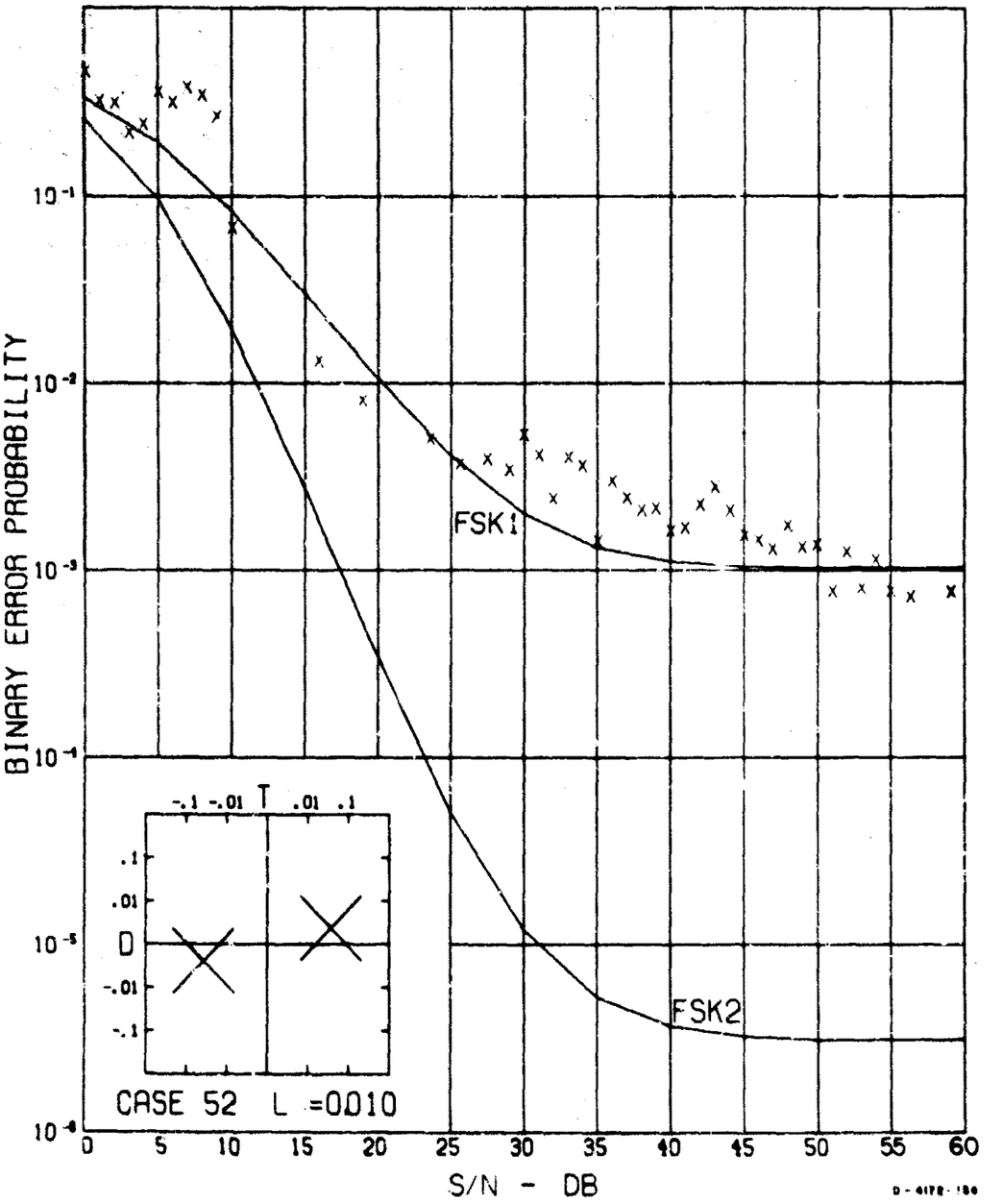

FIG. 52 DATA CLASS TD5 — $0.25 < 2\sigma_r < 0.75$; $0.25 < 2\sigma_\lambda < 0.5$

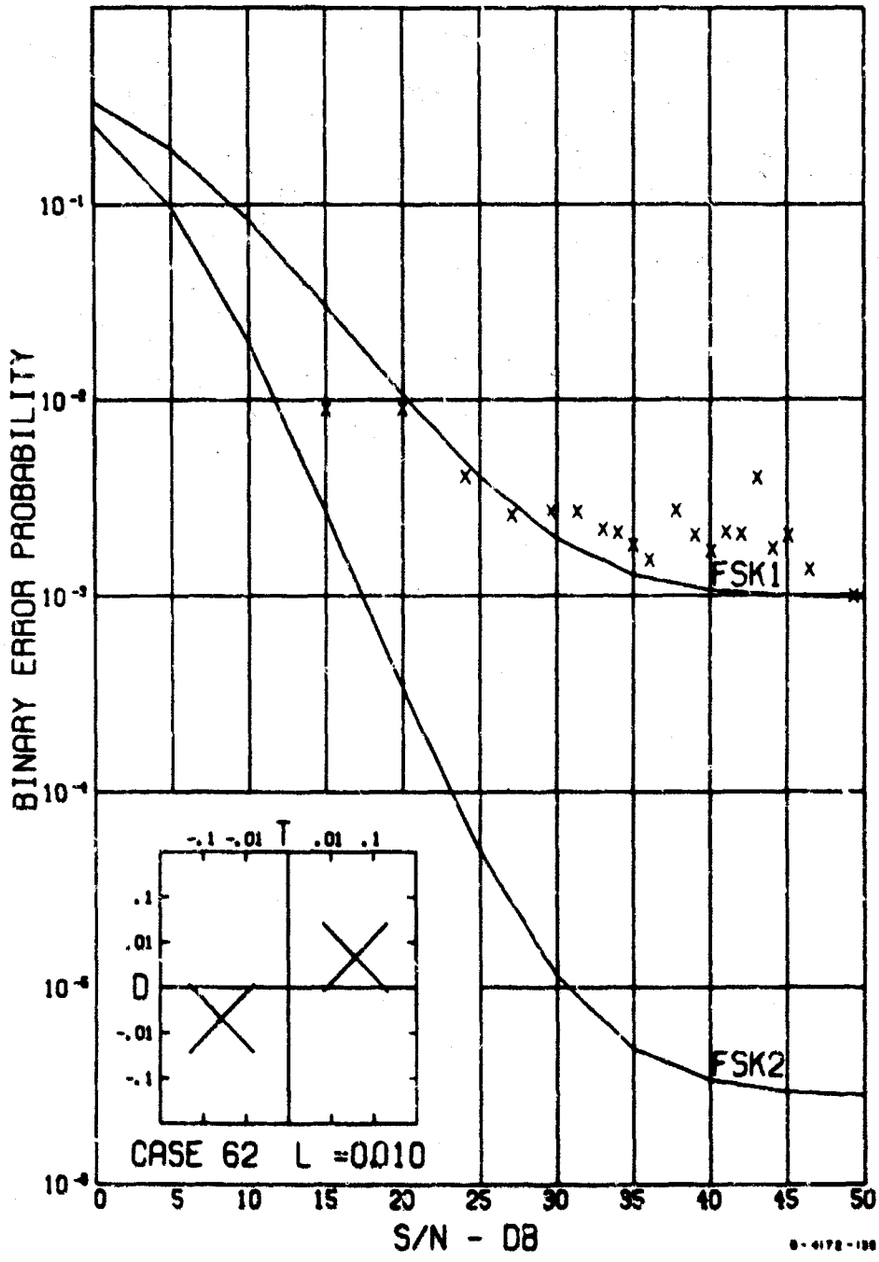

FIG. 53 DATA CLASS TD6 — $0.25 < 2\sigma_r < 0.75$; $0.5 < 2\sigma_\lambda < 1.0$

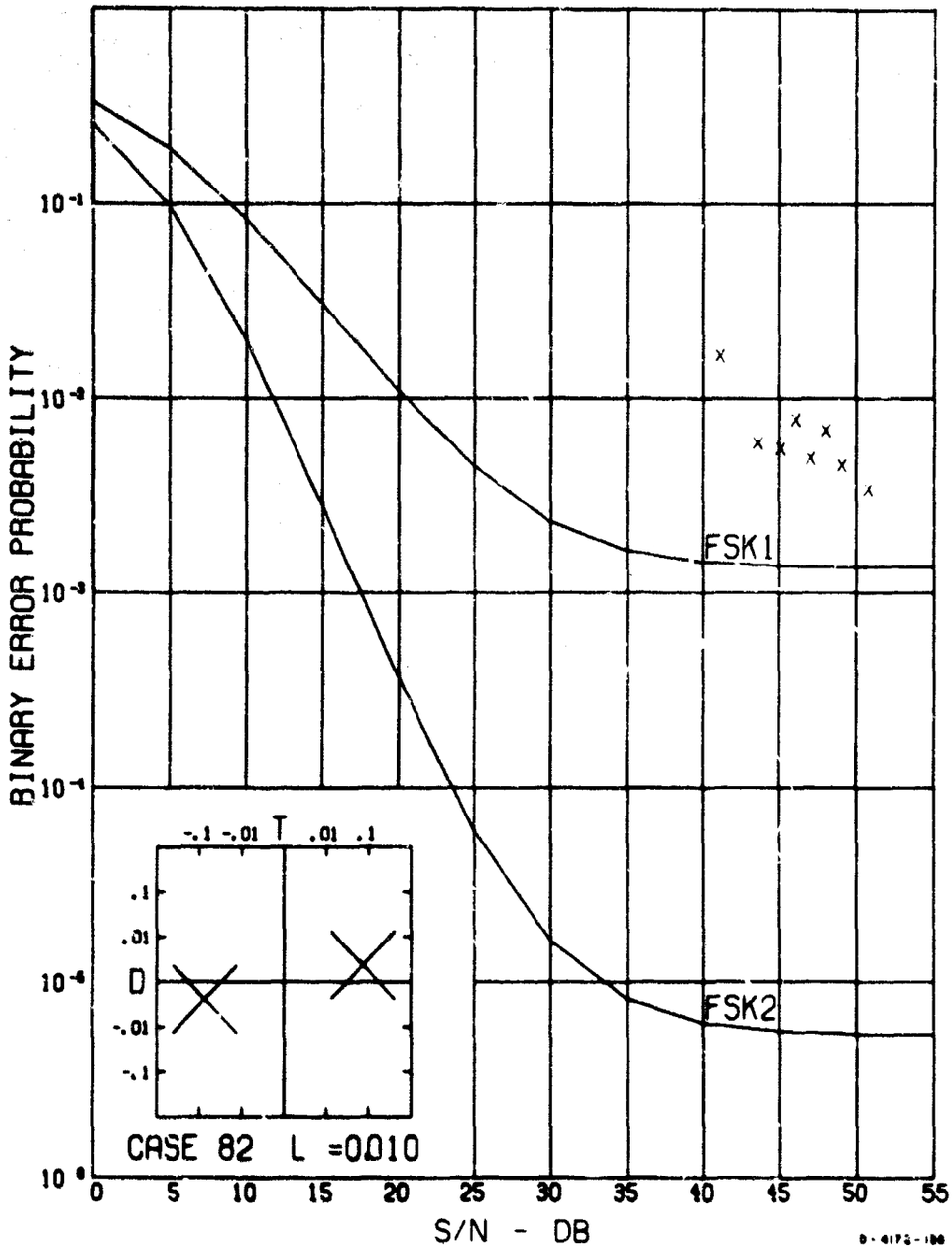

FIG. 54 DATA CLASS TD8 — $0.75 < \hat{\tau}_r < 1.5$; $0.25 < 2\sigma_\lambda < 0.5$

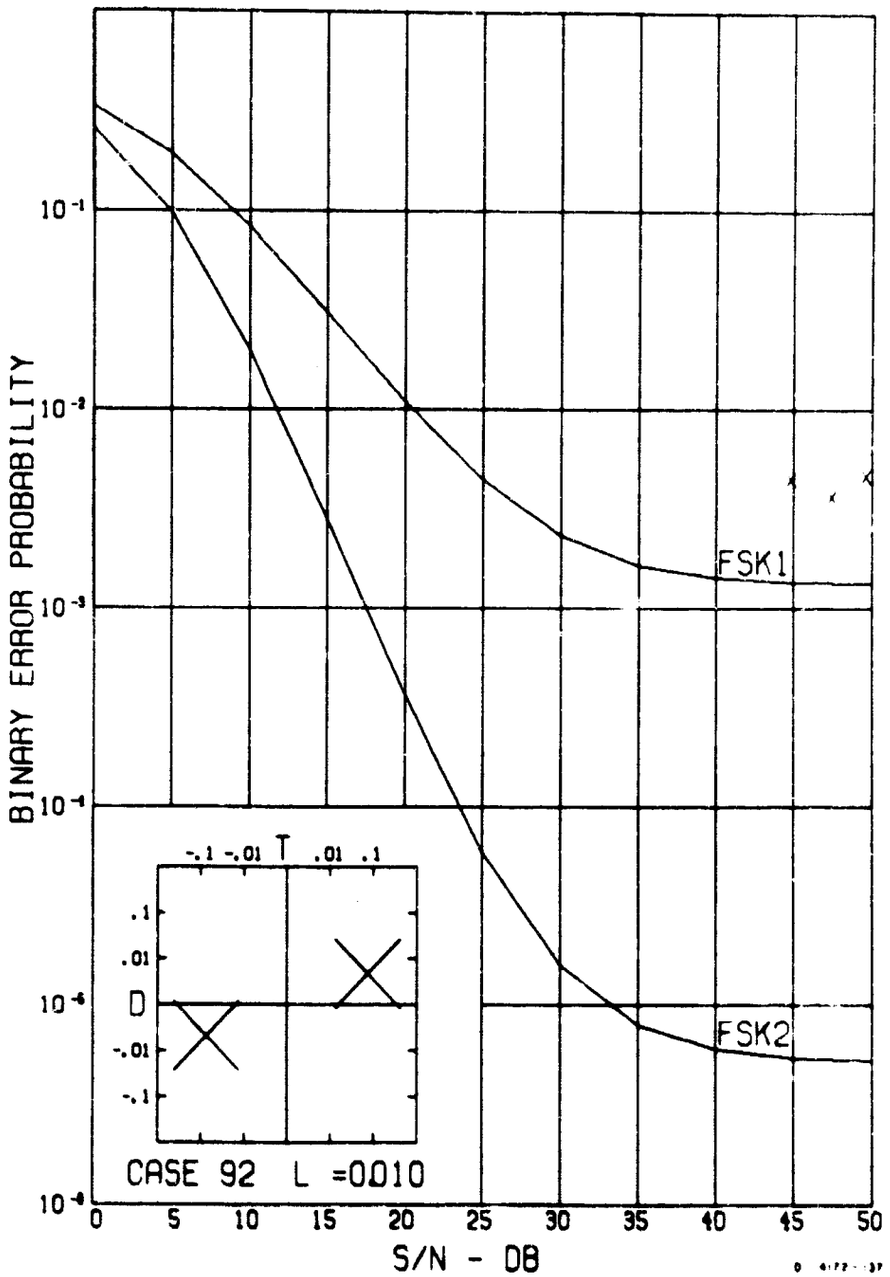

FIG. 55 DATA CLASS TD9 — $0.75 < 2\sigma_\tau < 1.5$; $0.5 < 2\sigma_\lambda < 1.0$

TD8, and TD9 indicate definite departures from the theoretical model. Data Class TD1 is the minimum time-delay-spread and minimum Doppler-spread class; TD8 is the maximum time-delay-spread and median Doppler-spread class; and TD9 is the maximum time-delay-spread and maximum Doppler-spread class.

It is interesting to note that the measured irreducible error probability for Data Class TD1 is lower than that predicted by the theoretical model. The theoretical model bottoms out at an error probability of approximately 1×10^{-3}, whereas the measured data of TD1 display a definite bottoming out at an error probability of 5×10^{-4}. Since a complete analysis of the experimental system is not available, we are not in a position to give exact technical reasons for this departure; however, in view of the differences between the experimental system and the theoretical model which have been discussed, such departures are not surprising. It is significant that the measured irreducible error probability is lower than the predicted irreducible error probability for the data class corresponding to the *minimum* observed time-delay and Doppler spreads, which implies that the experimental system is more effective than the theoretical model in combating a small amount of time- and frequency-selective fading.

On the other hand, the irreducible error probability indicated by the measured data of Data Class TD9 is approximately 4.2×10^{-3}, whereas the theoretical model bottoms out at approximately 1.5×10^{-3}. Hence, the irreducible error probability for the experimental system is higher than the irreducible error probability predicted by the theoretical model for the maximum observed time-delay and Doppler spreads. This indicates that the experimental system is less effective than the theoretical model in combating the degree of time- and frequency-selective fading associated with the maximum observed time-delay and Doppler spreads.

The fact that the experimental system shapes and smooths the time and frequency characteristics of the received signal pulses to a greater degree than does the incoherent matched-filter model is probably responsible for the superior performance of the experimental system for small amounts of time- and frequency-selective fading. Roughly speaking, appropriate shaping of the time structure of the received pulses would aid in combating frequency-selective (time-delay) effects, and appropriate shaping of the frequency structure of the received pulses would aid in combating the time-selective (Doppler) effects.

To continue this speculative reasoning, it is plausible that, as the degree of selective fading on the channel increases, a point is reached where the energy-quenching property of the theoretical model accounts for its superiority at the more severe observed time- and frequency-selective fading conditions. In other words, the performance of the experimental system is hindered by the possibility of an unequal bias condition in which the stored energies in the mark and space filters are different enough to cause a deterioration in detection capability. Observe that frequency-selective fading can cause one of the signaling frequencies to be in a fade over several signaling elements; the resulting difference in stored energy in the two filters will intensify the detrimental effects of frequency-selective fading.

Finally, to complete this speculative picture, it is reasonable to assume that the two opposing effects discussed above may have compensated for each other, so that when all of the data were plotted without regard to the dispersive state of the channel (Data Class A) a reasonably good fit with the theoretical curve was obtained.

The measured irreducible error rate as a function of time-delay and Doppler spread is plotted in Figs. 56 and 57, respectively. The three measured points of irreducible error probability as a function of time-delay spread were derived from Data Classes TD2, TD5, and TD8; similarily, the three measured points of irreducible error probability as a function of Doppler spread were derived from Data Classes TD1, TD2, and TD3. The theoretical irreducible error probability curves for no diversity and for dual diversity are also plotted in these figures. Comparison of the theoretical and measured curves of irreducible error probability emphasizes the greater sensitivity of the experimental system to time- and frequency-selective fading effects. Observe that the experimental system displays a bottoming-out effect at the low spread values which is in agreement with the transition-time bottoming out predicted by the theoretical model.

c. DATA CLASSES T1, T2, AND T3

The results of classifying the error-rate data according to minimum, median, and maximum observed time-delay spread (Data Classes T1, T2, and T3) without regard to Doppler spread are plotted in Figs. 58, 59, and 60 respectively.

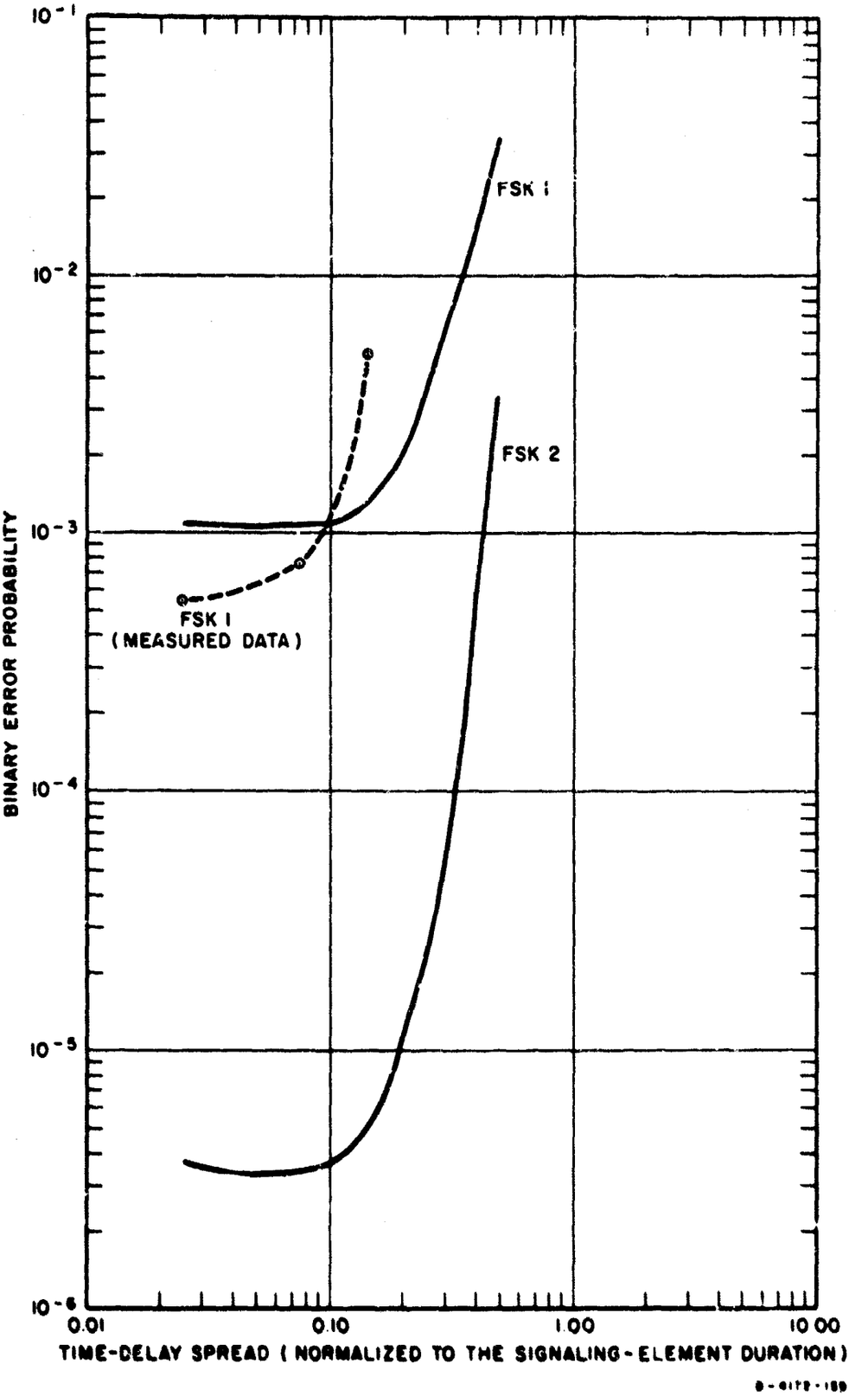

FIG. 56 MEASURED IRREDUCIBLE ERROR PROBABILITY AS A FUNCTION OF TIME-DELAY SPREAD

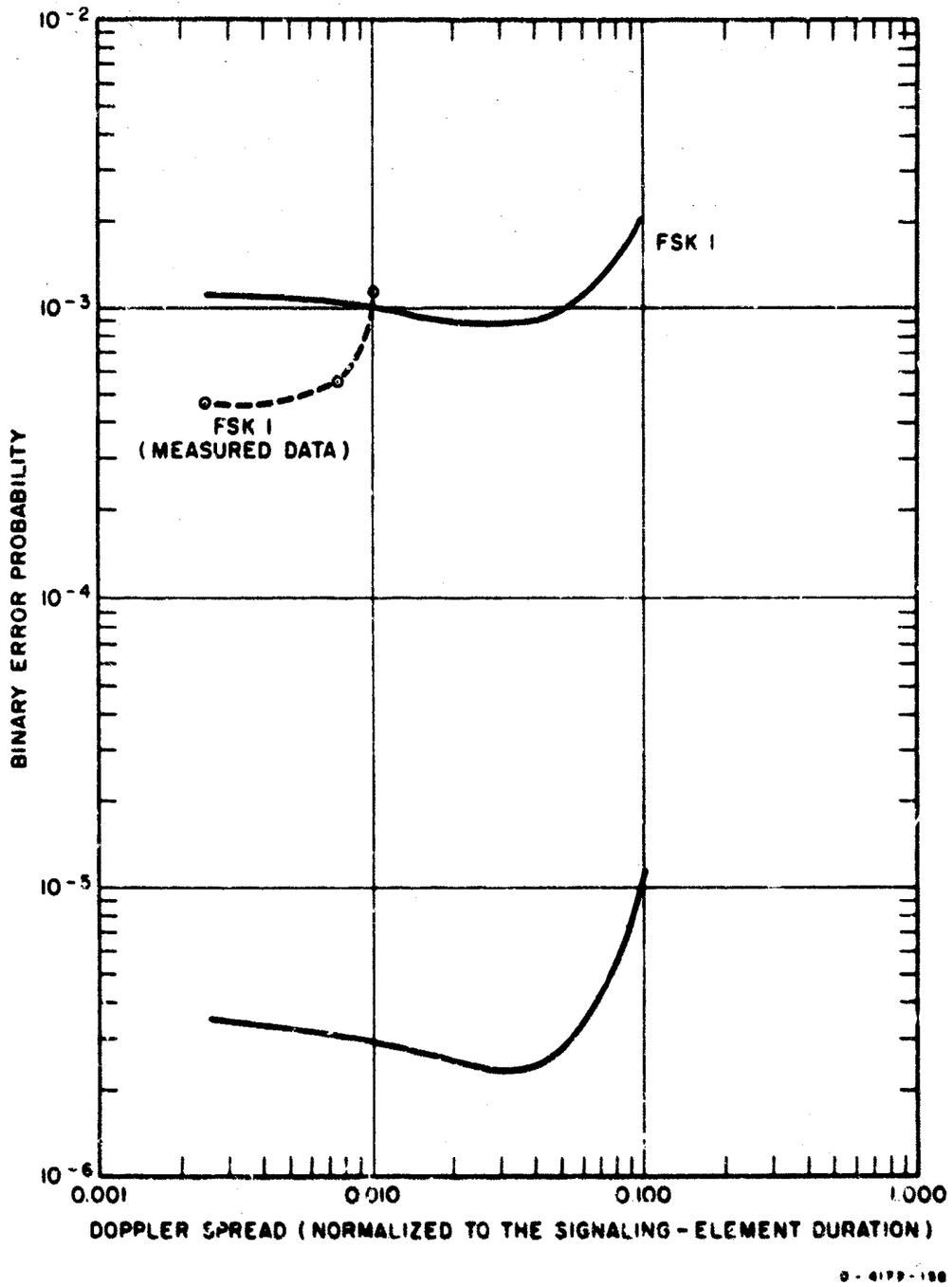

FIG. 57 MEASURED IRREDUCIBLE ERROR PROBABILITY AS A FUNCTION OF DOPPLER SPREAD

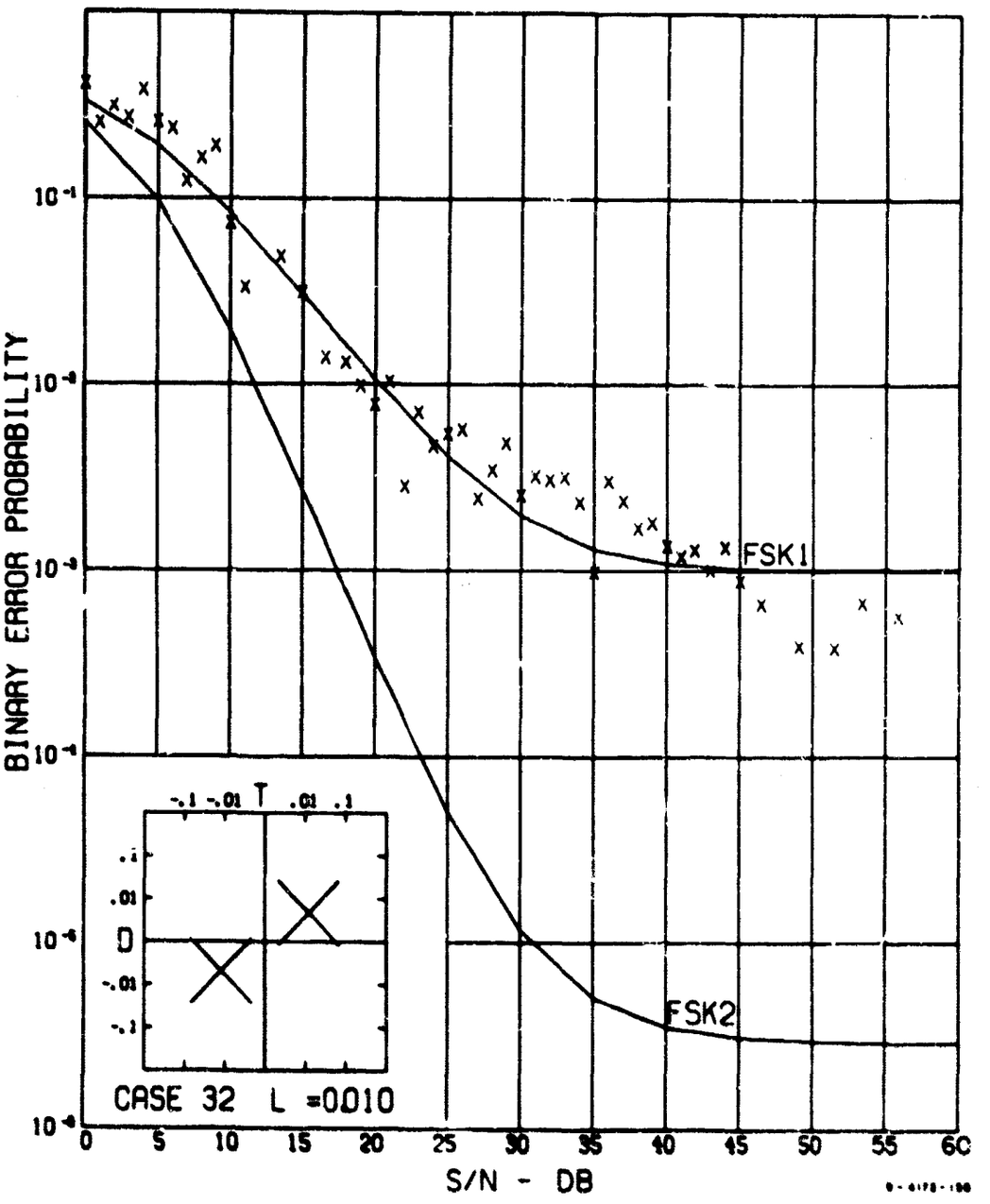

FIG. 58 DATA CLASS T1 — $0 < 2\sigma_r < 0.25$; $0 < 2\sigma_\lambda < 1.0$

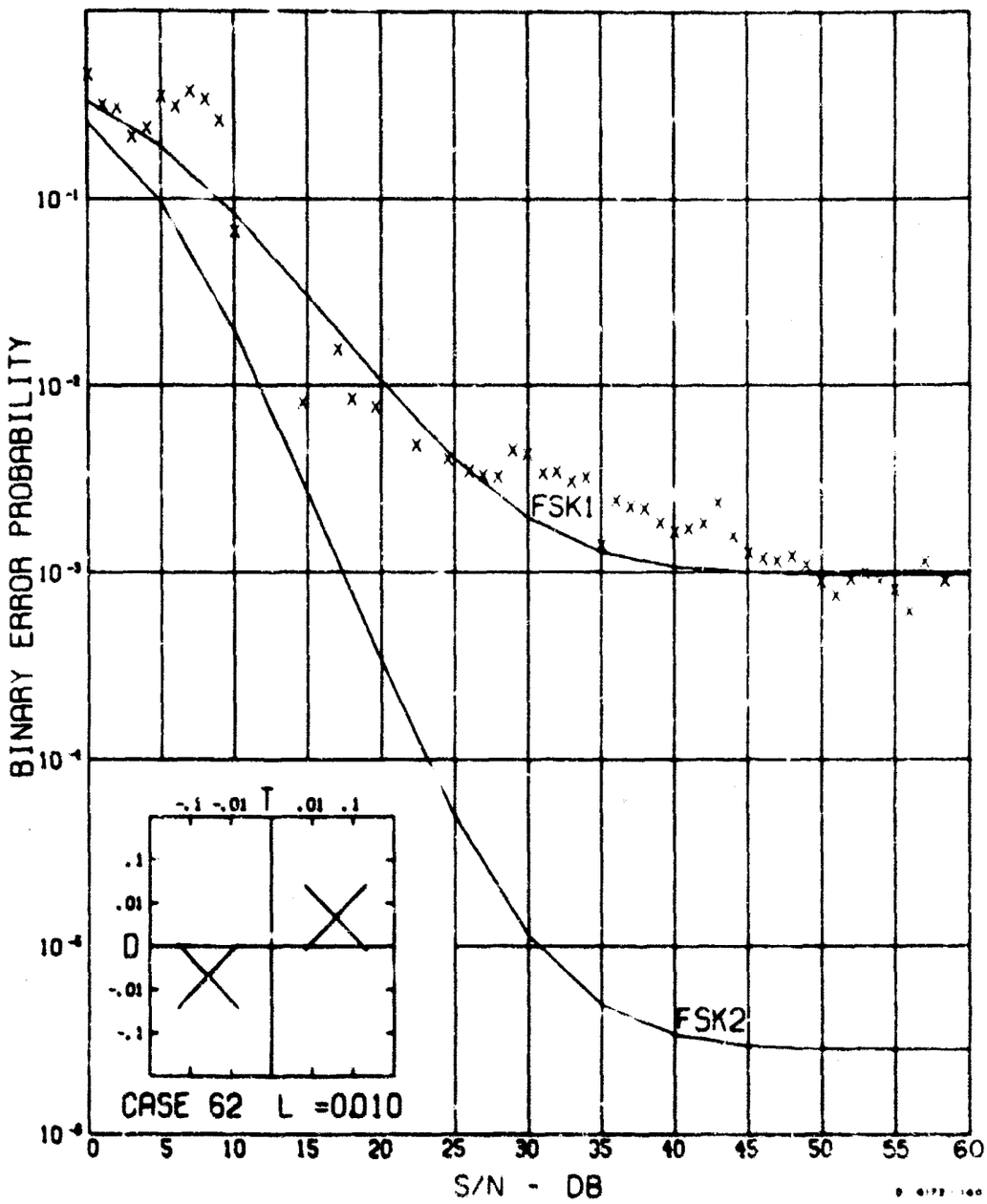

FIG. 59 DATA CLASS T2 — 0.25 $2\sigma_r$ 0.75. 0 $2\sigma_A$ 1.0

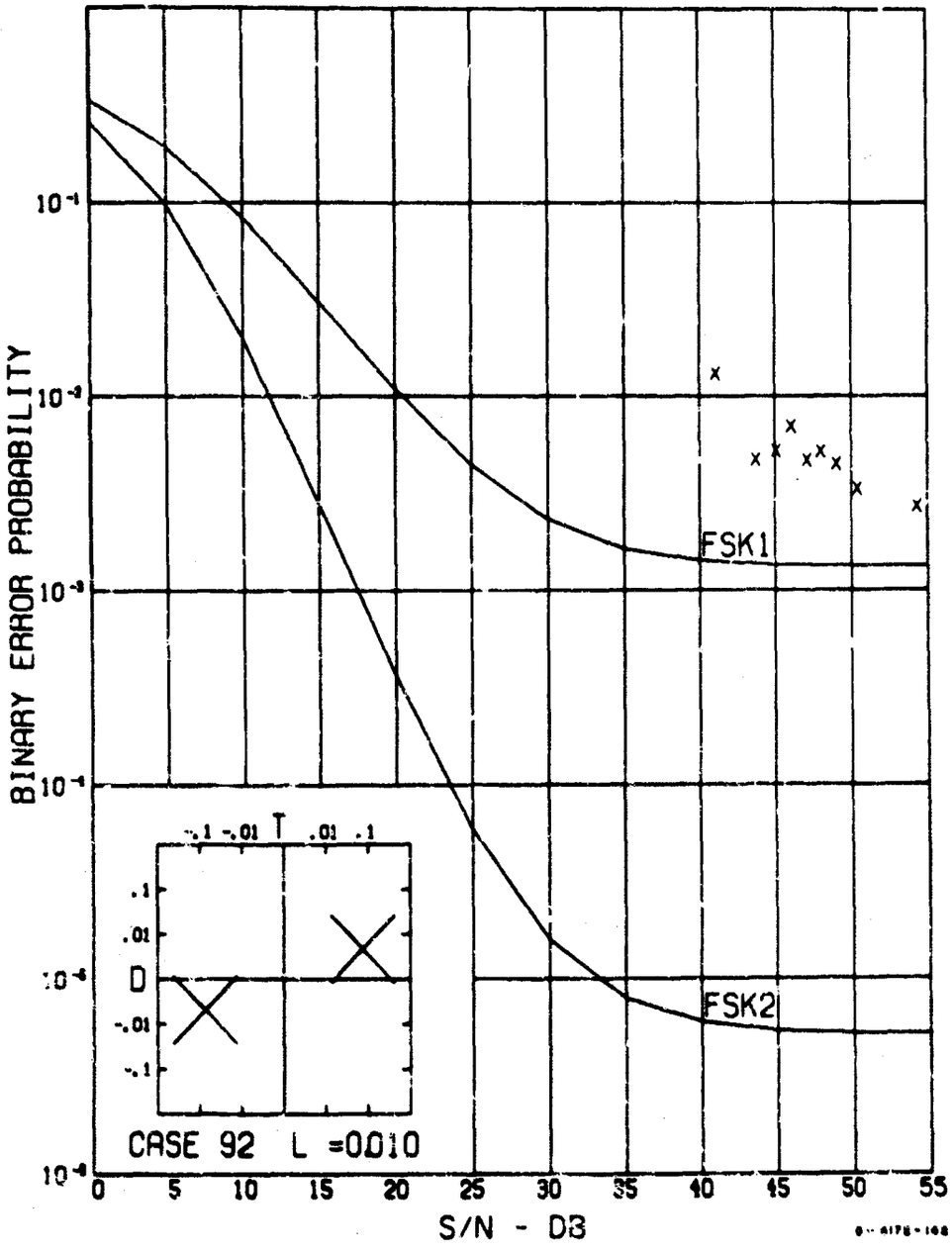

FIG. 60 DATA CLASS T3 — $0.75 < 2\sigma_r < 1.5$; $0 < 2\sigma_\lambda < 1.0$

The best fit of measured data with the theoretical curve is obtained for Data Class T2 (the median time-delay-spread class); departures between the measured and theoretical irreducible error probability are observed in the low and high time-delay-spread classes. The measured data display the same behavior observed in the previous classification procedure and emphasize the sensitivity of the performance of the experimental system to frequency-selective effects. The irreducible error probability measured for Data Class T3 is approximately ten times that measured for Data Class T1. This is an impressive variation of error rate for the relatively small variation of time-delay spread associated with the two data classes.

d. DATA CLASSES D1, D2, AND D3

The results of classifying the error-rate data according to minimum, median, and maximum observed Doppler spread (Data Classes D1, D2, and D3) without regard to time-delay spread are plotted in Figs. 61, 62, and 63

It is interesting to observe that the experimental data display a definite detectable sensitivity to Doppler spread. For the range of Doppler spread observed on the channel, the theoretical model is not sensitive to time-selective effects, since the frequency-selective and transition-time effects are the major contributing factors affecting the performance of the theroretical model for the range of observed time-delay and Doppler spreads. However, the measured irreducible error probability of Data Classes D1, D2, and D3, indicates a small but definite time-selective sensitivity.

C. EXPERIMENT REVIEW

The experience obtained from conducting such a complex experiment as this naturally suggests improvements that could be made if the experiment were repeated. Some suggestions are offered for possible future reference:

(1) *Record all raw data automatically and directly in a computer-compatible input medium.* Many processing problems that caused delays were directly traceable to errors in the manual recording of data, for example, mispunched data cards and omitted log entries. A small sample of erroneous data can significantly bias the results in such an experiment.

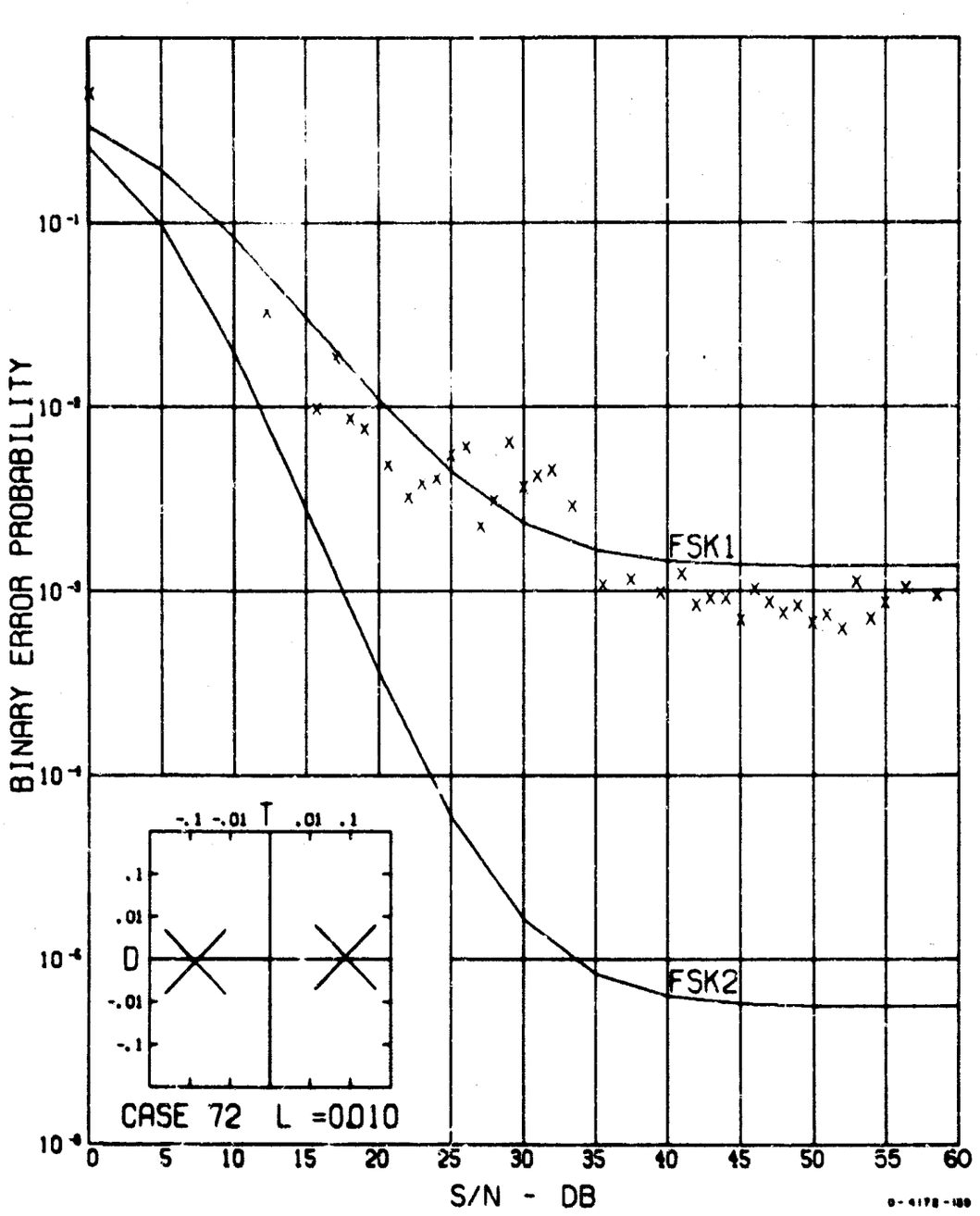

FIG. 61 DATA CLASS D1 — $0 < 2\sigma_r < 1.5$; $0 < 2\sigma_\lambda < 0.25$

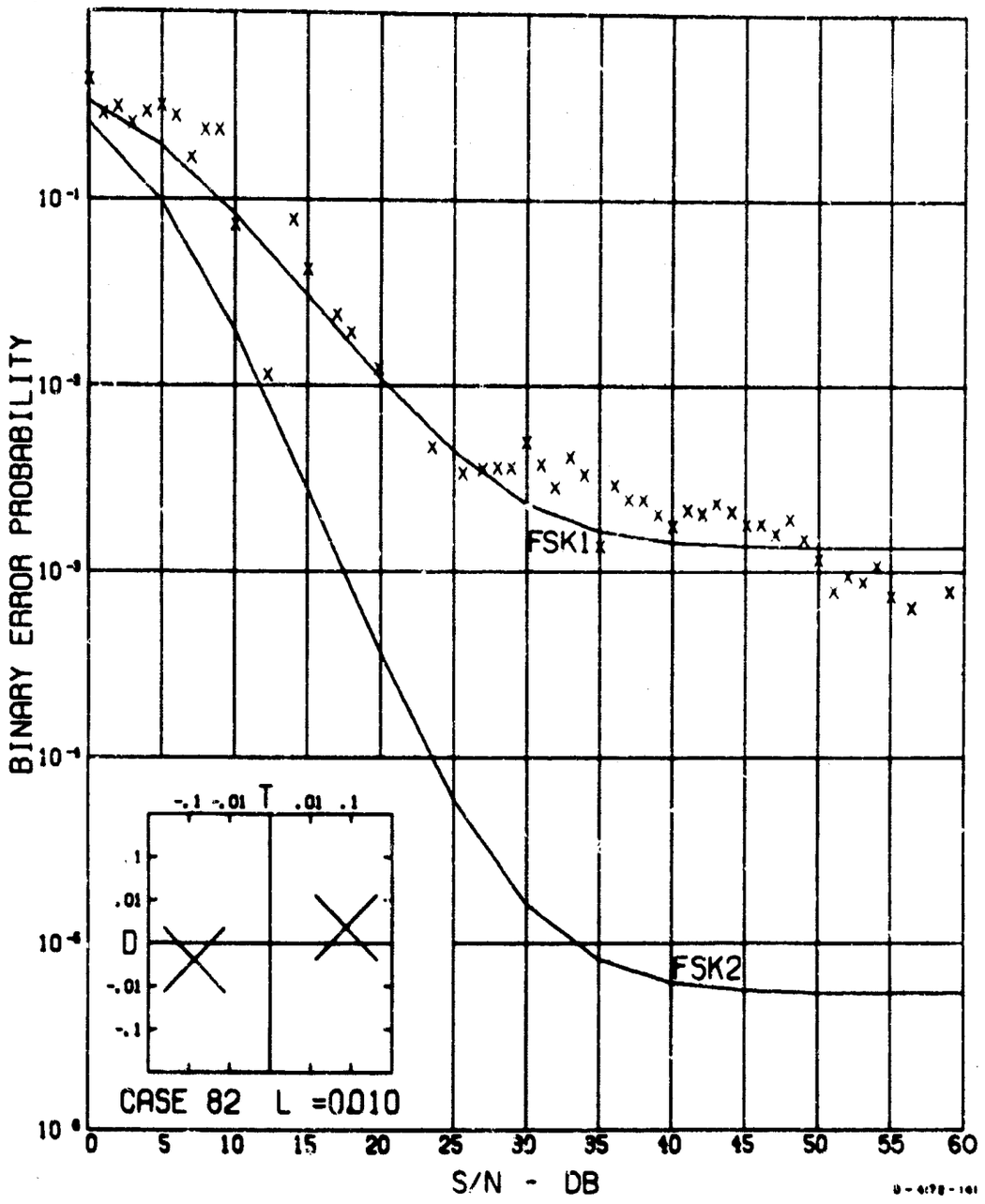

FIG. 62 DATA CLASS D2 — $0 < 2\sigma_r < 1.5$; $0.25 < 2\sigma_\lambda < 0.5$

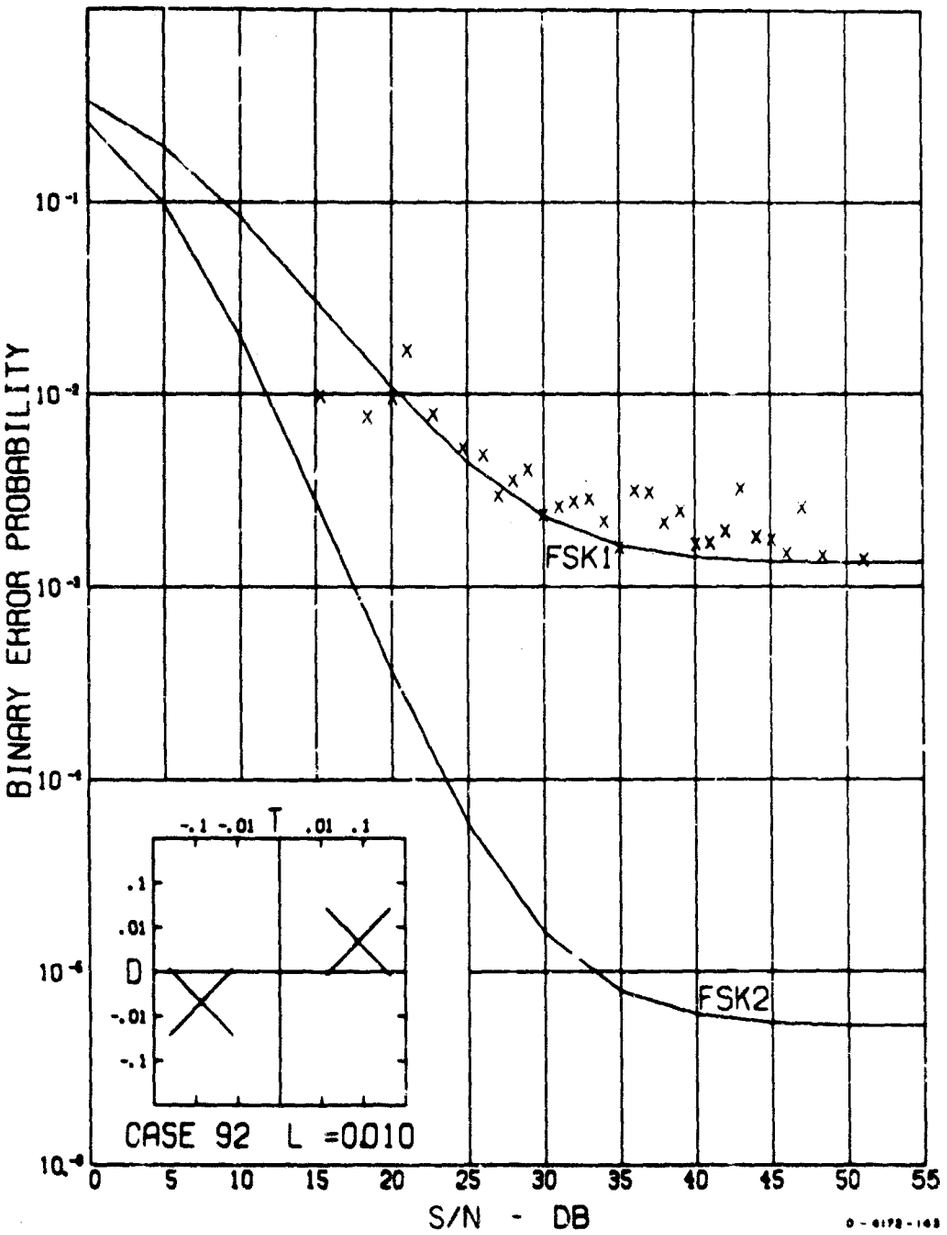

FIG. 63 DATA CLASS D3 — $0 < 2\sigma_r < 1.5$; $0.5 < 2\sigma_\lambda < 1.0$

(2) *Increase the data transmission rate.* It was desirable to obtain the error rate for a number of classes of channel conditions. However, the 100-baud maximum transmission rate and the over-all time schedule limited the amount of data that could be collected for each class. Confident error-rate estimations at low error rates require a large number of transmitted bits. More accurate validation of error-rate characteristics of diversity systems would require the measurement of much lower error rates than attempted here. With more data, the parameter of diversity channel correlation could be more accurately accounted for. The data rate for the AN/FGC-29 system could be increased simply by adding frequency-division multiplexed channels. This would also permit experiments to be conducted on the effect of interchannel distortions.

(3) *Transmit other binary sequences.* The alternating 10-msec keying sequence used was the most sensitive sequence possible for observing effects of time-delay spread on error rate. The error rate with the alternating sequence cannot be more than four times the error rate with a random sequence and is probably closer to two times. However, a random sequence may be more realistic for evaluating the performance of an actual data system under various channel conditions.

The error-rate model uses channel-spread parameters that are normalized to the transmission rate and to the mark-space frequency spacing. Therefore increasing the element length affords a method of effectively simulating reduced channel time-delay-spread conditions. Transmission of a simple 11001100 sequence would reduce the inter-symbol interference effects by one half. In fact, with sufficiently long signaling elements, measurement of the error rate with a sequence of all marks may greatly reduce frequency-selective fading effects and may permit error-rate validation of an essentially pure Doppler-spread channel.

In like manner, the spacing of the mark-space frequencies could be widened to simulate reduced Doppler-spread channels. This could be done conveniently in the AN/FGC-29 system by signaling with frequencies in different channels.

(4) *Conduct the experiment over a shorter path length.* Time-delay and Doppler effects on the Fort Monmouth to Palo Alto path were minimal. A shorter path would give much more variation of time-delay-spread conditions. This would permit better validation of error-rate models for higher time-delay spreads.

(5) *Conduct the experiment over a path with different ionospheric history.* A path where auroral effects or spread-*F* conditions are more prevalent would give more Doppler variations and hence a better verification of the error-rate models under various Doppler-spread conditions.

Measurements at additional transmission frequencies and at different times of day would also provide data at other spread conditions.

Everything considered, it was felt that the experiment was very sucessful. We are unaware of any reported channel error-rate experiment conducted in this depth; simultaneous measurement of appropriate channel parameters and real system error rate to verify assumptions associated with a mathematical model for both the channel and the system.

VI FREQUENCY-SELECTIVE WAVEFORM ANALYSIS

A. INTRODUCTION

The word analyzer used in the error-rate experiment provided immediate detection of received data bit errors. With this capability, it was possible to record, by oscilloscope photography, received signal waveforms at various processing stages in the receiver system for the time interval immediately following a detected error. The basic technique utilized a fast-response, dual-channel oscilloscope to display the waveforms and a Polaroid Land camera to photograph them. By triggering one or two such oscilloscope-cameras with the error signals, it was possible to record in detail as many as four received waveforms simultaneously in the time interval immediately following the occurrence of an error. During that interval, several errors usually occurred because of the burst character of the errors. Some of these records and their interpretation are presented in this chapter.

B. DESCRIPTION OF EXPERIMENT

Detrimental frequency-selective effects for an FSK system would be evidenced by unequal and time-varying channel attenuations at the mark and space signaling frequencies. To observe whether this condition occurred, it was necessary to compare the amplitude of the mark and space frequencies as a function of time. The AN/FGC-29 transmitter sent FSK tones separated by 85 cps. Alternate mark and space frequencies were transmitted in 10-msec intervals. Because of certain diversity-combining techniques used in the AN/FGC-29 receiver, it was not convenient to obtain a true picture of channel frequency-selective fading effects in the normal signal processing by this receiver. Hence a special mark-space filter was constructed, designed to provide separation of the two frequencies. This filter was connected to the output of the delay amplifier of the AN/FGC-29 receiver.

A block diagram of this mark-space filter is shown in Fig. 6.4. The received signal passed by the mark filter was envelope detected with a positive polarity. The received signal passed by the space filter was detected with a negative polarity. These two outputs were combined across

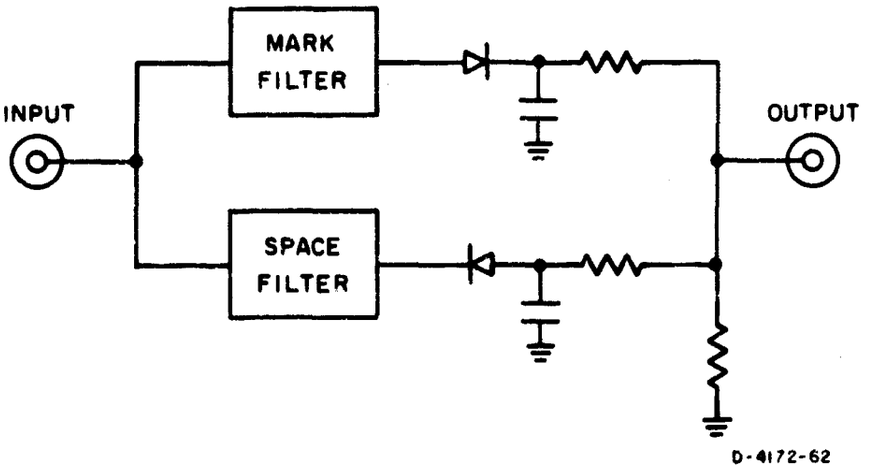

FIG. 64 BLOCK DIAGRAM OF MARK-SPACE FILTER

a grounded common load resistor. The voltage across this resistor then increased positively when a mark frequency was received, in proportion to the strength of the received signal, and similarly increased negatively when a space frequency was received. The 3-db bandwidth of each filter was about 40 cps.

The output of the mark-space filter was connected to one input of a dual-channel oscilloscope, as shown in Fig. 65. Error pulses generated by the word analyzer triggered the oscilloscope. The triggering mode was set to "single-sweep" mode operation. In this mode, after the triggering circuit was manually "armed," the first external trigger pulse to arrive triggered a single scope sweep. Additional trigger pulses had no effect on the scope until the trigger circuit was again armed.

Transient waveforms were recorded during detected errors by the following procedure:

(1) Prepare the Polaroid camera on the oscilloscope.

(2) Open the camera shutter.

(3) Arm the scope trigger circuit.

(4) Wait for a detected error to occur.

(5) Close shutter and process the photograph.

Alternating mark and space signaling elements of 10-msec duration were transmitted. To observe the distortion details of each pulse, the scope speed was adjusted to 20 or 50 msec cm. Frequency-selective fading characteristics on the channel were observed with a slower sweep speed.

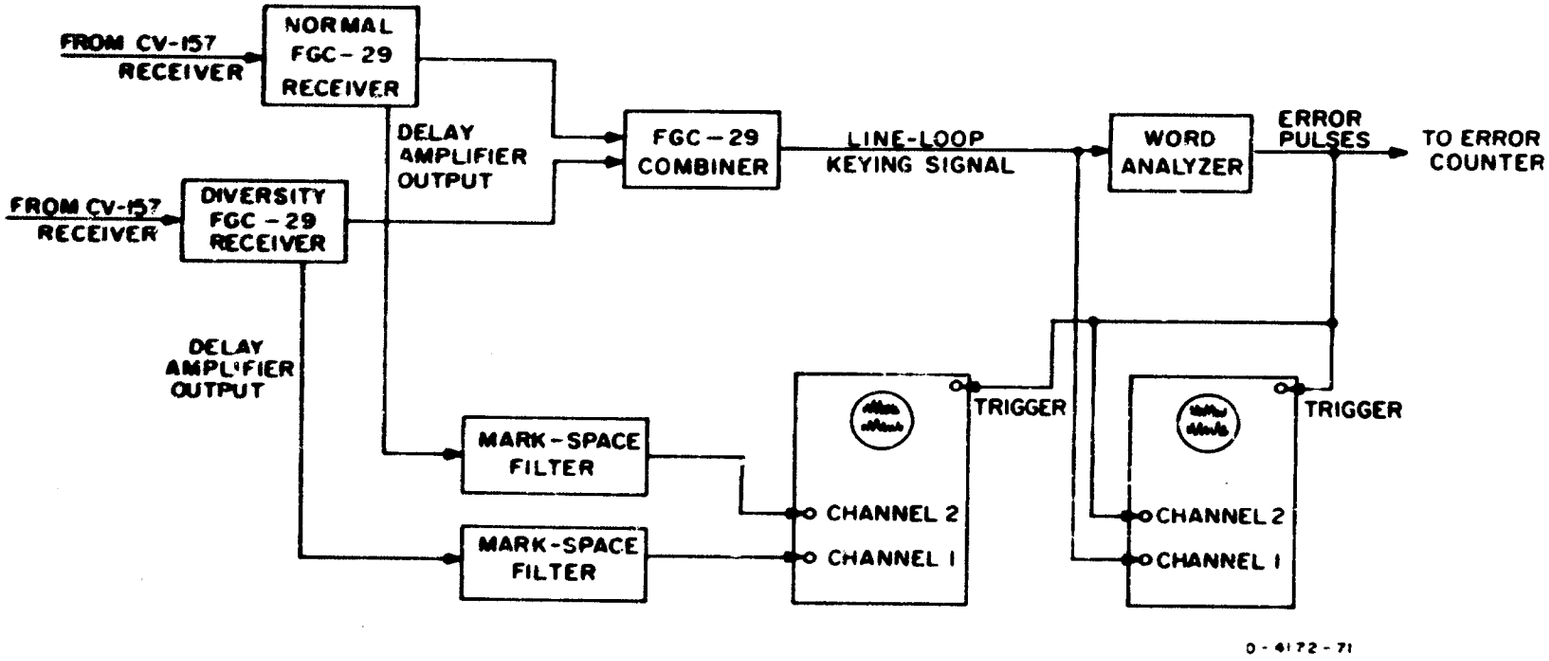

FIG. 65 SIGNAL WAVEFORM RECORDING SETUP

The recordings were made during operation at 7.3 or 14.3 Mc. The 14-Mc recordings were made between the hours of 1800 and 2300 GMT and the 7.3-Mc recordings between 0000 and 0200 GMT. The exact date and time of each recording is indicated on the figures. The average S/N when these recordings were made was generally higher than 20 db.

C. WAVEFORMS WITH FREQUENCY-SELECTIVE FADING

Figure 66 shows an example of almost identical fading properties on the mark and space frequencies. For a channel of this type, error probabilities are predicted by assuming a channel model in which the signaling frequencies fade simultaneously: produce fading that is "flat" or completely correlated at the two signaling frequencies.

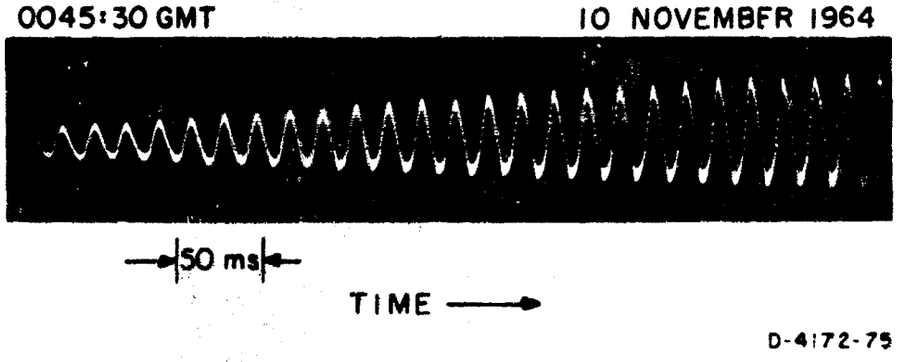

FIG. 66 FREQUENCY-FLAT FADING

Figure 67 shows two examples of noticeable frequency selectivity between the mark and space frequencies. The time positions of actual detected errors are shown immediately below this waveform as a series of dots. The occurrence of error bursts was quite common during frequency-selective fading of this sort. Furthermore, as can be seen from these examples, bit errors tended to occur alternately. This implies, because of the alternating sequence transmitted, that the errors were of one type (either a mark transposed to a space or a space transposed to a mark).

Figure 68 shows two examples of frequency flat fading on a longer time scale. Figure 69 shows two examples of frequency-selective fading on the same time scale as that of Fig. 68. Here it can be seen that the simultaneous channel gains in the mark and space channels were quite different. There are at least two occasions on these records where the gain at one frequency was in a null, while at a frequency only 85 cps away the

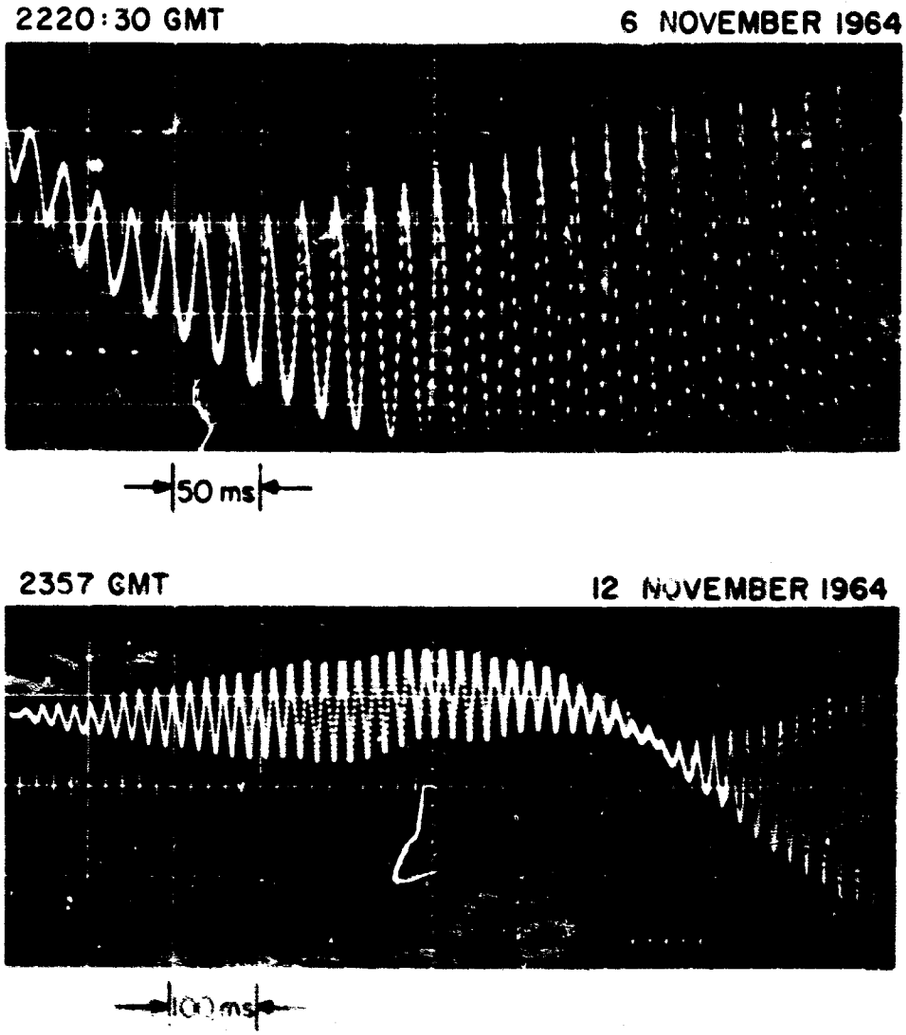

FIG. 67 FREQUENCY-SELECTIVE FADING

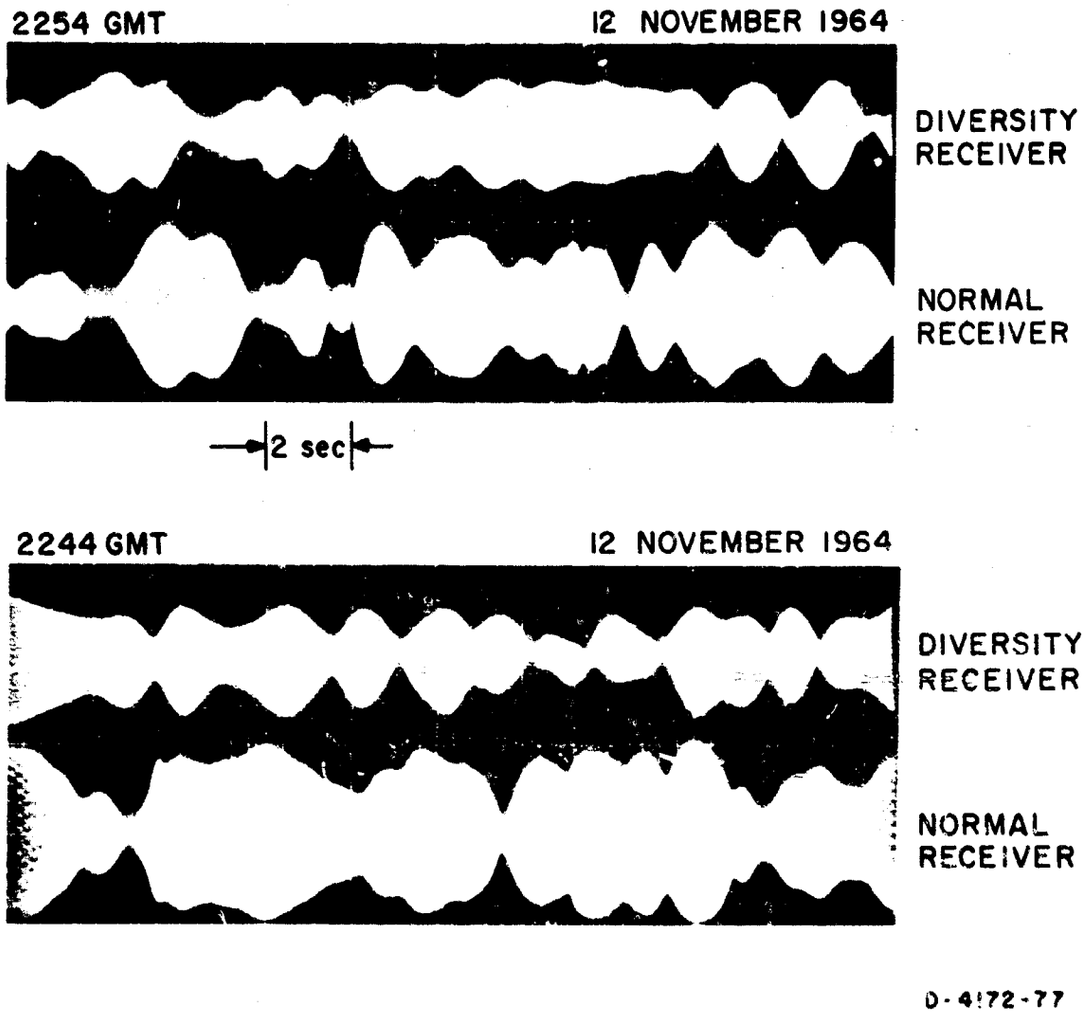

FIG. 68 FREQUENCY-FLAT FADING ON SPACE-DIVERSITY ANTENNAS

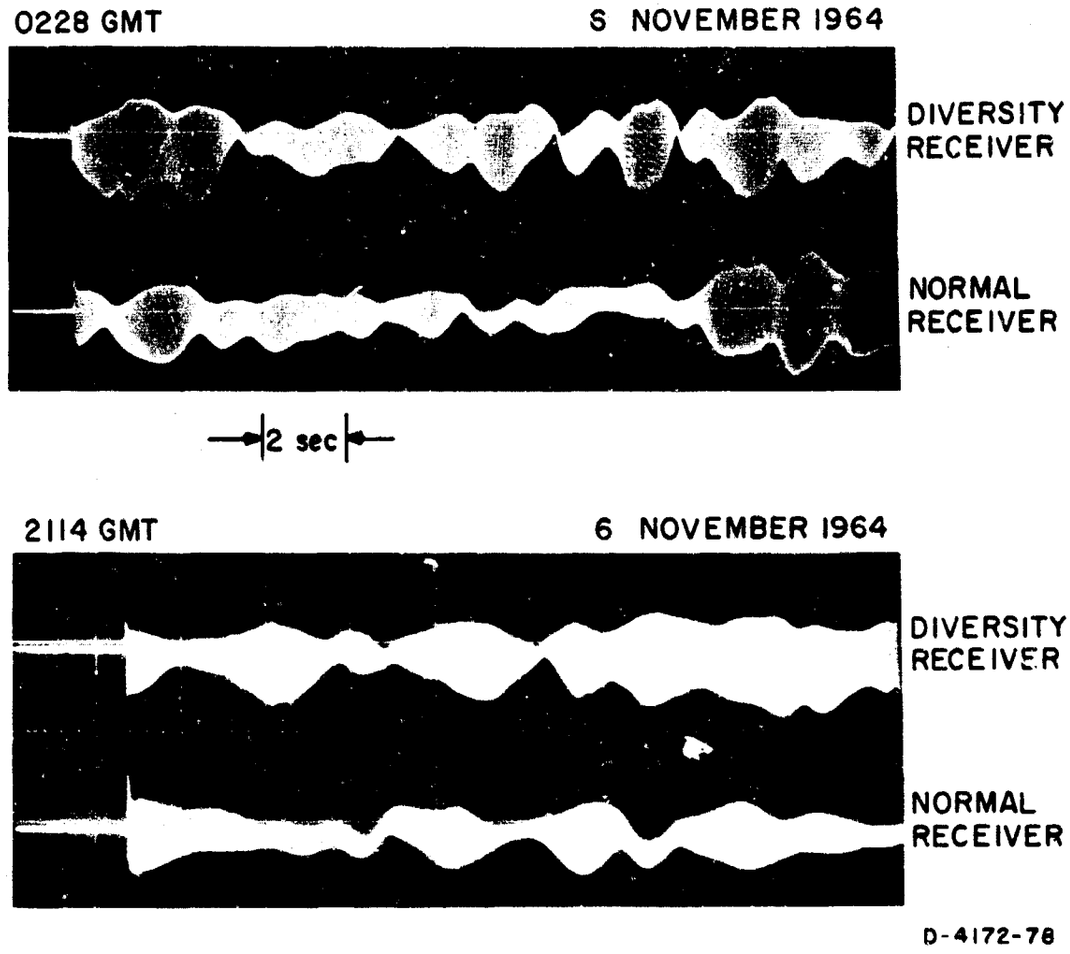

FIG. 69 FREQUENCY-SELECTIVE FADING ON SPACE-DIVERSITY ANTENNAS

the channel gain was at a relative maximum. These frequency-selective effects can be attributed to the differential time delays associated with multipath propagation modes.

D. WAVEFORMS ON SPACE ANTENNAS

The upper waveform in Figs. 68 and 69 was obtained simultaneously with the lower waveform from a second AN FGC-29 receiver and mark-space filter connected to the second channel of the dual-channel scope. The antenna for this receiver, however, was spaced some 1,000 feet away from the first antenna. At these times, the waveforms seem to indicate that the time fading on these two antennas was uncorrelated, because no deep fading occurred simultaneously on both antennas.* However, it is

* Detailed measurements of antenna correlations were made. These are discussed in chapter VII.

significant that the frequency-selective characteristics on the two antennas were similar.

The straight line at the beginning of the sweep in the waveforms of Fig. 69 occurred because the sweep was manually triggered while the tones were off at the transmitter. This occurred every 30 seconds in the transmission schedule; it provides a convenient zero reference level in these records.

E. LINE-LOOP CURRENT WAVEFORMS

In this experiment it was also possible to observe the waveforms of the dc line-loop keying signal. This signal, available as the output of the AN/FGC-29 combiner unit, is the limited version of the discriminator output normally delivered to the user. Distortion on this signal is often measured and evaluated to determine the usefulness of the channel. This signal is the input to the word analyzer in this experiment. Figure 70 shows two examples of this keying waveform. An error detected by the word

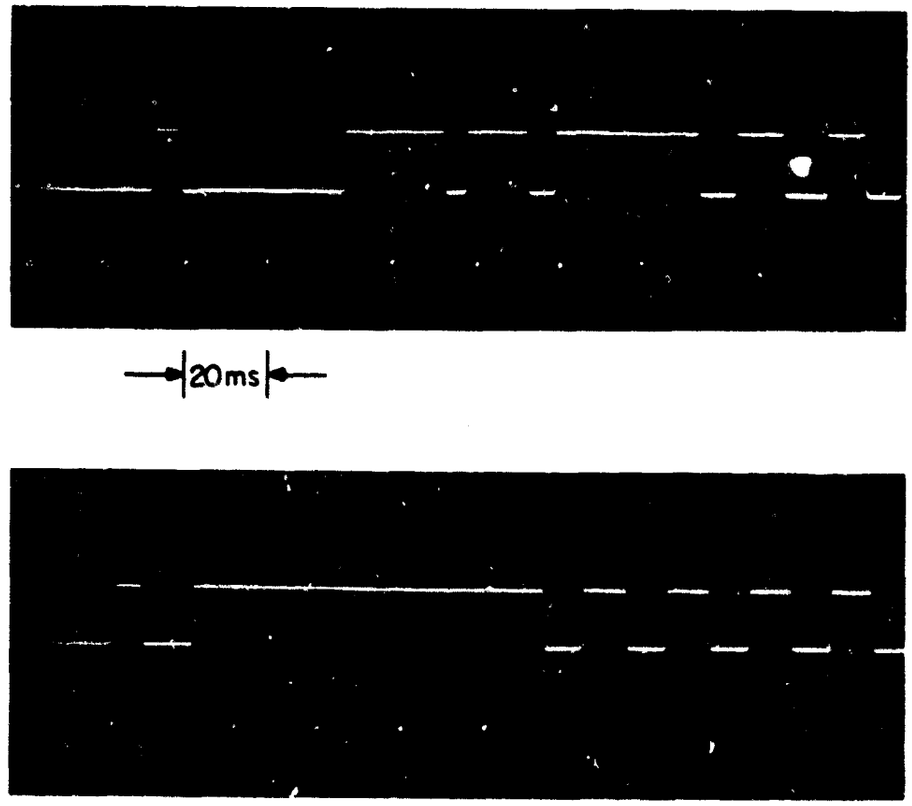

FIG. 70 LINE-LOOP CURRENT WAVEFORMS

analyzer using this signal is indicated on the figure by a dot immediately below the waveform.

If a mark state is arbitrarily defined as the upper level on this waveform, then the initial portion of the top waveform shows what is known as spacing-bias distortion. Spacing bias tends to cause transmitted marks to be erroneously interpreted as spaces. Notice, however, that the distortion soon reverses to marking bias, and errors of the opposite type occur. Such behavior can be explained by frequency-selective fading on the mark and space channels.

F. SIMULTANEOUS WAVEFORMS DURING ERRORS

Through the use of two dual-channel oscilloscopes and Polaroid cameras, triggered by the same error pulse, it was possible to record simultaneously four waveforms. Figures 71 through 76 show examples of these

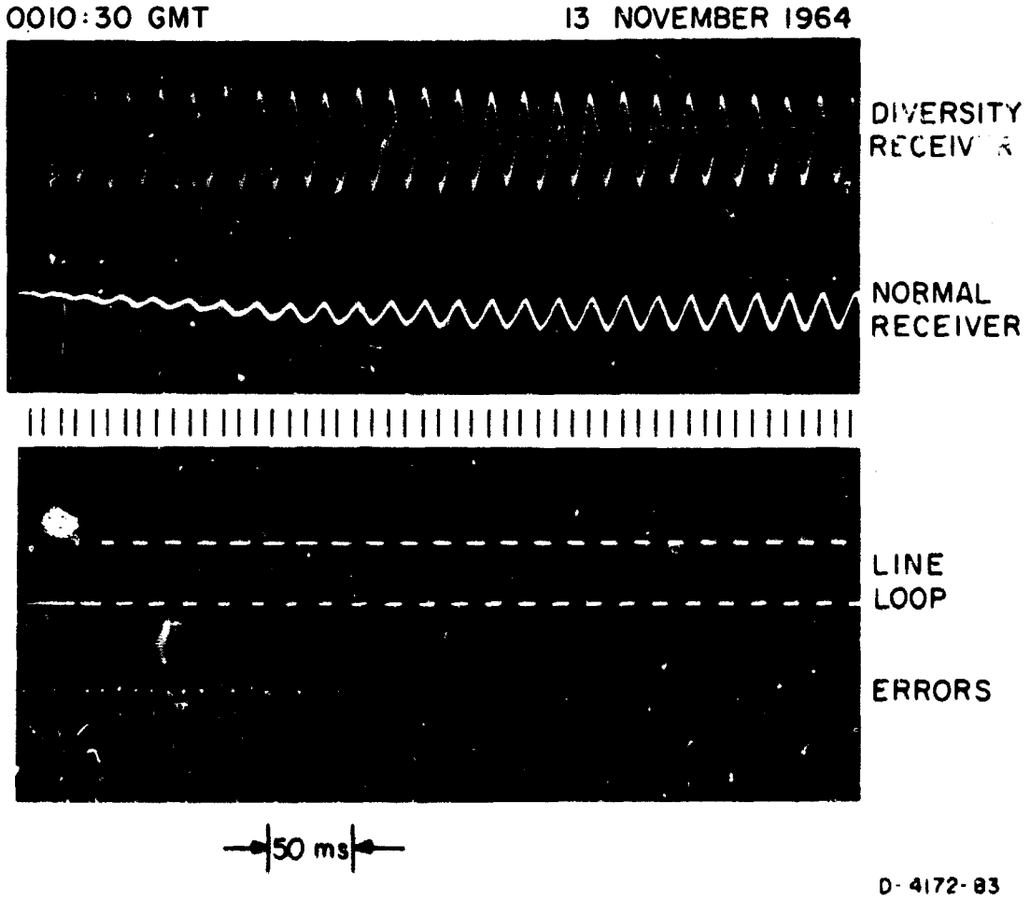

FIG. 71 SIMULTANEOUS WAVEFORMS DURING ERRORS

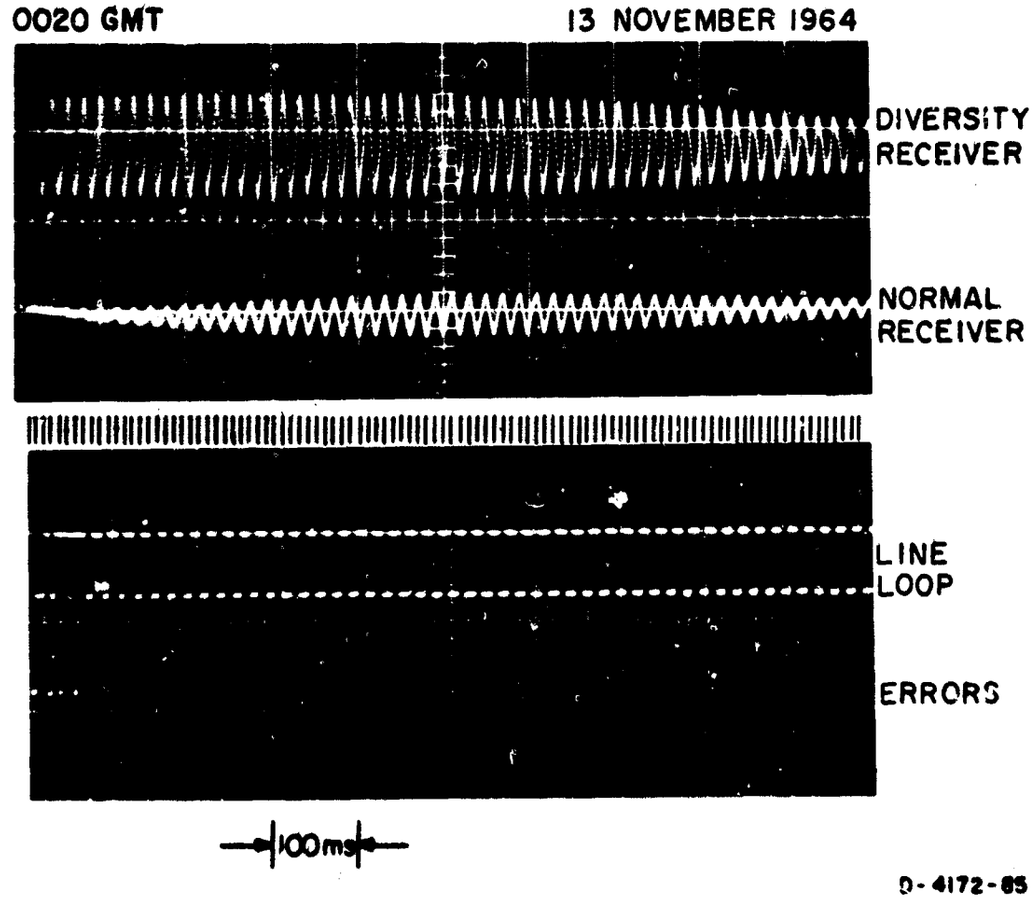

FIG. 72 SIMULTANEOUS WAVEFORMS DURING ERRORS

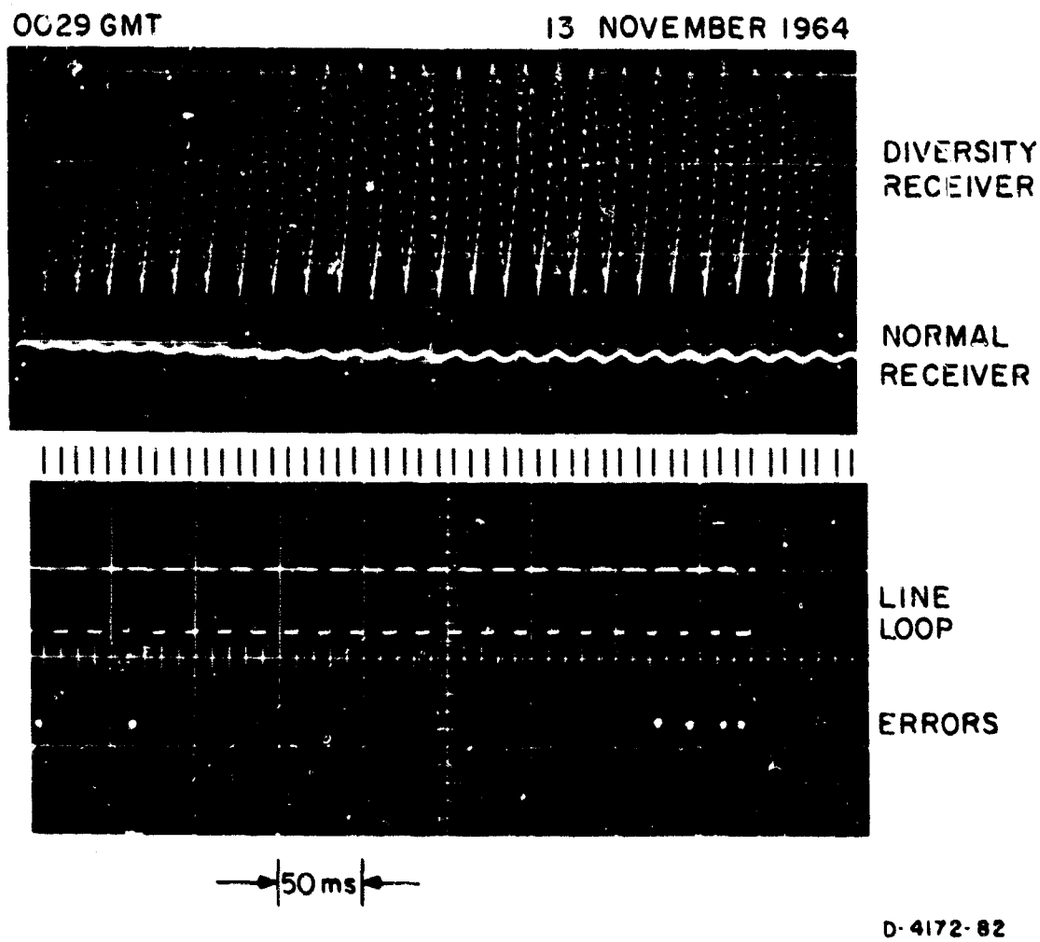

FIG. 73 SIMULTANEOUS WAVEFORMS DURING ERRORS

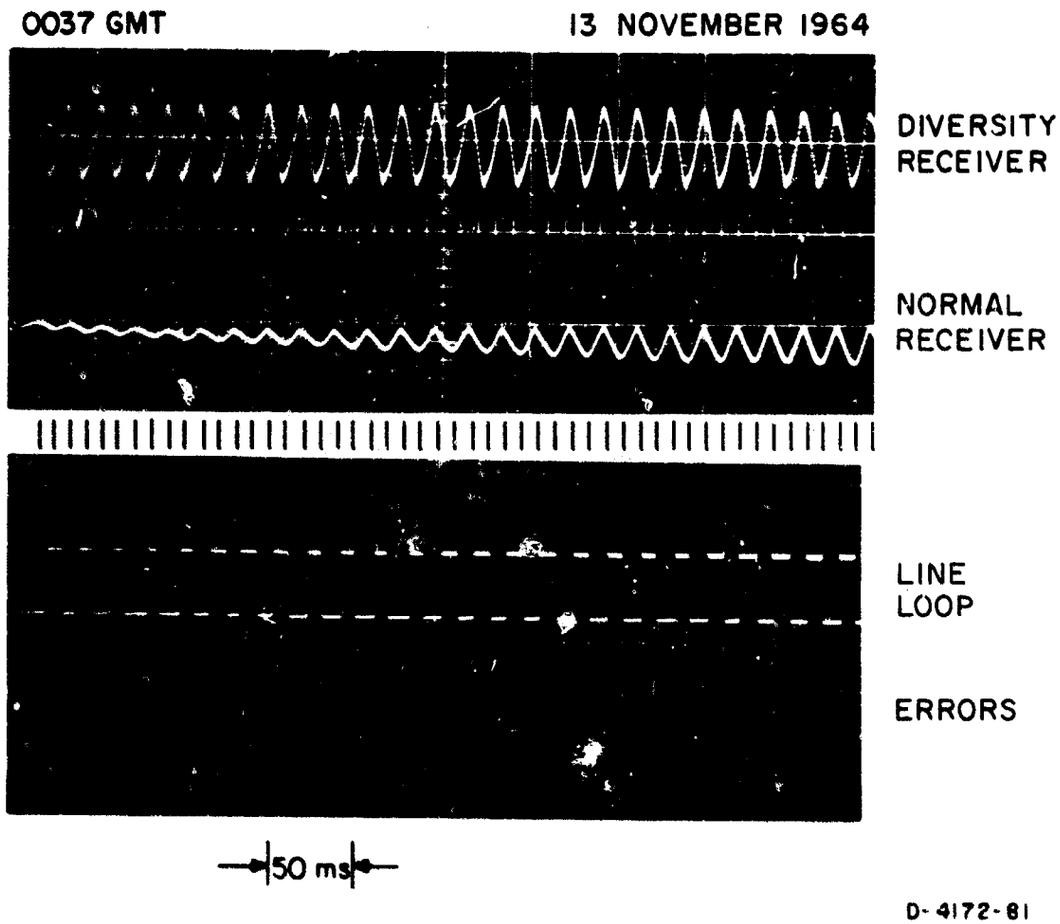

FIG. 74 SIMULTANEOUS WAVEFORMS DURING ERRORS

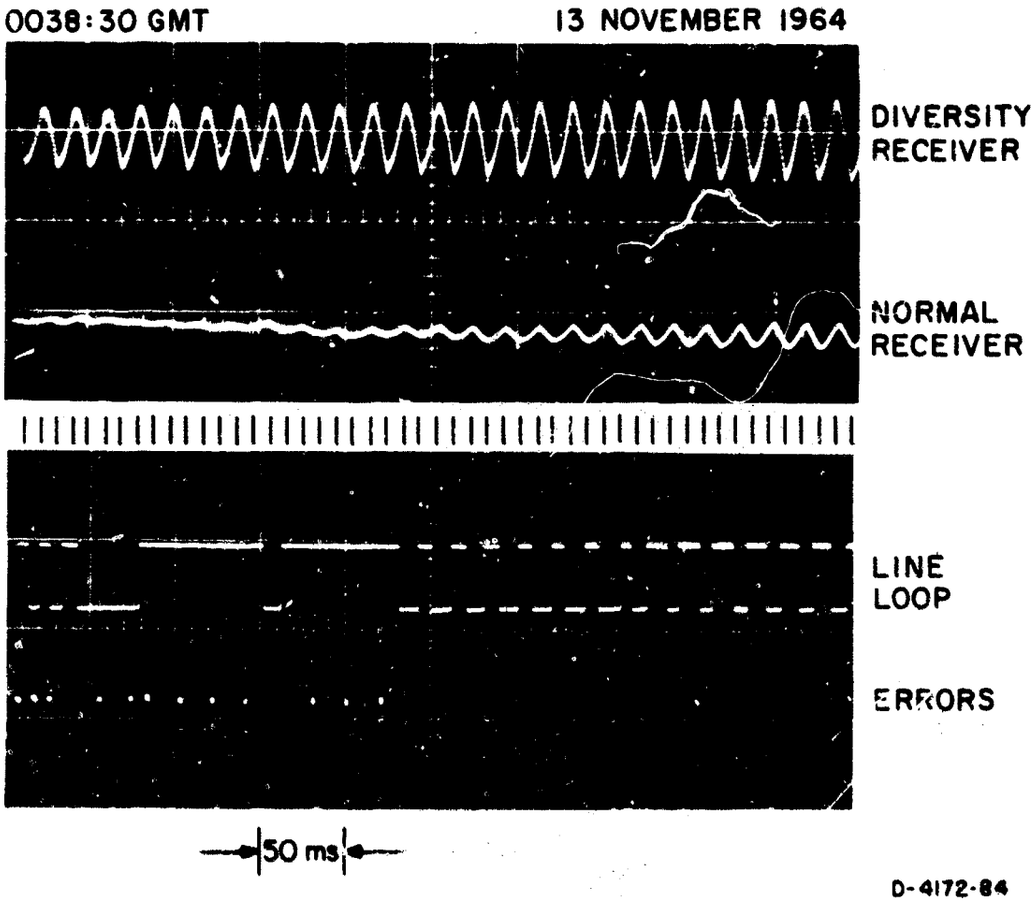

FIG. 75 SIMULTANEOUS WAVEFORMS DURING ERRORS

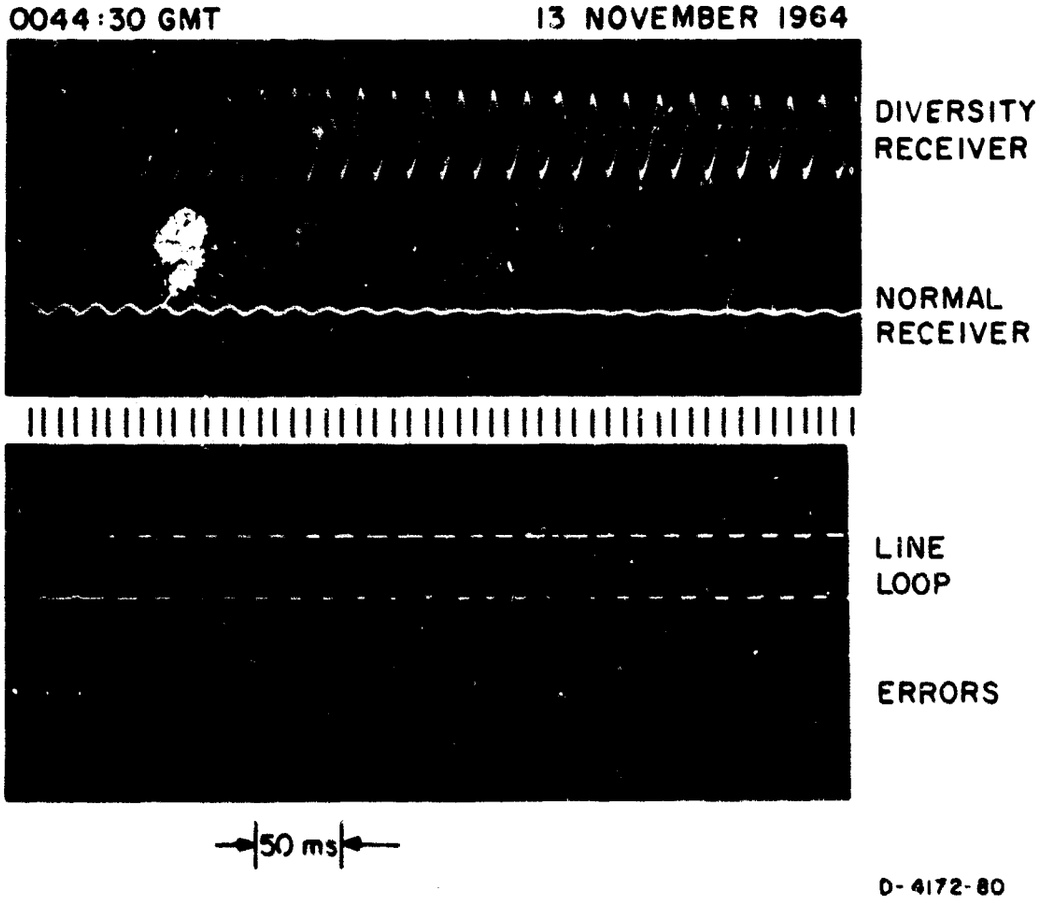

FIG. 76 SIMULTANEOUS WAVEFORMS DURING ERRORS

records. The horizontal time scale for Figs. 71 through 75 is 50 msec per grid line. In Fig. 76 the scale is 100 msec per grid line. The waveforms from top to bottom are as follows:

(1) Mark-space filter output from space-diversity receiver

(2) Mark-space filter output from normal receiver

(3) Line-loop keying signal from normal receiver

(4) Dots indicating signaling elements detected in error from normal receiver only.

The gains of the two mark-space waveforms were equalized with a common signal into the antenna terminal. An attempt was made to center the mark-space filter output displays vertically so that zero output was on a horizontal grid line. The line-loop keying signal waveform is reversed in polarity with respect to its corresponding mark-space signal shown above it. Hence frequency-selective fading in the space frequency (upper level) will be evident by the trace remaining below the zero threshold. At the same time, the line-loop keying waveform will be distorted with marking bias.

Figure 71 is an interesting example. At the start of the sweep, the channel was evidently in a selective fade on the mark channel but not in the space channel. As a result, there was heavy spacing bias as indicated on the loop keying waveform, and errors were made on every reception of a mark signaling element. Then there followed a period where the fading was apparently more or less equal on the mark and space channels and the keying waveform is not noticeably distorted. However, errors were detected *for eight signaling elements in a row*. The channel then went into a condition of selective fading on the space channel, and errors were made only in the detection of space signaling elements. One possible explanation of this phenomen is to hypothesize the simultaneous existence of the three propagation modes, two of which were rather strong and equal in strength but with small differential time delay. The third mode would have had to be weaker with a relatively long delay. During the time that the two stronger modes arrived at the antenna in phase opposition, the weaker mode dominated. However, because synchronization was still determined by the arrival time of the two stronger paths, sampling of the signaling elements with reception from the longer path was sufficiently displaced to cause errors in every element.

G. WAVEFORMS WITH DIVERSITY OPERATION

An attempt was made to observe waveforms after a detected error during operation with spaced diversity. However, diversity operation errors were so rare that the waiting time to obtain records following the detection of an error, was prohibitive. Observation of the diversity waveforms shown in the previous figures indicates, however that when errors were detected on the normal receiver, very few errors would have been made had the system been operating with diversity. At the time these waveform records were made, antenna correlation measurements were all under 0.6.

H. CONCLUSIONS

High-time-resolution waveform recordings for a time interval immediately following the detection of an error were made on an FSK communications system over an HF path. These have shown the significance of frequency-selective effects on the performance of a no-diversity system. The observations of these records can be summarized as follows:

(1) Even with the rather narrow frequency separation of 85 cps used in the AN/FGC-29 system, the assumption that the two signaling frequencies always fade together is not valid.

(2) Many of the errors observed occurred in bursts and were all of one type: either a mark transposed to a space or a space transposed to a mark. In many cases, the errors at the beginning of the burst were of one type, and a transition to errors of the opposite type occurred during the burst. No cases were observed where the type of errors during a burst was random. Thus the errors during a burst cannot be explained simply by a low S/N.

(3) Bias distortion of the line-loop keying waveform is correlated with observed frequency-selective effects on the channel.

The number of records made was insufficient for the formation of confident statistics as to the length of error bursts or the type of error. Several cases were recorded where only an isolated error occurred. However, bursts of five to fifteen errors were also quite common.

VII SPATIAL CORRELATION MEASUREMENTS

A. INTRODUCTION

1. Diversity Systems

Radio communications systems have long utilized diversity techniques to combat the effects of signal fading and thereby improve performance. In strategic HF military links, the use of dual spaced-antenna diversity is almost standard. The key to the success of a diversity technique is the availability of uncorrelated signals at the detector of the receiver. A comparison of dual- and no-diversity systems with respect to error rates as a function of S/N shows that dual diversity considerably improves performance. Futhermore, the margin of improvement increases with increasing S/N up to the point where dispersive effects predominate. Previous work by Staras,[21] Packard,[22] and Pierce and Stein[23] has attempted to assess the effect on system performance of partially correlated diversity signals. The results have indicated that for signal correlations up to 0.6 there is negligible deterioration in performance over the zero-correlation case. Little analysis has been made for time- and frequency-selective fading of the channel with correlated inputs.

2. Correlation Coefficient

Assume that before detection each received signal of a dual-diversity communications system can be represented by sample functions from two complex random processes, $x(t)$ and $y(t)$. A convenient measure of the effectiveness of diversity combining is the normalized covariance or correlation coefficient, ρ_{xy}, of these functions at zero time shift,

$$\rho_{xy} = \frac{E[(x - \bar{x})(y - \bar{y})]}{[\sigma_x^2 \sigma_y^2]^{\frac{1}{2}}} \tag{1}$$

where $\bar{x}$ and $\bar{y}$ are the respective means, and σ_x^2 and σ_y^2 are the respective variances of $x(t)$ and $y(t)$. The value of ρ_{xy} is generally constrained to the range from -1 to $+1$. A ρ_{xy} of $+1$ or -1 indicates that with probability one, a deterministic linear relationship exists between $x(t)$ and

$y(t)$, while a ρ_{xy} of zero indicates they are uncorrelated and, if $x(t)$ and $y(t)$ are jointly Gaussian, independent.

It is interesting that the correlation coefficient between the squared envelopes of Gaussian processes, $x(t)$ and $y(t)$, is simply the square of ρ_{xy}. This would indicate that the aquared envelope correlation coefficient should always be greater than zero. It is also true that the envelope correlation coefficient for the jointly Gaussian process is greater than zero. Departures from this would indicate that the sample functions are not derived from Gaussian random processes.

3. Purpose of the Measurement

The original objective of the measurement of correlation coefficient was to provide information that would permit comparison of a theoretical error-rate model for dual diversity with experimental error-rate data. Unfortunately, it was not possible to collect enough dual-diversity error-rate data for definite conclusions. Measurements of correlation coefficient were made, however, and at selected times the data receiver was operated in dual diversity. From the data taken, certain interesting facts emerged: (1) when the dual-diversity system made errors, the envelope correlation coefficient was high; (2) a relationship existed between long-term trends in envelope correlation coefficient and time-delay spread; and (3) previously held rules for space-diversity antenna spacing may not be correct. In this chapter, physical models for space-selective phenomena are given; the measurement techniques are described; and the results of the measurement are discussed.

B. PHYSICAL NATURE OF SPACE-SELECTIVE FADING

At HF, a common technique for obtaining uncorrelated received signals is to use signals received on antennas physically spaced by several wavelengths. Recent work by Ames, however, has shown that this simple rule may not be adequate.[24] He has experimentally demonstrated the presence of quasi-periodic interference patterns along the ground, which arise from differences in arrival angle between ionospheric modes. On this basis, correlation of signals received on spaced antennas will be highest when the center line between the two antennas is perpendicular to the interference patterns and lowest when it is parrallel to the interference patterns.

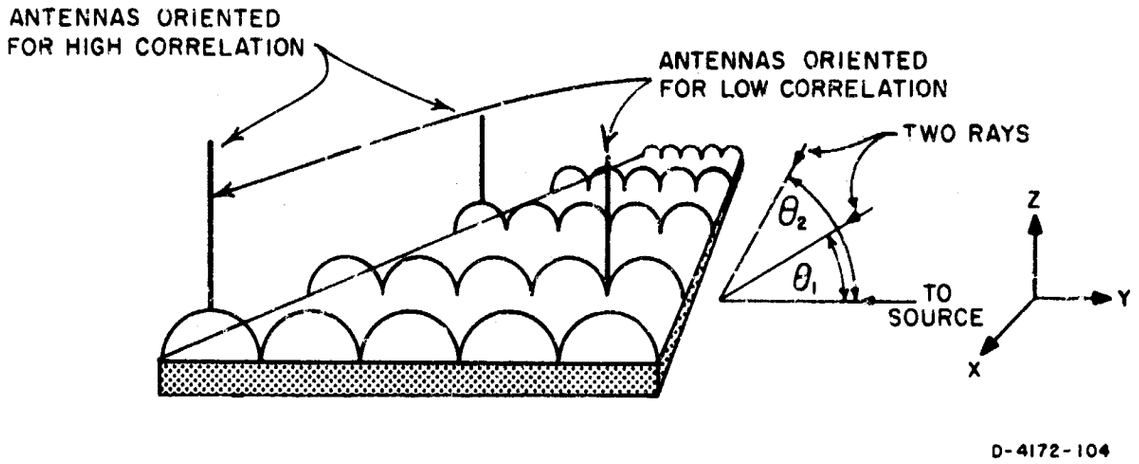

FIG. 77 TYPICAL MODE INTERFERENCE PATTERNS

1. Mode Interference Patterns

Shown in Fig. 77 are two modes differing in elevation angle but identical in azimuth. This could represent, for example, high- and low-ray F-propagating modes, each with a different time delay, Doppler frequency, and incoming angle of arrival. If the transmitted signal is represented as

$$y(t) = \mathrm{Re}\{e^{i2\pi f_0 t}\} \quad , \tag{2}$$

the received signal, $Z(x,y,z,t) \triangleq Z(r,t)$, is thus

$$Z(r,t) = \mathrm{Re}\left(\left\{A_1 e^{i[2\pi\lambda_1(t+\tau_1)+\vec{k}_1\cdot\vec{r}]} + A_2 e^{i[2\pi\lambda_2(t+\tau_2)+\vec{k}_2\cdot\vec{r}]}\right\} e^{i2\pi f_0 t}\right) \tag{3}$$

where

λ_i = ith mode Doppler frequency

τ_i = ith mode time delay

k_i = mode vector wave number, $= k_{x_i}\vec{i} + k_{y_i}\vec{j} + k_{z_i}\vec{k}$

r = $x\vec{i} + y\vec{j} + z\vec{k}$ = general position vector

A_i = complex amplitude of ith mode.

For illustration, suppose

$$A_1 e^{i2\pi\lambda_1\tau_1} = A_2 e^{i2\pi\lambda_2\tau_2+\delta} = A \quad . \tag{4}$$

Then Eq. (3) becomes

$$Z(r,t) = \mathrm{Re}\left(Ae^{i[2\pi(\lambda_1+f_0)t+\vec{k}_1\cdot\vec{r}]}\left\{1+e^{i[2\pi(\lambda_2-\lambda_1)t+(\vec{k}_2-\vec{k}_1)\cdot\vec{r}+\delta]}\right\}\right). \tag{5}$$

$Z(r,t)$ will be zero when

$$\delta + 2\pi(\lambda_2-\lambda_1)t + (\vec{k}_2-\vec{k}_1)\cdot\vec{r} = (2n-1)\pi \qquad n = 0,\mp1,\mp2\ \ldots \tag{6}$$

and will be a maximum when

$$\delta + 2\pi(\lambda_2-\lambda_1)t + (\vec{k}_2-\vec{k}_1)\cdot\vec{r} = 2n\pi \qquad n = 0,\mp1, = 2, \ldots \tag{7}$$

The effect of time delay is merely to put a fixed phase shift in the system of traveling waves. If the two modes have unequal amplitudes, Eq. (7) still describes the occurrence of maxima, but Eq. (6) describes the occurrence of minima rather than zeros.

At a given point in space [$(\vec{k}_2-\vec{k}_1)\cdot\vec{r}$ = a constant], a zero occurs every $1/(\lambda_2-\lambda_1)$ seconds. If one stood at a given point and measured field intensity on a narrow-band receiver, the time between minima (or maxima) would depend only on the Doppler-frequency difference between the two modes.

Suppose that instead of standing at a given point we position many antennas along a straight line. For simplicity (with reference to Fig. 77), we make this line have the same azimuth as our two rays. From Eq. (7) we see that the locus of maxima is satisfied by the equation of the plane

$$(\vec{k}_2-\vec{k}_1)\cdot\vec{r} = 2n\pi - 2\pi(\lambda_2-\lambda_1)t \quad , \tag{8}$$

or, by expanding,

$$(k_{x2}-k_{x2})x + (k_{y2}-k_{y1})y + (k_{z2}-k_{z1})z = 2n\pi - 2\pi(\lambda_2-\lambda_1)t \quad . \tag{9}$$

By the choice of the coordinate system, the two waves have no contribution in the x direction, $k_{x2} = k_{x1} = 0$, and furthermore we are observing on the plane $z = 0$. Under these conditions, only the middle term on the left-hand side of Eq. (9) survives, and by solving for y

$$y = \frac{2\pi[n - (\lambda_2 - \lambda_1)t]}{k_{y2} - k_{y1}} \qquad n = 0, \mp 1, \mp 2, \ldots \tag{10}$$

The distance between successive maxima (or minima) will be $2\pi/(k_{y2} - k_{y1})$. This is the period of the interference pattern shown in Fig. 77. This pattern moves with time at a velocity of $2\pi(\lambda_2 + \lambda_1)/(k_{y2} - k_{y1})$ along the y axis.

Certain physical constraints are imposed by virtue of the fact that a scalar wave funtion

$$Z(r, t) = \mathrm{Re}\left\{e^{i[2\pi(\lambda + f_0)t + \vec{k} \cdot \vec{r}]}\right\} \tag{11}$$

must satisfy the wave equation

$$\nabla^2 Z = \mu\epsilon \frac{\partial^2 Z}{\partial t^2} , \tag{12}$$

which leads to the relationship

$$(2\pi)^2 \mu\epsilon(\lambda + f_0)^2 = |\vec{k}|^2 = k_x^2 + k_y^2 + k_z^2 . \tag{13}$$

As might be expected, the wave numbers in the three principal directions are constrained by the physics of the medium.

2. Numerical Examples

For our first example, let us assume that our two waves are a $2F$ high and low ray on the 4100-km Fort Monmouth to Palo Alto path. On the basis of virtual-height geometry, we can assume θ_1 and θ_2 to be 11 and 15 degrees, respectively. If we assume a frequency of 14 Mc and that λ_1 and $\lambda_2 \ll f_0$, we get, since $k_x = 0$,

$$k_{yi}^2 + k_{zi}^2 \cong (2\pi)^2 \left(\frac{1}{3 \times 10^8}\right)^2 (14 \times 10^6)^2 \quad , \tag{14}$$

and

$$\frac{k_{z2}}{k_{y2}} = \text{Tan}^{-1}\ 15^\circ \ ; \quad \frac{k_{z1}}{k_{y1}} = \text{Tan}^{-1}\ 11^\circ \quad . \tag{15}$$

Solving, we get

$$\begin{aligned} k_{y1} &= 0.267\ (\text{meter})^{-1} \\ k_{y2} &= 0.262\ (\text{meter})^{-1} \quad . \end{aligned} \tag{16}$$

The distance between maxima is then

$$\frac{2\pi}{k_{y1} - k_{y2}} = \frac{2\pi}{0.005} = 1256 \text{ meters} \tag{17}$$

for a frequency of 14 Mc. (At 7 Mc, k_{y1} and k_{y2} become much closer, and the distance between maxima is greatly increased.)

Suppose now that our two incoming rays are $2F$ and $3F$ low rays having arrival angles of 11° and 20°, respectively. Under these conditions, at 14 Mc,

$$\begin{aligned} k_{y1} &= 0.267 \\ k_{y2} &= 0.236 \end{aligned} \tag{18}$$

and

$$\frac{2\pi}{k_{y1} - k_{y2}} = 202 \text{ meters} \quad .$$

The distance between minima (or period of the interference pattern) for $2F$ and $3F$ is only about one-sixth that of the period of the pattern produced by high and low $2F$. This drastic change shows the difficulty of using a single antenna spacing for different propagation conditions. In practice, spacings on the order of ten wavelengths, chosen to satisfy

constraints of land use, should probably be adequate, provided that the line between antennas is approximately in the azimuthal direction of the incoming waves (not necessarily the great-circle bearing).

3. Interference Patterns as Random Processes

The preceding two sections treat a somewhat special case of only two modes at constant amplitude. Generally, it is necessary to consider many modes having amplitudes that are random processes. In order to do this, an approach similar to that used by Daly in describing time- and frequency-selective fading will be employed.[6]

Assume that the transmitted signal is continuous of frequency f_0. The channel is assumed to be varying in time and giving rise in space to a number of discrete plane waves having different Doppler shifts and directions. Since we are dealing with a band of frequencies only a few cycles at most removed from f_0, we neglect frequency-selective effects. Under these conditions, the output of the channel, analogous to Eq. (3) in the last section, is for n plane waves

$$Z(r,t) = \mathrm{Re}\left(\left\{\sum_{i=1}^{n} a_i e^{i[2\pi\lambda_i t + \vec{k}_i \cdot \vec{r}]}\right\} e^{i2\pi f_0 t}\right) \quad . \tag{19}$$

The complex envelope of $Z(r,t)$ denoted $H(r,t)$

$$H(r,t) = \sum_{i=1}^{n} a_i e^{i[2\pi\lambda_i t + \vec{k}_i \cdot \vec{r}]} \quad . \tag{20}$$

It is assumed that the a_i are zero-mean complex Gaussian random variables having independent real and imaginary parts. This last constraint imposes uniformity upon the phase of the a_i. Furthermore we assume that

$$\begin{aligned} E[a_i a_j] &= \sigma_i^2 \qquad i = j \\ &= 0 \qquad i \neq j \quad ; \end{aligned} \tag{21}$$

σ_i^2 is then the average power associated with each plane wave, and it is assumed that any two plane waves are uncorrelated. Under these conditions, $H(r,t)$ will be a homogeneous Gaussian random field.

The correlation coefficient described in Sec. A.2 has an interesting physical interpretation: the correlation of two complex envelopes at

different points in space and at some additional time delay. We define the function $R_H(\Delta r \Delta t)$ as the space-time correlation function

$$R_H(\Delta r, \Delta t) = E[H(\vec{r}, t)H^*(\vec{r} + \Delta\vec{r}, t + \Delta t)]$$

$$= \sum_{i=1}^{n} \sigma_i^2 e^{-i[2\pi\lambda_i \Delta t + k_i \cdot \Delta\vec{r}]} \quad . \tag{22}$$

The correlation coefficient is simply the normalized space-time covariance function evaluated at zero time shift, and $\Delta\vec{r}_{12}$ is the spacing between antennas located at x_1, y_1, z_1 and x_2, y_2, z_2,

$$\rho = \frac{R_H(0, \Delta\vec{r}_{12})}{\sum_{i=1}^{n} \sigma_i^2} = \frac{\sum_{i=1}^{n} \sigma_i^2 e^{-i\vec{k}_i \cdot \Delta\vec{r}_{12}}}{\sum_{i=1}^{n} \sigma_i^2} \quad . \tag{23}$$

The Fourier transform of $R_H(\Delta t, \Delta\vec{r})$ is the scattering function

$$S(\lambda, k_x, k_y, k_z) = \iiint\!\!\int R_H(\Delta t, \Delta r) e^{-i[2\pi\lambda\Delta t + \vec{k} \cdot \Delta\vec{r}]} d\Delta t\, d\Delta x\, d\Delta y\, d\Delta z \tag{24}$$

where

$$\vec{k} \cdot \Delta\vec{r} = k_x \Delta x + k_y \Delta y + k_z \Delta z \quad . \tag{25}$$

For $R_H(\Delta t, \Delta r)$ of the form of Eq. (22), Eq. (24) becomes

$$S(\lambda, k_x, k_y, k_z) = \sum_{i=1}^{n} \sigma_i^2 \delta(\lambda - \lambda_i)\delta(k_x - k_{xi})\delta(k_y - k_{yi})\delta(k_z - k_{zi}) \quad . \tag{26}$$

Equation (26) shows that the scattering function consists of a number of delta functions.

Let us define a new function, the wave-number dispersion function $W(k_x, k_y, k_y, k_z)$. We integrate over-all Doppler shift λ to obtain a scattering function in wave number only

$$W(k_x, k_y, k_z) = \int S(\lambda, k_x, k_y, k_z)\, d\lambda$$

$$= \sum_{i=1}^{n} \sigma_i^2 \delta(k_x - k_{xi}) \delta(k_y - k_{yi}) \delta(k_z - k_{zi}) \quad . \qquad (27)$$

The wave-number dispersion function is the Fourier transform of $R_H(0,\Delta r)$. It indicates how the channel disperses a single plane wave into many plane waves of varying magnitude and direction. In any principal direction, a slowly converging wave-number dispersion function implies a rapidly converging spacial autocorrelation function $R_H(0,\Delta r)$. This implies that antennas spaced only a short distance apart will have independent complex envelopes and hence that one need not increase antenna spacing to have effective space-diversity correlation. Conversely, a narrow wave-number dispersion function in one principal direction implies a wide spacial autocorrelation function in that direction and that space diversity is rather ineffective.

The results of this section are applicable only where there is no polarization-selective fading or if only circularly polarized antennas are used. The more general case, where time-varying polarization causes changes in amplitude on an elliptically polarized antenna is not treated here.

C. MEASUREMENTS

In this section, the measurements made to determine normalized covariance between spaced antennas are outlined. No effort is made to determine the wave-number dispersion function. Since only two antennas were available, the only measurement made was the recording of correlation between these two antennas during periods of error-rate measurement.

For convenience, it was decided to measure the correlation between the envelopes of the transmitted carrier signal as received on two receivers each connected to its respective antenna. The two receivers were Technical Material Corporation Model GFR-90, having about 100-cps IF bandwidth. The envelopes were obtained by monitoring the AGC voltage of each receiver. The amplitude response of the AGC is quasi-logarithmic and is approximately the same as the response of the combination of R-390A URR and CV-157 described in Chapter III. Figure 78 shows a block diagram of the measurement.

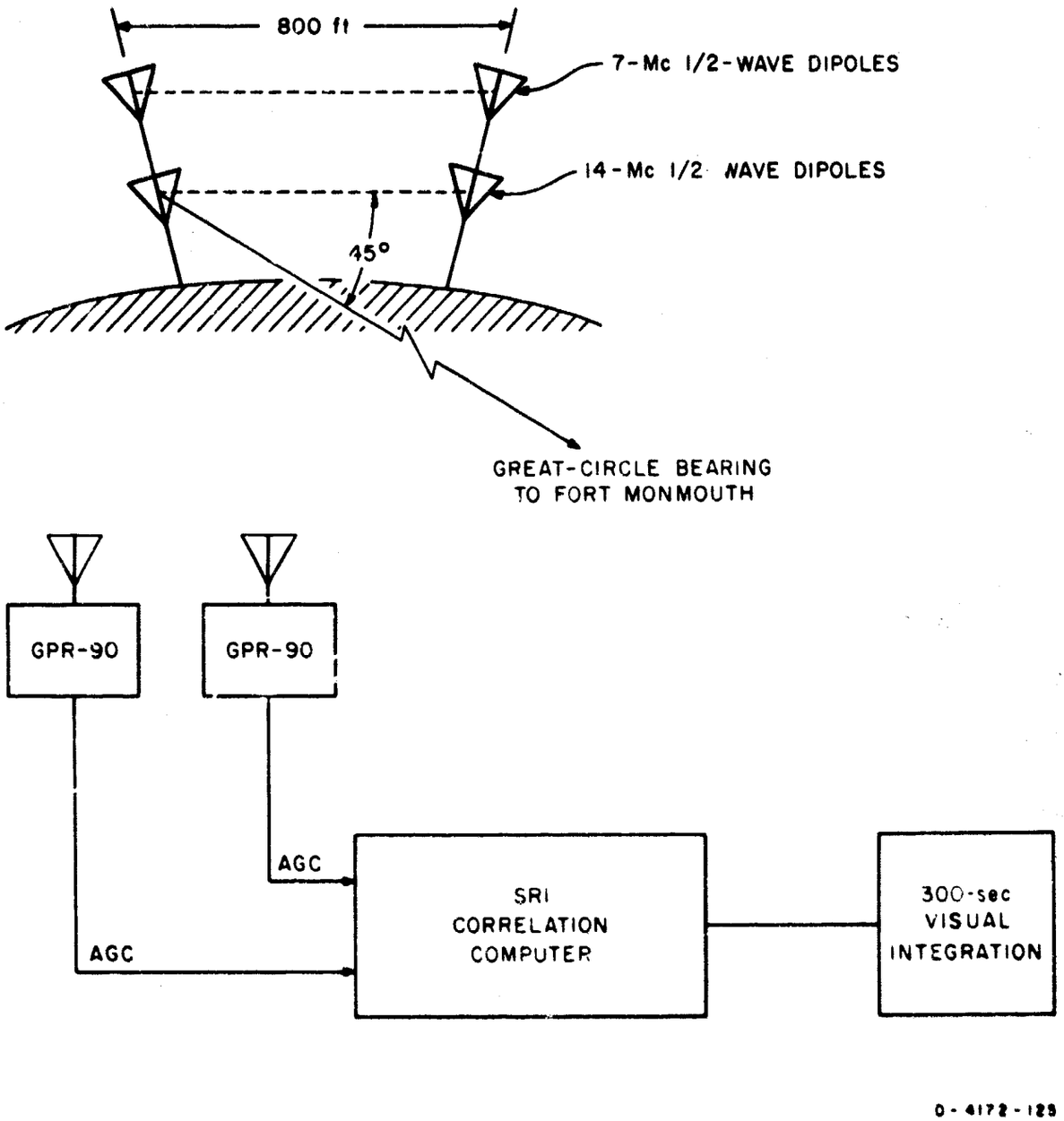

FIG. 78 BLOCK DIAGRAM OF OVER-ALL CORRELATION MEASUREMENT

1. Correlation Computer—Principles Of Operation

The correlation computer (see Fig. 79) provides an output that is an approximation to the correlation defined in Eq. (1). The approximation consists of correlation of a clipped version of each input after removal of their respective means.

The input signals are amplified and each is fed into a 100-second integrator. The output of each of the integrators is approximately of the form

$$\frac{K}{T}\int_0^T x(t)dt \tag{28}$$

where K is a circuit constant. The integrator output is then an estimate of the mean based on the previous 100 seconds of input.

The output of each integrator is subtracted from the input and clipped at a very low level by a two-sided clipper. The clipper gives a positive 6 volts if the signal is greater than its mean and a negative 6 volts if the signal is less than its mean.

The output from the two clippers is combined in an "exclusive-or" circuit. This circuit gives a positive output when both inputs are of the same sign and a negative output when the inputs are of different sign. Thus if input signals tend to deviate from their mean in opposite senses ($\rho < 0$), the circuit will give a negative voltage. When the signals deviate from their means in the same sense ($\rho > 0$), the output will be positive. If the signals are uncorrelated ($\rho = 0$), the output will be positive half the time and negative the other half. The output is integrated with a time constant of 100 seconds and recorded. An example of this record is shown in Fig. 80. This integrated output is approximately proportional to the correlation coefficient between the two input signals.

2. Accuracy of the Clipped Correlation Approximation

Assume the input signals to the correlator are cosine functions differing only in a constant phase angle, θ. The true correlation of these two signals as a function of the phase angle difference (also called the autocorrelation) is easily found. Similarly, the correlation of the clipped version of this autocorrelation has been determined. It is plotted

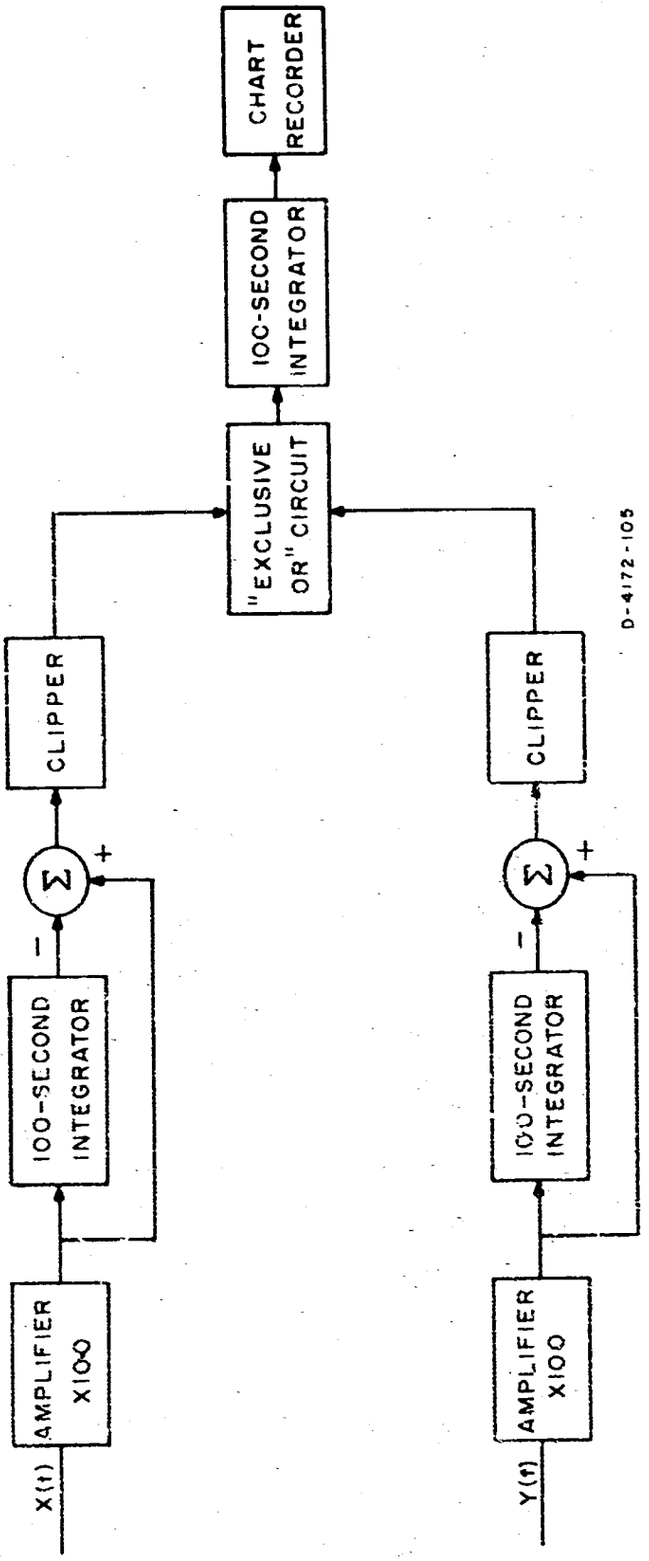

FIG. 79 BLOCK DIAGRAM OF CORRELATION COMPUTER

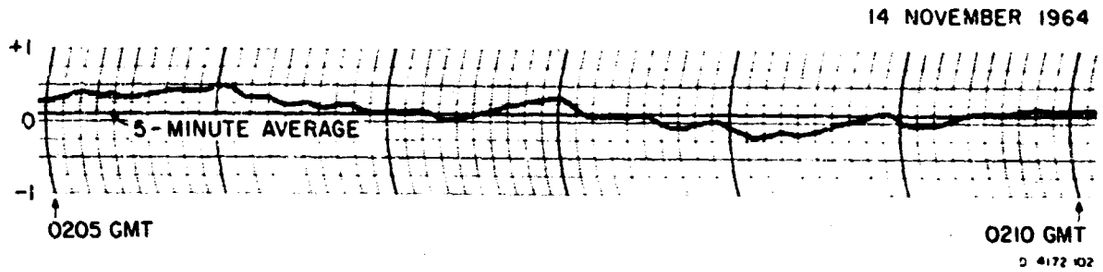

FIG. 80 EXAMPLE OF CORRELATION COMPUTER OUTPUT

in Fig. 81 along with the true autocorrelation. The greatest difference occurs at $\tau = \pi/4$, where the true correlation is 0.707 while the clipped approximation is 0.5.

For a Gaussian random process, Van Vleck[25] has shown that if $x(t)$ is the original process and $x_1(t)$ its clipped version, then the normalized autocorrelation function of the original process, ρ_x, in terms of the clipped version, ρ_{x1} is

$$\rho_x(\tau) = \text{Sin}\left[\frac{\pi}{2}\rho_{x1}(\tau)\right] \quad . \tag{29}$$

Thus for a Gaussian random process, a deterministic relationship exists between the two autocorrelation functions.

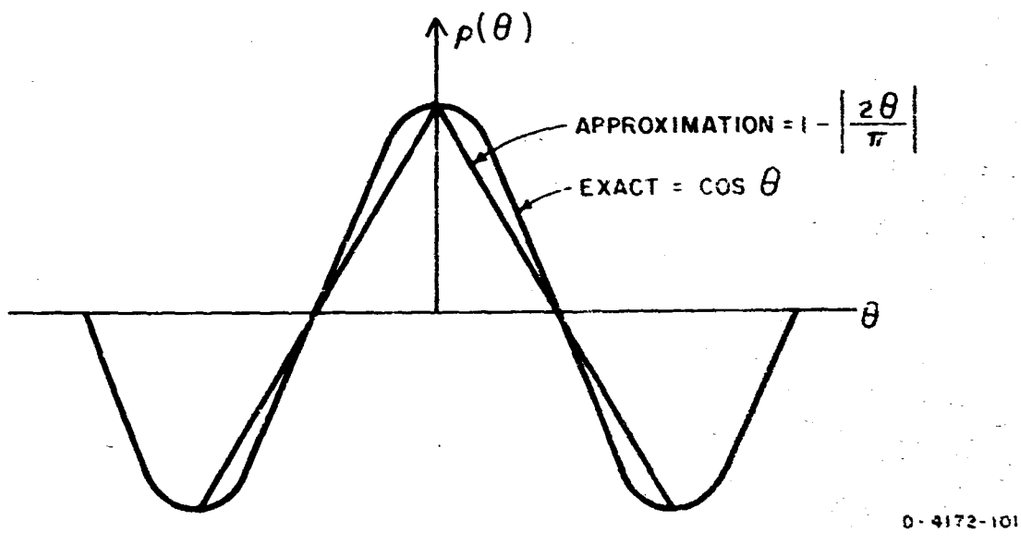

FIG. 81 CORRELATION COMPUTER APPROXIMATION TO TRUE CORRELATION FOR A SINUSOID

D. COMPARISON OF SPACE-DIVERSITY CORRELATION AND TIME SPREAD

It is interesting to compare the hourly trends between space-diversity correlation and time spread. In Sec. B.3 it was shown that a large spread in wave number would cause antennas spaced only a short distance apart to have uncorrelated envelopes. If it is further assumed that a situation in which modes are separated in wave number will also be one in which large separations exist in time delay, then a large time spread should indicate low correlation and vice versa.

The apparent validity of this assumption is illustrated in Fig. 82 for 7 Mc and to a lesser extent in Fig. 83 for 14 Mc. These curves consist of averages over each 5-minute period for space-diversity correlation 9 October to 14 November 1964 and for time spread from 4 to 14 November 1964. They show the hourly trends of each parameter and thus tend to average out daily fluctuations from these trends.

The 7-Mc average time spread and space correlation shown in Fig. 82 appear to be almost negatives of each other. This is not quite as apparent for the 14-Mc data. A possible reason for this difference between the two frequencies is the consistent presence of a greater number of modes on the lower frequency. At 14 Mc much of the uncorrelated fading may have been due to differences in polarization between the two antennas and correspondingly less to spread in wave number. It should be noted that from 2200 to 2300 the 14-Mc time-delay spread dropped to about 100 μsec, which would correspond to a single plane wave. The space-diversity correlation did not rise as fast during this period, nor did it attain a correlation of +1 which would be indicated for a single mode. Investigators such as Balser and Smith[26] and Hedlund and Edwards[27] have noted the presence of polarization fading on a single mode. Furthermore, with such a narrow wave-number dispersion function as would be present with a single mode, the presence of receiver noise or variation in antenna patterns would also tend to lower the correlation.

Figures 84 and 85 show the day-to-day variance of space-diversity correlation and time spread for both 7 and 14 Mc. The variance of each was computed for the same data as the averages cited previously. A high variance indicates a large day-to-day variation for the particular parameter at the particular time, while a small variance indicates relatively high day-to-day stability. For the 7-Mc data, it is clear that the change in variance of time spread with time of day is opposite to

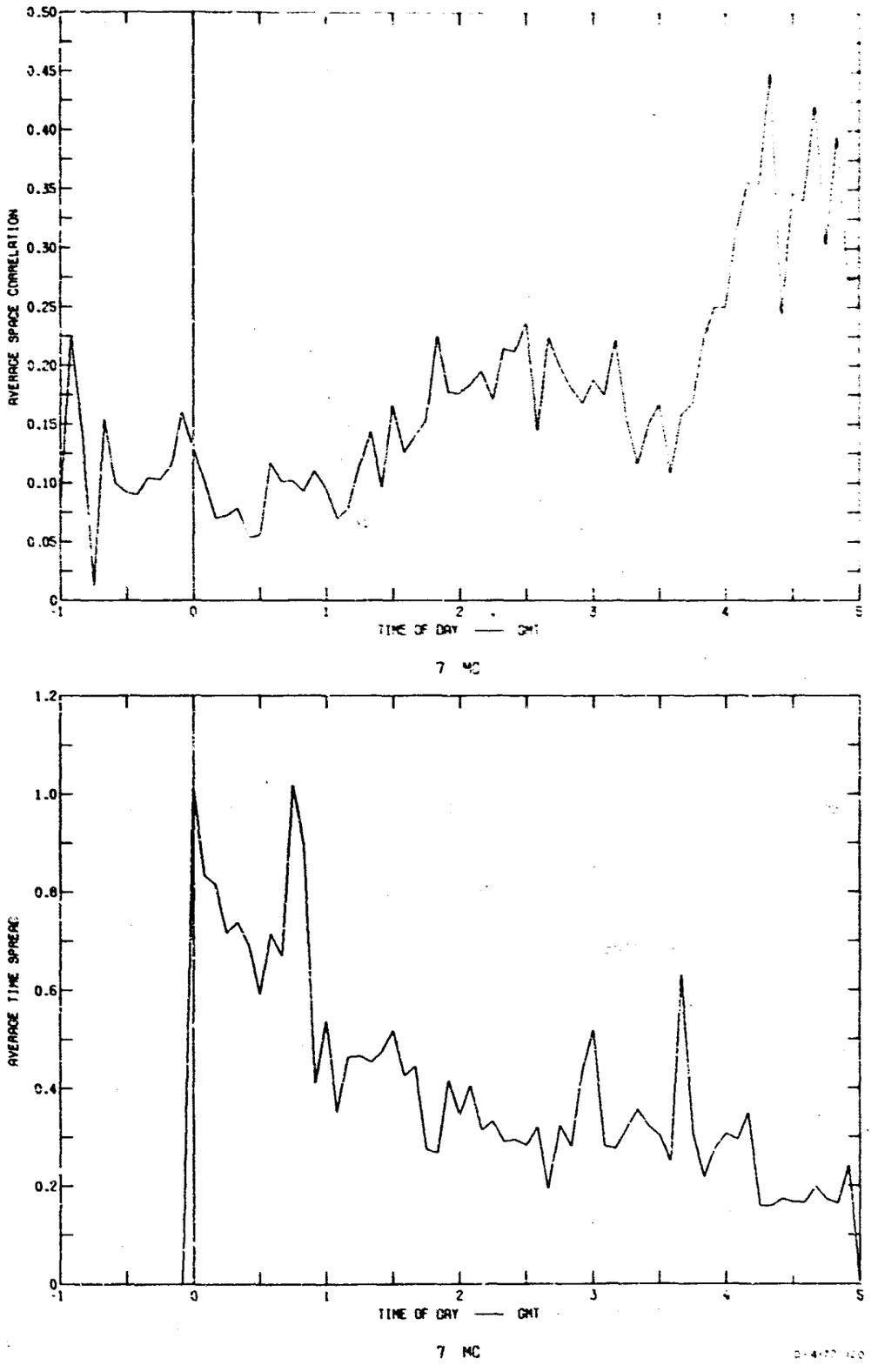

FIG. 82 COMPARISON OF AVERAGE CORRELATION AND TIME-DELAY SPREAD, 7 Mc

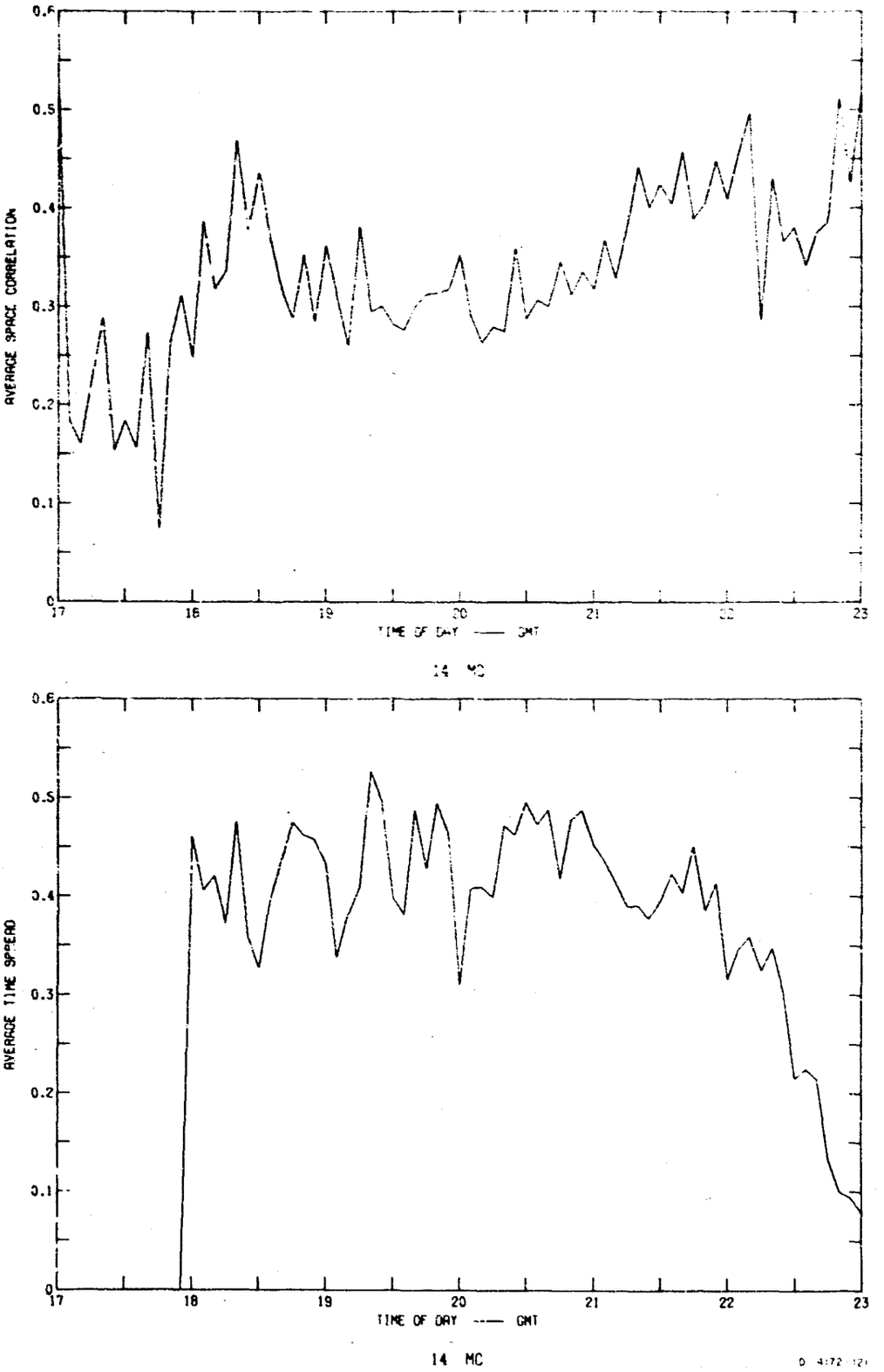

FIG. 83 COMPARISON OF AVERAGE CORRELATION AND TIME-DELAY SPREAD, 14 Mc

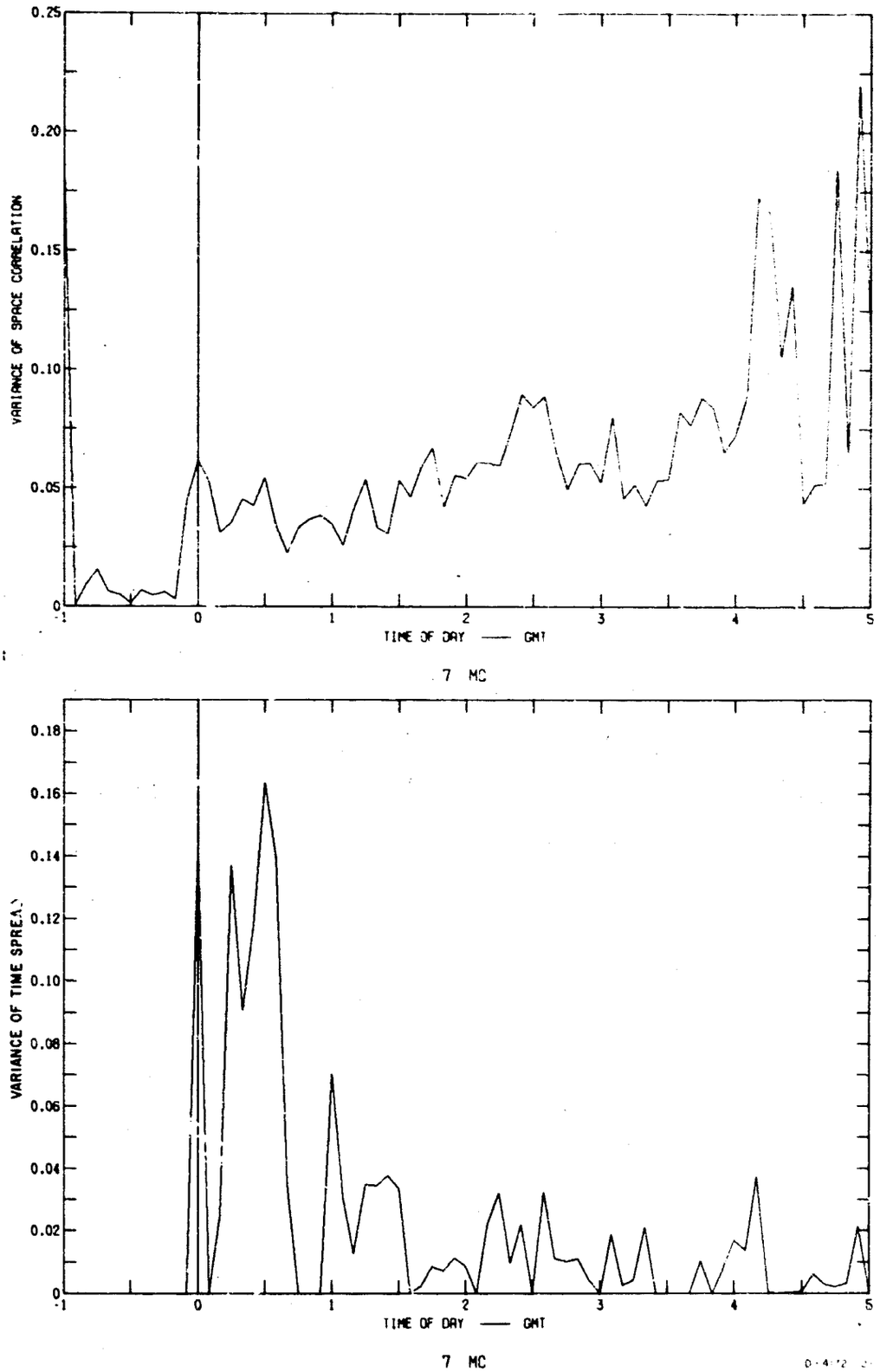

FIG. 84 COMPARISON OF VARIANCES OF CORRELATION AND TIME-DELAY SPREAD, 7 Mc

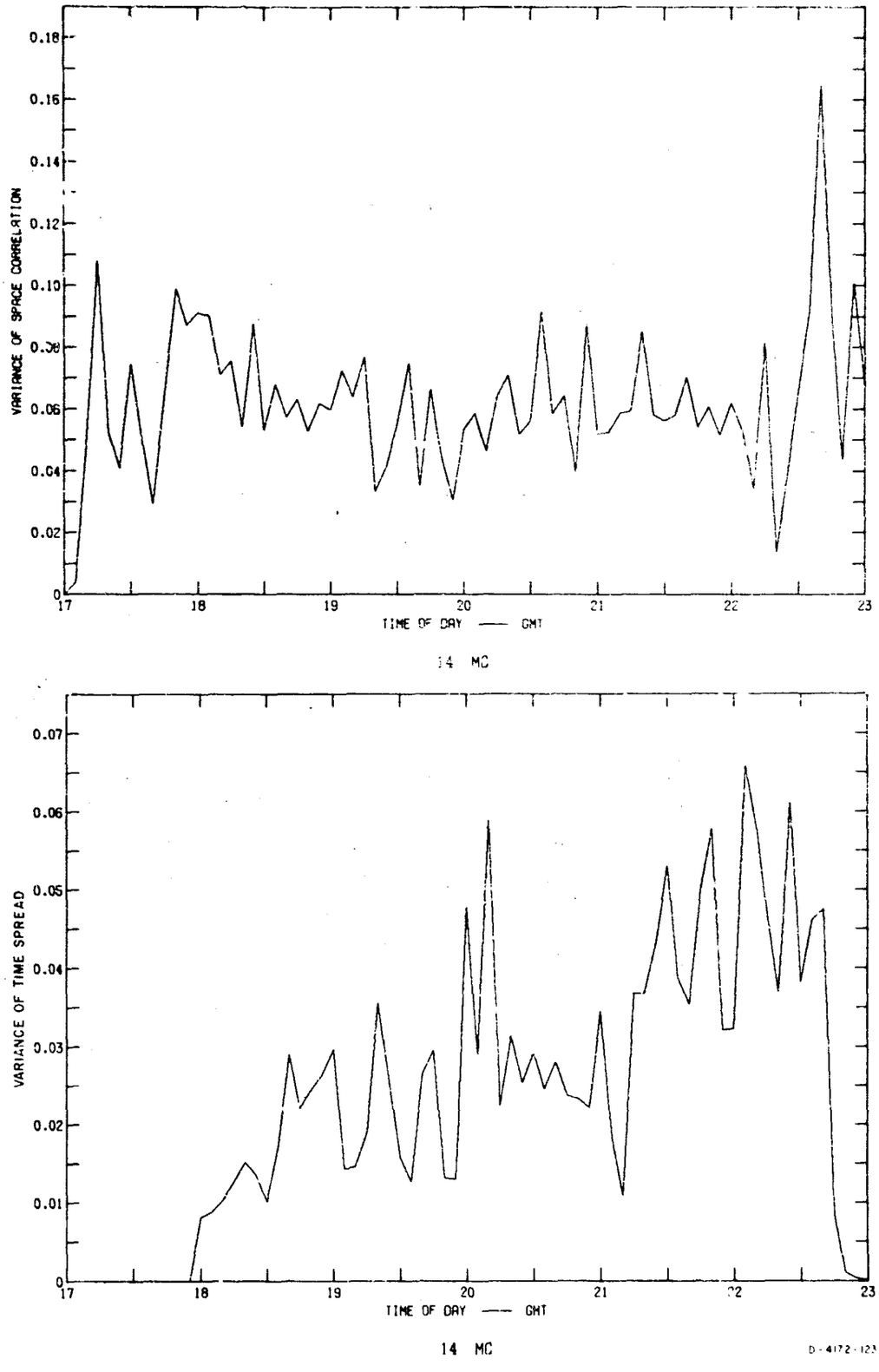

FIG. 85 COMPARISON OF VARIANCES OF CORRELATION AND TIME-DELAY SPREAD, 14 Mc

that of space-diversity correlation and that the change in variance of both time spread and space-diversity correlation with time of day is roughly the same as the change with time of day of their respective averages.

It may be deduced that a stable situation as far as time spread is concerned (*i.e.*, very few modes) is relatively unstable as far as space-diversity correlation is concerned. If few modes are present (stable variance), a change in elevation or azimuth of any one will have more drastic effects on the wave-number dispersion function (and hence on the space-diversity correlation) than if many modes were present.

The tendency of the averages to follow the variances indicates that day-to-day variations in a parameter are proportional to the magnitude of the parameter at that time. This, in turn, indicates a somewhat consistent measurement. Again, both these trends are somewhat less apparent at 14 Mc than at 7 Mc. The explanation is probably the same as that for the averages discussed earlier.

Figure 86 shows the histograms of 7- and 14-Mc space-diversity correlation. For each frequency, the number of occurrences is given without regard for time of day. The 7 Mc data are, on the average, more uncorrelated than those taken at 14 Mc, although the 1000-foot spacing between each set of antennas represented about 7-1/2 wavelengths at 7 Mc and 15 wavelengths at 14 Mc. This is certainly contradictory to much engineering practice, which assumes that the greater the spacing in wavelengths, the lower is the correlation between antennas. Again, the explanation probably lies in the fact that more modes were present in the 7-Mc data than in the 14-Mc.

In Sec. A.2, it was pointed out that the correlation coefficient between the envelopes of two jointly Gaussian random processes should never be negative. The appearance on the histograms of negative correlations may indicate that 5-minute samples were not long enough to average out the low-frequency variations of the processes. It is felt that if the sampling period had been increased to 10 minutes the average correlation would have been negative.

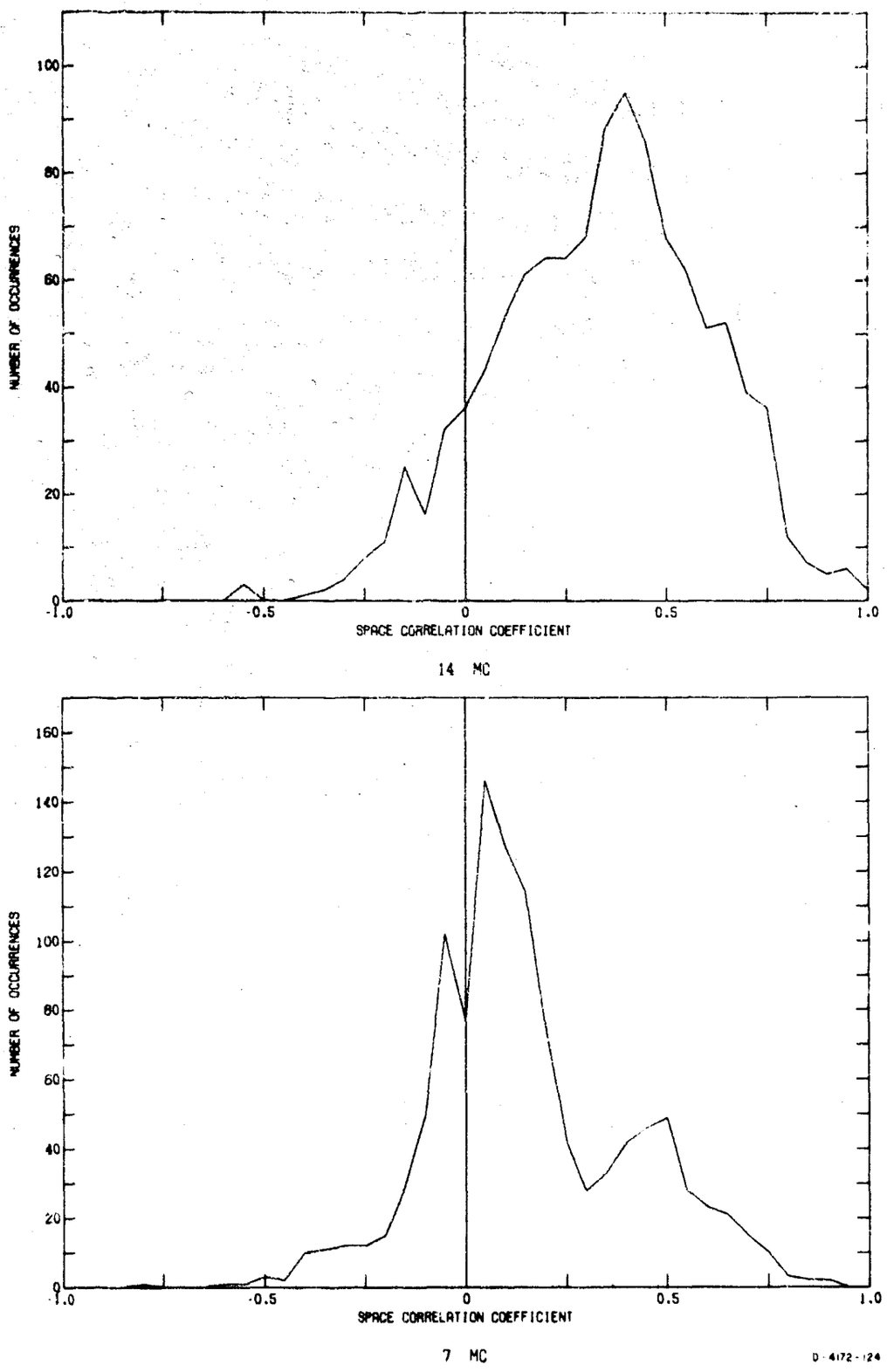

FIG. 86 HISTOGRAMS OF SPACE CORRELATION, 7 AND 14 Mc

E. OCCURRENCE OF ERRORS WITH DUAL DIVERSITY

Figure 87 shows the binary error probability for all the data taken with the use of a dual-diversity system. These data were taken from 9 to 12 November on both 7 and 14 Mc. It is clear that almost all of the points fall between the values that would be expected if no correlation existed (FSK 2) and those that would be obtained if complete correlation existed (FSK 1).

On 12 November errors were made during five non-contiguous 30-second intervals. Shown in Fig. 88 are raw data (without 300-second visual integration) 5 minutes before and after the 30-second interval in question. In each case, the correlation stayed above 0.6 for several minutes after the errors were made. Because of the 100-second time constant, the condition of the channel (for space correlation) for a given time was best obtained by observing the space-correlation data for at least 100 seconds after the given time. These results indicate that errors were made when the correlation coefficient was high. It should not be assumed that the converse is true: high correlation coefficient does not cause errors. The most probable explanation is that time- or frequency-selective fading is more likely to cause errors when correlation coefficient is high than when it is low.

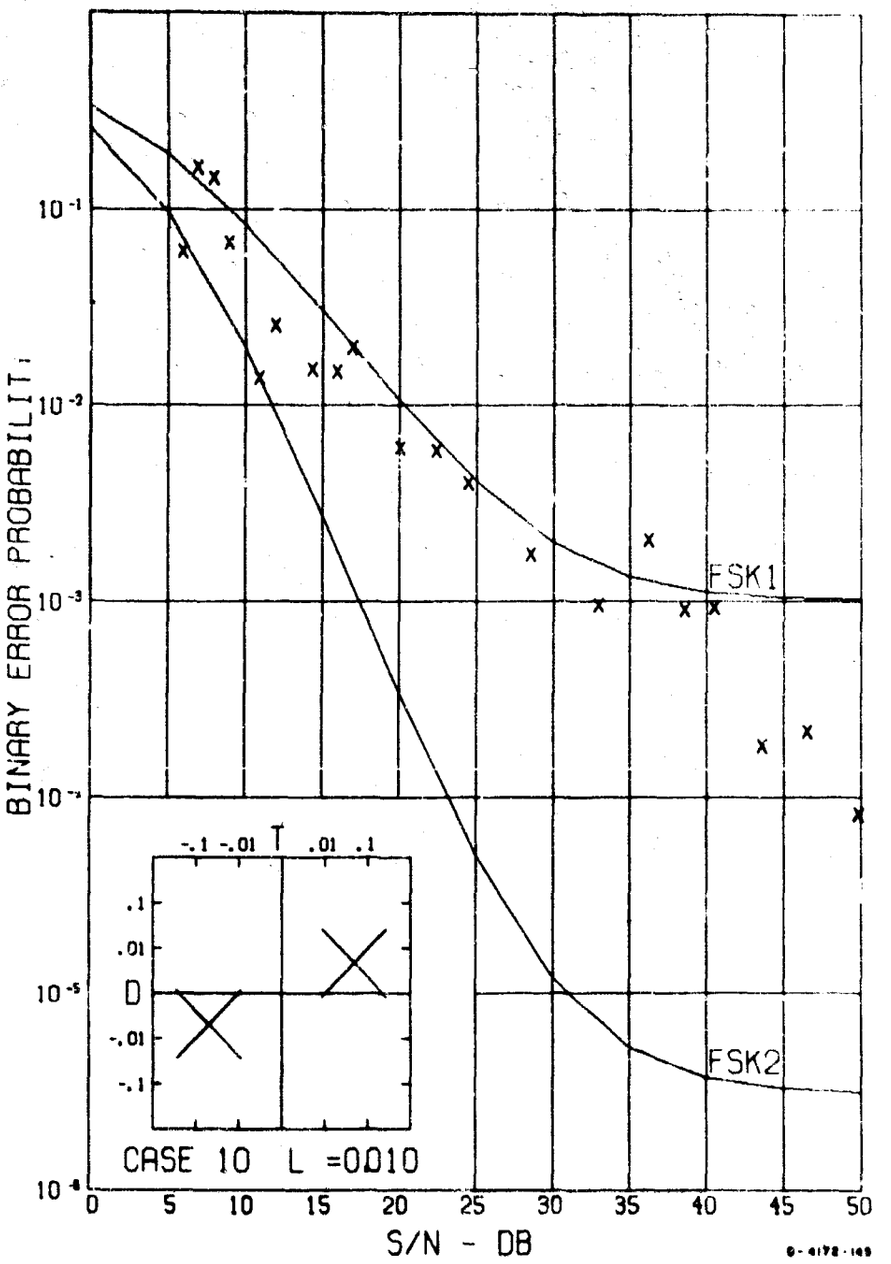

FIG. 87 MEASURED BINARY ERROR PROBABILITY vs. MEASURED S/N, ALL DIVERSITY DATA

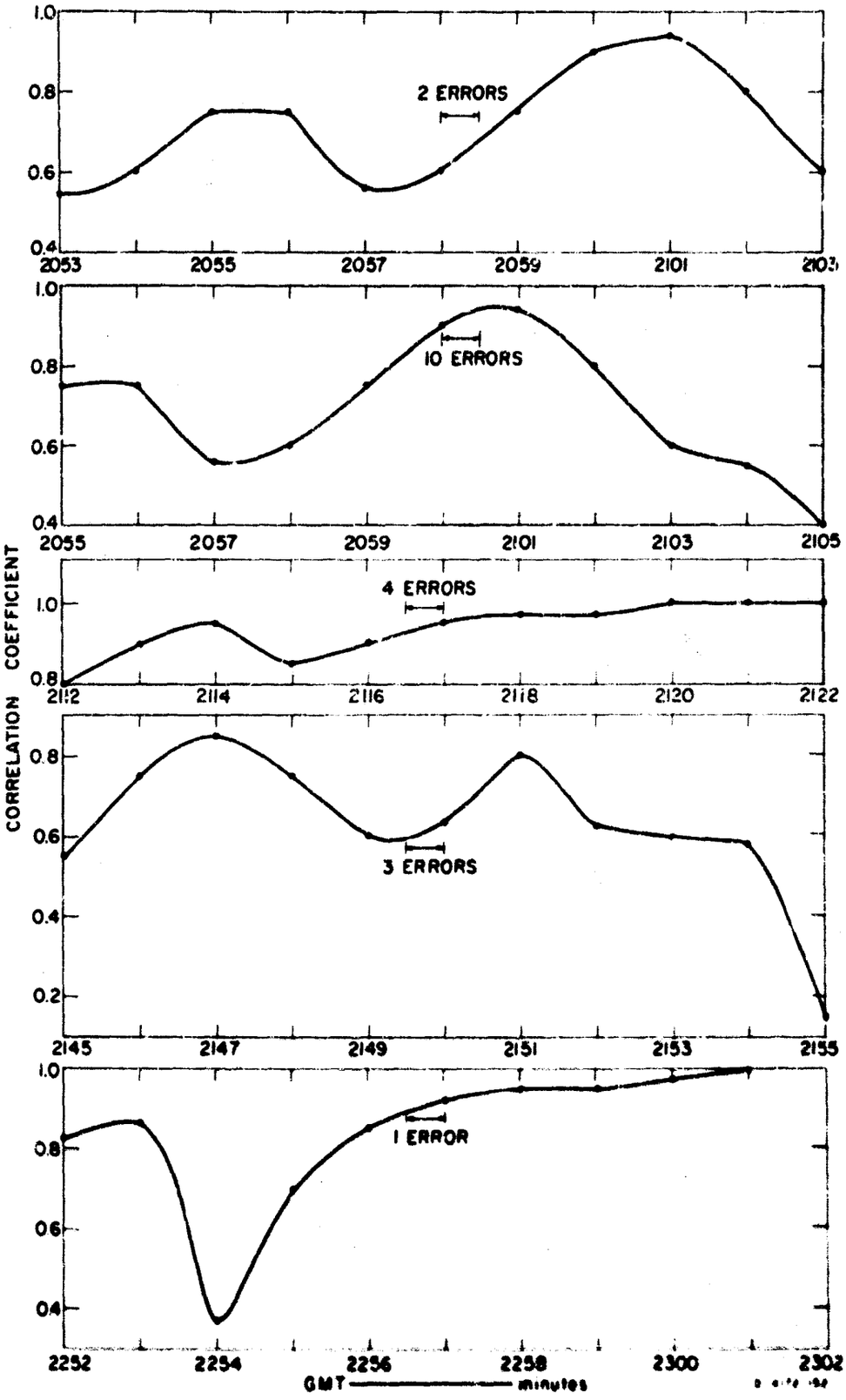

FIG. 88 SPACE CORRELATION BEFORE AND AFTER DETECTED ERRORS, 14 Mc 12 NOVEMBER 1964

VIII CONCLUSIONS

A mathematical model for an FSK data transmission system operating through an HF channel was developed by SRI to predict binary error rate. The channel portion of this model considers S/N as well as time-delay and Doppler-frequency effects introduced by the channel. The system portion of the model incorporates various realistic FSK system features including a finite transition time between the modulation states.

An experiment was conducted to simultaneously measure the binary error rate of an AN/FGC-29-type FSK system and the S/N, time-delay spread and Doppler-frequency spread of the channel. The results of this experiment are summarized in Figs. 46 through 55. The asymptotic bottoming out of the error-rate curves at high S/Ns for various channel conditions is clearly demonstrated.

For normalized time-delay and Doppler spreads less than 0.05, the asymptotic error rate for the theoretical model is much more sensitive to system transition time than to changes in the time-delay or Doppler-frequency spreading of the channel. The model shows that a reduction of system transition time from 200 to 50 μsec would reduce the asymptotic error rate from 1×10^{-3} to approximately 1×10^{-4} for relatively low spread conditions on the channel. This design feature should receive careful consideration in future FSK systems.

Although the ranges of time-delay and Doppler spread observed in the experiment were small, the performance of the experimental system showed a well-defined sensitivity to time- and frequency-selective effects. Although this sensitivity was greater than that predicted by the model, it was reasonable in view of the differences between the detection procedure of the modeled system and that of the experimental system.

Insufficient data were collected with dual-diversity operation to permit a confident comparison with the theoretical model. However, indications were that the existence of correlated space-diversity channels would produce higher measured error rates than predicted for the independent dual-diversity model. Measurements of antenna correlation have shown appreciable time intervals when correlation coefficients exceeded 0.6.

The alternative transmission sequence used in the experiment was chosen to maximize the frequency-selective effects. With a more random transmission sequence, representative of normal traffic, it could be expected that the irreducible error rate would be lower than measured here. The 100-baud transmission rate used in this experiment was slightly higher than the 75-baud rate used operationally with this system; the irreducible error rate would be slightly lower when used at the lower rate.

For a shorter HF propagation path than the 4100-km circuit used in this experiment, larger time-delay spreads and hence a higher irreducible error rate could be expected. Similarly, on paths through auroral activity or other highly turbulent ionospheric conditions, a higher irreducible error rate would be likely. A longer path would probably display smaller variations in time-delay and Doppler spread.

In general, the results of the experiment indicate the importance of the dispersive channel effects in limiting the performance of a communications system. For the range of spread conditions observed on the channel, the model yields a good fit to the average performance of the experimental system over all dispersive states observed. However, to obtain a more accurate error-rate estimation for lower and higher channel-spread conditions, it may be necessary to include in the model noninstantaneous energy-quenching and other filtering characteristics of the particular experimental system.

The adequacy of this, or any, error-rate model depends on its intended application. If this theoretical FSK model is to be used to compare the performance of the AN/FGC-29 system with the performance predicted by the theoretical model of another system under a wide range of channel conditions, it may be necessary to model the FSK system more closely. The results of the experiment give positive indications that the present FSK model can be modified to yield an adequate model of the AN/FGC-29 system for arbitrary dispersive states of the channel. Consideration should be given, however, to the variation of critical system parameters among AN/FGC-29 systems.

If, however, the model is to be used to estimate *outage time* of a circuit—based on some modest user-defined minimum preformance threshold—then the model is very likely to be adequate, especially if the variations in propagation conditions are extreme. Redundant-language traffic typically requires binary error rates of 10^{-3} for intelligibility. Probably

the high-accuracy requirement for data transmission will be achieved in current HF systems by the use of coding. Such systems will still operate with channel binary error rates in the 10^{-3} range. In a case where one is interested only in predicting whether the binary error rate is above or below that required for minimum performance, the range of interest in predicted error rates will be limited to moderate values, and the present system model will suffice.

APPENDIX A

ESTIMATION OF RMS VOLTAGE LEVELS WITH AN ENVELOPE DETECTOR

APPENDIX A

ESTIMATION OF RMS VOLTAGE LEVELS WITH AN ENVELOPE DETECTOR

Let $x(t)$ be a narrowband random process with zero mean. Consider the estimation of the power in the process by the detection scheme shown in Fig. A-1.

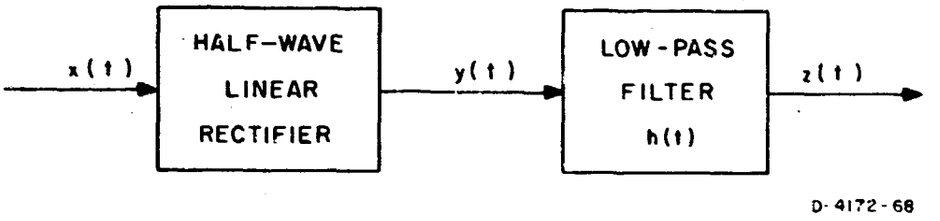

FIG. A-1 ENVELOPE DETECTOR–FILTER COMBINATION

The input may be written in the form

$$x(t) = V(t) \cos [2\pi f_0 t + \phi(t)]$$

where the envelope, $V(t) \geq 0$ for all t. A measure of the power in the input signal, $x(t)$, is the variance, $\sigma_x^2(t)$.

The output of the half-wave linear rectifier, $y(t)$, is

$$y(t) = V(t) \cos [2\pi f_0 t + \phi(t)] \quad \text{when } \cos [2\pi f_0 t + \varphi(t) \geq 0$$

$$= 0 \quad \text{otherwise} \quad .$$

By a Fourier series expansion, $y(t)$ may be written as

$$y(t) = V(t)\left(b_0 + b_1 \cos [2\pi f_0 t + \phi(t)] + b_2 \cos \{2[2\pi f_0 t + \phi(t)]\} + \ldots\right) \quad .$$

Since $z(t)$ is a low-pass filtered version of $y(t)$ with a cutoff frequency much smaller than f_0, then

$$z(t) = [b_0 V(t)] * h(t)$$

$$= b_0 \int_{-\infty}^{\infty} V(\tau) h(t - \tau) d\tau \quad .$$

Without any loss in generality, both b_0 and $\int_{-\infty}^{\infty} h(t - \tau) d\tau$ will be chosen equal to one, since these are arbitrary gain constants. The value of $z(t)$ will be chosen as an estimate of $\sigma_x(t)$, the rms value of the input signal process. The expected value of the estimate is

$$\overline{z}(t) = \int_{-\infty}^{\infty} \overline{V}(\tau) h(t - \tau) d\tau \quad . \tag{A-1}$$

If the mean of $V(t)$ does not vary appreciably during the memory of the low-pass filter, then Eq. (A-1) reduces to

$$\overline{z}(t) = \overline{V}(t) \quad .$$

For a simple *RC* filter, a realistic value of the filter memory is on the order of two or three time constants.

It will be shown that for some processes the square root of the input power and the expected value of the input signal envelope are approximately proportional,

$$\overline{V}(t) \simeq K \sigma_x(t) \tag{A-2}$$

where $\sigma_x(t)$ is the rms value of the input signal process at time t and K is a constant dependent upon the process. The functional dependence upon t is retained to include nonstationary processes. When power ratios are formed, as in S/N calculations, the constants will cancel if the noise and signal plus noise processes have the same constant. If the constants for the two processes are not identical, then an additional bias is introduced into the result.

To illustrate possible values of K, the expected value of the random variable V may be obtained for various assumed distributions. If V has a Rayleigh distribution, then

$$\overline{V} = \sqrt{\pi/2}\,\sigma \quad , \quad i.e., \; K = \sqrt{\pi/2} \quad .$$

If the input signal is a sinusoid of fixed amplitude A, the output, $z(t)$, will be a constant value equal to A. The output is thus equal to $\sqrt{2}$ times the rms value of the input signal.

If V has a Rice distribution, and $\sigma_x(t)$, the rms value of $x(t)$, is $[(A^2/2) + \sigma^2]^{1/2}$; then[28]

$$\bar{V} = \sqrt{\frac{\pi}{2}}\,\sigma\ {}_1F_1\left(-\frac{1}{2}\ ;\quad 1\ ;\quad -\frac{A^2}{2\sigma^2}\right)$$

where ${}_1F_1$ is a hypergeometric function. If

$$\frac{A^2}{2\sigma^2} \geq 10$$

then, by using the first two terms in the expansion of the hypergeometric function, the following result may be obtained.

$$\bar{V} \simeq A + \frac{1}{2}\left(\frac{\sigma}{A}\right)\sigma$$

$$= \sqrt{2}\left[\frac{A^2}{2} + \sigma^2\left(\frac{1}{2} + \frac{1}{8}\,\frac{\sigma^2}{A^2}\right)\right]^{1/2}$$

$$\simeq \sqrt{2}\,\sigma_x \quad .$$

In this case we do not have a linear relationship between $\bar{V}$ and σ_x, the rms value of $x(t)$. However, under the conditions of the approximation, the relationship is roughly true with the constant of proportionality equal to $\sqrt{2}$.

It is interesting to note that a parameter designated V_d and defined as

$$V_d \triangleq 20\ \log\left[\left.\overline{\left(\frac{V}{\sqrt{2}}\right)^2}^{1/2}\middle/\left(\frac{\bar{V}}{\sqrt{2}}\right)\right.\right]$$

$$= 10\ \log\left(\left.\overline{V^2}\middle/\bar{V}^2\right.\right)$$

has been extensively investigated experimentally for HF atmospheric noise by the National Bureau of Standards.[29] The parameter is related to K as given in Eq. (A-2) by

$$V_d = 20 \log \left(\frac{\sqrt{2}}{K}\right) .$$

The NBS work indicates that the value of V_d lies between 2 and 4 for the frequency range 7 to 15 Mc with the variation occurring between winter daytime and summer nighttime. These values correspond to values of K equal to 1.12 and 0.89, respectively. The values are strictly valid only for a particular year and the site near Boulder, Colorado; however, they give some indication of the values of K that might be expected for atmospheric noise.

As a result of higher values of K for signal measurement than for noise measurement, calculated S/N assuming equal values of K may be as much as 4 db high. This is the worst-case estimate; however, the calculation may be 2 and possibly 3 db high.

APPENDIX B

ESTIMATION OF POWER AND POWER RATIOS

APPENDIX B

ESTIMATION OF POWER AND POWER RATIOS

It has been shown in Appendix A that if the time variations of the input envelope are slow compared to the filter memory, then the expected output of a linear detector-filter combination, $\bar{z}(t)$, is the expected value of the envelope, $\bar{V}(t)$, of the input signal. Further, it has been shown that the square of the expected value of the envelope is approximately proportional to the power in the input signal.

Suppose we wish to obtain an estimate of the average power in the signal over a time interval T'. Assume that a series of n independent sample values, $z(t_1)$, $z(t_2)$, ..., $z(t_n)$, are available. The actual power (the time average of the ensemble average power), $\langle P \rangle_{T'}$, is given by

$$\langle P \rangle_{T'} = \frac{1}{T'} \int_0^{T'} \sigma^2(t)\,dt$$

and by approximating the integration by a summation becomes

$$\langle P \rangle_{T'} \approx \frac{1}{n} \sum_{i=1}^{n} \sigma^2(t_i) \qquad t_i \text{ in } [0, T']$$

where $\sigma^2(t)$ is the ensemble variance of the signal process $x(t)$ at time t. For a stationary process

$$\langle P \rangle_{T'} = \frac{1}{T'} \int_0^{T'} \sigma^2\,dt$$

$$= \sigma^2 .$$

It has been shown that for the cases of interest

$$\bar{z}(t) = \bar{V}(t) = K\sigma(t)$$

Define an error term

$$\varepsilon_i = z(t_i) - K\sqrt{\langle P\rangle_{T'}}$$

which has zero mean for the stationary case. Assuming that the errors are independently, jointly normally distributed, the joint probability density function is

$$P\left(z_1, z_2, \ldots, z_n; K\sqrt{\langle P\rangle_T}\right) = \frac{1}{(2\pi\sigma^2)^{n/2}} \exp\left[-\frac{1}{2\sigma^2}\sum_{i=1}^{n}\left(z_i - K\sqrt{\langle P\rangle_{T'}}\right)^2\right] \tag{B-1}$$

where $z(t_i)$ is defined as z_i. Given $(z_1, \ldots, z_n)$, the best estimate of $K\sqrt{\langle P\rangle_{T'}}$ is known to be the maximum-likelihood estimate.[30] This estimate,

$$\widehat{\left(K\sqrt{\langle P\rangle_T}\right)},$$

is determined by maximizing the likelihood function

$$P\left[z_1, z_2, \ldots, z_n; \quad \widehat{\left(K\sqrt{\langle P\rangle_{T'}}\right)}\right]$$

for each $(z_1, z_2, \ldots, z_n)$. For the function of Eq. (B-1), this is most easily achieved by maximizing the natural logarithm of the function. The resulting maximum-likelihood estimate becomes

$$\widehat{\left(K\sqrt{\langle P\rangle_{T'}}\right)} = \frac{1}{n}\sum_{i=1}^{n} z_i ,$$

and the best estimate of the power becomes

$$\hat{\langle P\rangle}_T = \frac{1}{K^2}\left[\frac{1}{n}\sum_{i=1}^{n} z_i\right]^2 .$$

It is often necessary to estimate S/Ns from the power estimate of S + N and noise. Define a measure of the power as W where

$$W = \left[\frac{1}{n}\sum_{i=1}^{n} z_i\right]^2 .$$

For S + N and for noise only present, respectively, we have

$$\overline{W_{S+N}} = K_{S+N}^2 \sigma_{S+N}^2$$

$$\overline{W_N} = K_N^2 \sigma_N^2 .$$

Since the signal and noise are independent and zero mean processes, the total power is equal to the sum of the individual powers,

$$\sigma_{S+N}^2 = \sigma_S^2 + \sigma_N^2 .$$

The true S/N is given by

$$\frac{S}{N} = \frac{\sigma_S^2}{\sigma_N^2}$$

$$= \frac{\sigma_{S+N}^2}{\sigma_N^2} - 1$$

$$= \frac{K_N^2\ \overline{W_{S+N}}}{K_{S+N}^2\ \overline{W_N}} - 1 .$$

Since we have insufficient information to specify the ratio (K_N/K_{S+N}) with any degree of confidence, we choose as our S/N estimate

$$\left(\frac{\hat{S}}{N}\right) = \frac{W_{S+N}}{W_N} - 1 .$$

The expected value of the estimate is

$$\overline{\left(\frac{\hat{S}}{N}\right)} = \overline{\left(\frac{W_{S+N}}{W_N}\right)} - 1$$

$$= \overline{\left(\frac{W_{S+N}}{\overline{W_N} - \epsilon_N}\right)} - 1$$

where ϵ_N represents the variation of the noise power estimate about its mean. Since the noise power estimate will always be greater than zero,

$$\overline{\left(\frac{\hat{S}}{N}\right)} = \overline{\left(\frac{W_{S+N}}{\overline{W_N}}\right)\left[1 + \frac{\overline{\epsilon_N}}{\overline{W_N}} + \frac{\overline{\epsilon_N^2}}{\overline{W_N}^2} + \frac{\overline{\epsilon_N^3}}{\overline{W_N}^3} + \ldots\right]} - 1$$

$$= \left(\frac{K_{S+N}^2}{K_N^2}\right)\left(\frac{S}{N}\right)\left[1 + \frac{\overline{\epsilon_N^2}}{\overline{W_N}^2} + \frac{\overline{\epsilon_N^3}}{\overline{W_N}^3} + \ldots\right]$$

$$+ \frac{K_{S+N}^2}{K_N^2}\left[1 + \frac{\overline{\epsilon_N^2}}{\overline{W_N}^2} + \frac{\overline{\epsilon_N^3}}{\overline{W_N}^3} + \ldots\right] - 1 \quad .$$

With the assumption that the sum,

$$\frac{\overline{\epsilon_N^2}}{\overline{W_N}^2} + \frac{\overline{\epsilon_N^3}}{\overline{W_N}^3} + \frac{\overline{\epsilon_N^4}}{\overline{W_N}^4} + \ldots$$

is negligible compared to one, we have approximately

$$\overline{\left(\frac{\hat{S}}{N}\right)} \approx \left(\frac{K_{S+N}^2}{K_N^2}\right)\left(\frac{S}{N}\right) + \left(\frac{K_{S+N}^2}{K_N^2} - 1\right) \quad .$$

Normally the last term will be insignificant, since K_{S+N} is of the same order of magnitude as K_N. The multiplicative constant, $(K_{S+N}/K_N)^2$, in the first term introduces an additive bias when the S/N is expressed in decibels. The constant will normally be greater than one and increase with S/N (see Appendix A). The resulting estimate may thus be 2 or 3 db high.

APPENDIX C

ERROR ANALYSIS OF S/N ESTIMATIONS

APPENDIX C

ERROR ANALYSIS OF S/N ESTIMATIONS

In the formulation of the S/N in decibels, the logarithm of a power ratio is formed. In the error analysis, the effect of errors in the power measurement upon the S/N (expressed in decibels) must be considered. In the material that follows, the error propagation effects are analyzed.

First, consider the expansion of the estimate in a Taylor series about the true value:

$$ln\left(\frac{x + \epsilon_x}{y + \epsilon_y}\right) = ln\left(\frac{x}{y}\right) - \sum_{n=1}^{\infty}\left[-\frac{\epsilon}{\left(\frac{x}{y}\right)}\right]^n \frac{1}{n!}$$

$$= ln\left(\frac{x}{y}\right) + 1 - \exp\left[-\frac{\epsilon}{\left(\frac{x}{y}\right)}\right]$$

where

$$\epsilon = \frac{x + \epsilon_x}{y + \epsilon_y} - \frac{x}{y} = \frac{\epsilon_x}{y + \epsilon_y} - \left(\frac{x}{y}\right)\frac{\epsilon_y}{(y + \epsilon_y)} .$$

Therefore,

$$ln\left(\frac{x + \epsilon_x}{y + \epsilon_y}\right) = ln\left(\frac{x}{y}\right) + 1 - \exp\left[\frac{\epsilon_y}{(y + \epsilon_y)} - \frac{y\epsilon_x}{(y + \epsilon_y)x}\right] .$$

If the error of the original measurements may be bounded in the following way,

$$\frac{|\epsilon_x|}{x} \leq e$$

$$\frac{|\epsilon_y|}{y} \leq e .$$

that is, if we can bound both terms with a fixed percentage error, then

$$1 - \exp\left(\frac{2e}{1+e}\right) \leq 1 - \exp\left[\frac{\epsilon_y}{y+\epsilon_y} - \frac{y\epsilon_x}{(y+\epsilon_y)x}\right] \leq 1 - \exp\left(\frac{-2e}{1-e}\right) .$$

In the Taylor series expansion it has been convenient to use natural logarithms: an error bound may be given in decibels that is independent of the S/N and depends only upon the percentage error, e, assumed for the original power measurements. The lower bound is

$$\frac{10}{ln\ 10}\left[1 - \exp\left(\frac{2e}{1+e}\right)\right]$$

and the upper bound is

$$\frac{10}{ln\ 10}\left[1 - \exp\left(\frac{-2e}{1-e}\right)\right] .$$

These error bounds are plotted as a function of the percentage error in the original power estimate in Fig. C-1. To illustrate, an error of ±25 percent in the power measurement ($e = 0.25$) will result in, at most, an error of ±2 db in the S/N.

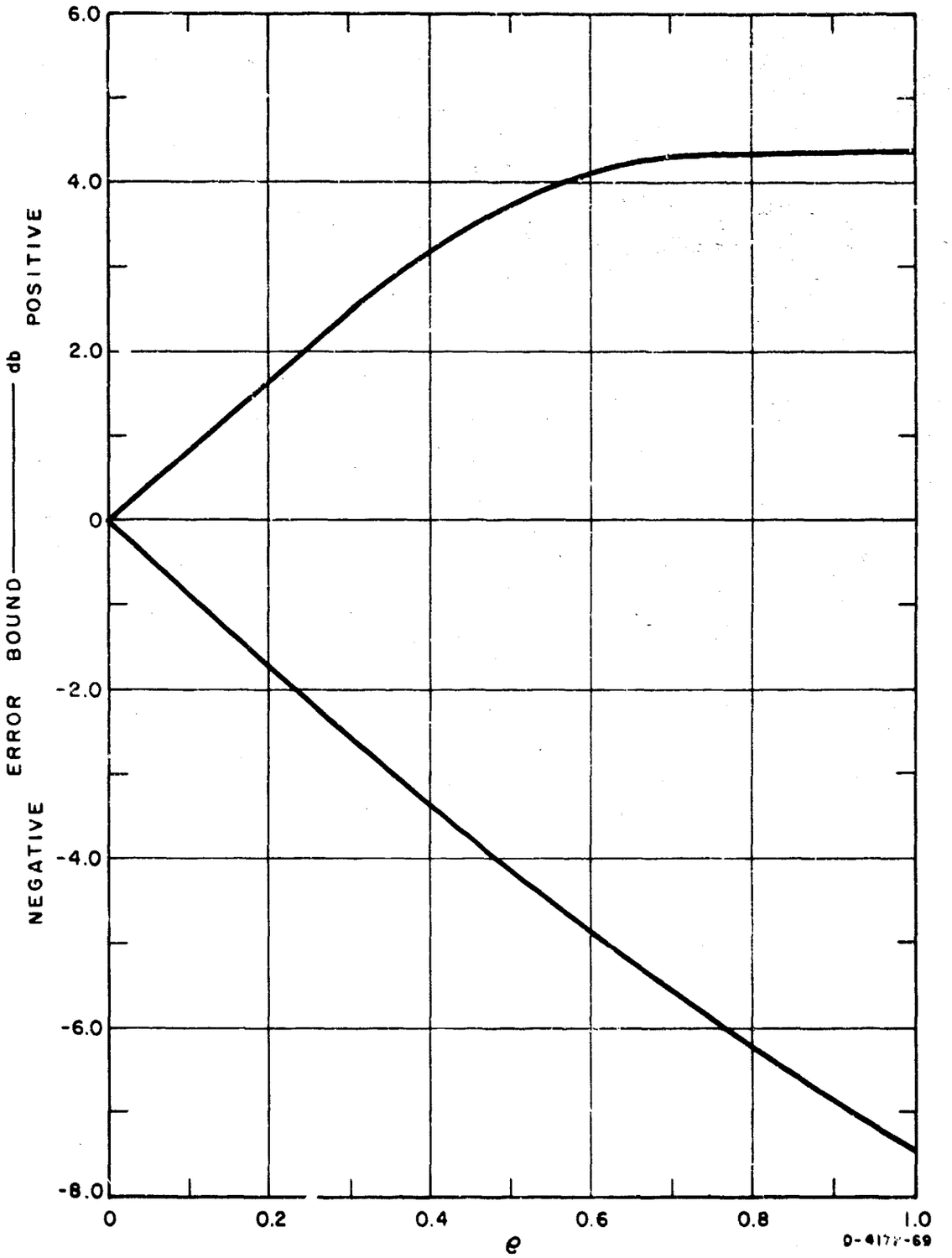

FIG. C-1 THE ERROR BOUNDS FOR S/N IN DECIBELS WHEN THE POWER ESTIMATES, P, ARE BOUNDED BY AN ERROR OF ±eP

APPENDIX D

CONFIDENCE LIMITS IN THE MEASUREMENT OF LOW ERROR PROBABILITIES

APPENDIX D

CONFIDENCE LIMITS IN THE MEASUREMENT OF LOW ERROR PROBABILITIES

1. INTRODUCTION

The experimental validation of an error-rate model for a communications system requires an estimate of the true binary error rate from a finite set of measurements. Two questions then arise: How much confidence can be placed in error-rate estimates made with limited measured data? How much measuring must be done to obtain a given degree of confidence in an estimate?

The general technique for measuring the binary error rate of a communications system is to transmit a known binary sequence over the channel, compare the receiver's decision with a local reference, and compute the ratio of the number of errors to the number of transmitted bits for some interval. The receiver decides, only through its normal detection scheme, which binary signal was transmitted. After some measuring interval, we are asked to give an estimate of the true binary error rate for the system from this data. Because our estimate must be based on a finite number of samples of a random phenomenon, it will be subject to some error. If we can describe this error in terms of a probability law, we can better assess the accuracy of our answer. When the true error rate is small, we may obtain a very few errors in our sample. We then have the classical problem of estimating the rate of occurrence of rare events from a small sample.

2. ERROR-RATE PROBABILITY LAW

A binary communications system transmits one of two possible signals (mark or space), and the receiver must decide at the end of each signaling element time which signal was transmitted. These receiver decisions can be described by Bernoulli trials where the results are traditionally termed success or failure. In this Appendix, the occurrence of an error will be designated by success and the absence of an error by failure. This definition is consistent with statistical conventions.

For a symmetrical binary channel, we define p as the probability of a detected error, where a detected error is defined as a mark received when a space was transmitted or a space received when a mark was transmitted. We desire to estimate the parameter p from our measurements.

3. LOW-ERROR CONFIDENCE INTERVALS

From a Bernoulli probability distribution, if we take n independent samples where the probability of error (or success) is p, the probability of obtaining x errors will follow a binomial distribution. (The case when the samples are not independent is discussed later.) If we know *a priori* that the probability of error is low (*i.e.* $p < 0.1$), we can approximate this adequately by a Poisson distribution.

We then find confidence intervals for this distribution by determining probabilities that k_1 or less errors occur and k_2 or more errors occur, given that the true error rate is p:

$$P[x \leq k_1] = \sum_{x=0}^{k_1} \frac{e^{-np}(np)^x}{x!}$$

$$P[x \geq k_2] = \sum_{x=k_2}^{\infty} \frac{e^{-np}(np)^x}{x!} \quad ,$$

where n is the number of samples taken.

Note that the product, np, is also the expected number of errors we would observe with this error rate and number of samples. The expected number of errors (or successes) is more conventionally defined as the parameter of the Poisson distribution.

If we have observed a particular number of errors in an experiment but do not know the value of the parameter, we can reverse the procedure and determine ranges of parameters that could still give the observed value within a given probability.

From cumulative Poisson distribution tables we determine the following:

(1) The smallest integer value of the parameter, np_1, such that with k observed errors

$$\sum_{x=0}^{k} \frac{e^{-np_1}(np_1)^x}{x!} \leq C$$

(2) The largest integer value of the parameter, np_2, such that with k observed errors

$$\sum_{x=k}^{\infty} \frac{e^{-np_2}(np_2)^x}{x!} \leq C$$

where C is some confidence level (*e.g.*, 0.05).

If we observe k errors in a sample of n, the best estimator, $\hat{p}$, of the true binary error rate is simply the ratio k/n. The upper and lower confidence limits at some confidence level, C, are p_1 and p_2. Values of np_1 and np_2 for a confidence level of 5 percent are shown in Table D-I.

4. CONFIDENCE CRITERIA

It is convenient at this stage to seek a single-valued confidence parameter. For example, we could define a ratio, A, in terms of the upper and lower confidence estimates as

$$A = \frac{p_1}{p_2} .$$

Or we could define a percentage error, P, between the confidence estimates and the estimate itself as follows:

$$P = \frac{p_1 - p_2}{\hat{p}} \cdot 100$$

Table D-I

UPPER AND LOWER 90-PERCENT CONFIDENCE ESTIMATES
OF POISSON PARAMETER WITH k OBSERVED SUCCESSES

k	UPPER CONFIDENCE LEVEL* (np_1)	LOWER CONFIDENCE LEVEL* (np_2)	RATIO (A)	PERCENTAGE ERROR (P)
0	3.0	--	--	--
1	4.75	0.052	91.3	470
2	6.3	0.36	17.5	297
3	7.76	0.82	9.46	231
4	9.15	1.38	6.63	191
5	10.5	1.97	5.33	171
6	11.85	2.61	4.54	151
7	13.15	3.29	4.0	141
8	14.43	3.98	3.62	131
9	15.8	4.7	3.36	123
10	17.	5.44	3.12	116
11	18.2	6.18	2.94	109
12	19.5	6.94	2.81	105
13	20.8	7.7	2.7	101
14	21.9	8.46	2.59	96
15	23.1	9.25	2.50	92
17	25.8	10.85	2.38	88
20	29.2	13.27	2.20	80
25	34.9	17.3	2.02	70
30	40.6	22.4	1.81	61
50	64.	39.9	1.60	48
70	86.5	58.1	1.49	41
100	118.8	85.6	1.39	33
200	228.	182.	1.25	23
300	335.	279.	1.20	19
500	543.	467.	1.16	15
10^3	1063.	961.	1.11	10

* Confidence level = 0.05.

Both of these parameters are also tabulated in Table D-I. Notice that these confidence criteria depend directly on the number of *errors observed* and not on the number of samples taken.

We are now in a position to determine the amount of sampling we must do to obtain a given degree of confidence in our parameter estimate. If we use one of the above confidence definitions, our rule is to continue to sample until the observed errors are greater than a required number. Note that as the sample size is always increased until the number of observed errors exceeds a constant, then the number of samples required will

be roughly inversely proportional to the error-rate estimate. This is intuitively satisfying in that more samples are required for lower error-rate estimates.

5. EXAMPLE

Assume we desire to state with 90-percent confidence that the difference between the upper and lower confidence levels is always less than the estimate itself. From Table D-I we see that this would require a minimum of 14 observed errors in our sample. If the number of observed errors in a string of 1000 transmitted bits were 6, we would defer making an error probability estimate until we observed, say, an additional 1000 bits. If the next 1000 bits contained 8 errors we would estimate the error probability as 14/2000 or 7×10^{-3}. And we could say with 90-percent confidence that the true error probability lies within 4.2×10^{-3} and 1.1×10^{-2}.

6. CORRECTIONS FOR NONINDEPENDENT ERRORS

It has been observed at HF that errors do not occur independently. However, without a detailed knowledge of the exact statistics of the error distributions, we assume that the errors occur in average bursts of length, L, and that the *bursts* of errors are independent. To obtain confidence limits we consider that an "error" is in reality a burst of L errors so that the minimum number of actual errors required for a given confidence is L times the previously defined errors.

In the previous example, assume that the average burst is 7 errors in length. To observe 14 independent bursts of errors, we would need to accumulate slightly over 100 errors before obtaining the degree of confidence desired.

APPENDIX E

TIME INTERVAL CLASSIFICATIONS OF CHANNEL ACCORDING TO MEASURED TIME-DELAY- AND DOPPLER-FREQUENCY-SPREAD CONDITIONS

APPENDIX E

TIME INTERVAL CLASSIFICATIONS OF CHANNEL ACCORDING TO MEASURED TIME-DELAY- AND DOPPLER-FREQUENCY-SPREAD CONDITIONS

TABLE	TIME-DELAY-SPREAD RANGE (msec)	DOPPLER-FREQUENCY-SPREAD RANGE (cps)
1	0 - 0.25	0 - 0.25
2	↓	0.25 - 0.5
3	↓	0.5 - 1.0
4	0.25 - 0.75	0 - 0.25
5	↓	0.25 - 0.5
6	↓	0.5 - 1.0
7	0.75 - 1.5	0 - 0.25
8	↓	0.25 - 0.5
9	↓	0.5 - 1.0

DATA TIME INIERVALS

						TABLE
11- 4	1108: 0	TO	11- 4	1834:31		4
11- 4	1834:31	TO	11- 4	1838: 0		4
11- 4	1838: 0	TO	11- 4	1859:31		4
11- 4	1859:31	TO	11- 4	1904:31		4
11- 4	1904:31	TO	11- 4	1909:30		4
11- 4	1909:30	TO	11- 4	1914:30		4
11- 4	1914:30	TO	11- 4	1919:31		4
11- 4	1919:31	TO	11- 4	1924:31		4
11- 4	1924:31	TO	11- 4	1929:31		4
11- 4	1929:31	TO	11- 4	1934:30		4
11- 4	1934:30	TO	11- 4	1938: 0		4
11- 4	1938: 0	TO	11- 4	1942: 1		4
11- 4	1942: 1	TO	11- 4	1949:31		4
11- 4	1949:31	TO	11- 4	1954:30		4
11- 4	1954:30	TO	11- 4	1959:30		4
11- 4	1959:30	TO	11- 4	2007: 1		1
11- 4	2007: 1	TO	11- 4	2019:30		4
11- 4	2019:30	TO	11- 4	2032: 1		4
11- 4	2032: 1	TO	11- 4	2038: 0		4
11- 4	2038: 0	TO	11- 4	2039:30		5
11- 4	2039:30	TO	11- 4	2044:30		5
11- 4	2044:30	TO	11- 4	2049:31		5
11- 4	2049:31	TO	11- 4	2054:31		5
11- 4	2054:31	TO	11- 4	2059:30		5
11- 4	2059:30	TO	11- 4	2104:30		5
11- 4	2104:30	TO	11- 4	2109:31		5
11- 4	2109:31	TO	11- 4	2114:31		5
11- 4	2114:31	TO	11- 4	2119:31		5
11- 4	2119:31	TO	11- 4	2124:30		5
11- 4	2124:30	TO	11- 4	2129:30		5
11- 4	2129:30	TO	11- 4	2134:31		5
11- 4	2134:31	TO	11- 4	2138: 0		5
11- 4	2138: 0	TO	11- 4	2139:31		5
11- 4	2139:31	TO	11- 4	2144:30		5
11- 4	2144:30	TO	11- 4	2149:30		5
11- 4	2149:30	TO	11- 4	2154:31		5
11- 4	2154:31	TO	11- 4	2159:31		5
11- 4	2159:31	TO	11- 4	2204:31		5
11- 4	2204:31	TO	11- 4	2209:30		5
11- 4	2209:30	TO	11- 4	2214:30		5
11- 4	2214:30	TO	11- 4	2219:31		5
11- 4	2219:31	TO	11- 4	2224:31		5
11- 4	2224:31	TO	11- 4	2229:31		5
11- 4	2229:31	TO	11- 4	2234:30		5
11- 4	2234:30	TO	11- 4	2239:31		5
11- 4	2239:31	TO	11- 4	2244:31		5
11- 4	2244:31	TO	11- 4	2249:31		2
11- 4	2249:31	TO	11- 4	2254:30		2
11- 4	2254:30	TO	11- 4	2302:10		2
11- 4	2342: 0	TO	11- 5	19:30		8
11- 5	19:30	TO	11- 5	38: 0		5
11- 5	38: 0	TO	11- 5	47: 0		5
11- 5	47: 0	TO	11- 5	57: 1		8

11- 5	57: 1	TO	11- 5	109:34	8
11- 5	109:34	TO	11- 5	119:34	5
11- 5	119:34	TO	11- 5	124:31	5
11- 5	124:31	TO	11- 5	134:31	5
11- 5	134:31	TO	11- 5	138: 0	5
11- 5	138: 0	TO	11- 5	144:31	4
11- 5	144:31	TO	11- 5	154:31	4
11- 5	154:31	TO	11- 5	212: 1	4
11- 5	212: 1	TO	11- 5	224:31	4
11- 5	224:31	TO	11- 5	237: 1	4
11- 5	237: 1	TO	11- 5	238: 0	1
11- 5	238: 0	TO	11- 5	249:31	2
11- 5	249:31	TO	11- 5	259:31	2
11- 5	259:31	TO	11- 5	322: 1	2
11- 5	322: 1	TO	11- 5	338: 0	5
11- 5	338: 0	TO	11- 5	407: 4	5
11- 5	407: 4	TO	11- 5	1117:59	2
11- 5	1137: 4	TO	11- 5	1839:31	4
11- 5	1839:31	TO	11- 5	1844:30	4
11- 5	1844:30	TO	11- 5	1847:59	4
11- 5	1847:59	TO	11- 5	1849:30	4
11- 5	1849:30	TO	11- 5	1854:31	4
11- 5	1854:31	TO	11- 5	1859:31	4
11- 5	1859:31	TO	11- 5	1904:31	4
11- 5	1904:31	TO	11- 5	1909:30	4
11- 5	1909:30	TO	11- 5	1914:30	4
11- 5	1914:30	TO	11- 5	1919:31	4
11- 5	1919:31	TO	11- 5	1924:31	4
11- 5	1924:31	TO	11- 5	1929:31	4
11- 5	1929:31	TO	11- 5	1934:30	4
11- 5	1934:30	TO	11- 5	1938: 0	4
11- 5	1938: 0	TO	11- 5	1939:31	4
11- 5	1939:31	TO	11- 5	1944:31	4
11- 5	1944:31	TO	11- 5	1949:31	4
11- 5	1949:31	TO	11- 5	1954:30	4
11- 5	1954:30	TO	11- 5	1959:30	4
11- 5	1959:30	TO	11- 5	2004:31	4
11- 5	2004:31	TO	11- 5	2009:31	4
11- 5	2009:31	TO	11- 5	2014:30	4
11- 5	2014:30	TO	11- 5	2019:30	4
11- 5	2019:30	TO	11- 5	2024:31	4
11- 5	2024:31	TO	11- 5	2029:31	4
11- 5	2029:31	TO	11- 5	2034:31	4
11- 5	2034:31	TO	11- 5	2038: 0	4
11- 5	2038: 0	TO	11- 5	2039:30	4
11- 5	2039:30	TO	11- 5	2044:30	4
11- 5	2044:30	TO	11- 5	2049:31	4
11- 5	2049:31	TO	11- 5	2054:31	4
11- 5	2054:31	TO	11- 5	2059:30	4
11- 5	2059:30	TO	11- 5	2104:30	4
11- 5	2104:30	TO	11- 5	2109:31	4
11- 5	2109:31	TO	11- 5	2114:31	4
11- 5	2114:31	TO	11- 5	2119:31	4
11- 5	2119:31	TO	11- 5	2124:30	4
11- 5	2124:30	TO	11- 5	2129:30	4

11- 5	2129:30	TO	11- 5	2134:31	4
11- 5	2134:31	TO	11- 5	2138: 0	4
11- 5	2138: 0	TO	11- 5	2139:31	4
11- 5	2139:31	TO	11- 5	2144:30	4
11- 5	2144:30	TO	11- 5	2149:30	4
11- 5	2149:30	TO	11- 5	2154:31	4
11- 5	2154:31	TO	11- 5	2159:31	4
11- 5	2159:31	TO	11- 5	2204:31	4
11- 5	2204:31	TO	11- 5	2209:30	4
11- 5	2209:30	TO	11- 5	2214:30	4
11- 5	2214:30	TO	11- 5	2219:31	4
11- 5	2219:31	TO	11- 5	2224:31	4
11- 5	2224:31	TO	11- 5	2229:31	4
11- 5	2229:31	TO	11- 5	2234:30	4
11- 5	2234:30	TO	11- 5	2239:31	4
11- 5	2239:31	TO	11- 5	2244:31	4
11- 5	2244:31	TO	11- 5	2249:31	4
11- 5	2249:31	TO	11- 5	2254:30	1
11- 5	2254:30	TO	11- 5	2259:32	1
11- 6	7: 0	TO	11- 6	14:31	9
11- 6	14:31	TO	11- 6	19:31	6
11- 6	19:31	TO	11- 6	27: 0	9
11- 6	27: 0	TO	11- 6	37: 1	6
11- 6	37: 1	TO	11- 6	38: 0	9
11- 6	38: 0	TO	11- 6	44:30	9
11- 6	44:30	TO	11- 6	52: 0	9
11- 6	52: 0	TO	11- 6	102: 1	6
11- 6	102: 1	TO	11- 6	109:30	6
11- 6	109:30	TO	11- 6	114:30	6
11- 6	114:30	TO	11- 6	119:31	6
11- 6	119:31	TO	11- 6	124:31	6
11- 6	124:31	TO	11- 6	129:31	6
11- 6	129:31	TO	11- 6	138: 0	6
11- 6	138: 0	TO	11- 6	142: 1	5
11- 6	142: 1	TO	11- 6	154:30	5
11- 6	154:30	TO	11- 6	159:30	5
11- 6	159:30	TO	11- 6	204:31	5
11- 6	204:31	TO	11- 6	209:31	5
11- 6	209:31	TO	11- 6	214:30	5
11- 6	214:30	TO	11- 6	219:30	5
11- 6	219:30	TO	11- 6	224:31	5
11- 6	224:31	TO	11- 6	229:31	5
11- 6	229:31	TO	11- 6	234:35	5
11- 6	234:35	TO	11- 6	238: 0	5
11- 6	238: 0	TO	11- 6	239:35	5
11- 6	239:35	TO	11- 6	247: 1	5
11- 6	247: 1	TO	11- 6	254:31	2
11- 6	254:31	TO	11- 6	302: 0	5
11- 6	302: 0	TO	11- 6	309:31	5
11- 6	309:31	TO	11- 6	314:34	2
11- 6	314:34	TO	11- 6	319:33	2
11- 6	319:33	TO	11- 6	324:30	5
11- 6	324:30	TO	11- 6	329:30	5
11- 6	329:30	TO	11- 6	334:31	5
11- 6	334:31	TO	11- 6	338: 0	2

11- 6	3381 0	TO	11- 6	3421 1	2
11- 6	3421 1	TO	11- 6	3541:31	2
11- 6	3541:31	TO	11- 6	4041:31	5
11- 6	4041:31	TO	11- 6	4091:30	5
11- 6	4091:30	TO	11- 6	4241:31	5
11- 6	4241:31	TO	11- 6	4391:31	5
11- 6	4391:31	TO	11- 6	4441:31	5
11- 6	4441:31	TO	11- 6	4491:31	2
11- 6	4491:31	TO	11- 6	4541:30	2
11- 6	4541:30	TO	11- 6	4591:30	5
11- 6	4591:30	TO	11- 6	1117:59	5
11- 6	1924:31	TO	11- 6	1929:31	4
11- 6	1929:31	TO	11- 6	1934:36	4
11- 6	1934:36	TO	11- 6	1938: 0	4
11- 6	1938: 0	TO	11- 6	1939:36	4
11- 6	1939:36	TO	11- 6	1944:31	4
11- 6	1944:31	TO	11- 6	1949:31	4
11- 6	1949:31	TO	11- 6	1954:34	4
11- 6	1954:34	TO	11- 6	2002: 4	4
11- 6	2002: 4	TO	11- 6	2017: 1	4
11- 6	2017: 1	TO	11- 6	2029:31	4
11- 6	2029:31	TO	11- 6	2034:31	4
11- 6	2034:31	TO	11- 6	2038: 0	4
11- 6	2038: 0	TO	11- 6	2039:30	5
11- 6	2039:30	TO	11- 6	2044:30	5
11- 6	2044:30	TO	11- 6	2049:31	5
11- 6	2049:31	TO	11- 6	2054:31	5
11- 6	2054:31	TO	11- 6	2059:30	5
11- 6	2059:30	TO	11- 6	2104:30	5
11- 6	2104:30	TO	11- 6	2109:31	5
11- 6	2109:31	TO	11- 6	2114:35	5
11- 6	2114:35	TO	11- 6	2119:35	5
11- 6	2119:35	TO	11- 6	2124:30	5
11- 6	2124:30	TO	11- 6	2129:30	5
11- 6	2129:30	TO	11- 6	2134:31	5
11- 6	2134:31	TO	11- 6	2138: 0	5
11- 6	2138: 0	TO	11- 6	2139:31	5
11- 6	2139:31	TO	11- 6	2144:30	5
11- 6	2144:30	TO	11- 6	2149:30	5
11- 6	2149:30	TO	11- 6	2154:31	5
11- 6	2154:31	TO	11- 6	2159:31	5
11- 6	2159:31	TO	11- 6	2204:31	5
11- 6	2204:31	TO	11- 6	2209:30	5
11- 6	2209:30	TO	11- 6	2214:36	5
11- 6	2214:36	TO	11- 6	2219:36	5
11- 6	2219:36	TO	11- 6	2224:31	5
11- 6	2224:31	TO	11- 6	2232: 3	5
11- 6	2232: 3	TO	11- 6	2239:33	2
11- 6	2239:33	TO	11- 6	2244:31	2
11- 6	2244:31	TO	11- 6	2249:31	2
11- 6	2249:31	TO	11- 6	2254:36	2
11- 6	2254:36	TO	11- 6	2308: 0	2
11- 6	2308: 0	TO	11- 7	19:36	3
11- 7	19:36	TO	11- 7	381 0	5
11- 7	381 0	TO	11- 7	1181 0	5

11- 7	118: 0	TO	11- 7	144:31	6
11- 7	144:31	TO	11- 7	149:31	3
11- 7	149:31	TO	11- 7	209:31	3
11- 7	209:31	TO	11- 7	217:59	3
11- 7	217:59	TO	11- 7	319:31	1
11- 7	319:31	TO	11- 7	338: 0	1
11- 7	338: 0	TO	11- 7	414:34	1
11- 7	414:34	TO	11- 7	419:35	1
11- 7	419:35	TO	11- 7	424:31	1
11- 7	424:31	TO	11- 7	429:31	1
11- 7	429:31	TO	11- 7	434:30	1
11- 7	434:30	TO	11- 7	442: 1	1
11- 7	442: 1	TO	11- 7	449:31	1
11- 7	449:31	TO	11- 7	454:30	1
11- 7	454:30	TO	11- 8	1108: 0	1
11-10	1904:31	TO	11-10	1909:30	1
11-10	1909:30	TO	11-10	1914:30	4
11-10	1914:30	TO	11-10	1919:31	4
11-10	1919:31	TO	11-10	1924:31	4
11-10	1924:31	TO	11-10	1929:31	4
11-10	1929:31	TO	11-10	1934:30	4
11-10	1934:30	TO	11-10	1938: 0	4
11-10	1938: 0	TO	11-10	1939:31	4
11-10	1939:31	TO	11-10	1944:31	4
11-10	1944:31	TO	11-10	1949:31	4
11-10	1949:31	TO	11-10	1954:30	4
11-10	1954:30	TO	11-10	2004:31	4
11-10	2004:31	TO	11-10	2017: 1	1
11-10	2017: 1	TO	11-10	2024:31	4
11-10	2024:31	TO	11-10	2029:31	4
11-10	2029:31	TO	11-10	2034:31	4
11-10	2034:31	TO	11-10	2039:31	4
11-10	2039:31	TO	11-10	2044:31	4
11-10	2044:31	TO	11-10	2049:31	4
11-10	2049:31	TO	11-10	2054:31	4
11-10	2054:31	TO	11-10	2058:30	4
11-10	2058:30	TO	11-10	2059:31	5
11-10	2059:31	TO	11-10	2104:31	5
11-10	2104:31	TO	11-10	2109:31	5
11-10	2109:31	TO	11-10	2114:31	5
11-10	2114:31	TO	11-10	2122: 1	5
11-10	2122: 1	TO	11-10	2129:31	5
11-10	2129:31	TO	11-10	2134:31	5
11-10	2134:31	TO	11-10	2139:31	5
11-10	2139:31	TO	11-10	2144:31	5
11-10	2144:31	TO	11-10	2149:31	5
11-10	2149:31	TO	11-10	2154:31	5
11-10	2154:31	TO	11-10	2159: 0	5
11-10	2159: 0	TO	11-10	2159:31	5
11-10	2159:31	TO	11-10	2204:31	5
11-10	2204:31	TO	11-10	2209:30	5
11-10	2209:30	TO	11-10	2214:30	5
11-10	2214:30	TO	11-10	2218:59	5
11-10	2218:59	TO	11-10	2219:31	4
11-10	2219:31	TO	11-10	2224:31	4

11-10	2224:31	TO	11-10	2229:31	1
11-10	2229:31	TO	11-10	2234:30	1
11-10	2234:30	TO	11-10	2239:31	1
11-10	2239:31	TO	11-10	2244:31	1
11-10	2244:31	TO	11-10	2249:31	1
11-10	2249:31	TO	11-10	2254:30	1
11-10	2254:30	TO	11-10	2316:29	1
11-10	2316:29	TO	11-11	9:31	2
11-11	9:31	TO	11-11	36: 0	5
11-11	36: 0	TO	11-11	136: 0	6
11-11	136: 0	TO	11-11	204:31	5
11-11	204:31	TO	11-11	236: 0	5
11-11	236: 0	TO	11-11	254:31	5
11-11	254:31	TO	11-11	304:31	2
11-11	304:31	TO	11-11	309:31	2
11-11	309:31	TO	11-11	314:34	2
11-11	314:34	TO	11-11	319:34	2
11-11	319:34	TO	11-11	324:31	2
11-11	324:31	TO	11-11	329:31	5
11-11	329:31	TO	11-11	334:31	2
11-11	334:31	TO	11-11	336: 0	2
11-11	336: 0	TO	11-11	339:31	2
11-11	339:31	TO	11-11	344:31	2
11-11	344:31	TO	11-11	349:31	2
11-11	349:31	TO	11-11	354:31	2
11-11	354:31	TO	11-11	359:31	2
11-11	359:31	TO	11-11	404:31	2
11-11	404:31	TO	11-11	409:30	2
11-11	409:30	TO	11-11	414:30	2
11-11	414:30	TO	11-11	419:31	2
11-11	419:31	TO	11-11	424:31	2
11-11	424:31	TO	11-11	429:31	2
11-11	429:31	TO	11-11	434:30	2
11-11	434:30	TO	11-11	439:31	2
11-11	439:31	TO	11-11	444:31	2
11-11	444:31	TO	11-11	449:31	5
11-11	449:31	TO	11-11	454:36	2
11-11	454:36	TO	11-11	459:36	5
11-11	1814:31	TO	11-11	1819:31	4
11-11	1819:31	TO	11-11	1824:31	4
11-11	1824:31	TO	11-11	1829:31	4
11-11	1829:31	TO	11-11	1834:31	4
11-11	1834:31	TO	11-11	1836: 0	4
11-11	1836: 0	TO	11-11	1839:31	4
11-11	1839:31	TO	11-11	1844:31	4
11-11	1844:31	TO	11-11	1849:31	4
11-11	1849:31	TO	11-11	1854:31	4
11-11	1854:31	TO	11-11	1859:31	4
11-11	1859:31	TO	11-11	1904:31	4
11-11	1904:31	TO	11-11	1909:30	4
11-11	1914:30	TO	11-11	1919:31	4
11-11	1919:31	TO	11-11	1924:31	4
11-11	1924:31	TO	11-11	1929:31	4
11-11	1929:31	TO	11-11	1934:30	4
11-11	1934:30	TO	11-11	1936: 0	4

11-11	1938: 0	TO	11-11	1939:31	4
11-11	1939:31	TO	11-11	1944:31	4
11-11	1944:31	TO	11-11	1949:31	4
11-11	1949:31	TO	11-11	1954:30	4
11-11	1954:30	TO	11-11	1959:31	4
11-11	1959:31	TO	11-11	2007: 1	1
11-11	2007: 1	TO	11-11	2017: 1	4
11-11	2017: 1	TO	11-11	2024:31	4
11-11	2024:31	TO	11-11	2029:31	4
11-11	2029:31	TO	11-11	2034:31	4
11-11	2034:31	TO	11-11	2038: 0	4
11-11	2038: 0	TO	11-11	2039:31	5
11-11	2039:31	TO	11-11	2044:31	5
11-11	2044:31	TO	11-11	2049:31	5
11-11	2049:31	TO	11-11	2054:34	5
11-11	2054:34	TO	11-11	2059:34	5
11-11	2059:34	TO	11-11	2104:31	5
11-11	2104:31	TO	11-11	2109:31	5
11-11	2109:31	TO	11-11	2114:31	5
11-11	2114:31	TO	11-11	2119:31	2
11-11	2119:31	TO	11-11	2124:31	2
11-11	2124:31	TO	11-11	2129:31	2
11-11	2129:31	TO	11-11	2134:31	2
11-11	2134:31	TO	11-11	2138: 0	2
11-11	2138: 0	TO	11-11	2139:31	2
11-11	2139:31	TO	11-11	2144:31	2
11-11	2144:31	TO	11-11	2149:31	2
11-11	2149:31	TO	11-11	2154:31	2
11-11	2154:31	TO	11-11	2159:31	2
11-11	2159:31	TO	11-11	2204:31	2
11-11	2204:31	TO	11-11	2209:30	2
11-11	2209:30	TO	11-11	2214:30	2
11-11	2214:30	TO	11-11	2219:31	2
11-11	2219:31	TO	11-11	2224:31	2
11-11	2224:31	TO	11-11	2229:31	2
11-11	2229:31	TO	11-11	2234:30	2
11-11	2234:30	TO	11-11	2239:31	2
11-11	2239:31	TO	11-11	2244:31	2
11-11	2244:31	TO	11-11	2249:31	2
11-11	2249:31	TO	11-11	2254:30	2
11-11	2254:30	TO	11-11	2259:33	2
11-11	2352: 3	TO	11-12	52: 1	6
11-12	52: 1	TO	11-12	135:59	3
11-12	135:59	TO	11-12	149:32	3
11-12	149:32	TO	11-12	236: 0	6
11-12	236: 0	TO	11-12	239:32	6
11-12	239:32	TO	11-12	322: 1	3
11-12	322: 1	TO	11-12	336: 0	6
11-12	336: 0	TO	11-12	404:31	6
11-12	404:31	TO	11-12	409:30	6
11-12	409:30	TO	11-12	414:30	3
11-12	414:30	TO	11-12	419:31	3
11-12	419:31	TO	11-12	424:31	3
11-12	424:31	TO	11-12	429:31	3
11-12	434:34	TO	11-12	439:34	3

11-12	439:34	TO	11-12	444:31	3
11-12	444:31	TO	11-12	449:31	3
11-12	449:31	TO	11-12	454:30	3
11-12	454:30	TO	11-12	459:31	3
11-12	1132: 2	TO	11-12	1704:32	4
11-12	1804:32	TO	11-12	1809:31	4
11-12	1809:31	TO	11-12	1814:31	4
11-12	1814:31	TO	11-12	1819:31	4
11-12	1819:31	TO	11-12	1824:31	4
11-12	1824:31	TO	11-12	1829:31	4
11-12	1829:31	TO	11-12	1834:31	4
11-12	1834:31	TO	11-12	1836: 0	4
11-12	1836: 0	TO	11-12	1839:31	4
11-12	1839:31	TO	11-12	1844:31	4
11-12	1844:31	TO	11-12	1849:31	4
11-12	1849:31	TO	11-12	1854:31	4
11-12	1854:31	TO	11-12	1859:31	4
11-12	1859:31	TO	11-12	1907: 1	4
11-12	1907: 1	TO	11-12	1914:30	4
11-12	1914:30	TO	11-12	1919:31	4
11-12	1919:31	TO	11-12	1924:31	4
11-12	1924:31	TO	11-12	1929:31	4
11-12	1929:31	TO	11-12	1934:30	4
11-12	1934:30	TO	11-12	1935:59	4
11-12	1935:59	TO	11-12	1939:31	5
11-12	1939:31	TO	11-12	1944:31	8
11-12	1944:31	TO	11-12	1949:31	5
11-12	1949:31	TO	11-12	1954:30	5
11-12	1954:30	TO	11-12	1959:31	5
11-12	1959:31	TO	11-12	2004:31	5
11-12	2004:31	TO	11-12	2009:31	5
11-12	2009:31	TO	11-12	2014:31	8
11-12	2014:31	TO	11-12	2019:31	5
11-12	2019:31	TO	11-12	2024:31	5
11-12	2024:31	TO	11-12	2029:31	5
11-12	2029:31	TO	11-12	2034:34	5
11-12	2034:34	TO	11-12	2036: 0	5
11-12	2036: 0	TO	11-12	2039:34	5
11-12	2039:34	TO	11-12	2044:31	5
11-12	2044:31	TO	11-12	2049:31	5
11-12	2049:31	TO	11-12	2054:31	5
11-12	2054:31	TO	11-12	2059:31	5
11-12	2312: 1	TO	11-12	2339:31	5
11-12	2339:31	TO	11-12	2344:31	2
11-12	2349:31	TO	11-12	2354:31	5
11-12	2359:31	TO	11-13	19:35	2
11-13	19:35	TO	11-13	36: 0	5
11-13	36: 0	TO	11-13	39:35	6
11-13	39:35	TO	11-13	44:31	3
11-13	44:31	TO	11-13	49:31	3
11-13	49:31	TO	11-13	54:31	3
11-13	54:31	TO	11-13	107: 1	3
11-13	107: 1	TO	11-13	119:31	3
11-13	119:31	TO	11-13	124:31	3
11-13	124:31	TO	11-13	129:31	3

11-13	129:31	TO	11-13	144:33	3
11-13	144:33	TO	11-13	206: 0	3
11-13	206: 0	TO	11-13	214:34	1
11-13	214:34	TO	11-13	237: 1	1
11-13	237: 1	TO	11-13	252: 1	1
11-13	252: 1	TO	11-13	304:31	1
11-13	304:31	TO	11-13	309:31	1
11-13	309:31	TO	11-13	314:31	4
11-13	314:31	TO	11-13	319:31	4
11-13	319:31	TO	11-13	324:31	1
11-13	324:31	TO	11-13	329:31	4
11-13	329:31	TO	11-13	336: 0	4
11-13	336: 0	TO	11-13	339:31	5
11-13	339:31	TO	11-13	352: 1	5
11-13	352: 1	TO	11-13	359:31	5
11-13	359:31	TO	11-13	409:31	5
11-13	409:31	TO	11-13	419:31	5
11-13	419:31	TO	11-13	424:31	5
11-13	424:31	TO	11-13	429:31	5
11-13	429:31	TO	11-13	437: 0	5
11-13	437: 0	TO	11-13	1115:59	5
11-13	1132: 1	TO	11-13	1824:31	5
11-13	1824:31	TO	11-13	1829:31	5
11-13	1829:31	TO	11-13	1834:31	5
11-13	1834:31	TO	11-13	1839:31	5
11-13	1839:31	TO	11-13	1844:31	5
11-13	1844:31	TO	11-13	1845:59	5
11-13	1845:59	TO	11-13	1849:31	4
11-13	1849:31	TO	11-13	1854:31	4
11-13	1854:31	TO	11-13	1859:31	4
11-13	1859:31	TO	11-13	1904:31	4
11-13	1904:31	TO	11-13	1909:30	4
11-13	1909:30	TO	11-13	1914:30	4
11-13	1914:30	TO	11-13	1919:31	4
11-13	1919:31	TO	11-13	1924:31	4
11-13	1924:31	TO	11-13	1929:31	4
11-13	1929:31	TO	11-13	1934:30	4
11-13	1934:30	TO	11-13	1935:59	4
11-13	1935:59	TO	11-13	1939:31	4
11-13	1939:31	TO	11-13	1944:31	4
11-13	1944:31	TO	11-13	1949:31	4
11-13	1949:31	TO	11-13	1954:30	4
11-13	1954:30	TO	11-13	1959:31	4
11-13	1959:31	TO	11-13	2004:31	4
11-13	2004:31	TO	11-13	2009:31	4
11-13	2009:31	TO	11-13	2014:31	4
11-13	2014:31	TO	11-13	2019:31	4
11-13	2019:31	TO	11-13	2024:31	4
11-13	2024:31	TO	11-13	2029:31	4
11-13	2029:31	TO	11-13	2034:31	4
11-13	2034:31	TO	11-13	2036: 0	4
11-13	2036: 0	TO	11-13	2039:31	5
11-13	2039:31	TO	11-13	2044:31	5
11-13	2044:31	TO	11-13	2049:31	5
11-13	2049:31	TO	11-13	2054:31	5

11-13	2054:31	TO	11-13	2059:31	5
11-13	2059:31	TO	11-13	2104:31	5
11-13	2104:31	TO	11-13	2109:31	5
11-13	2109:31	TO	11-13	2114:31	5
11-13	2114:31	TO	11-13	2119:31	5
11-13	2119:31	TO	11-13	2124:31	5
11-13	2124:31	TO	11-13	2129:31	5
11-13	2129:31	TO	11-13	2134:31	5
11-13	2134:31	TO	11-13	2136: 0	5
11-13	2136: 0	TO	11-13	2139:31	4
11-13	2139:31	TO	11-13	2144:31	4
11-13	2144:31	TO	11-13	2152: 1	4
11-13	2152: 1	TO	11-13	2159:31	4
11-13	2159:31	TO	11-13	2204:31	1
11-13	2204:31	TO	11-13	2209:30	1
11-13	2209:30	TO	11-13	2214:30	1
11-13	2214:30	TO	11-13	2219:31	1
11-13	2219:31	TO	11-13	2224:31	1
11-13	2224:31	TO	11-13	2229:31	1
11-13	2229:31	TO	11-13	2234:30	1
11-13	2234:30	TO	11-13	2239:31	1
11-13	2239:31	TO	11-13	2244:31	1
11-13	2244:31	TO	11-13	2249:31	1
11-13	2249:31	TO	11-13	2254:30	1
11-13	2254:30	TO	11-13	2306:59	1
11-13	2337: 1	TO	11-14	19:31	5
11-14	19:31	TO	11-14	24:31	5
11-14	24:31	TO	11-14	29:31	5
11-14	29:31	TO	11-14	34:31	2
11-14	34:31	TO	11-14	38: 0	5
11-14	38: 0	TO	11-14	39:31	6
11-14	39:31	TO	11-14	57: 1	6
11-14	57: 1	TO	11-14	114:32	6
11-14	114:32	TO	11-14	119:32	6
11-14	119:32	TO	11-14	124:31	6
11-14	124:31	TO	11-14	138: 0	6
11-14	138: 0	TO	11-14	207: 1	5
11-14	207: 1	TO	11-14	238: 0	5
11-14	238: 0	TO	11-14	249:31	5
11-14	249:31	TO	11-14	254:31	5
11-14	254:31	TO	11-14	259:31	5
11-14	259:31	TO	11-14	304:31	5
11-14	304:31	TO	11-14	309:31	5
11-14	309:31	TO	11-14	314:31	5
11-14	314:31	TO	11-14	319:31	5
11-14	319:31	TO	11-14	332: 1	5
11-14	332: 1	TO	11-14	338: 0	5
11-14	338: 0	TO	11-14	344:31	5
11-14	344:31	TO	11-14	349:31	5
11-14	349:31	TO	11-14	354:31	2
11-14	354:31	TO	11-14	359:31	5
11-14	359:31	TO	11-14	404:31	5
11-14	404:31	TO	11-14	409:30	5
11-14	409:30	TO	11-14	1632: 0	5

APPENDIX F

TABULATED RESULTS OF MEASURED S/N AND BINARY ERROR RATE CLASSIFIED BY TIME-DELAY- AND DOPPLER-FREQUENCY-SPREAD CONDITIONS

APPENDIX F

TABULATED RESULTS OF MEASURED S/N AND BINARY ERROR RATE CLASSIFIED BY TIME-RELAY- AND DOPPLER-FREQUENCY-SPREAD CONDITIONS

DESCRIPTION OF COLUMN HEADINGS

MAXIMUM S/N	Maximum possible measured S/N in any 30-second data block in this data bracket.
AVERAGE S/N	Weighted average S/N of data in this bracket.
BER	Estimated binary error rate for data accumulated in this S/N bracket.
TOTAL	Total number of transmitted bits accumulated in this bracket.
TOTAL ERRORS	Total number of bit errors accumulated in this bracket.

TIME DELAY SPREAD: 0.00 TO 1.50 MS
DOPPLER SPREAD: 0.00 TO 1.00 CPS

MAXIMUM S/N	AVERAGE S/N	BER	TOTAL BITS	TOTAL ERRORS
0.5	0.0	4.35E-01	49522	21520
1.5	1.0	2.85E-01	18008	5137
2.5	2.0	3.09E-01	20259	6267
3.5	3.0	2.53E-01	29263	7413
4.5	4.0	2.91E-01	24761	7202
5.5	5.0	3.15E-01	38267	12067
6.5	6.0	2.79E-01	36016	10040
7.5	7.0	1.67E-01	49522	8261
8.5	8.0	2.35E-01	56275	13227
9.5	9.0	2.35E-01	29263	6887
10.5	10.0	7.15E-02	15757	1127
11.5	11.0	3.29E-02	4502	148
14.5	13.5	3.54E-02	24761	877
15.5	15.0	2.77E-02	11255	312
16.5	16.0	8.66E-03	18008	156
17.5	17.0	1.92E-02	20259	389
18.5	18.0	1.18E-02	47271	557
19.5	19.0	9.90E-03	40518	401
20.5	20.0	7.16E-03	38267	274
21.5	21.0	1.02E-02	40518	413
22.5	22.0	2.85E-03	49522	141
23.5	23.0	5.98E-03	76534	458
24.5	24.0	4.16E-03	85538	356
25.5	25.0	5.18E-03	101295	525
26.5	26.0	4.92E-03	126056	620
27.5	27.0	2.79E-03	119303	333
28.5	28.0	3.38E-03	146315	494
29.5	29.0	4.73E-03	162072	767
30.5	30.0	3.58E-03	182331	653
31.5	31.0	3.36E-03	182331	613
32.5	32.0	3.32E-03	186833	620
33.5	33.0	3.14E-03	218347	685
34.5	34.0	2.97E-03	229602	682
35.5	35.0	1.26E-03	344403	435
36.5	36.0	2.65E-03	357909	948
37.5	37.0	2.33E-03	330897	770
38.5	38.0	2.09E-03	389423	812
39.5	39.0	1.87E-03	456702	849
40.5	40.0	1.58E-03	468208	738
41.5	41.0	1.78E-03	560499	998
42.5	42.0	1.72E-03	549244	945
43.5	43.0	2.04E-03	569503	1162
44.5	44.0	1.65E-03	650539	1076
45.5	45.0	1.36E-03	738328	1007
46.5	46.0	1.41E-03	700061	987
47.5	47.0	1.38E-03	821615	1135
48.5	48.0	1.29E-03	785599	1014
49.5	49.0	1.20E-03	799105	960
50.5	50.0	9.17E-04	871137	799
51.5	51.0	7.91E-04	745081	589
52.5	52.0	7.75E-04	601017	466
53.5	53.0	1.00E-03	562750	563
54.5	54.0	9.21E-04	398427	367
55.5	55.0	7.92E-04	333148	264
56.5	56.0	5.96E-04	184582	110
57.5	57.0	1.12E-03	114801	129
59.5	58.4	8.95E-04	146315	131
60.5	60.7	5.71E-04	31514	18

TIME DELAY SPREAD: 0.00 TO 0.25 MS
DOPPLER SPREAD: 0.00 TO 0.25 CPS

MAXIMUM S/N	AVERAGE S/N	BER	TOTAL BITS	TOTAL ERRORS
14.5	12.3	3.29#-02	6753	222
16.5	15.7	9.77#-03	13506	132
17.5	17.0	1.84#-02	9004	166
18.5	18.0	9.58#-03	20259	194
19.5	19.0	7.02#-03	22510	158
21.5	20.6	4.91#-03	36016	177
22.5	22.0	3.28#-03	36016	118
23.5	23.0	4.07#-03	42769	174
24.5	24.0	4.66#-03	45020	210
25.5	25.0	5.37#-03	27012	145
26.5	26.0	6.44#-03	40518	261
28.5	27.5	2.55#-03	90040	230
29.5	29.0	5.14#-03	47271	243
30.5	30.0	2.72#-03	38267	104
31.5	31.0	4.22#-03	27012	114
32.5	32.0	3.29#-03	38267	126
35.5	34.2	1.27#-03	78785	100
42.5	38.8	4.79#-04	229602	110
47.5	44.9	4.97#-04	227351	113
52.5	50.0	4.48#-04	245359	110
60.5	54.1	8.42#-04	42769	36

TIME DELAY SPREAD: 0.00 TO 0.25 MS
DOPPLER SPREAD: 0.25 TO 0.50 CPS

MAXIMUM S/N	AVERAGE S/N	BER	TOTAL BITS	TOTAL ERRORS
0.5	0.0	4.05E-01	20259	8215
1.5	1.0	2.53E-01	9004	2278
2.5	2.0	3.13E-01	4502	1410
3.5	3.0	2.70E-01	20259	5476
4.5	4.0	3.81E-01	9004	3428
5.5	5.0	2.57E-01	15757	4049
6.5	6.0	2.35E-01	15757	3704
7.5	7.0	1.20E-01	40518	4866
8.5	8.0	1.64E-01	33765	5554
9.5	9.0	1.90E-01	11255	2134
10.5	10.0	7.24E-02	13506	978
14.5	13.1	5.01E-02	15757	789
15.5	15.0	4.20E-02	4502	189
17.5	17.0	4.93E-02	2251	111
18.5	18.0	3.07E-02	6753	207
24.5	21.7	1.50E-02	6753	101
32.5	29.6	2.77E-03	56275	156
34.5	33.6	3.17E-03	36016	114
37.5	36.3	1.96E-03	72032	141
38.5	38.0	3.80E-03	36016	137
39.5	39.0	1.66E-03	60777	101
40.5	40.0	2.14E-03	51773	111
41.5	41.0	1.79E-03	56275	101
43.5	42.6	1.12E-03	146[illegible]5	164
44.5	44.0	1.63E-03	81036	132
45.5	45.0	1.26E-03	94542	119
47.5	46.5	7.45E-04	139562	104
51.5	49.8	3.93E-04	330897	130
54.5	52.9	4.82E-04	213845	103
59.5	55.9	4.44E-04	92291	41

TIME DELAY SPREAD: 0.00 TO 0.25 MS
DOPPLER SPREAD: 0.50 TO 1.00 CPS

MAXIMUM S/N	AVERAGE S/N	BER	TOTAL BITS	TOTAL ERRORS
19.5	17.6	7.70E-03	20259	156
20.5	20.0	1.00E-02	11255	113
21.5	21.0	2.19E-02	11255	246
23.5	22.6	1.04E-02	22510	235
25.5	24.8	5.26E-03	45020	237
26.5	26.0	5.55E-03	36016	200
28.5	27.6	3.78E-03	60777	230
29.5	29.0	4.58E-03	29263	134
31.5	30.5	2.64E-03	67530	178
33.5	32.5	2.94E-03	58526	172
34.5	34.0	2.12E-03	47271	100
36.5	35.5	3.04E-03	123805	376
37.5	37.0	3.24E-03	51773	168
39.5	38.5	2.05E-03	99044	203
41.5	40.6	1.18E-03	132809	157
43.5	42.4	1.37E-03	83287	114
45.5	44.5	1.09E-03	101295	110
52.5	47.3	1.03E-03	58526	60

TIME DELAY SPREAD: 0.25 TO 0.75 MS
DOPPLER SPREAD: 0.25 TO 0.50 CPS

MAXIMUM S/N	AVERAGE S/N	BER	TOTAL BITS	TOTAL ERRORS
0.5	0.0	4.47E-01	24761	11065
1.5	1.0	3.18E-01	9004	2859
2.5	2.0	3.08E-01	15757	4857
3.5	3.0	2.15E-01	9004	1937
4.5	4.0	2.40E-01	15757	3774
5.5	5.0	3.56E-01	22510	8018
6.5	6.0	3.13E-01	20259	6336
7.5	7.0	3.77E-01	9004	3395
8.5	8.0	3.41E-01	22510	7673
9.5	9.0	2.64E-01	18008	4753
10.5	10.0	6.62E-02	2251	149
17.5	16.0	1.30E-02	9004	117
20.5	19.0	8.16E-03	18008	147
24.5	23.6	5.06E-03	22510	114
26.5	25.6	3.74E-03	42769	160
28.5	27.5	3.96E-03	49522	196
29.5	29.0	3.47E-03	36016	125
30.5	30.0	5.30E-03	56275	298
31.5	31.0	4.16E-03	56275	234
32.5	32.0	2.40E-03	51773	124
33.5	33.0	4.00E-03	76534	306
34.5	34.0	3.63E-03	76534	278
35.5	35.0	1.43E-03	123805	177
36.5	36.0	3.00E-03	123805	372
37.5	37.0	2.46E-03	148566	366
38.5	38.0	2.13E-03	171076	365
39.5	39.0	2.16E-03	175578	379
40.5	40.0	1.64E-03	191335	314
41.5	41.0	1.70E-03	189084	322
42.5	42.0	2.25E-03	207092	465
43.5	43.0	2.79E-03	177829	497
44.5	44.0	2.11E-03	209343	441
45.5	45.0	1.56E-03	186033	292
46.5	46.0	1.47E-03	175578	258
47.5	47.0	1.31E-03	238606	313
48.5	48.0	1.78E-03	272371	479
49.5	49.0	1.34E-03	256614	345
50.5	50.0	1.38E-03	274622	379
51.5	51.0	7.83E-04	256614	201
52.5	52.0	1.26E-03	200339	252
53.5	53.0	8.14E-04	189084	154
54.5	54.0	1.14E-03	162072	185
55.5	55.0	7.85E-04	141813	111
57.5	56.4	7.31E-04	139562	102
64.5	59.1	7.75E-04	105797	82

TIME DELAY SPREAD: 0.25 TO 0.75 MS
DOPPLER SPREAD: 0.00 TO 0.25 CPS

MAXIMUM S/N	AVERAGE S/N	BER	TOTAL BITS	TOTAL ERRORS
0.5	0.0	4.98E-01	4502	2240
27.5	23.7	3.76E-03	29263	110
29.5	28.6	9.08E-03	15757	143
31.5	30.5	5.53E-03	24761	137
32.5	32.0	7.33E-03	18008	132
34.5	33.6	3.62E-03	45020	163
36.5	35.6	1.64E-03	67530	111
38.5	37.5	1.74E-03	78785	137
40.5	39.5	1.42E-03	135060	192
41.5	41.0	1.45E-03	85538	124
43.5	42.5	8.88E-04	243108	216
44.5	44.0	9.91E-04	175578	174
45.5	45.0	8.16E-04	220598	180
46.5	46.0	1.20E-03	256614	307
47.5	47.0	9.24E-04	342152	316
48.5	48.0	8.67E-04	321893	279
49.5	49.0	9.29E-04	342152	318
50.5	50.0	6.43E-04	407431	262
51.5	51.0	7.57E-04	319642	242
52.5	52.0	7.21E-04	267869	193
53.5	53.0	1.20E-03	249861	299
54.5	54.0	7.14E-04	166574	119
55.5	55.0	9.04E-04	132809	120
57.5	56.4	9.89E-04	119303	118
61.5	58.5	6.37E-04	58526	37

TIME DELAY SPREAD: 0.25 TO 0.75 MS
DOPPLER SPREAD: 0.50 TO 1.00 CPS

MAXIMUM S/N	AVERAGE S/N	BER	TOTAL BITS	TOTAL ERRORS
16.5	15.0	8.8##E-03	11255	100
21.5	20.0	9.05#E-03	18008	163
25.5	24.1	4.11#E-03	36016	148
28.5	27.1	2.61#E-03	58526	153
30.5	29.6	2.70#E-03	65279	176
32.5	31.4	2.72#E-03	76534	208
33.5	33.0	2.22#E-03	54024	120
34.5	34.0	2.12#E-03	49522	105
35.5	35.0	1.84#E-03	67530	124
36.5	36.0	1.55#E-03	76534	119
38.5	37.7	2.72#E-03	85538	233
39.5	39.0	2.07#E-03	67530	140
40.5	40.0	1.71#E-03	60777	104
41.5	41.0	2.11#E-03	112550	238
42.5	42.0	2.09#E-03	96793	202
43.5	43.0	4.01#E-03	83287	334
44.5	44.0	1.76#E-03	81036	143
45.5	45.0	2.04#E-03	90040	184
47.5	46.4	1.38#E-03	155319	214
53.5	49.3	1.02#E-03	101295	103

TIME DELAY SPREAD: 0.75 TO 1.50 MS
DOPPLER SPREAD: 0.25 TO 0.[illegible] CPS

MAXIMUM S/N	AVERAGE S/N	BER	TOTAL BITS	TOTAL ERRORS
41.5	41.0	1.66E-02	6753	112
44.5	43.5	5.94E-03	18008	107
45.5	45.0	5.61E-03	24761	139
46.5	46.0	7.85E-03	24761	194
47.5	47.0	4.98E-03	33765	168
48.5	48.0	6.96E-03	20259	141
49.5	49.0	4.58E-03	42769	196
53.5	50.8	3.45E-03	38267	132
56.5	54.9	1.71E-03	15757	27

TIME DELAY SPREAD: 0.75 TO 1.50 MS
DOPPLER SPREAD: 0.50 TU 1.00 CPS

MAXIMUM S/N	AVERAGE S/N	BER	TOTAL BITS	TOTAL ERRORS
46.5	44.8	4.42E-03	38267	169
48.5	47.4	3.62E-03	31514	114
51.5	49.7	4.59E-03	13506	62

TIME DELAY SPREAD: 0.00 TO 1.50 MS
DOPPLER SPREAD: 0.00 TO 0.25 CPS

MAXIMUM S/N	AVERAGE S/N	BER	TOTAL BITS	TOTAL ERRORS
0.5	0.0	4.98E-01	4502	2240
14.5	12.3	3.29E-02	6753	222
16.5	15.7	9.77E-03	13506	132
17.5	17.0	1.64E-02	9004	166
18.5	18.0	8.71E-03	22510	196
19.5	19.0	7.66E-03	27012	207
21.5	20.6	4.91E-03	36016	177
22.5	22.0	3.28E-03	36016	118
23.5	23.0	3.86E-03	45020	174
24.5	24.0	4.11E-03	51773	213
25.5	25.0	5.49E-03	31514	173
26.5	26.0	6.10E-03	42769	261
27.5	27.0	2.26E-03	49522	112
28.5	28.0	3.13E-03	54024	169
29.5	29.0	6.45E-03	56275	363
30.5	30.0	3.70E-03	49522	183
31.5	31.0	4.25E-03	40518	172
32.5	32.0	4.58E-03	56275	258
34.5	33.4	2.94E-03	81036	238
36.5	35.5	1.08E-03	153068	166
38.5	37.5	1.16E-03	141813	165
40.5	39.5	9.91E-04	204841	203
41.5	41.0	1.26E-03	119303	150
42.5	42.0	8.50E-04	130558	111
43.5	43.0	9.2 -04	184582	171
44.5	44.0	9.27E-04	207092	192
45.5	45.0	7.12E-04	283628	202
46.5	46.0	1.03E-03	299383	309
47.5	47.0	8.83E-04	380419	336
48.5	48.0	7.66E-04	375917	288
49.5	49.0	8.40E-04	391674	329
50.5	50.0	6.82E-04	450200	307
51.5	51.0	7.54E-04	364682	275
52.5	52.0	6.37E-04	321893	205
53.5	53.0	1.13E-03	276873	313
54.5	54.0	7.19E-04	171076	123
55.5	55.0	8.74E-04	137311	120
57.5	56.4	1.03E-03	123805	127
61.5	58.5	9.54E-04	60777	58

TIME DELAY SPREAD: 0.00 TO 1.50 MS
DOPPLER SPREAD: 0.25 TO 0.50 CPS

MAXIMUM S/N	AVERAGE S/N	BER	TOTAL BITS	TOTAL ERRORS
0.5	0.0	4.28E-01	45020	19280
1.5	1.0	2.85E-01	18008	5137
2.5	2.0	3.09E-01	20259	6267
3.5	3.0	2.53E-01	29263	7413
4.5	4.0	2.91E-01	24761	7202
5.5	5.0	3.15E-01	38267	12067
6.5	6.0	2.79E-01	36016	10040
7.5	7.0	1.67E-01	49522	8261
8.5	8.0	2.35E-01	56275	13227
9.5	9.0	2.35E-01	29263	6887
10.5	10.0	7.15E-02	15757	1127
13.5	12.3	1.13E-02	9004	102
14.5	14.0	7.75E-02	9004	698
15.5	15.0	4.20E-02	4502	189
17.5	17.0	2.41E-02	9004	217
18.5	18.0	1.92E-02	15757	303
20.5	19.8	1.24E-02	11255	140
24.5	23.5	4.66E-03	27012	126
26.5	25.6	3.38E-03	47271	160
27.5	27.0	3.55E-03	29263	104
28.5	28.0	3.62E-03	31514	114
29.5	29.0	3.64E-03	47271	172
30.5	30.0	4.92E-03	63028	310
31.5	31.0	3.78E-03	65279	247
32.5	32.0	2.85E-03	65279	186
33.5	33.0	4.10E-03	92291	378
34.5	34.0	3.31E-03	96793	320
35.5	35.0	1.35E-03	139562	189
36.5	36.0	2.88E-03	141813	409
37.5	37.0	2.45E-03	186833	458
38.5	38.0	2.42E-03	207092	502
39.5	39.0	2.03E-03	236355	480
40.5	40.0	1.75E-03	243108	425
41.5	41.0	2.12E-03	252112	535
42.5	42.0	2.04E-03	274622	560
43.5	43.0	2.32E-03	263367	612
44.5	44.0	2.10E-03	301636	634
45.5	45.0	1.80E-03	306136	550
46.5	46.0	1.80E-03	272371	491
47.5	47.0	1.61E-03	339901	546
48.5	48.0	1.91E-03	344403	657
49.5	49.0	1.50E-03	369164	553
50.5	50.0	1.16E-03	405180	469
51.5	51.0	7.88E-04	366913	289
52.5	52.0	9.44E-04	270120	255
53.5	53.0	8.74E-04	281375	246
54.5	54.0	1.07E-03	227351	244
55.5	55.0	7.35E-04	195837	144
57.5	56.4	6.38E-04	175578	112
64.5	59.0	7.77E-04	117052	91

TIME DELAY SPREAD: 0.00 TO 1.50 MS
DOPPLER SPREAD: 0.50 TO 1.00 CPS

MAXIMUM S/N	AVERAGE S/N	BER	TOTAL BITS	TOTAL ERRORS
16.5	15.3	9.52E-03	15757	150
19.5	18.4	7.51E-03	22510	169
20.5	20.0	9.33E-03	13506	126
21.5	21.0	1.64E-02	20259	333
23.5	22.7	7.70E-03	33765	260
25.5	24.7	5.16E-03	69781	360
26.5	26.0	4.72E-03	54024	255
27.5	27.0	2.89E-03	40518	117
28.5	28.0	3.47E-03	60777	211
29.5	29.0	3.96E-03	58526	232
30.5	30.0	2.29E-03	69781	160
31.5	31.0	2.53E-03	76534	194
32.5	32.0	2.70E-03	65279	176
33.5	33.0	2.79E-03	81036	226
34.5	34.0	2.12E-03	96793	205
35.5	35.0	1.57E-03	132809	208
36.5	36.0	3.04E-03	135060	411
37.5	37.0	2.99E-03	76534	229
38.5	38.0	2.11E-03	108048	228
39.5	39.0	2.41E-03	119303	287
40.5	40.0	1.61E-03	119303	192
41.5	41.0	1.66E-03	189084	313
42.5	42.0	1.90E-03	144064	274
43.5	43.0	3.12E-03	121554	379
44.5	44.0	1.76E-03	141813	250
45.5	45.0	1.72E-03	148566	255
46.5	46.0	1.46E-03	128307	187
47.5	47.0	2.50E-03	101295	253
49.5	48.4	1.42E-03	103546	147
53.5	51.1	1.36E-03	42769	58

TIME DELAY SPREAD: 0.00 TO 0.25 MS
DOPPLER SPREAD: 0.00 TO 1.00 CPS

MAXIMUM S/N	AVERAGE S/N	BER	TOTAL BITS	TOTAL ERRORS
0.5	0.0	4.05E-01	20259	8215
1.5	1.0	2.53E-01	9004	2278
2.5	2.0	3.13E-01	4502	1410
3.5	3.0	2.70E-01	20259	5476
4.5	4.0	3.81E-01	9004	3428
5.5	5.0	2.57E-01	15757	4049
6.5	6.0	2.35E-01	15757	3704
7.5	7.0	1.20E-01	40518	4866
8.5	8.0	1.64E-01	33765	5554
9.5	9.0	1.90E-01	11255	2134
10.5	10.0	7.24E-02	13506	978
11.5	11.0	3.29E-02	4502	148
14.5	13.4	4.79E-02	18008	863
15.5	15.0	3.12E-02	9004	281
17.5	16.5	1.38E-02	27012	373
18.5	18.0	1.31E-02	33765	441
19.5	19.0	9.74E-03	31514	307
20.5	20.0	7.77E-03	27012	210
21.5	21.0	1.03E-02	31514	326
22.5	22.0	2.81E-03	47271	133
23.5	23.0	7.07E-03	56275	398
24.5	24.0	4.64E-03	56275	261
25.5	25.0	5.38E-03	63028	339
26.5	26.0	5.69E-03	81036	461
27.5	27.0	2.42E-03	72032	174
28.5	28.0	3.42E-03	90040	308
29.5	29.0	4.83E-03	87789	424
30.5	30.0	2.51E-03	78785	198
31.5	31.0	3.20E-03	69781	223
32.5	32.0	3.05E-03	83287	254
33.5	33.0	3.14E-03	67530	212
34.5	34.0	2.32E-03	78785	183
35.5	35.0	9.77E-04	123805	121
36.5	36.0	3.01E-03	119303	359
37.5	37.0	2.35E-03	121554	286
38.5	38.0	1.70E-03	114801	195
39.5	39.0	1.81E-03	137311	248
40.5	40.0	1.35E-03	155319	210
41.5	41.0	1.19E-03	164323	196
42.5	42.0	1.32E-03	132809	175
43.5	43.0	1.00E-03	168825	169
44.5	44.0	1.34E-03	162072	217
45.5	45.0	8.79E-04	209343	184
47.5	46.5	6.61E-04	258865	171
50.5	49.1	3.91E-04	396176	155
52.5	51.5	3.81E-04	270120	103
54.5	53.4	6.72E-04	175578	118
60.5	55.9	5.70E-04	103546	59

TIME DELAY SPREAD: 0.25 TO 0.75 MS
DOPPLER SPREAD: 0.00 TO 1.00 CPS

MAXIMUM S/N	AVERAGE S/N	BER	TOTAL BITS	TOTAL ERRORS
0.5	0.0	4.55E-01	29263	13305
1.5	1.0	3.18E-01	9004	2859
2.5	2.0	3.08E-01	15757	4857
3.5	3.0	2.15E-01	9004	1937
4.5	4.0	2.40E-01	15757	3774
5.5	5.0	3.56E-01	22510	8018
6.5	6.0	3.13E-01	20259	6336
7.5	7.0	3.77E-01	9004	3395
8.5	8.0	3.41E-01	22510	7673
9.5	9.0	2.64E-01	18008	4753
10.5	10.0	6.62E-02	2251	149
16.5	14.7	8.22E-03	13506	111
17.5	17.0	1.57E-02	6753	106
18.5	18.0	8.59E-03	13506	116
20.5	19.6	7.80E-03	20259	158
23.5	22.4	4.92E-03	31514	155
25.5	24.6	4.16E-03	67530	281
26.5	26.0	3.53E-03	45020	159
27.5	27.0	3.36E-03	47271	159
28.5	28.0	3.31E-03	56275	186
29.5	29.0	4.62E-03	74283	343
30.5	30.0	4.39E-03	103546	455
31.5	31.0	3.47E-03	112550	390
32.5	32.0	3.53E-03	103546	366
33.5	33.0	3.14E-03	150817	473
34.5	34.0	3.31E-03	150817	499
35.5	35.0	1.42E-03	220598	314
36.5	36.0	2.47E-03	238606	589
37.5	37.0	2.31E-03	209343	484
38.5	38.0	2.25E-03	274122	617
39.5	39.0	1.89E-03	317191	601
40.5	40.0	1.69E-03	312389	528
41.5	41.0	1.77E-03	387172	684
42.5	42.0	1.84E-03	414184	763
43.5	43.0	2.41E-03	393925	951
44.5	44.0	1.63E-03	465957	758
45.5	45.0	1.32E-03	497471	656
46.5	46.0	1.23E-03	526734	647
47.5	47.0	1.19E-03	641535	761
48.5	48.0	1.24E-03	634782	787
49.5	49.0	1.13E-03	628029	712
50.5	50.0	9.28E-04	691057	641
51.5	51.0	7.80E-04	587511	458
52.5	52.0	9.50E-04	474961	451
53.5	53.0	1.03E-03	443447	457
54.5	54.0	9.25E-04	328656	304
55.5	55.0	8.41E-04	274622	231
56.5	56.0	6.41E-04	157570	101
57.5	57.0	1.17E-03	101295	119
59.5	58.5	9.03E-04	135060	122
64.5	60.8	3.08E-04	29263	9

TIME DELAY SPREAD: 0.75 TO 1.50 MS
DOPPLER SPREAD: 0.00 TO 1.00 CPS

MAXIMUM S/N	AVERAGE S/N	BER	TOTAL BITS	TOTAL ERRORS
41.5	41.0	1.31@-02	9004	118
44.5	43.6	4.76@-03	31514	150
45.5	45.0	5.30@-03	31514	167
46.5	46.0	7.06@-03	40518	286
47.5	47.0	4.76@-03	54024	257
48.5	48.0	5.27@-03	31514	166
49.5	49.0	4.54@-03	49522	225
51.5	50.4	3.40@-03	38267	130
56.5	54.3	2.75@-03	22510	62

DUAL DIVERSITY-ALL DATA

TIME DELAY SPREAD: 0.00 TO 5.00 MS
DOPPLER SPREAD: 0.00 TO 5.00 CPS

MAXIMUM S/N	AVERAGE S/	BER	TOTAL BITS	TOTAL ERRORS
6.5	6.0	6.15e-02	6753	415
7.5	7.0	1.65e-01	6753	1114
8.5	8.0	1.45e-01	9004	1310
9.5	9.0	6.78e-02	6753	458
11.5	11.0	1.39e-02	11255	156
12.5	12.0	2.56e-02	11255	288
13.5	14.4	1.55e-02	22510	349
16.5	16.0	1.50e-02	11255	169
17.5	17.0	1.98e-02	6753	134
21.5	20.1	6.10e-03	40518	247
23.5	22.5	5.91e-03	45020	266
25.5	24.5	4.04e-03	42769	173
31.5	28.6	1.75e-03	132809	233
34.5	33.0	9.66e-04	103546	100
37.5	36.2	2.07e-03	157570	326
39.5	38.5	9.16e-04	144068	132
41.5	40.5	9.43e-04	164323	155
45.5	43.6	1.45e-04	699543	122
47.5	46.5	2.20e-04	463706	102
59.5	49.8	8.26e-05	763049	63

APPENDIX G

FSK CROSS AMBIGUITY FUNCTIONS

APPENDIX G

FSK CROSS AMBIGUITY FUNCTIONS

In this appendix the cross ambiguity functions are documented for FSK transmissions possessing a linear frequency variation at the transition intervals. We require the function

$$A_r^{010}(\lambda,\tau) = \int_0^W S_r(t) S_{010}^*(t-\tau) e^{-i2\lambda t} dt$$

where $S_0(t)$ and $S_1(t)$ are the two ideal FSK transmissions, and $S_{010}(t)$ is the non-ideal FSK transmission depicted in Fig. 1. The signaling-element duration is W seconds, the mark and space frequencies are $-1/2W$ cps and $1/2W$ cps, respectively; and the total transition time is $2L$ seconds.

For $|\tau| \geq L$, the ambiguity functions assume the form:

$$A_1^{010}(\lambda,\tau) = \frac{2E}{\pi\lambda W} \exp\left\{-i\pi\left(\frac{\tau}{W} + \lambda W + \lambda\tau + (\operatorname{sgn}\tau)\lambda L\right)\right\} \sin\left\{\pi\lambda\left[W - |\tau| - L\right]\right\}$$

$$+ \frac{2E}{\pi(1+\lambda W)} \exp\left\{i\pi\left[(\operatorname{sgn}\tau)(1+\lambda W)\frac{L}{W} - \lambda\tau + (\operatorname{sgn}\tau - 1)\lambda W\right]\right\} \sin\left\{\pi(1+\lambda W)\left(\frac{|\tau|}{W} - \frac{L}{W}\right)\right\}$$

$$+ 2\,\mathrm{Re}\left\{\frac{2E\sqrt{LW}}{W(1-i)} \exp\left\{-i\pi\left[2\lambda^2 W + 2\lambda L - 2\lambda|\tau| + \frac{|\tau|}{W}(\operatorname{sgn}\tau - 1)\lambda W\right]\right\}\right.$$

$$\left.\cdot\left\{\Phi\left[(1-i)\sqrt{\frac{\pi L}{W}}(1+\lambda W)\right] - \Phi\left[(1-i)\lambda\sqrt{\pi L W}\right]\right\}\right\}$$

$$A_0^{010}(\lambda,\tau) = \frac{2E}{\pi(1-\lambda W)} \exp\left\{i\pi\left[(\operatorname{sgn}\tau)L\left(\frac{1}{W} - \lambda\right) - \lambda(\tau + L)\right]\right\} \sin\left\{\pi\lambda\left(|\tau| + \lambda L - \frac{|\tau|}{W} - \frac{L}{W} - \lambda W\right)\right\}$$

$$+ \frac{2E}{\pi\lambda W} \exp\left\{i\pi\left[\frac{\tau}{W} - \lambda\tau + (\operatorname{sgn}\tau)\lambda L + (\operatorname{sgn}\tau - 1)\lambda W\right]\right\} \sin\pi\lambda(|\tau| - L)$$

$$+ 2\,\mathrm{Re}\left\{\frac{2E\sqrt{LW}}{(1+i)W} \exp\left\{i\pi\left[\frac{(1-\operatorname{sgn}\tau)}{2}(1-2\lambda W) - \frac{|\tau|}{W} + \lambda(|\tau| - 2L) + 2L\lambda^2 W\right]\right\}\right.$$

$$\left.\cdot\left\{\Phi\left[\sqrt{\pi L W}(1+i)\lambda\right] - \Phi\left[\sqrt{\frac{\pi L}{W}}(1+i)(\lambda W - 1)\right]\right\}\right\}$$

For $|\tau| \le L$, the ambiguity functions assume the form:

$$A_1^{010}(\lambda,\tau) = \frac{2E}{\pi\lambda W}\exp\left\{-i\pi\left[\frac{\tau}{W}+2\lambda\tau+\lambda W\right]\right\}\sin\left\{\pi\lambda(W-2L)\right\}$$

$$+\frac{2E\sqrt{LW}}{W(1-i)}\exp\left\{-i\pi\left[2L\lambda^2W+2\lambda L+2\lambda\tau+\frac{\tau}{W}\right]\right\}$$

$$\times\left\{\Phi\left[\frac{(1-i)}{2}\sqrt{\frac{\pi}{LW}}(2L\lambda W+L+\tau)\right]-\Phi\left[(1-i)\lambda\sqrt{\pi LW}\right]\right\}$$

$$+\frac{2E\sqrt{LW}}{W(1+i)}\exp\left\{i\pi\left[2L\lambda^2W+2\lambda L-2\lambda\tau-2\lambda W-\frac{\tau}{W}\right]\right\}$$

$$\times\left\{\Phi\left[\frac{(1+i)}{2}\sqrt{\frac{\pi}{LW}}(2L\lambda W+L-\tau)\right]-\Phi\left[(1+i)\lambda\sqrt{\pi LW}\right]\right\}.$$

$$A_0^{010}(\lambda,\tau) = \frac{2E}{(1-\lambda W)}\exp\left[i\pi\left(\frac{\tau}{W}-2\lambda\tau-\lambda W\right)\right]\sin\left[(1-\lambda W)\left(\frac{2L}{W}-1\right)\right]$$

$$+\frac{2E\sqrt{LW}}{W(1-i)}\exp\left[-i\pi\left(2LW\lambda^2+2\lambda\tau-2\lambda L-\frac{\tau}{W}\right)\right]$$

$$\times\left\{\Phi\left[\sqrt{\frac{\pi}{LW}}\frac{1-i}{2}(2L\lambda W+\tau-L)\right]-\Phi\left[\sqrt{\frac{\pi L}{W}}(1-i)(\lambda W-1)\right]\right\}$$

$$+\frac{2E\sqrt{LW}}{W(1+i)}\exp\left[i\pi\left(2L\lambda^2W-2\lambda W-2\lambda\tau-2\lambda L+\frac{\tau}{W}\right)\right]$$

$$\times\left\{\Phi\left[\sqrt{\frac{\pi}{LW}}\frac{1+i}{2}(2L\lambda W-\tau-L)\right]-\Phi\left[\sqrt{\frac{\pi L}{W}}(1+i)(\lambda W-1)\right]\right\}.$$

$$\Phi(x) = \frac{2}{\sqrt{\pi}}\int_0^x e^{-t^2}dt \quad ,$$

where x is a complex variable.

REFERENCES

1. Edel M. Young and M. Pollack, "Outputs from the Network Analysis Computer Programs: A Summary Report," Final Technical Report 3 Contract DA 36-039SC-85052, SRI Project 3340, Stanford Research Institute, Menlo Park, California (December 1962).

2. Edel M. Young and E. A. Clarke, "The HF Propagation Prediction Programs for the IBM 7090 Computer," Final Technical Report 2, Contract DA 36-039-SC-85052, SRI Project 3340, Stanford Research Institute, Menlo Park, California (May 1962).

3. Bruce M. Sifford, "Link Evaluation and Tape Merging Computer Programs," Final Technical Report 7, Contract DA 36-039-SC-85052, SRI Project 3340, Stanford Research Institute, Menlo Park, California (December 1962).

4. M. Pollack and G. Wallace, "The Network Routing and Evaluation Program," Final Technical Report 9, Contract DA 36-039-SC-85052, SRI Project 3340, Stanford Research Institute, Menlo Park, California (December 1962).

5. P. A. Bello and B. D. Nelin, "The Effect of Frequency-Selective Fading on the Binary Error Probabilities of Incoherent and Differentially Coherent Matched Filter Receiver," *IRE Trans. PGCS*-11, pp. 170-186 (June 1963).

6. Robert F. Daly, "Analysis of Multipath Effects on FSK Error Probability for a Simple HF Channel Model," Research Memorandum 1, Contract SD-189, SRI Project 4554, Stanford Research Institute, Menlo Park, California (February 1964).

7. Robert F. Daly, "On Modeling the Time-Varying Frequency-Selective Radio Channel," Technical Report 2, Part II, Contract DA 36-039-SC-90859, SRI Project 4172, Stanford Research Institute, Menlo Park, California (July 1964).

8. N. T. Gaarder, "An Error-Rate Expression for HF DPSK Communication Systems," Technical Report 3, Contract DA-36-039-SC-90859, SRI Project 4172, Stanford Research Institute, Menlo Park, California (August 1964).

9. Granger Associates, "Handbook of Operation and Maintenance Instructions for Granger Associates Model 540 Programmer," Palo Alto, California (June 1962).

10. Rixon Electronics, Inc., "Digital Word Generator and Analyzer Operation and Maintenance Manual," Silver Spring, Maryland (January 1963).

11. Department of the Army, "Telegraph Terminal AN/FGC-29," TM11-2245 (August 1956).

12. Department of the Army, "Radio Receiver R-390A/URR," TM11-856A (January 1956).

13. Departments of the Army and the Air Force, "Single-Sideband Converter CV-157 URR," TM11-266 and TO 31R1-2URR-231 (October 1955).

14. D. G. Brennan, "Linear Diversity Combining Techniques," *Proc. IRE*, Vol. 47, pp. 1075-1102 (June 1959).

15. R. G. Gallager, "Characterization and Measurement of Time- and Frequency-Spread Channels," Technical Report 352, Lincoln Laboratory, Massachusetts Institute of Technology, Lexington, Massachusetts (30 April 1964).

16. T. Kailath, "Channel Characterization: Time-Variant Dispersive Channels," in E. J. Baghdady, editor, *Lectures on Communication System Theory*, pp. 95-123 (McGraw-Hill, New York 1961).

17. P. Bello, "Characterization of Randomly Time Variant Linear Channels," *IEEE Trans. PGCS*-11, pp. 360-393 (December 1963).

18. R. F. Daly, "A Power Spectrum Program for Estimating the Doppler Profile of a Radio Channel," Research Memorandum 15, Contract DA 36-039-SC-27197, DASA Subtask 938 01-011, SRI Project 3670, Stanford Research Institute, Menlo Park, California (October 1964).

19. R. A. Shepherd, "HF Communication Effects Simulation: Instrumentation and Operation of the Field Experiment," Interim Report 3, Contract DA 36-039-SC-87197, DASA Subtask 938 01-011, SRI Project 3670, Stanford Research Institute, Menlo Park, California (December 1963).

20. Bruce M. Sifford, "HF Communication Effects Simulation: Computer Processing of Oblique Sounder Data," Interim Report 5, Contract DA 36-039-SC-87197 DASA, Subtask 938 01-011, SRI Project 3670, Stanford Research Institute, Menlo Park, California (February 1964).

21. H. Staras, "Diversity Reception with Correlated Signals," *J. Appl. Phys.*, Vol. 27, pp. 93-94 (January 1956).

22. F. S. Packard, "Effect of Correlation on Combined Diversity," *Proc. IRE*, Vol. 46, pp. 362-363 (January 1958).

23. J. N. Pierce and S. Stein, "Multiple Diversity with Non-Independent Fading," *Proc. IRE*, Vol. 48, pp. 89-104 (January 1960).

24. J. W. Ames, "Spatial Properties of Amplitude Fading of Continuous 17-Mc Radio Waves," Technical Report 87, Contract Nonr-225(64), NR 088-019, ARPA Order 196-64, Report SEL-64-022, Stanford Electronics Laboratories, Stanford University, Stanford, California (March 1964).

25. J. H. Van Vleck, "The Spectrum of Clipped Noise," Report 51, Radio Research Laboratory, Harvard University, Cambridge, Massachusetts (1943).

26. M. Balser and W. B. Smith, "Some Statistical Properties of Pulsed Oblique HF Ionospheric Transmissions," *J. Research NBS*, Vol 66D, No. 6, pp. 721-730 (November-December 1962).

27. D. A. Hedlund and L. C. Edwards, "Polarization Fading over an Oblique Incidence Path," *IRE Trans. PGAP*-6, pp. 21-25 (January 1958).

28. S. O. Rice, "Mathematical Analysis of Random Noise," *BSTJ*, Vols. 23 and 24, pp. 1-162, also in Nelson Wax, editor, *Selected Papers on Noise and Stochastic Processes*, pp. 133-294 Dover Publications, Inc., New York, 1954).

29. W. Q. Crichlow, Q. D. Spaulding, C. J. Roubique, and R. T. Disney, "Amplitude-Probability Distributions for Atmospheric Radio Noise," NBS Monograph 23, National Bureau of Standards (November 4, 1960).

30. D.A.S. Fraser, *Statistics—An Introduction*, p. 224 (Wiley and Sons, Inc., 1958).

STANFORD RESEARCH INSTITUTE

MENLO PARK
CALIFORNIA

Regional Offices and Laboratories

Southern California Laboratories
820 Mission Street
South Pasadena, California 91031

Washington Office
808–17th Street, N.W.
Washington, D.C. 20006

New York Office
270 Park Avenue, Room 1770
New York, New York 10017

Detroit Office
1025 East Maple Road
Birmingham, Michigan 48011

European Office
Pelikanstrasse 37
Zurich 1, Switzerland

Japan Office
Nomura Security Building, 6th Floor
1–1 Nihonbashidori, Chuo ku
Tokyo, Japan

Retained Representatives

Toronto, Ontario, Canada
Cyril A. Ing
67 Yonge Street, Room 710
Toronto 1, Ontario, Canada

Milan, Italy
Lorenzo Franceschini
Via Macedonio Melloni, 49
Milan, Italy